Institute of Nutritional Science
Chair of Food Science
Justus Liebig University Giessen

Development of on-surface metabolisation systems for food analysis

Cumulative dissertation

for the degree of

Doctor rerum naturalium (Dr. rer. nat.)

Submitted to the

Faculty of Agricultural Science, Nutritional Science, and Environmental Management

Justus Liebig University Giessen

by

Isabel Müller (M. Sc.)

Siegburg, Germany

Giessen, 2025

With permission of the faculty Agricultural Science,
Nutritional Science, and Environmental Management
Justus Liebig University Giessen

Examining committee:

1st Reviewer: Prof. Dr. Gertrud Morlock
2nd Reviewer: Prof. Dr. Bernd Lindemann
3rd Examiner: Prof. Dr. Sylvia Schnell
3rd Examiner: Prof. Dr. Mathias Faßhauer

Table of contents

Declaration

I declare that this dissertation is a work of my own, written without any illegitimate help by any third party, and only with the materials indicated in the dissertation. I have indicated in the text where I have used texts from already published sources, either word for word or in substance, and where I have made statements based on the oral information given to me. At any time during the investigations carried out by me and described in the dissertation, I followed the principles of good scientific practice as defined in the "Justus Liebig University Giessen Statute for Ensuring Good Scientific Practice".

Giessen, May 2025

_____

Isabel Müller

Acknowledgments

I would like to thank my supervisor, Prof. Dr. Gertrud Morlock, for the opportunity to write my doctoral dissertation in her research group. Thank you for your patience in advising my scientific journey, reading and editing my publications, and this thesis. I appreciated your support overall.

Additionally, I want to thank all other reviewers and examiners of this thesis for reading my dissertation during perpetually stressful days.

Special thanks go to Prof. em. Dr. Wolfgang Schwack as the haven of peace for the research group. May you remain healthy for a long time to continue your passion for research.

As life as a doctoral student may sometimes be stressful, exhausting, and frustrating, colleagues will be there to bring back the sunshine, strengthen your back, and are always ready to listen. Thanks to the first round of comrade-in-arms: Stefanie Kruse, Tamara Schreiner, Annabel Mehl, Daniel Meyer, Alisa Ronzheimer and Kevin Jakob, and for the second round: Katharina Schmidtmann, Marlene Fischer, Stefan Roling, Annika Haase, Max Haumann, Cande Ochoa Romero, Bastian Loderhose and Anne Ringelmann.

Accompanying students on their scientific journey has not only been my profession, but also to ignite their passion for research. Thank you to Jessica Richardson, Alexander Gulde, Bianca Schmid, Loredana Bosa, Ilka Scheibelhut, Sophie Kolitsch, Viktoria Englert, Saad Samir, Maja Bücker and Lisa-Marie Niemeier for joining me during my doctorate. You all have contributed so much!

Thank is owed to all my friends and family, who have supported me, no matter how. Without you, I would not have been where I am today.

How can you tell if you've been working on your doctorate for too long? – The list of fellows is perhaps a little long!

So, let us dive into my contribution to science!

Scientific contributions

Peer-reviewed original research paper

I) **Müller I**, Morlock GE. (2023) Quantitative saccharide release of hydrothermally treated flours by validated salivary/pancreatic on-surface amylolysis (nanoGIT) and high-performance thin-layer chromatography. *Food Chem.* 432: 137145. doi: 10.1016/j.foodchem.2023.137145

Author contributions: Isabel Müller: Conceptualization, Methodology, Data curation, Validation, Writing – original draft. **Gertrud E. Morlock:** Conceptualization, Methodology, Supervision, Writing – review & editing.

II) **Müller I**, Gulde A, Morlock GE (2023) Bioactive profiles of edible vegetable oils determined using 10D hyphenated comprehensive high-performance thin-layer chromatography (HPTLC×HPTLC) with on-surface metabolism (nanoGIT) and planar bioassays. *Front. Nutr.* 10: 1227546. doi: 10.3389/fnut.2023.1227546

Author contributions: Isabel Müller: Conceptualization, Methodology, Experimental analysis, Data analysis, and Writing—original draft. **Alexander Gulde:** Experimental analysis and Data analysis. **Gertrud E. Morlock:** Conceptualization, Methodology, Supervision, and Writing—review and editing.

III) **Müller I**, Schmid B, Bosa L, Morlock GE (2024) Screening of α-amylase/trypsin inhibitor activity in wheat, spelt and einkorn by high-performance thin-layer chromatography. *Anal. Methods*. 16: 997-3006. doi: 10.1039/D4AY00402G

Author contributions: Isabel Müller: Conceptualization, Methodology, Experimental analysis, Data analysis, Witing – original draft. **Loredana Bosa:** Experimental analysis, Data analysis. **Bianca Schmid:** Experimental analysis, Data analysis. **Gertrud E. Morlock:** Conceptualization, Methodology, Supervision, Writing – original draft, Writing – review and editing.

IV) **Müller I**, Scheibelhut I, Morlock GE Study of the quantitative α-amylase or trypsin inhibition by refined and whole wheat and einkorn using high-performance thin-layer chromatography–nanoGIT versus conventional spectrophotometry, in preparation

Author contributions: Isabel Müller: Conceptualization, Methodology, Experimental analysis, Data analysis, Writing – original draft. **Ilka Scheibelhut**: Experimental analysis, Data analysis. **Gertrud E. Morlock**: Conceptualization, Methodology, Supervision, Writing – review and editing.

V) **Müller I**, Englert VH, Morlock GE Feasibility of HPTLC on-surface enzyme assays for the determination of enzyme activity in comparison to spectrophotometric approaches using invertase from *S. cerevisiae*, in preparation

Author contributions: Isabel Müller: Conceptualization, Methodology, Experimental analysis, Data analysis, Writing – original draft. **Viktoria H. Englert**: Experimental analysis, Data analysis. **Gertrud E. Morlock**: Conceptualization, Methodology, Supervision, Writing – review and editing.

Conference talks

I) Progress in Nutritional Science, Justus-Liebig University Giessen, Germany, 06.07.2022: **I. Müller**, G. Morlock "Miniaturized on-surface digestion of starches"

II) 34. Doktorandenseminar Separation Science, Hotelpark Hohenroda, Germany, 07.-09.01.2024: **I. Müller**, A. Gulde, G. Morlock "On-surface Untersuchung der Verdauung von Kohlenhydraten und Fetten unter Verwendung von Mund- und Darmenzymen"

List of abbreviations

AA	Amino acids
ATI	α-amylase/trypsin inhibitor
DAD	Diode array detection
DAG	Diacylglycerol
EDA	Effect-directed analysis
FA	Fatty acid
FLD	Fluorescence detector
GC	Gas chromatography
GIT	Gastrointestinal tract
HESI	Heated electro spray ionisation
HILIC	Hydrophilic interaction liquid chromatography
HPLC	High-performance liquid chromatography
HPTLC	High-performance thin-layer chromatography
HR	High resolution
LADME	Liberation, Absorption, Distribution, Metabolism, Excretion
MAG	Monoacylglycerol
MS	Mass spectrometry
NMR	Nuclear magnetic resonance spectroscopy
NP	Normal phase
RP	Reversed phase
TAG	Triacylglycerol
UV	Ultraviolet light
Vis	Visible light

List of figures

List of tables

Introduction

The innate curiosity of humans drives them to investigate and comprehend the unknown. The earliest attempts at explanation by pioneering women and men in science established the groundwork for what would become the field of analytics. Today, the field of analytics covers various interconnected disciplines, each holding its own significance. An important area within analytics is the study of the metabolome, which focuses on investigating products released by metabolic reactions in organisms [1]. By examining metabolites and their interactions in the discipline of metabolomics, researchers can gain valuable insights into biological and chemical processes. This knowledge contributes significantly to our understanding of life. Metabolomics finds applications across various organisms and ecosystems in examining their biochemical pathways [2] and identifying biomarkers [3]. It is essential for pharmaceutical research, environmental sciences, clinical investigations, as well as in nutrition and agricultural studies.

1. The impact of food metabolomics on nutrition and food processing

As part of foodomics, food metabolomics applies advanced analytical techniques to study the metabolites present in food and those resulting from human metabolic processes after food consumption [4]. It has wide-ranging applications, from the routine monitoring of contaminants [5] and improving food processing [6] to understanding the impact of food on human health [7].

The consumption of food implies biochemical transformations during the digestive process that enable the human body to access nutrients, minerals, and as well as potentially harmful substances. As food enters the oral cavity, digestion starts and the bolus passes through the oesophagus into the gastrointestinal tract and ends in the colon, where undigested matter is excreted through the anus (Figure 1). According to the LADME model [8, 9], the metabolic processes of substances within organisms, including those found in food, occur in five distinct phases: **L**iberation, **A**bsorption, **D**istribution, **M**etabolism and **E**xcretion. The organs of the digestive system (mouth, stomach, and intestines) establish an optimal environment for the decomposition of food into its constituent parts [10–13] and liberate them into their respective digestive fluids. Once released, these substances are absorbed into the circulatory system and distributed to their target locations in the human body where they undergo metabolism. If not required elsewhere in the body, they are excreted via urine or faeces. However, metabolism does not occur exclusively after absorption into the circulatory

system; the process begins immediately as soon as digestive fluids come into contact with food. Digestive fluids, which contain enzymes and bacteria, contribute to the creation of an optimal environment and support further release of nutrients via direct enzymatic conversion or bacterial metabolism [10–14]. The survival of the human body relies on the metabolism of the macronutrients carbohydrates, lipids, and proteins as they are a sophisticated source of energy [15]. The body can directly absorb only a limited number of small-molecule macronutrients [16]. The majority require an initial breakdown through enzymatic digestion (Figure 1).

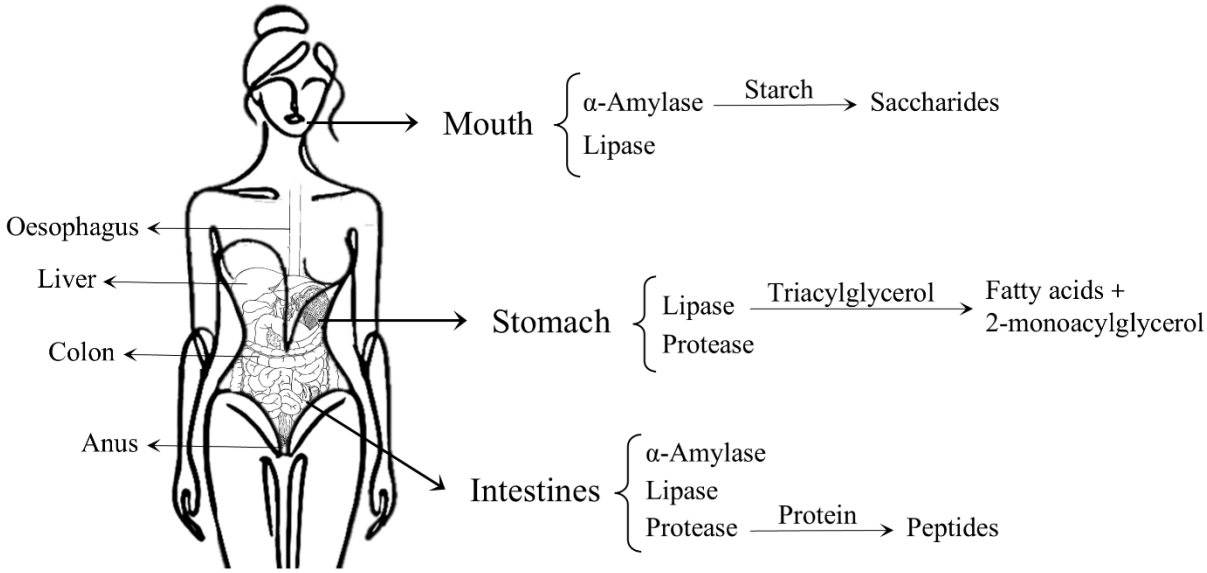

Figure 1 The human digestive system consisting of the digestive organs mouth, stomach, and intestines including their most important enzymes and the corresponding metabolic reactions.
AI-generated image mixed with an image from hatchcr (Vecteezy.com).

The initial stage is oral digestion, which involves α-amylase, the most prevalent salivary enzyme [17]. Known as amylolysis, α-amylase metabolises starch, converting it into its smaller molecules such as maltotriose, maltose, and glucose [18, 19]. Saliva also contains antibacterial enzymes such as lysozyme, lactoperoxidase, lactoferrin, and immunoglobulin A, which maintain a healthy oral microbiota [20].

Carbohydrate metabolism is crucial not only for survival but also for investigating starch bioavailability [18, 21]. In the last decades, dietary trends have shifted towards an excess of carbohydrates, leading to widespread obesity and its associated health issues emerging as a major concern for modern society [22–24]. The effects of carbohydrate intake on human health can be determined by various factors including the diverse botanical origins of starch [25], genetically engineered crops [26], different flour milling techniques (refined or whole grain) [27, 28], and food preparation methods such as cooking, baking, and serving [29, 30].

Carbohydrate-rich foods not only supply energy through starch but also contain dietary fibres (non-digestible or partially digestible polysaccharides). They escape amylolysis because of their molecular structure, which is inaccessible to α-amylase, and some become fermented in the gut. However, dietary fibre intake is poor in modern diets and a daily intake of 20–30 g is recommended [31, 32]. They serve a dual purpose: they counteract excessive calorie intake by rapidly promoting satiety and enhancing human health through beneficial metabolites produced during fermentation [33]. Furthermore, the investigation of cereal-based foods also plays an important role in the field of food metabolomics regarding intolerances such as coeliac disease and allergies caused by metabolites [34]. In addition to nutritional aspects of carbohydrates, analysis of the metabolic profile of food plays a decisive role in food fraud investigations. The geographical and botanical origin of exemplary honey, as well as any unauthorised addition of sugars, can be verified by chemometric analysis of its carbohydrate profile [35]. Concluding, the detailed analysis of the carbohydrate profile of foods is of major interest.

However, not all metabolic pathways in the human body are as well-known as amylolysis. For example, the secretion of lipase in saliva by acinar cells [36]. No matter of lingual, gastric or pancreatic lipase, they catalyse the conversion of triacylglycerols into free fatty acids (FA) and 2-monoacyglycerols [37, 38]. Although lingual lipase may exist, it is the gastric lipase in the stomach that is crucial for newborns, as their pancreatic lipase secretion is not yet fully developed [39].

Similar to the trend observed for carbohydrates, the consumption of fats has increased in recent years, resulting in health problems such as obesity and cardiovascular diseases [24, 40, 41]. Nutritional guidelines suggest limiting fat intake to 30–35% of the total energy consumption, as lipids have the highest caloric density among macronutrients [31, 42]. However, FAs, as metabolites of digestive lipolysis, not only function as an energy source but also fulfil numerous other roles within the human organism. They contribute to intercellular communication, regulate metabolic activities, and are part of the cellular membrane [43]. FAs are categorised as either saturated or unsaturated, with the latter containing at least one double bond in their structure. In the typical diet, the predominant saturated FAs are lauric acid (C12:0), myristic acid (C14:0), palmitic acid (C16:0), and stearic acid (C18:0). Conversely, oleic acid (C18:1), linoleic acid (C18:2), and linolenic acid (C18:3) represent the most frequently consumed unsaturated FAs [44–46]. While FAs of atypical lengths (shorter or longer) are found in trace amounts in our diet, they serve important functions in human physiology. The body can produce most of these FAs

independently, with linoleic acid (ω-6) and linolenic acid (ω-3) being exceptions that must be obtained from dietary sources [47]. Experts suggest an optimal dietary ratio of ω-6 to ω-3 FAs, ranging from 1:1 to 5:1 [48]. This recommendation has led to an expanding market for nutritional supplements, as the typical diet is notably deficient in ω-3 FAs [48]. In general, a lower intake of saturated FAs compared to unsaturated FAs is recommended, as realised by the Mediterranean diet [49, 50]. Concluding, the analysis of the comprehensive FA profile of plant-based and animal-derived food is of major importance to support an optimal diet and facilitate the development of more nutritionally beneficial processed food. In addition, examining the metabolic profile of fats can reveal food adulteration, which is frequently used to assess olive oil composition [35].

Proteins, along with lipids and carbohydrates, represent the third macronutrient to be discussed. In the stomach, initial protein breakdown occurs through the action of the protease pepsin into smaller peptide fragments. Following their transport to the small intestine, these peptides undergo further enzymatic digestion via pancreatic proteases such as trypsin and chymotrypsin. [51] The breakdown of peptides yields smaller peptides and amino acids (AA), which are essential for either supporting the body's internal protein synthesis, undergoing oxidation to function as an energy source or neurotransmitter [52, 53]. In humans, 21 of the numerous AAs are proteinogenic and act as precursors for the synthesis of proteins. Nine of those 21 AAs (histidine, isoleucine, leucine, lysine, methionine, phenylalanine, tryptophan, threonine, and valine) are categorised as essential and must be obtained through dietary intake. [52] Beside the amino acid profile of food, proteins are of great interest to the food processing industry. As plant-based diets grow in popularity, alternative protein sources have gained the focus of research, particularly in the context of processed foods. Within a few years, plant-based meat alternatives have emerged as the most lucrative products in the protein food sector. Their success has been so remarkable that certain companies have ceased production of their traditional meat offerings [54]. Moreover, the food industry has acknowledged the growing health trend of fighting against poor modern nutrition and is constantly developing innovative products, such as high-protein dairy products, sweets, or bars enhanced with supplementary proteins. Thus, protein, peptide and AAs profiles are important in the field of food metabolomics and of great interest in the food industry.

The intestinal tract, comprising the small and large intestines, represents the most sophisticated organ of the digestive system, where the chyme, departing from the stomach, is further metabolised. In addition to the three most prevalent pancreatic enzymes (α-

amylase, lipase, and the proteases trypsin and chymotrypsin), a diverse microbial community, including numerous bacteria, bacteriophages, human viruses, and yeast, colonises the intestinal tract. The human microbiota contains trillions of microorganisms that support the health and digestion of the human body. [55, 56] Over the past few years, the significance of the gut microbiome in food digestion has been greatly underappreciated, resulting in its own distinct field, known as microbiome metabolomics. Complementary to amylolytic, lipolytic, and proteolytic metabolism, the microbiota metabolises a variety of other nutrients contained in food, making them accessible to the human body. The gut microbiome is strongly individual, and digestive disorders often arise from imbalanced microbial gut colonisation [55, 57]. In response to these concerns, the food and pharmaceutical industries offer an array of supplements. The probiotic microorganisms *Lactobacillus* and *Bifidobacterium*, along with prebiotic substances such as inulin or fructooligosaccharides, are available as dietary supplements or food additives [57–59]. As an innovative medical treatment, faecal microbiota transplantation from healthy donors is being extensively researched across various scientific disciplines [60, 61].

However, the complexity of the human digestive system and the discipline of food metabolomics encompass numerous other factors, including individual physiology, environmental influences, genetics, medication and drugs, sex, age, and culture. In conclusion, metabolites play an important role in nutrition and digestion and are essential for both survival and human health. Therefore, the pharmaceutical and food industries are committed to advancing research on drug development, dietary supplements, and food processing.

2. Analytical techniques in food metabolomics

A wide range of analytical methods are available for examining enzymes and metabolites, ranging from sophisticated approaches, such as mass spectrometry (MS) linked to high-performance liquid chromatography (HPLC) or gas chromatography (GC) and nuclear magnetic resonance spectroscopy (NMR), to simpler techniques, such as spectrophotometric assays and high-performance thin-layer chromatography (HPTLC). [7, 62–64]

2.1. Liquid and gas chromatography coupled to mass spectrometry

One of the main analytical techniques used to evaluate the food metabolome is the separation of metabolites using HPLC or GC coupled with MS. HPLC has proven to be the best method in the field of proteomics and separation of polar metabolites and pesticides [65, 66]. GC has proven its pioneering position in lipidomics and the separation of apolar metabolites, such as flavourings [67]. Both methods offer unique advantages, with HPLC providing better separation of complex mixtures [68] and GC offering higher sensitivity for apolar compounds, making them complementary tools for comprehensive food metabolome analysis. Hyphenation with MS enables identification of the separated metabolites. If financial resources and expertise are available, high-resolution MS (HRMS) is preferred to obtain more information about the sample, especially regarding non-targeting analysis [69]. Nonetheless, MS detection relies on ionisable compounds, and the examination of complex sample mixtures complicates interpretation, requiring substantial analytical experience. Additionally, sample preparation and method development can be challenging for achieving the best analytical results. Analysing metabolic reactions, separate sample withdrawal to analyse metabolic products, and often additional sample preparation are necessary. [69] Although MS is frequently employed, it is important to recognise that HPLC and GC systems can be used in conjunction with various detection methods for metabolite analyses [70, 71].

2.2. Nuclear magnetic resonance spectroscopy

NMR analysis of the food metabolome represents another important analytical method that offers non-destructive metabolite profiling. Qualitative and quantitative analyses can be performed on a broad spectrum of analytes such as carbohydrates, lipids, AAs, and organic acids, without compromising the integrity of the sample [72]. Compared to HPLC or GC techniques, NMR requires minimal sample preparation, which helps to maintain sample integrity. This feature renders NMR particularly advantageous for identifying food adulteration and performing quality control in the food industry [63]. As no separation occurs

prior to detection, the complete sample can be examined at any time, allowing for transitions between various analytical approaches (targeted, non-targeted, profiling/screening, and identification) without the need for additional measurements but with limitations regarding sensitivity [64]. Nevertheless, this results in increased difficulty in interpreting NMR spectra as the sample complexity increases. The advanced nature of this method leads to substantial costs, both in terms of equipment and specialist training. However, examining the metabolic profile of food via NMR is commonly employed to investigate alterations during food processing, evaluate the effects and interactions of nutritional components, and detect food contaminants and additives [73, 74].

2.3. Spectrophotometric assays

The analysis of food metabolites by spectrophotometric assays remains an underappreciated analytical technique. They are predominantly used to assess enzymatic activity or quantify the resulting metabolic products. Two principal detection approaches are employed for the analysis. The first method utilises substrates that incorporate chromophores or fluorophores, which yield a detectable signal upon enzymatic transformation. The second approach is the use of derivatisation agents that react with either the substrate or product, forming a compound that can be identified through spectrophotometry. This technique is particularly well-suited for observing metabolic activities and enzyme inhibition reactions in a simple and economical manner. Nutrient profiling and quantification of various food components, including proteins, carbohydrates, lipids, and contaminants, can be readily accomplished using derivatisation reagents. [75–77] Screening of bioactive compounds represents another application area, as these substances can be directly identified through their biological activities, such as their capacity to act as antioxidants [78]. Although spectrophotometric assays are simple to execute, they require highly standardised conditions and are both resource-intensive and time-consuming, particularly in the context of high-throughput methodologies. The sensitivity of the method is significantly affected by complex and matrix-rich samples because no separation stage is included. Thus, sample preparation plays a crucial role. Because separation is missing, spectrophotometric assays are only able to determine sum parameters. Spectrophotometric methods are rarely employed as a single analytical technique but are typically supported by additional separation procedures to provide a comprehensive analysis [79, 80].

2.4. High-performance thin-layer chromatography

Although HPTLC is a simple and cost-effective separation method with diverse applications, it is rarely included in the list of analytical techniques for food metabolomics. The robustness of HPTLC enables it to handle complex and matrix-rich sample mixtures with minimal sample preparation requirements [81, 82]. Furthermore, the development of methods for this technique is less complex compared to GC or HPLC, as there is considerable flexibility in the composition of both mobile and stationary phases. The integration of separation techniques with diverse detection methods makes this approach well suited for fingerprinting and metabolite profiling. The scope extends from the basic qualitative or quantitative examination of macronutrients [19, 81] to the recognition of bioactive compounds through the application of chemical assays or bioassays [83]. In contrast to spectrophotometric assays, HPTLC has the option of determining the sum parameters but also identify the specific causative substance. The integration of hyphenation with additional analytical methods such as MS/MS or HPLC-MS/MS significantly broadens the scope of separation and identification [84, 85].

The all-in-one HPTLC-nanoGIT technique (Figure 2) offers a novel approach for examining metabolic reactions directly within the HPTLC plate [86]. It evaluates metabolic reactions of the gastrointestinal tract (GIT) at the nanomolar level. The metabolic reaction and subsequent separation process occurr on the same surface, eliminating the need for a separate sample collection step and dilution after the enzymatic reaction. This methodology facilitates complete analysis of the sample and prevents any loss or modification of substances during sample preparation. Once the metabolites have been separated, the HPTLC plate is subjected to derivatisation. This process involves either a single reagent or multiple reagents in sequence, enabling visualisation of specific metabolites. This visualisation technique allows the identification of metabolite classes, including carbohydrates, lipids, and proteins, as well as the recognition of specific substances by the use of standard substances [19, 81, 86–88]. Alternatively, a bioassay can be applied to the HPTLC plate to detect various biological effects [81, 86]. Both visualisation methods can also be combined to identify the class of metabolites responsible for these biological effects [81, 89]. The HPTLC chromatogram obtained is subsequently detected either qualitatively through plate imaging or quantitatively via densitometric evaluation. MS/MS analysis or further separation via heart-cut HPLC before MS/MS analysis can be performed directly on the HPTLC plate whether derivatised or containing bioassays, facilitating more accurate identification of co-eluting metabolites

[81, 90]. The process is entirely automated through an autoTLC interface, which allows elution by selecting zones from the previously visualised HPTLC chromatogram [84].

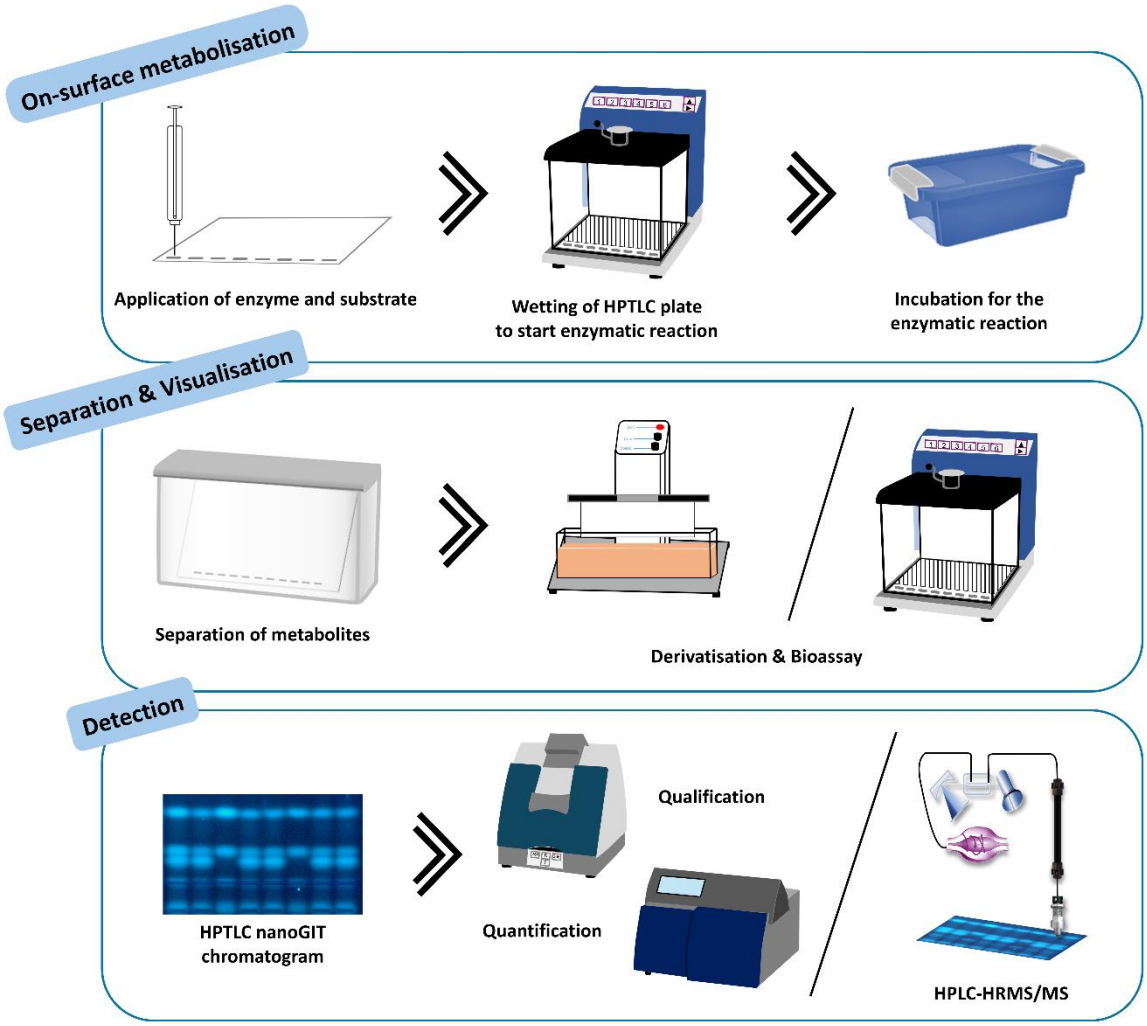

Figure 2 Schematic workflow of the HPTLC-nanoGIT method from application of enzyme and substrate solutions to the qualitative and quantitative detection of the metabolic products.

In summary, the all-in-one HPTLC-nanoGIT approach is the superior balanced method in assessing metabolic processes.

2.5. *In vitro* digestion systems

In vitro digestion models are applied in a variety of disciplines including food science, nutrition, pharmacology, and toxicology. They are used to examine the digestibility of nutrients or novel food products and investigate the release of beneficial or harmful compounds during digestion. [91, 92]

These systems were designed to simulate human digestive processes under controlled conditions and replicate the major compartments of the gastrointestinal tract (oral cavity,

stomach, and intestine). Comparability is supported by the integration of digestive enzymes such as amylases, proteases, and lipases, along with precise pH adjustments and mechanical forces to accurately mimic the physiological breakdown of food. The complexity of in vitro digestion models varies widely, ranging from simple static systems (constant conditions throughout the digestion process) to complex dynamic models. These dynamic systems consider additional factors that provide a more realistic representation of the digestive process, for example gastric emptying rates, peristaltic movements, and intestinal absorption. [91, 93, 94] Some advanced models additionally try to represent the gut microbiota to study interactions between food components and intestinal bacteria [93, 94].

One of the most important advantages of *in vitro* digestion systems is their ability to overcome ethical and practical limitations associated with *in vivo* studies. They provide a controlled environment for experiments that would be challenging in human trials, beside the uncomfortable sampling. Unfortunately, *in vitro* digestion systems cannot fully simulate the complexity of human digestion. Incorporating hormonal regulation or the dynamic gut microbiome into these models is challenging [91, 93, 94]. Ongoing developments promise to further increase the reliability of *in vitro* digestion systems, potentially leading to more effective strategies for improving human health through the diet. Nevertheless, they are particularly useful for initial screening and hypothesis confirmation in food and nutritional research.

3. Bioactivity of food metabolites

Food metabolomics studies have included two distinct areas. The first area examines endogenous metabolites resulting from the body's metabolic processes, and the second area investigates exogenous metabolites originating from consumed food. Examining not only the metabolome of food samples derived from plants or animals but also their bioactivity allows for assumptions about the impact of metabolites on human health. Activity metabolomics, a relatively recent branch of food metabolomics, has been established as a distinct field of study [95].

Metabolic pathways can be influenced by bioactive compounds, resulting in the stimulation, inhibition, or modification of human organisms. The chemical structure, concentration, and potency of these substances determine their bioactivity [96, 97]. Bioactive substances have the potential to affect every metabolic pathway; therefore, the possibilities of their effects are endless (Figure 3), and often a single substance causes multiple effects simultaneously. The most significant health-beneficial properties include the potential to be anti-carcinogenic, anti-microbial, anti-inflammatory, neuroprotective, and metabolic-activating. Food metabolites that exclusively cause positive biological effects are referred to as nutribiotics or nutraceuticals [97, 98]. The most significant adverse effects are various forms of toxicity (genotoxic, cytotoxic, neurotoxic, immunotoxic, or reprotoxic), carcinogenesis, disruption of the endocrine system, or deactivation of metabolic processes. Food contaminants or ingredients that cause pathological effects are termed xenobiotics and typically exit the body via xenobiotic metabolism [96, 98].

Food metabolites can be classified into two categories. On the one hand primary metabolites, including proteins derived from plants or animals, fatty acids, and dietary fibres. On the other hand, secondary metabolites, such as plant polyphenols, alkaloids, and endogenous animal metabolites, such as taurine and creatine. Predominantly, bioactive compounds are secondary metabolites. [99, 100]

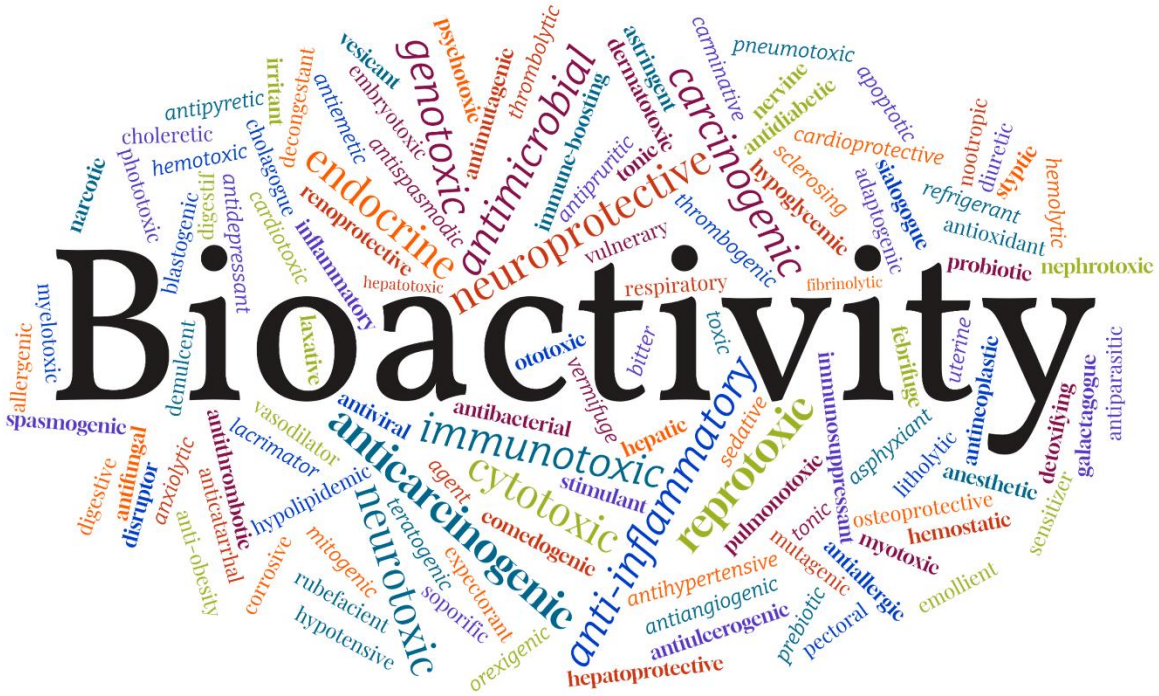

Figure 3 Health-beneficial and harmful effects associated with bioactivity, presented as word cloud. Generated by wordclouds.com.

Comprehensive analysis of bioactive effects is elaborating and requires multidisciplinary approaches. Bioactive substances are present in complex matrices, such as plant parts, and need to be made accessible for analysis. However, the extraction process was identified as the first major challenge because bioactivity needs to be preferably maintained without any loss, depending on the analytical approach. Extracting the entirety of all bioactive substances in one sample is practically unfeasible due to their diverse physical and chemical properties. For example, lipophilic compounds can be extracted using apolar organic solvents, and conversely, hydrophilic substances can be extracted using highly polar solutions such as water or acidified alcohols. The process may require multiple extraction steps or the use of a universal extraction solvent, potentially resulting in the loss of full bioactive potential or, in the worst case, entire substances. Insufficient isolation of a substance leads to a higher concentration of matrix compounds, which hinders the identification of bioactivity. Bioactivity can be detected by direct identification via effect-directed analysis (EDA), or indirect detection solely by identifying previously described bioactive compounds and their concentrations [101, 102].

EDA combines chemical analysis (fractionation, characterisation, and identification) with biological testing (bioassays and evaluation of synergistic, agonistic, and antagonistic effects) [103]. This approach enables the identification of the components responsible for

the bioactive effects. Separation techniques allow isolation via fractionation and characterisation of specific bioactive compounds within complex matrices, whereas distinct bioassays are used to evaluate their bioactive potential. A pioneering technique in terms of EDA is HPTLC, in which crude extracts are easily separated and subsequently subjected to multiple bioassays in sequence [104, 105]. Finally, heart-cutting hyphenation techniques such as HPTLC-MS [106, 107] or HPTLC-HPLC-MS [85, 90] can be used to directly identify bioactive compounds without additional sample application. EDA is both expensive and time-consuming, except for high-throughput approaches; however, it is by far the most comprehensive analytical method. This approach is crucial for the detection of new bioactive substances and is widely used for both target and non-target substance screening.

Another approach is to detect and identify known bioactive substances without confirming their activities. This method relies on established databases of known bioactive compounds and their associated bioactivity. The quantification of these compounds can be related to their bioactive potential. The key advantage of this approach is its independence from biological activities and the possible application of destructive analytical methods. However, this approach has limitations as it may fail to account for the synergistic effects between multiple substances or missing bioactive compounds that are not catalogued. [102, 108]

4. Current challenges in the analysis of metabolites

As previously outlined, the chapter on food metabolomics and examination of food metabolites addresses a wide range of aspects. Due to the diverse properties of metabolites, no single analytical technique can detect and quantify all metabolites and their effects. It is often necessary to combine multiple methods, each with a specific strength, to identify classes of metabolites (Table 1).

Table 1 Advantages, disadvantages, and application areas of various analytical techniques used for the evaluation of food metabolomics, including HPLC-MS, GC-MS, NMR, HPTLC, and spectrophotometric assays.

Advantages	Disadvantages	Application areas
HPLC-MS		
- High-through put option - Optimal for polar substances - Separation of complex mixtures - High sensitivity	- Complex method development - Limited to soluble substances - Sample withdrawal necessary - Organic solvents - Matrix prone	- Proteomics - Targeted and non-targeted screening - Qualification and quantification
GC-MS		
- High-through put option - Optimal for apolar substances - High sensitivity	- Limited to evaporable and volatile substances - Complex sample preparation - Sample withdrawal necessary	- Lipidomics - Targeted and non-targeted screening - Qualification and quantification
NMR		
- Structural identification - Minimal sample preparation - Non-destructive - High reproducibility	- Sample withdrawal necessary - Complex evaluation - Expensive - Low sensitivity - No separation technique - Matrix prone - Organic solvents	- Proteomics - Targeted and non-targeted screening - Qualification and quantification
HPTLC		
- Cheap - Simple - Minimal sample preparation	- Organic solvents - Semi-automatic method - Low sensitivity - Immobilised enzyme reaction	- Lipidomics - Peptidomics - Targeted and non-targeted screening

Advantages	Disadvantages	Application areas
- Flexible method development - Flexible detection options - High-through put option - Separation of complex mixtures - All-in-one approach possible - Trace analysis		- Qualification and quantification - Effect-directed analysis
Spectrophotometric assays		
- Cheap - Aqueous solvents - Simple - High-through put option - Real time analysis - Flexible detection options - Application of enzymes possible	- Stringent standardisation - Time-consuming - High material consumption - Sample withdrawal necessary - Low selectivity and sensitivity - Matrix prone - Indirect measurement - Sample withdrawal necessary	- Non-targeted screening - Analysis of nutrients - Effect-directed analysis

Metabolite analysis includes significant challenges, where sample preparation being the first critical step. The process of extracting all metabolites while maintaining their integrity is complex, particularly in matrix-rich food samples. Various classes of metabolites require multiple extraction techniques. Therefore, standardisation of sample preparation protocols is essential to ensure reproducibility and comparability of results; however, standardisation is often lacking. The additional sample preparation required for the analytical method after the metabolic reaction can further affect the integrity of the extracted metabolites.

Metabolites are products of processes involving enzymes, bacteria, and organisms. They often exist at trace levels and require sensitive detection techniques. HPTLC offers a broad detection range to achieve a balance between sensitivity and precision, whereas MS provides the best overall sensitivity. However, accurate quantification is complicated by matrix effects and lack of references. Additionally, the development and validation of quantification methods for a wide range of metabolites are both time- and resource-intensive. The field of non-targeted metabolomics, especially when managing completely unknown compounds,

remains challenging. HRMS/MS and NMR are considered gold standards because of the possibility of structural elucidation.

Moreover, connecting metabolite profiles to their bioactivity and understanding the complex interactions between multiple metabolites are difficult tasks. The integration of enzyme assays into *in vitro* studies is essential for establishing the relevance of the identified metabolites. HPTLC supports EDA by combining a separation technique with bioassays. Despite efforts to generate *in vitro* metabolite profiles, their translation into *in vivo* effects remains a challenge. A comparison of the bioavailability and metabolism of food compounds in the human body using *in vitro* digestion systems requires expert knowledge. Nevertheless, *in vitro* digestion models are necessary to overcome ethical limitations associated with human trials. The development of advanced *in vitro* models that closely simulate human digestion is a growing research area. By optimising the automation and miniaturisation, reduced sample consumption and enhanced throughput can be achieved. HPTLC is an effective method to balance the demands of high-throughput screening with the need to maintain quality, particularly in the context of miniaturisation.

Addressing the challenges associated with metabolite identification and quantification is essential for achieving advancements in the field of food metabolomics. Ongoing improvements in analytical methodologies and standardised protocols are required.

5. Scope

This thesis addresses the potential of HPTLC in high-throughput screening and maintaining the reliability in miniaturised food metabolomics studies. The impact of miniaturisation on the separation efficiency and metabolite detection is evaluated in detail. The scope of this thesis is a more profound understanding of how the performance of miniaturised HPTLC systems is comparable to that of conventional well-established spectrophotometric assays. Chien-Shiung Wu, a prominent scientist, once expressed her concerns of the modern scientific world, 'I am not afraid of the unknown. I am afraid of the known that isn't true.' Can HPTLC unlock a further understanding of enzymatic reactions and initiate new advancements in the field of food metabolomics?

Given that HPTLC is recognised as the most reliable technique for sample preparation and for reducing matrix effects, its potential as an alternative method for metabolite analysis and analysis of complex food samples is being explored. Consequently, it is essential to develop protocols for the standardisation of on-surface HPTLC systems, including plate selection, sample application, and critical development conditions. Moreover, to improve the detection of trace metabolites, it is essential to validate quantitative HPTLC methods in line with the established guidelines. The potential of establishing HPTLC-based methodologies for detailed metabolite profiling of food samples is investigated. Specifically, the effect of the food matrix components on the separation and detection capabilities of HPTLC is investigated. Moreover, the ability of HPTLC-EDA to detect bioactive compounds in complex food extracts following metabolic processes is examined.

6. Improvements in analysing food metabolites using HPTLC

The following publications provide a detailed summary of the development and application of HPTLC hyphenated with on-surface metabolism (nanoGIT), establishing it as a novel analytical tool in the field of food metabolomics.

Quantification and characterisation of fundamental metabolic processes, including starch digestibility, lipid metabolism, and enzyme inhibition, were demonstrated. In the first publication, the release of saccharides during amylolysis of various flours was investigated using the HPTLC-nanoGIT system. This method was further extended to lipolysis in vegetable oils using an advanced hyphenated 10D technique to determine fatty acid profiles and identify potential genotoxic and antibacterial properties. In addition, innovative HPTLC screening methodologies were developed for qualitative and quantitative evaluation of enzyme inhibition, specifically α-amylase/trypsin inhibitors. These results were compared with those obtained using traditional spectrophotometric techniques. Furthermore, assessment of the feasibility of HPTLC on-surface metabolisation using invertase demonstrated enhanced sensitivity and dynamic range. However, limitations in determining the kinetic parameters and impact of immobilised enzyme systems are acknowledged.

6.1. Publication I – On-surface amylolysis of various grains

For the first time, HPTLC-nanoGIT on-surface metabolism was used for quantification (Figure 4). The starch digestibility of ten distinct hydrothermally treated flour suspensions was evaluated via quantitative saccharide release of glucose, maltose, and maltotriose using salivary/pancreatic on-surface amylolysis [19]. To ensure successful quantification, the method was validated to ensure reliability and reproducibility of the results.

The analysis revealed variations in the digestibility of refined and whole flours and among different grain types, including wheat, spelt, rye, einkorn, amaranth, emmer, and oats. These findings could play a significant role in the use of grain-based products for individuals with obesity or diabetes. Analysing individual saccharides distinctly allows for a unique evaluation from a nutritional perspective, in contrast to the evaluation of sum parameter values from spectrophotometric assays. Whole-grain products generally displayed lower saccharide release than refined flours, suggesting potential nutritional benefits. This observation aligns with the current dietary guidelines that recommend increased consumption of whole-grain products [28, 33]. Moreover, the differences between salivary and pancreatic amylolysis showed increased glucose release during prolonged pancreatic

digestion. This suggests that the duration of food transit through the digestive system may influence the overall glycaemic response.

This cost- and time-efficient methodology offers advantages over the traditional *in vitro* digestion methods. Reduced sample preparation and the all-in-one approach combining on-surface metabolisation, identification, and quantification enables comprehensive analysis with minimal effort. The ability to simultaneously analyse multiple samples on one HPTLC plate makes it suitable for high-throughput screening of starch digestibility in various food products. The HPTLC-nanoGIT technique sheds light on specific enzymatic products at the nanomolar scale, uncovering previously unnoticed matrix effects that could affect spectrophotometric detection without being detected. This contributes to our understanding of nutritional recommendations at the molecular level and how various grains and processing methods (whole-grain or refined) influence saccharide release during digestion.

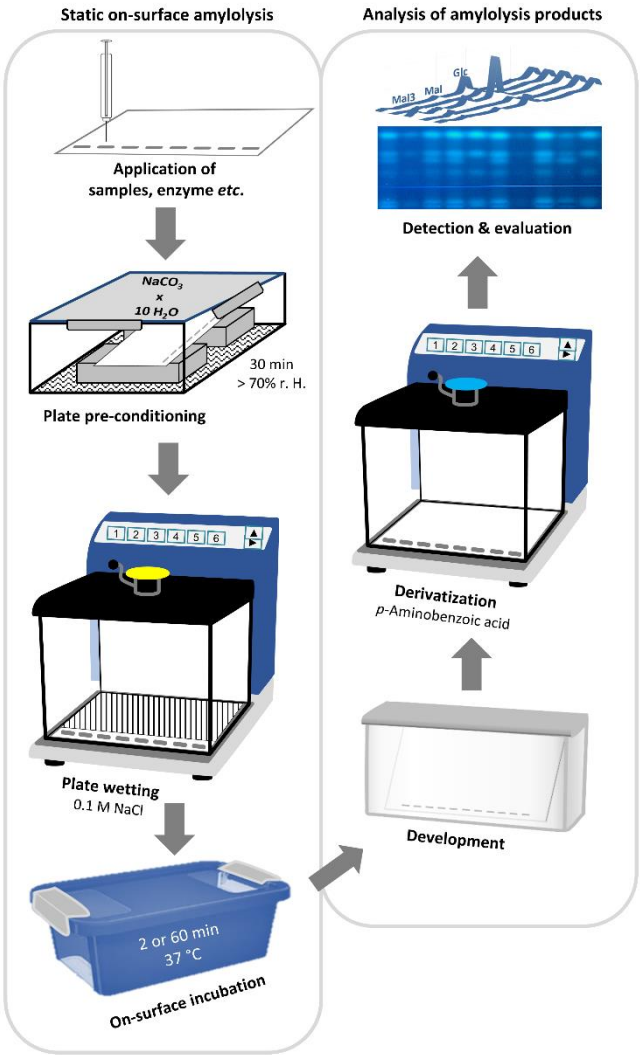

Figure 4 Validated HPTLC-nanoGIT workflow for the qualitative and quantitative determination of on-surface amylolysis [19].

6.2. Publication II – On-surface lipolysis of various vegetable oils

To fully exploit the potential of the HPTLC-nanoGIT method, the bioactive profiles of nine edible vegetable oils were investigated via a 10D hyphenated technique (Figure 5), namely nanoGIT-HPTLC×HPTLC-Vis/FLD-bioassay-heart cut-RP-HPLC-DAD-HESI-HRMS/MS [81]. The comprehensive HPTLC×HPTLC method in conjunction with on-surface metabolism (nanoGIT), planar bioassays, and subsequent heart cut HPLC-HRMS/MS metabolite identification offers full potential for the evaluation of pancreatic lipolysis. The methodology was applied to nine vegetable oils commonly used in culinary applications and in the food industry, including rapeseed, flaxseed, hemp, walnut, soybean, sunflower, olive, coconut, and palm oils.

Investigation of triacylglycerol (TAG) digestion is challenging because of the markedly different physicochemical properties of the resultant FAs, which hinders the application of aqueous-based spectrophotometric methods. To conduct the aqueous enzymatic reaction on-surface, a hybrid reversed-phase (RP) HPTLC plate with hydrophilic characteristics (RP18-W) was used, creating simultaneously a 2D orthogonal separation system (1st dimension with HILIC/NP separation and 2nd dimension with RP separation). In the first dimension, the separation of TAGs, diacylglycerols (DAGs), and monoacylglycerols (MAGs) from FAs demonstrated the success of the metabolic reaction, whereas the second dimension further distinguished the FAs to determine the FA profile for each digested oil. Additionally, the chromatogram obtained was subsequently analysed using EDA to identify antibacterial effects against Gram-negative *Aliivibrio fischeri* and Gram-positive *Bacillus subtilis* as well as genotoxic effects using the SOS-Umu-C assay. The causative substances were further separated using heart cut-RP-HPLC and identified using HRMS/MS [90, 109]. The digested oils were found to have genotoxic effects, which were linked to the presence of oxidised fatty acid species and contaminants. Arising potential for reconsideration of current risk assessments for edible vegetable oils. The antibacterial effect was significantly influenced by the degree of saturation, which aids in assessing potential new health-enhancing antibacterial agents.

Despite its limitations in the metabolism of only one oil at a time, this novel method stands out in the study of lipolytic profiles. The developed method represents a significant tool for the comprehensive evaluation of complex samples and their potentially harmful or beneficial metabolic products using an integrated and holistic approach.

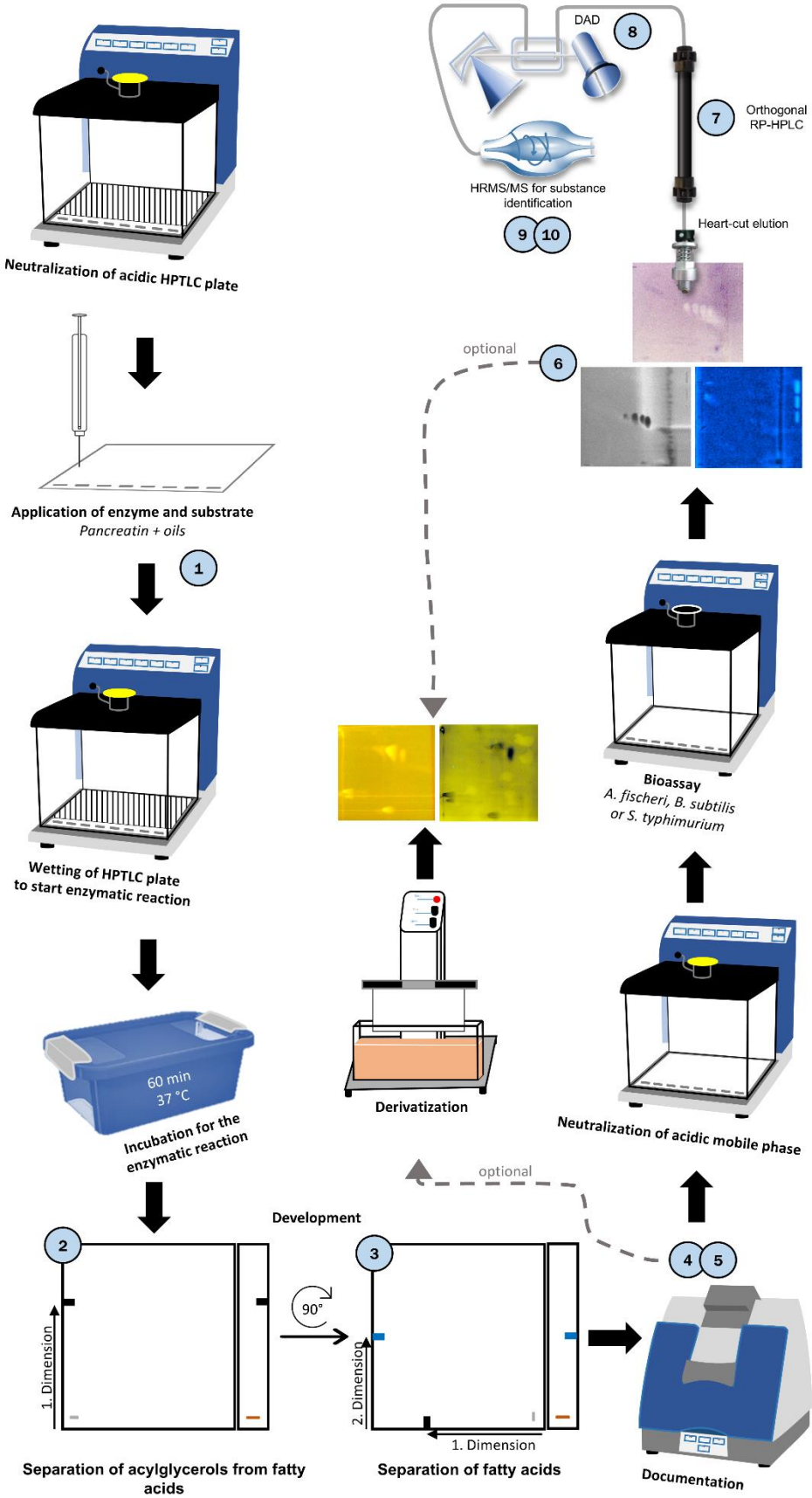

Figure 5 Workflow of the nanoGIT-HPTLC×HPTLC-Vis/FLD-bioassay-heart cut-RP-HPLC-DAD-HESI-HRMS/MS used for the qualification of on-surface lipolysis and bioactive profiling [81].

6.3. Publication III – Qualitative on-surface amylolysis/proteolysis inhibition

After the successful implementation of an optimised qualitative and quantitative HPTLC-nanoGIT method, the concept was expanded to investigate inhibitory reactions. α-Amylase/trypsin inhibitor proteins (ATIs) have been identified as potential triggers for non-celiac gluten sensitivity, an intolerance with increasing attention due to its impact on digestive health and overall well-being [110]. Therefore, two novel HPTLC screening methodologies were developed to evaluate the inhibitory properties of ATI-containing matrix-rich flour extracts derived from wheat, spelt, and einkorn [87].

The NP-HPTLC-nanoGIT method (Figure 6) was designed to analyse α-amylase inhibition in a two-step process: in-vial pre-incubation, followed by on-surface amylolysis. The reduction in the released saccharides was used to evaluate the inhibitory potential. This approach allowed for a more detailed investigation of the inhibitory effects on α-amylase activity, surpassing the limitations of matrix-susceptible spectrophotometric methods. Furthermore, HPTLC analysis provided novel insights into the amylolysis of acarbose, a well-established α-amylase inhibitor, and elucidated the influence on amylolysis. To evaluate trypsin inhibition, in-vial pre-incubation and proteolysis were performed, followed by separation of the released peptides on a wettable RP-HPTLC plate (Figure 6). This approach offers a detailed evaluation of trypsin inhibition and potential effects of ATIs on protein digestion. While the results for both amylolysis and proteolysis did not fully correspond with the existing literature, it is possible that additional non-proteinogenic inhibitors influenced the observed inhibitory effects.

Unfortunately, these methods do not achieve full on-surface digestion; thus, they lack an integrated, all-in-one approach. Nonetheless, the developed screening techniques have shown the ability to identify individual saccharides or peptides. Offering more details than spectrophotometric assays, the HPTLC methods are a more cost-effective option than HPLC-MS methods. Additionally, the simultaneous analysis of up to 17 samples increased the throughput and efficiency. By providing more detailed and accurate information on enzyme inhibition at the molecular level, these methods will pave the way for the assessment of food processing and potential health impacts of cereals.

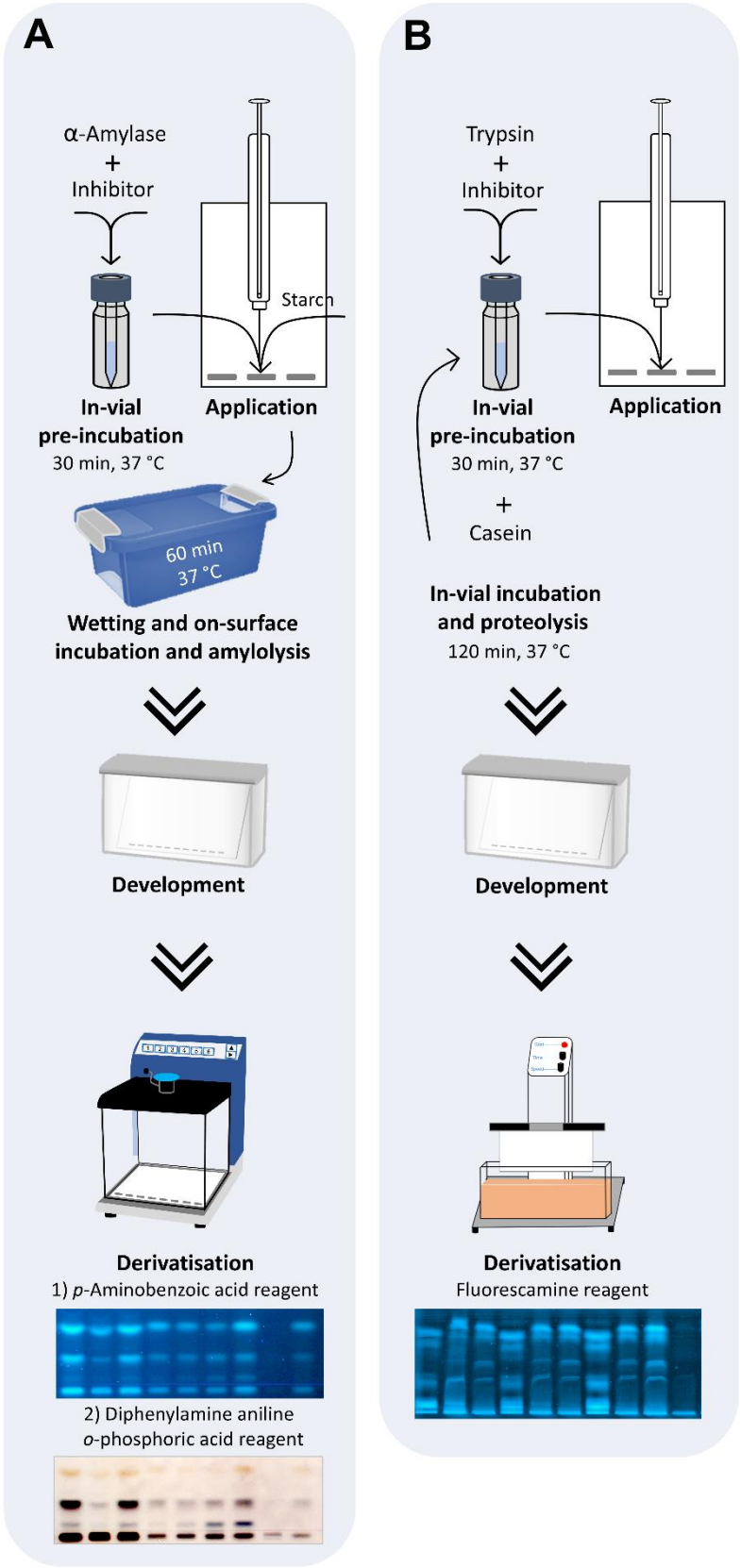

Figure 6 Workflow of the inhibitory semi-on-surface amylolysis HPTLC-nanoGIT assay (**A**) and inhibitory HPTLC proteolysis assay (**B**) for the qualification of the inhibitory potential of ATI-containing extracts [87].

6.4. Publication IV – Quantitative on-surface amylolysis/proteolysis inhibition

Based on the previously discussed HPTLC-nanoGIT inhibition method, which evaluated the inhibitory effects of ATI-containing wheat and einkorn flour extracts, the method was refined into two novel on-surface assays, resulting in a unified all-in-one approach [88].

For α-amylase inhibition, the optimised technique allowed for quantitative evaluation of the inhibitory effects of different cereal extracts. The results revealed that einkorn flour extract showed lower α-amylase inhibition than the refined and whole-wheat extracts. This finding points to potential differences in ATI content and activity among various cereal types, which could influence their digestibility and nutritional value. In addition, proteolytic inhibition was optimised using a fully integrated on-surface method. A comparative analysis of trypsin inhibition across different ATI-containing flour extracts via on-surface metabolization effectively eliminated the need for additional sample withdrawal and dilution. However, on-surface trypsin inhibition was only suitable for semi-quantification because of the dominant blank peptide signals. This limitation highlights the complexity of analysing trypsin inhibition initiated by proteins and emphasises the necessity for further improvement in analytical techniques. To validate the results, the on-surface methods were compared with conventional spectrophotometric assays. For α-amylase inhibition, the HPTLC approach provided more differentiated results regarding individual saccharides released during amylolysis. For trypsin inhibition, the spectrophotometric assay showed nearly total inhibition for all three cereal types, whereas the on-surface HPTLC method only partially confirmed this result. This discrepancy emphasises the need to use multiple analytical techniques to gain a more accurate insight into enzyme inhibition in complex samples.

Research on ATIs is limited and highlights the potential role of HPTLC on-surface metabolisation as a decisive link. The HPTLC approach effectively connects non-specific spectrophotometric assays, which assess inhibitory potential, with more precise HPLC-MS/MS techniques that confirm the identity of the inhibitors present. Furthermore, the developed HPTLC methods have the potential to identify both known and unidentified inhibitors when combined with further purification. This capability opens new avenues for the discovery and characterisation of known and novel inhibitors in food products.

6.5. Publication V – Feasibility of HPTLC in on-surface metabolisation

In the course of evaluating both qualitative and quantitative on-surface metabolisation processes in complex samples, including suspensions and matrix-rich samples, certain limitations were identified. Consequently, a detailed investigation of a simple enzymatic reaction was conducted to assess the feasibility of HPTLC in on-surface metabolisation processes. A quantitative HPTLC nano assay was developed to investigate the enzyme invertase, sourced from *Saccharomyces cerevisiae*, and its function in catalysing the conversion of sucrose into glucose and fructose. To ensure comparability, the validated results were compared to those obtained using conventional spectrophotometric techniques. [111]

The innovative HPTLC approach exhibited significantly enhanced sensitivity, necessitating 12,500 times less substrate while requiring equivalent enzyme quantities compared to traditional spectrophotometric methods. This significant reduction in substrate requirements demonstrated the efficiency of the assay and enable the study of enzymes present in trace amounts or at low activity levels. Furthermore, the larger linear range of the HPTLC method provides greater flexibility for measuring enzyme activity, reducing the need for sample dilution or multiple runs. Another key advantage of the HPTLC method was its ability to quantify glucose and fructose separately, enabling the detection of non-equimolar conversions and potential side reactions. This features a detailed insight into the enzymatic process, allowing the identification and investigation of unexpected products or reaction pathways that may occur during enzymatic conversion. However, a significant discrepancy between the calculated enzyme activity and the theoretical activity was revealed, resulting from the use of an immobilised enzyme system on solid surfaces. Different enzyme-to-substrate ratios and potential side reactions can influence the comparison with other analytical techniques. These findings highlight the need for careful optimisation and standardisation of assay conditions, particularly for immobilised enzyme systems. Moreover, limitations in determining certain kinetic parameters, such as the Michaelis-Menten constant, were observed. While the HPTLC method offers advantages in terms of sensitivity and product separation, it may need to be complemented with other techniques for complete characterisation of enzyme kinetics.

Nevertheless, these improvements have opened new possibilities for enzyme characterisation and metabolic reaction studies, potentially enabling researchers to investigate enzymatic processes at previously unattainable levels of detail and sensitivity.

References

[1] O. Fiehn, Metabolomics — the link between genotypes and phenotypes, in: C. Town (Ed.), Functional Genomics, 1st ed., Springer Netherlands; Imprint Springer, Dordrecht, 2002, pp. 155–171.

[2] C.H. Johnson, J. Ivanisevic, G. Siuzdak, Metabolomics: beyond biomarkers and towards mechanisms, Nat Rev Mol Cell Biol 17 (2016) 451–459. https://doi.org/10.1038/nrm.2016.25.

[3] M.D. Luque de Castro, F. Priego-Capote, The analytical process to search for metabolomics biomarkers, J. Pharm. Biomed. Anal. 147 (2018) 341–349. https://doi.org/10.1016/j.jpba.2017.06.073.

[4] S. Kim, J. Kim, E.J. Yun, K.H. Kim, Food metabolomics: from farm to human, Curr. Opin. Biotechnol. 37 (2016) 16–23. https://doi.org/10.1016/j.copbio.2015.09.004.

[5] E. Tengstrand, J. Rosén, K.-E. Hellenäs, K.M. Aberg, A concept study on non-targeted screening for chemical contaminants in food using liquid chromatography-mass spectrometry in combination with a metabolomics approach, Anal Bioanal Chem 405 (2013) 1237–1243. https://doi.org/10.1007/s00216-012-6506-5.

[6] M. Utpott, E. Rodrigues, A.d.O. Rios, G.D. Mercali, S.H. Flôres, Metabolomics: An analytical technique for food processing evaluation, Food Chem. 366 (2022) 130685. https://doi.org/10.1016/j.foodchem.2021.130685.

[7] M.M. Ulaszewska, C.H. Weinert, A. Trimigno, R. Portmann, C. Andres Lacueva, R. Badertscher, L. Brennan, C. Brunius, A. Bub, F. Capozzi, M. Cialiè Rosso, C.E. Cordero, H. Daniel, S. Durand, B. Egert, P.G. Ferrario, E.J.M. Feskens, P. Franceschi, M. Garcia-Aloy, F. Giacomoni, P. Giesbertz, R. González-Domínguez, K. Hanhineva, L.Y. Hemeryck, J. Kopka, S.E. Kulling, R. Llorach, C. Manach, F. Mattivi, C. Migné, L.H. Münger, B. Ott, G. Picone, G. Pimentel, E. Pujos-Guillot, S. Riccadonna, M.J. Rist, C. Rombouts, J. Rubert, T. Skurk, P.S.C. Sri Harsha, L. van Meulebroek, L. Vanhaecke, R. Vázquez-Fresno, D. Wishart, G. Vergères, Nutrimetabolomics: An Integrative Action for Metabolomic Analyses in Human Nutritional Studies, Mol. Nutr. Food Res. 63 (2019) e1800384. https://doi.org/10.1002/mnfr.201800384.

[8] M.J. Rein, M. Renouf, C. Cruz-Hernandez, L. Actis-Goretta, S.K. Thakkar, M. da Silva Pinto, Bioavailability of bioactive food compounds: a challenging journey to

bioefficacy, Br. J. Clin. Pharmacol. 75 (2013) 588–602. https://doi.org/10.1111/j.1365-2125.2012.04425.x.

[9] E. Fernández-García, I. Carvajal-Lérida, A. Pérez-Gálvez, In vitro bioaccessibility assessment as a prediction tool of nutritional efficiency, Nutr. Res. 29 (2009) 751–760. https://doi.org/10.1016/j.nutres.2009.09.016.

[10] M. Boland, Human digestion - a processing perspective, J. Sci. Food Agric. 96 (2016) 2275–2283. https://doi.org/10.1002/jsfa.7601.

[11] I. Sensoy, A review on the food digestion in the digestive tract and the used in vitro models, Current Research in Food Science 4 (2021) 308–319. https://doi.org/10.1016/j.crfs.2021.04.004.

[12] A. Andrés, A. Heredia, Advanced Research in Food Digestion, Foods (Basel, Switzerland) 10 (2021) 122. https://doi.org/10.3390/foods10010122.

[13] S. Fernández-Tomé, Role of Food Digestion and Digestive System in the Nutritional, Functional and Health Properties of Food Bioactives, Nutrients 16 (2024) 712. https://doi.org/10.3390/nu16050712.

[14] J.C. Stearns, M.D.J. Lynch, D.B. Senadheera, H.C. Tenenbaum, M.B. Goldberg, D.G. Cvitkovitch, K. Croitoru, G. Moreno-Hagelsieb, J.D. Neufeld, Bacterial biogeography of the human digestive tract, Sci Rep 1 (2011) 170. https://doi.org/10.1038/srep00170.

[15] A.M. Prentice, Macronutrients as sources of food energy, Public Health Nutrition 8 (2005) 932–939. https://doi.org/10.1079/PHN2005779.

[16] N.G. MacFarlane, Digestion and absorption, Anaesthesia & Intensive Care Medicine 19 (2018) 125–127. https://doi.org/10.1016/j.mpaic.2018.01.001.

[17] E. Roblegg, A. Coughran, D. Sirjani, Saliva: An all-rounder of our body, Eur. J. Pharm. Biopharm. 142 (2019) 133–141. https://doi.org/10.1016/j.ejpb.2019.06.016.

[18] S. Dhital, F.J. Warren, P.J. Butterworth, P.R. Ellis, M.J. Gidley, Mechanisms of starch digestion by α -amylase—Structural basis for kinetic properties, Crit. Rev. Food Sci. Nutr. 57 (2017) 875–892. https://doi.org/10.1080/10408398.2014.922043.

[19] I. Müller, G.E. Morlock, Quantitative saccharide release of hydrothermally treated flours by validated salivary/pancreatic on-surface amylolysis (nanoGIT) and high-performance thin-layer chromatography, Food Chem. 432 (2023) 137145. https://doi.org/10.1016/j.foodchem.2023.137145.

[20] A.M. Lynge Pedersen, D. Belstrøm, The role of natural salivary defences in maintaining a healthy oral microbiota, Journal of Dentistry 80 Suppl 1 (2019) S3-S12. https://doi.org/10.1016/j.jdent.2018.08.010.

[21] P.J. Butterworth, F.J. Warren, P.R. Ellis, Human α-amylase and starch digestion: An interesting marriage, Starch/Stärke 63 (2011) 395–405. https://doi.org/10.1002/star.201000150.

[22] S. Swaminathan, M. Dehghan, J.M. Raj, T. Thomas, S. Rangarajan, D. Jenkins, P. Mony, V. Mohan, S.A. Lear, A. Avezum, P. Lopez-Jaramillo, A. Rosengren, F. Lanas, K.F. AlHabib, A. Dans, M.V. Keskinler, T. Puoane, B. Soman, L. Wei, K. Zatonska, R. Diaz, N. Ismail, J. Chifamba, R. Kelishadi, A. Yusufali, R. Khatib, L. Xiaoyun, H. Bo, R. Iqbal, R. Yusuf, K. Yeates, K. Teo, S. Yusuf, Associations of cereal grains intake with cardiovascular disease and mortality across 21 countries in Prospective Urban and Rural Epidemiology study: prospective cohort study, BMJ 372 (2021) m4948. https://doi.org/10.1136/bmj.m4948.

[23] M.I. Zafar, K.E. Mills, J. Zheng, A. Regmi, S.Q. Hu, L. Gou, L.-L. Chen, Low-glycemic index diets as an intervention for diabetes: a systematic review and meta-analysis, The American Journal of Clinical Nutrition 110 (2019) 891–902. https://doi.org/10.1093/ajcn/nqz149.

[24] V.J. Clemente-Suárez, A.I. Beltrán-Velasco, L. Redondo-Flórez, A. Martín-Rodríguez, J.F. Tornero-Aguilera, Global Impacts of Western Diet and Its Effects on Metabolism and Health: A Narrative Review, Nutrients 15 (2023). https://doi.org/10.3390/nu15122749.

[25] H. Kaur, B.S. Gill, B.L. Karwasra, In vitro digestibility, pasting, and structural properties of starches from different cereals, Int. J. Food Prop. 21 (2018) 70–85. https://doi.org/10.1080/10942912.2018.1439955.

[26] Derek Stewart, Louise V. T. Shepherd, Robert D. Hall, Paul D. Fraser, Crops and Tasty, Nutritious Food – How Can Metabolomics Help?, in: Annual Plant Reviews Volume 43, John Wiley & Sons, Ltd, 2011, pp. 181–217.

[27] D. Aune, N. Keum, E. Giovannucci, L.T. Fadnes, P. Boffetta, D.C. Greenwood, S. Tonstad, L.J. Vatten, E. Riboli, T. Norat, Whole grain consumption and risk of cardiovascular disease, cancer, and all cause and cause specific mortality: systematic review and dose-response meta-analysis of prospective studies, BMJ 353 (2016) i2716. https://doi.org/10.1136/bmj.i2716.

[28] S. am Kelly, L. Hartley, E. Loveman, J.L. Colquitt, H.M. Jones, L. Al-Khudairy, C. Clar, R. Germanò, H.R. Lunn, G. Frost, K. Rees, Whole grain cereals for the primary or secondary prevention of cardiovascular disease, Cochrane Database Syst Rev 8 (2017) CD005051. https://doi.org/10.1002/14651858.CD005051.pub3.

[29] C.H. Edwards, A.S. Veerabahu, A.J. Mason, P.J. Butterworth, P.R. Ellis, α-Amylase action on starch in chickpea flour following hydrothermal processing and different drying, cooling and storage conditions, Carbohydr. Polym. 259 (2021) 117738. https://doi.org/10.1016/j.carbpol.2021.117738.

[30] E. Urbinati, M. Di Nunzio, G. Picone, E. Chiarello, A. Bordoni, F. Capozzi, The Effect of Balsamic Vinegar Dressing on Protein and Carbohydrate Digestibility is Dependent on the Food Matrix, Foods (Basel, Switzerland) 10 (2021) 411. https://doi.org/10.3390/foods10020411.

[31] Deutsche Gesellschaft für Ernährung (DGE), Österreichische Gesellschaft für Ernährung (ÖGE), Schweizerische Gesellschaft für Ernährung (SGE), D-A-CH-Referenzwerte für die Nährstoffzufuhr, 2nd ed., Bonn, 2024.

[32] European Food Safety Authority, Scientific Opinion on Dietary Reference Values for carbohydrates and dietary fibre, EFSA Journal 8 (2010) 1462. https://doi.org/10.2903/j.efsa.2010.1462.

[33] T.M. Barber, S. Kabisch, A.F.H. Pfeiffer, M.O. Weickert, The Health Benefits of Dietary Fibre, Nutrients 12 (2020). https://doi.org/10.3390/nu12103209.

[34] L.J. Gilissen, I.M. van der Meer, M.J. Smulders, Reducing the incidence of allergy and intolerance to cereals, Journal of Cereal Science 59 (2014) 337–353. https://doi.org/10.1016/j.jcs.2014.01.005.

[35] E. Hong, S.Y. Lee, J.Y. Jeong, J.M. Park, B.H. Kim, K. Kwon, H.S. Chun, Modern analytical methods for the detection of food fraud and adulteration by food category, J. Sci. Food Agric. 97 (2017) 3877–3896. https://doi.org/10.1002/jsfa.8364.

[36] H. Brignot, G. Feron, Oral lipolysis and its association with diet and the perception and digestion of lipids: A systematic literature review, Archives of Oral Biology 108 (2019) 104550. https://doi.org/10.1016/j.archoralbio.2019.104550.

[37] N. Yadav, A.T. Paul, Pancreatic lipase and its related proteins: where are we now?, Drug Discovery Today 29 (2024) 103855. https://doi.org/10.1016/j.drudis.2023.103855.

[38] H. Mu, C.-E. Høy, The digestion of dietary triacylglycerols, Progress in Lipid Research 43 (2004) 105–133. https://doi.org/10.1016/S0163-7827(03)00050-X.

[39] S. Lindquist, O. Hernell, Lipid digestion and absorption in early life: an update, Current opinion in clinical nutrition and metabolic care 13 (2010) 314–320. https://doi.org/10.1097/MCO.0b013e328337bbf0.

[40] L. Wang, H. Wang, B. Zhang, B.M. Popkin, S. Du, Elevated Fat Intake Increases Body Weight and the Risk of Overweight and Obesity among Chinese Adults: 1991-2015 Trends, Nutrients 12 (2020) 3272. https://doi.org/10.3390/nu12113272.

[41] J. Xu, S. Eilat-Adar, C. Loria, U. Goldbourt, B.V. Howard, R.R. Fabsitz, E.M. Zephier, C. Mattil, E.T. Lee, Dietary fat intake and risk of coronary heart disease: the Strong Heart Study, The American Journal of Clinical Nutrition 84 (2006) 894–902. https://doi.org/10.1093/ajcn/84.4.894.

[42] G. Wolfram, A. Bechthold, H. Boeing, S. Ellinger, H. Hauner, A. Kroke, E. Leschik-Bonnet, J. Linseisen, S. Lorkowski, M. Schulze, P. Stehle, J. Dinter, Evidence-Based Guideline of the German Nutrition Society: Fat Intake and Prevention of Selected Nutrition-Related Diseases, Ann Nutr Metab 67 (2015) 141–204. https://doi.org/10.1159/000437243.

[43] P.C. Calder, Functional Roles of Fatty Acids and Their Effects on Human Health, JPEN. Journal of parenteral and enteral nutrition 39 (2015) 18S-32S. https://doi.org/10.1177/0148607115595980.

[44] V. Kostik, S. Memeti, B. Bauer, Fatty acid composition of edible oils and fats, Journal of Hygienic Engineering and Design 4 (2013) 112–116.

[45] M. Kouba, J. Mourot, A review of nutritional effects on fat composition of animal products with special emphasis on n-3 polyunsaturated fatty acids, Biochimie 93 (2011) 13–17. https://doi.org/10.1016/j.biochi.2010.02.027.

[46] J.D. Wood, M. Enser, A.V. Fisher, G.R. Nute, P.R. Sheard, R.I. Richardson, S.I. Hughes, F.M. Whittington, Fat deposition, fatty acid composition and meat quality: A review, Meat Science 78 (2008) 343–358. https://doi.org/10.1016/j.meatsci.2007.07.019.

[47] G.L. Russo, Dietary n-6 and n-3 polyunsaturated fatty acids: from biochemistry to clinical implications in cardiovascular prevention, Biochem. Pharmacol. 77 (2009) 937–946. https://doi.org/10.1016/j.bcp.2008.10.020.

[48] A.P. Simopoulos, An Increase in the Omega-6/Omega-3 Fatty Acid Ratio Increases the Risk for Obesity, Nutrients 8 (2016) 128. https://doi.org/10.3390/nu8030128.

[49] L. Hooper, N. Martin, O.F. Jimoh, C. Kirk, E. Foster, A.S. Abdelhamid, Reduction in saturated fat intake for cardiovascular disease, Cochrane Database Syst Rev 5 (2020) CD011737. https://doi.org/10.1002/14651858.CD011737.pub2.

[50] A.S. Abdelhamid, N. Martin, C. Bridges, J.S. Brainard, X. Wang, T.J. Brown, S. Hanson, O.F. Jimoh, S.M. Ajabnoor, K.H. Deane, F. Song, L. Hooper, Polyunsaturated fatty acids for the primary and secondary prevention of cardiovascular disease, Cochrane Database Syst Rev 11 (2018) CD012345. https://doi.org/10.1002/14651858.CD012345.pub3.

[51] J.S. Bond, Proteases: History, discovery, and roles in health and disease, J. Biol. Chem. 294 (2019) 1643–1651. https://doi.org/10.1074/jbc.TM118.004156.

[52] G. Wu, Functional amino acids in growth, reproduction, and health, Adv. Nutr. 1 (2010) 31–37. https://doi.org/10.3945/an.110.1008.

[53] Z.-N. Ling, Y.-F. Jiang, J.-N. Ru, J.-H. Lu, B. Ding, J. Wu, Amino acid metabolism in health and disease, Sig Transduct Target Ther 8 (2023) 345. https://doi.org/10.1038/s41392-023-01569-3.

[54] Rügenwalder Mühle, Rügenwalder Mühle macht noch mehr Platz für pflanzliche Produkte: Schinken Spicker ab sofort nur noch vegan, Bad Zwischenahn, 2024.

[55] K. Hou, Z.-X. Wu, X.-Y. Chen, J.-Q. Wang, D. Zhang, C. Xiao, D. Zhu, J.B. Koya, L. Wei, J. Li, Z.-S. Chen, Microbiota in health and diseases, Sig Transduct Target Ther 7 (2022) 135. https://doi.org/10.1038/s41392-022-00974-4.

[56] S. Leviatan, S. Shoer, D. Rothschild, M. Gorodetski, E. Segal, An expanded reference map of the human gut microbiome reveals hundreds of previously unknown species, Nat Commun 13 (2022) 3863. https://doi.org/10.1038/s41467-022-31502-1.

[57] S.-K. Kim, R.B. Guevarra, Y.-T. Kim, J. Kwon, H. Kim, J.H. Cho, H.B. Kim, J.-H. Lee, Role of Probiotics in Human Gut Microbiome-Associated Diseases, J. Microbiol. Biotechnol. 29 (2019) 1335–1340. https://doi.org/10.4014/jmb.1906.06064.

[58] P.M. Bock, A.F. Martins, B.D. Schaan, Understanding how pre- and probiotics affect the gut microbiome and metabolic health, American journal of physiology. Endocrinology and metabolism 327 (2024) E89-E102. https://doi.org/10.1152/ajpendo.00054.2024.

[59] M.E. Sanders, D.J. Merenstein, G. Reid, G.R. Gibson, R.A. Rastall, Probiotics and prebiotics in intestinal health and disease: from biology to the clinic, Nature reviews.

Gastroenterology & hepatology 16 (2019) 605–616. https://doi.org/10.1038/s41575-019-0173-3.

[60] J.-W. Wang, C.-H. Kuo, F.-C. Kuo, Y.-K. Wang, W.-H. Hsu, F.-J. Yu, H.-M. Hu, P.-I. Hsu, J.-Y. Wang, D.-C. Wu, Fecal microbiota transplantation: Review and update, Journal of the Formosan Medical Association = Taiwan yi zhi 118 Suppl 1 (2019) S23-S31. https://doi.org/10.1016/j.jfma.2018.08.011.

[61] A. Yadegar, H. Bar-Yoseph, T.M. Monaghan, S. Pakpour, A. Severino, E.J. Kuijper, W.K. Smits, E.M. Terveer, S. Neupane, A. Nabavi-Rad, J. Sadeghi, G. Cammarota, G. Ianiro, E. Nap-Hill, D. Leung, K. Wong, D. Kao, Fecal microbiota transplantation: current challenges and future landscapes, Clinical microbiology reviews 37 (2024) e0006022. https://doi.org/10.1128/cmr.00060-22.

[62] W. Lu, X. Su, M.S. Klein, I.A. Lewis, O. Fiehn, J.D. Rabinowitz, Metabolite Measurement: Pitfalls to Avoid and Practices to Follow, Annu. Rev. Biochem. 86 (2017) 277–304. https://doi.org/10.1146/annurev-biochem-061516-044952.

[63] J.M. Cevallos-Cevallos, J.I. Reyes-De-Corcuera, E. Etxeberria, M.D. Danyluk, G.E. Rodrick, Metabolomic analysis in food science: a review, Trends in Food Science & Technology 20 (2009) 557–566. https://doi.org/10.1016/j.tifs.2009.07.002.

[64] N. Sharma, Anurag, H. Singh, A. Sharma, Application of high-performance thin layer chromatography mass spectrometry (HPTLC MS) in foodomics authenticity, Talanta Open 9 (2024) 100315. https://doi.org/10.1016/j.talo.2024.100315.

[65] P. Zhong, X. Wei, X. Li, X. Wei, S. Wu, W. Huang, A. Koidis, Z. Xu, H. Lei, Untargeted metabolomics by liquid chromatography-mass spectrometry for food authentication: A review, Comprehensive Reviews in Food Science and Food Safety 21 (2022) 2455–2488. https://doi.org/10.1111/1541-4337.12938.

[66] D. Dupont, Peptidomic as a tool for assessing protein digestion, Current Opinion in Food Science 16 (2017) 53–58. https://doi.org/10.1016/j.cofs.2017.08.001.

[67] S.P. Putri, M.M.M. Ikram, A. Sato, H.A. Dahlan, Della Rahmawati, Y. Ohto, E. Fukusaki, Application of gas chromatography-mass spectrometry-based metabolomics in food science and technology, J. Biosci. Bioeng. 133 (2022) 425–435. https://doi.org/10.1016/j.jbiosc.2022.01.011.

[68] A. Kaufmann, Combining UHPLC and high-resolution MS: A viable approach for the analysis of complex samples?, TrAC Trends in Analytical Chemistry 63 (2014) 113–128. https://doi.org/10.1016/j.trac.2014.06.025.

[69] J. Rubert, M. Zachariasova, J. Hajslova, Advances in high-resolution mass spectrometry based on metabolomics studies for food--a review, Food additives & contaminants. Part A, Chemistry, analysis, control, exposure & risk assessment 32 (2015) 1685–1708. https://doi.org/10.1080/19440049.2015.1084539.

[70] K. Kraboun, K. Rojsuntornkitti, N. Jittrepotch, T. Kongbangkerd, N. Uthai, C. Pechyen, Formation analysis of primary and secondary metabolites during angkak fermentation based on GC-TOF-MS, GC-FID, and HPLC and metabolomics analysis, The Microbe 1 (2023) 100006. https://doi.org/10.1016/j.microb.2023.100006.

[71] J.S. Ahn, W.K. Whang, The Development and Validation of Simultaneous Multi-Component Quantitative Analysis via HPLC–PDA Detection of 12 Secondary Metabolites Isolated from Drynariae Rhizoma, Separations 10 (2023) 601. https://doi.org/10.3390/separations10120601.

[72] M. Utpott, E. Rodrigues, A.d.O. Rios, G.D. Mercali, S.H. Flôres, Metabolomics: An analytical technique for food processing evaluation, Food Chem. 366 (2022) 130685. https://doi.org/10.1016/j.foodchem.2021.130685.

[73] C.R. Chowdhury, D. Kavitake, K.K. Jaiswal, K.S. Jaiswal, G.B. Reddy, V. Agarwal, P.H. Shetty, NMR-based metabolomics as a significant tool for human nutritional research and health applications, Food Bioscience 53 (2023) 102538. https://doi.org/10.1016/j.fbio.2023.102538.

[74] A. Ciampa, F. Danesi, G. Picone, NMR-Based Metabolomics for a More Holistic and Sustainable Research in Food Quality Assessment: A Narrative Review, Applied Sciences 13 (2023) 372. https://doi.org/10.3390/app13010372.

[75] K. Liu, Q. Liu, Enzymatic determination of total starch and degree of starch gelatinization in various products, Food Hydrocolloids 103 (2020) 105639. https://doi.org/10.1016/j.foodhyd.2019.105639.

[76] M. Stoytcheva, G. Montero, R. Zlatev, Jose A. Leon, V. Gochev, Analytical Methods for Lipases Activity Determination: A Review, Current Analytical Chemistry 8 400–407. https://doi.org/10.2174/157341112801264879.

[77] L. Call, E.V. Reiter, G. Wenger-Oehn, I. Strnad, H. Grausgruber, R. Schoenlechner, S. D'Amico, Development of an enzymatic assay for the quantitative determination of trypsin inhibitory activity in wheat, Food Chem. 299 (2019) 125038. https://doi.org/10.1016/j.foodchem.2019.125038.

[78] I.G. Munteanu, C. Apetrei, Analytical Methods Used in Determining Antioxidant Activity: A Review, Int. J. Mol. Sci. 22 (2021) 3380. https://doi.org/10.3390/ijms22073380.

[79] S. Tchewonpi Sagu, L. Zimmermann, E. Landgräber, T. Homann, G. Huschek, H. Özpinar, F.J. Schweigert, H.M. Rawel, Comprehensive Characterization and Relative Quantification of α-Amylase/Trypsin Inhibitors from Wheat Cultivars by Targeted HPLC-MS/MS, Foods 9 (2020). https://doi.org/10.3390/foods9101448.

[80] N. Jahn, C.F.H. Longin, K.A. Scherf, S. Geisslitz, No correlation between amylase/trypsin-inhibitor content and amylase inhibitory activity in hexaploid and tetraploid wheat species, Curr. Res. Food Sci. 7 (2023) 100542. https://doi.org/10.1016/j.crfs.2023.100542.

[81] I. Müller, A. Gulde, G.E. Morlock, Bioactive profiles of edible vegetable oils determined using 10D hyphenated comprehensive high-performance thin-layer chromatography (HPTLC×HPTLC) with on-surface metabolism (nanoGIT) and planar bioassays, Front. Nutr. 10 (2023) 1227546. https://doi.org/10.3389/fnut.2023.1227546.

[82] K. Jakob, W. Schwack, G.E. Morlock, All-in-one 2LabsToGo system for analysis of ergot alkaloids in whole rye, in submission (2024).

[83] T. Schreiner, D. Sauter, M. Friz, J. Heil, G.E. Morlock, Is Our Natural Food Our Homeostasis? Array of a Thousand Effect-Directed Profiles of 68 Herbs and Spices, Frontiers in pharmacology 12 (2021) 755941. https://doi.org/10.3389/fphar.2021.755941.

[84] A. Mehl, W. Schwack, G.E. Morlock, On-surface autosampling for liquid chromatography-mass spectrometry, J Chromatogr A 1651 (2021) 462334. https://doi.org/10.1016/j.chroma.2021.462334.

[85] T. Schreiner, G.E. Morlock, Non-target bioanalytical eight-dimensional hyphenation including bioassay, heart-cut trapping, online desalting, orthogonal separations and mass spectrometry, J Chromatogr A 1647 (2021) 462154. https://doi.org/10.1016/j.chroma.2021.462154.

[86] G.E. Morlock, L. Drotleff, S. Brinkmann, Miniaturized all-in-one nanoGIT+active system for on-surface metabolization, separation and effect imaging, Anal. Chim. Acta 1154 (2021) 338307. https://doi.org/10.1016/j.aca.2021.338307.

[87] I. Müller, B. Schmid, L. Bosa, G.E. Morlock, Screening of α-amylase/trypsin inhibitor activity in wheat, spelt and einkorn by high-performance thin-layer chromatography, Anal. Methods. https://doi.org/10.1039/D4AY00402G.

[88] I. Müller, I. Scheibelhut, G.E. Morlock, Study of the quantitative α-amylase or trypsin inhibition by refined and whole wheat and einkorn using high-performance thin-layer chromatography–nanoGIT versus conventional spectrophotometry in submission.

[89] S. Kruse, F. Pierre, G.E. Morlock, Effects of the Probiotic Activity of Bacillus subtilis DSM 29784 in Cultures and Feeding Stuff, J. Agric. Food. Chem. 69 (2021) 11272–11281. https://doi.org/10.1021/acs.jafc.1c04811.

[90] T. Schreiner, N.M. Eggerstorfer, G.E. Morlock, Ten-dimensional hyphenation including simulated static gastro-intestinal digestion on the adsorbent surface, planar assays, and bioactivity evaluation for meal replacement products, Food Funct. 14 (2023) 344–353. https://doi.org/10.1039/d2fo02610d.

[91] M. Minekus, M. Alminger, P. Alvito, S. Ballance, T. Bohn, C. Bourlieu, F. Carrière, R. Boutrou, M. Corredig, D. Dupont, C. Dufour, L. Egger, M. Golding, S. Karakaya, B. Kirkhus, S. Le Feunteun, U. Lesmes, A. Macierzanka, A. Mackie, S. Marze, D.J. McClements, O. Ménard, I. Recio, C.N. Santos, R.P. Singh, G.E. Vegarud, M.S.J. Wickham, W. Weitschies, A. Brodkorb, A standardised static in vitro digestion method suitable for food - an international consensus, Food Funct. 5 (2014) 1113–1124. https://doi.org/10.1039/c3fo60702j.

[92] A. Brodkorb, L. Egger, M. Alminger, P. Alvito, R. Assunção, S. Ballance, T. Bohn, C. Bourlieu-Lacanal, R. Boutrou, F. Carrière, A. Clemente, M. Corredig, D. Dupont, C. Dufour, C. Edwards, M. Golding, S. Karakaya, B. Kirkhus, S. Le Feunteun, U. Lesmes, A. Macierzanka, A.R. Mackie, C. Martins, S. Marze, D.J. McClements, O. Ménard, M. Minekus, R. Portmann, C.N. Santos, I. Souchon, R.P. Singh, G.E. Vegarud, M.S.J. Wickham, W. Weitschies, I. Recio, INFOGEST static in vitro simulation of gastrointestinal food digestion, Nat. Protoc. 14 (2019) 991–1014. https://doi.org/10.1038/s41596-018-0119-1.

[93] D. Dupont, M. Alric, S. Blanquet-Diot, G. Bornhorst, C. Cueva, A. Deglaire, S. Denis, M. Ferrua, R. Havenaar, J. Lelieveld, A.R. Mackie, M. Marzorati, O. Menard, M. Minekus, B. Miralles, I. Recio, P. van den Abbeele, Can dynamic in vitro digestion systems mimic the physiological reality?, Crit. Rev. Food Sci. Nutr. 59 (2019) 1546–1562. https://doi.org/10.1080/10408398.2017.1421900.

[94] I. Sensoy, A review on the food digestion in the digestive tract and the used in vitro models, Current Research in Food Science 4 (2021) 308–319. https://doi.org/10.1016/j.crfs.2021.04.004.

[95] M.M. Rinschen, J. Ivanisevic, M. Giera, G. Siuzdak, Identification of bioactive metabolites using activity metabolomics, Nat Rev Mol Cell Biol 20 (2019) 353–367. https://doi.org/10.1038/s41580-019-0108-4.

[96] A. Guaadaoui, S. Benaicha, N. Elmajdoub, M. Bellaoui, A. Hamal, What is a Bioactive Compound? A Combined Definition for a Preliminary Consensus, Int. J. Nutr. Food Sci. 3 (2014) 174. https://doi.org/10.11648/j.ijnfs.20140303.16.

[97] H.-K. Biesalski, L.O. Dragsted, I. Elmadfa, R. Grossklaus, M. Müller, D. Schrenk, P. Walter, P. Weber, Bioactive compounds: definition and assessment of activity, Nutrition 25 (2009) 1202–1205. https://doi.org/10.1016/j.nut.2009.04.023.

[98] C. Dima, E. Assadpour, S. Dima, S.M. Jafari, Bioavailability and bioaccessibility of food bioactive compounds; overview and assessment by in vitro methods, Comprehensive Reviews in Food Science and Food Safety 19 (2020) 2862–2884. https://doi.org/10.1111/1541-4337.12623.

[99] B. Kulczyński, A. Sidor, A. Gramza-Michałowska, Characteristics of Selected Antioxidative and Bioactive Compounds in Meat and Animal Origin Products, Antioxidants 8 (2019). https://doi.org/10.3390/antiox8090335.

[100] C. Jain, S. Khatana, R. Vijayvergia, Bioactivity of secondary metabolites of various plants: a review, IJPSR 10 (2019) 494–504.

[101] C. Barba-Ostria, S.E. Carrera-Pacheco, R. Gonzalez-Pastor, J. Heredia-Moya, A. Mayorga-Ramos, C. Rodríguez-Pólit, J. Zúñiga-Miranda, B. Arias-Almeida, L.P. Guamán, Evaluation of Biological Activity of Natural Compounds: Current Trends and Methods, Molecules 27 (2022) 4490. https://doi.org/10.3390/molecules27144490.

[102] S. Geisslitz, C. Ludwig, K.A. Scherf, P. Koehler, Targeted LC-MS/MS Reveals Similar Contents of α-Amylase/Trypsin-Inhibitors as Putative Triggers of Nonceliac Gluten Sensitivity in All Wheat Species except Einkorn, J. Agric. Food. Chem. 66 (2018) 12395–12403. https://doi.org/10.1021/acs.jafc.8b04411.

[103] S. Hong, J.P. Giesy, J.-S. Lee, J.-H. Lee, J.S. Khim, Effect-directed analysis: Current status and future challenges, Ocean Sci. J. 51 (2016) 413–433. https://doi.org/10.1007/s12601-016-0038-4.

[104] C. Riegraf, A.M. Bell, M. Ohlig, G. Reifferscheid, S. Buchinger, Planar chromatography-bioassays for the parallel and sensitive detection of androgenicity, anti-androgenicity and cytotoxicity, Journal of chromatography. A 1684 (2022) 463582. https://doi.org/10.1016/j.chroma.2022.463582.

[105] G.E. Morlock, D. Meyer, Designed genotoxicity profiling detects genotoxic compounds in staple food such as healthy oils, Food Chem. 408 (2023) 135253. https://doi.org/10.1016/j.foodchem.2022.135253.

[106] M.N. Taha, M.B. Krawinkel, G.E. Morlock, High-performance thin-layer chromatography linked with (bio)assays and mass spectrometry - a suited method for discovery and quantification of bioactive components? Exemplarily shown for turmeric and milk thistle extracts, Journal of chromatography. A 1394 (2015) 137–147. https://doi.org/10.1016/j.chroma.2015.03.029.

[107] G.E. Morlock, Chromatography Combined with Bioassays and Other Hyphenations – The Direct Link to the Compound Indicating the Effect, American Chemical Society, 2014.

[108] U. Bose, K. Byrne, C.A. Howitt, M.L. Colgrave, Targeted proteomics to monitor the extraction efficiency and levels of barley α-amylase trypsin inhibitors that are implicated in non-coeliac gluten sensitivity, J. Chromatogr. A 1600 (2019) 55–64. https://doi.org/10.1016/j.chroma.2019.04.043.

[109] T. Schreiner, N.M. Eggerstorfer, G.E. Morlock, Towards non-target proactive food safety: identification of active compounds in convenience tomato products by ten-dimensional hyphenation with integrated simulated gastrointestinal digestion, Anal Bioanal Chem (2023) 1–17. https://doi.org/10.1007/s00216-023-04656-0.

[110] M.G. Mumolo, F. Rettura, S. Melissari, F. Costa, A. Ricchiuti, L. Ceccarelli, N. de Bortoli, S. Marchi, M. Bellini, Is Gluten the Only Culprit for Non-Celiac Gluten/Wheat Sensitivity?, Nutrients 12 (2020) 3785. https://doi.org/10.3390/nu12123785.

[111] I. Müller, V.H. Englert, G.E. Morlock, Feasibility of HPTLC on-surface enzyme assays for the determination of enzyme activity in comparison to spectrophotometric approaches using invertase from S. cerevisiae in submission.

Publication I

Quantitative saccharide release of hydrothermally treated flours by validated salivary/pancreatic on-surface amylolysis (nanoGIT) and high-performance thin-layer chromatography

Isabel Müller, Gertrud E. Morlock

Published in Food Chemistry

Received 1st April 2023, Accepted 10th August 2023, Published 15th August 2023

Food Chemistry 432 (2024) 137145

Contents lists available at ScienceDirect

Food Chemistry

journal homepage: www.elsevier.com/locate/foodchem

Quantitative saccharide release of hydrothermally treated flours by validated salivary/pancreatic on-surface amylolysis (nanoGIT) and high-performance thin-layer chromatography

Isabel Müller, Gertrud E. Morlock [*,1]

Institute of Nutritional Science, Chair of Food Science, and Interdisciplinary Research Centre for Biosystems, Land Use, and Nutrition, Justus Liebig University Giessen, Heinrich-Buff-Ring 26–32, 35392 Giessen, Germany

ARTICLE INFO

Keywords:
All-in-one digestion and analysis system
Starch
α-Amylase
Human digestion
Oral phase
Intestinal phase

ABSTRACT

The susceptibility of hydrothermally treated flour products to amylolysis was studied. The human salivary α-amylase and porcine pancreatin enzyme mixture containing α-amylase were used on-surface to investigate the release of glucose, maltose, and maltotriose. On the same adsorbent surface (all-in-one), their high-performance thin-layer chromatography separation and detection via selective chemical derivatization was performed. For the first time, the all-in-one nanoGIT system was studied quantitatively and validated for the simulated static oral and intestinal on-surface amylolysis of ten different hydrothermally treated flours and soluble starch. Differences were detected in the digestibility of refined and whole flours from wheat, spelt, and rye as well as from einkorn, amaranth, emmer, and oat. Amaranth released the lowest amount of saccharides and spelt the highest in both oral and intestinal digestion systems. The results suggest that consumption of whole grain products may be beneficial because of their lower saccharide release, with particular attention to rye.

1. Introduction

Starch is a major energy-providing source for the human diet. The digestion of starchy foods leads to a release of saccharides, following a rise in blood glucose and a corresponding insulin response. This blood glucose rise is expressed as a glycaemic index (GI) value. Since the relationship is still unclear, a low GI value diet is controversially discussed as whether it reduces the risk of type 2 diabetes mellitus, overweight, obesity-related diabetes mellitus (diabesity), and cardiovascular disease (Jenkins et al., 2002; Zafar et al., 2019; Astrup & Finer, 2000; Han, Richmond, Avenell, & Lean, 1997; Vega-López, Venn, & Slavin, 2018). All these health problems are partially rooted in the saccharide release during the amylolysis of starch by α-amylase.

Food processing has a major influence on the digestibility of starch. The amylolysis of hydrothermally treated flour products and soluble starch by α-amylase depends on several factors such as botanical origin and thus particle structure (Slaughter, Ellis, & Butterworth, 2001), and processes such as milling of the grains and gelatinization of the starch (Dhital, Warren, Butterworth, Ellis, & Gidley, 2017). Hydrothermal treatment like cooking and baking leads to structural changes of starch at a molecular and granular level due to gelatinization (Tahir, Ellis, Bogracheva, Meares-Taylor, & Butterworth, 2011). The latter increases the availability of starch as substrate and therefore the digestibility of starchy foods (Chung, Lim, & Lim, 2006; Edwards, Veerabahu, Mason, Butterworth, & Ellis, 2021). Subsequent cooling of gelatinized starch causes retrogradation, which massively decreases the degree of digestion (Bird, Lopez-Rubio, Shrestha, & Gidley, 2009; Edwards et al., 2021). Both processes take place in succession and are important for the evaluation of the digestibility of cooked or baked starchy food but are hard to control.

In the last decade, the variety of flours used in baking products increased, generating growing consumer interest in refined flours and alternatives to wheat (*Triticum aestivum*), such as rye (*Secale cereale*), spelt wheat (*Triticum aestivum* subsp. *spelta*), oat (*Avena sativa*), pseudo cereals such as amaranth (*Amaranthus*), and the ancient einkorn (*Triticum monococcum*) and emmer (*Triticum dicoccum*). Next to white flour, whole grain flours are most relevant (Ahluwalia, Herrick, Terry, & Hughes, 2019). A higher intake of whole grain products (*e.g.*, bread and breakfast cereals) showed a reduction in the risk of cardiovascular disease (Aune et al., 2016; Ye, Chacko, Chou, Kugizaki, & Liu, 2012). This

* Corresponding author.
E-mail address: gertrud.morlock@uni-giessen.de (G.E. Morlock).
[1] Dedicated to the 85th birthday of Dr. Fred Rabel, ChromHELP, Woodbury, NJ, USA.

https://doi.org/10.1016/j.foodchem.2023.137145
Received 1 April 2023; Received in revised form 2 August 2023; Accepted 10 August 2023
Available online 15 August 2023

reduction could be associated with the higher nutrient and fibre content of whole grain flour, resulting in a slower digestion rate and lower GI value (Slavin, Jacobs, Marquart, & Wiemer, 2001; Hallfrisch et al., 2000). Consequently, whole grain products could be the better diet for diabetics and obese individuals. However, studies reported contradictory results due to the low overall quality of evidence and difficulties in the comparability of results from patients (Swaminathan et al., 2021; Kelly, 2017).

Amylolysis results comparing *in vivo* and *in vitro* data can vary between individuals, making their interpretation difficult. As far as the reaction is dependent on too many factors of influence, the exact mechanism of amylolysis is not revealed and the exact rates of all products can be seen as random (Slaughter et al., 2001). To predict dietary effects and clarify contradictory results, *in vitro* digestion experiments are preferred because of the complexity and individuality of the body and ethical concerns about animal testing and human trials. Since *in vitro* amylolysis strongly depends on the process conditions (such as digestion time, enzymes used, concentrations chosen, and physiological aspects), static *in vitro* digestion of macronutrients (carbohydrates, lipids, and proteins) was standardized by an international consensus (INFOGEST network, Minekus et al. (2014)). Based on this harmonized protocol, the nanoGIT$^{+active}$ system (Morlock, Drotleff, & Brinkmann, 2021) was recently developed as the first all-in-one digestion–analysis system. Static digestion and subsequent sensitive analysis including selective detection were performed on the same high-performance thin-layer chromatography (HPTLC) plate. The all-in-one workflow on the same HPTLC surface enabled the efficient and precise analysis of a broad spectrum of complex food samples and their change in macronutrients after oral, gastric, and intestinal digestion.

In this study, a quantitative HPTLC–nanoGIT–FLD method with static digestion and selective detection of the formed saccharides via post-chromatographic derivatization (Morlock, Morlock, & Lemo, 2014) was developed and validated (ICH, 1995/2005). The on-surface oral and intestinal amylolysis of ten different kinds of flours was studied using human salivary α-amylase (HSA) and porcine pancreatic α-amylase in a pancreatin enzyme mixture (Panc), respectively. Soluble starch and hydrothermally treated refined wheat flour type 405 (wheat 405) were selected for the method validation, whereby the wheat 405 was considered as a challenging worst-case scenario due to the poor solubility of native starch. Differences in the digestibility of seven botanically different flours (wheat, spelt, rye, einkorn, amaranth, emmer, and oat) were determined via the quantitatively released glucose (Glc), maltose (Mal) and maltotriose (Mal3).

2. Materials and methods

2.1. Chemicals and materials

D-(+)-Glucose (≥99.5%, Glc), D-(+)-maltose monohydrate (≥99%, Mal), maltotriose hydrate (97%, Mal3), D-(+)-lactose monohydrate (≥99.5%, Lac), 4-aminobenzoic acid (≥99%), bile extract porcine, sodium bicarbonate (≥99.7%), pancreatin from porcine pancreas (Panc; 8 × USP specifications) and α-amylase from human saliva (HSA; 190.4 U/mg solid) were purchased from Sigma Aldrich Fluka (Steinheim, Germany). 2-Propanol (≥99.8%) and *o*-phosphoric acid (85%, pure) were from Th. Geyer (Renningen, Germany). Acetic acid (99–100%), acetonitrile (≥99.9%), starch soluble (analytical grade), and sodium carbonate decahydrate (≥99%) were from Riedel-de Haen (Seelze, Germany). Acetone (≥99.9%) and sodium chloride (≥99%) were purchased from VWR International (Darmstadt, Germany). Calcium chloride (≥98%), monopotassium phosphate (≥99%), and magnesium chloride hexahydrate (≥98%) were from Carl Roth (Karlsruhe, Germany). Ammonium carbonate (extra pure) was from Bernd Kraft (Duisburg, Germany). Bi-distilled water was produced by a Heraeus Destamat B-18E (Thermo Fisher Scientific, Dreieich, Germany). HPTLC plates silica gel 60 (20 × 10 cm) and potassium chloride (≥99.5%) were supplied by Merck (Darmstadt, Germany). Flour samples were purchased from local mills or supermarkets (Table S1).

2.2. Preparation of enzymatic, calcium chloride, and standard solutions

Digestion fluid stock solutions (containing potassium chloride, monopotassium phosphate, sodium bicarbonate, sodium chloride, magnesium chloride hexahydrate and ammonium carbonate) were prepared as described by Minekus et al. (2014). Using the corresponding digestion fluid stock solutions, Panc (10 TAME mU/μL with 10.2 mg/mL bile extract porcine), HSA (75 mU/μL), and calcium chloride (6 pmol/μL for Panc, 750 pmol/μL for HSA) solutions were prepared according to Morlock et al. (2021). Standard stock solutions (1 mg/mL) for Glc, Mal, and Mal3 were prepared and diluted 1:10 or 1:100 with bi-distilled water (stored at 4 °C).

2.3. Flour and starch sample preparation

Each flour sample was freshly prepared daily by weighing 10 mg ± 0.2 mg into a 2-mL reaction tube and mixing with 1 mL bi-distilled water (10 mg/mL), followed by heating in a boiling water bath for 15 min and centrifugation at 17,000 × *g* for 10 min. The supernatant was discarded, and the flour sample was washed with 1 mL bi-distilled water and centrifuged at 17,000 × *g* for 10 min. After discarding the supernatant, the flour sample residue was re-suspended in 1 mL bi-distilled water and filled into a 1.5 mL sample vial. For each re-suspension, the centrifuged flour sample was shaken for 1 min with a vortex mixer equipped with a multi-tube holder (Vortex Genie 2, Scientific Industries, New York City, NY, USA). The soluble starch sample was dissolved in bi-distilled water (1 mg/mL), heated in a boiling water bath until the clarity of the solution, and stored at 4 °C (if needed, re-heated before application).

2.4. On-surface amylolysis and analysis via HPTLC–nanoGIT–FLD

HPTLC silica gel 60 plates were prewashed with acetonitrile by front-elution up to 90 mm. All solutions/suspensions were applied as 7-mm bands using the following settings (Automatic TLC Sampler ATS 4, CAMAG, Muttenz, Switzerland): track distance 10 mm, distance from the lower edge 10 mm (alternatively, 8 mm) and left edge minimal 20 mm, dosage speed 50 nL/s, filling speed 8 μL/s, filling vacuum time 4 s, and syringe volume 25 μL. The application was performed in three steps (Files S1 and S2). (I) The sample (substrate for the enzyme) was applied (2 μL/band). (II) Five standard levels for Glc (40–400 ng/band), Mal (475–2660 ng/band), and Mal3 (471–2823 ng/band) were applied. (III) The sample (substrate) was over-sprayed with the enzymatic and calcium chloride solution (each 1 μL/band). To obtain a standardized plate activity of 70% relative humidity, pre-conditioning was used for 30 min. Therefore, the plate was placed horizontally in a plastic box (IKEA 365+, 5.2 L, IKEA, Hofheim-Wallau, Germany) filled with 200 mL saturated sodium carbonate decahydrate solution having a relative humidity of at least 70% (Fig. S1A). This humid box was kept filled and reused over months. Alternatively, a twin trough chamber (CAMAG; 20 cm × 10 cm) can be used but must be prepared at least 1 h before preconditioning. Before starting the enzyme reaction by wetting the application area, the upper plate part was covered with another smaller plate (Fig. S2, cut to 20 cm × 8 cm or 8.5 cm, depending on the lowest hR_F of interest, which should still be covered by this plate; placed with the layer facing upwards). This package (sample plate and cover plate) was wetted with 2.5 mL 0.1 M sodium chloride solution by piezo-electrical spraying (yellow nozzle, level 6; Derivatizer, CAMAG) to start the enzyme reaction and incubated in another humid plastic box lined with wet filter paper and filled with 70 mL water (Fig. S1B; 26.5 cm × 16 cm × 10 cm, ABM, Wolframs-Eschenbach, Germany) at 37 °C for 60 min for Panc, whereas it was only 2 min for HSA. After drying (120 °C, 10 min; TLC Plate Heater III, CAMAG), which also terminates the enzyme reaction, the plate was developed in the twin trough chamber up

to 70 mm either with 8 mL acetonitrile/water/2-propanol/acetone 12:3:4:1 (*V/V/V/V*; after 5-min chamber saturation) or acetonitrile/water/2-propanol 3:1:1 (*V/V/V*; no chamber saturation). The plate was piezoelectrically sprayed with the *p*-aminobenzoic acid reagent (2 g *p*-aminobenzoic acid in 252 mL glacial acetic acid/water/acetone/*o*-phosphoric acid 1:1:3:0.04, *V/V/V/V*) for post-chromatographic derivatization (4 mL, yellow nozzle, level 6) and heated (140 °C, 5 min). The chromatograms were documented at 366 nm (TLC Visualizer 2, CAMAG) and the fluorescence was measured densitometrically at 366/>400 nm (slit 4.0 mm × 0.2 mm, mercury lamp, TLC Scanner 4, CAMAG). Instrument operation and data evaluation were performed using visionCATS software (version 3.1, CAMAG).

2.5. Validation parameters

The intestinal phase was selected for simulated static on-surface amylolysis due to the longer incubation time and higher Panc enzyme mixture complexity if compared to the oral phase. According to the International Council for Harmonisation of Technical Requirements for Pharmaceuticals for Human Use Q2(R1) guideline (ICH, 1995/2005), method validation was performed with regard to limits of detection and quantification (LOD/LOQ), working range (analytical response, regression analysis), interday and intraday precision, and recovery rate.

For determination of the LOD/LOQ and working range, a saccharide mixture was applied at 16 different standard levels, ranging from 5 to 800 ng/band for Glc, 10–2660 ng/band for Mal, and 47–2635 ng/band for Mal3. Although no enzyme was applied, the plate was also wetted and incubated to simulate its influence on the signal response. The signal-to-noise ratio (S/N) was calculated to determine the limit of detection (LOD, S/N ≥ 3) and the limit of quantification (LOQ, S/N ≥ 10). The noise signal was obtained by integrating a baseline area of the same size as the analyte signal on each track. The peak height signal and polynomial (quadratic) calibration curves were used to select the working range for each saccharide analysis.

Interday and intraday precisions were evaluated on three different days. Therefore, hydrothermally treated wheat 405 and soluble starch samples were applied fivefold, digested on-surface, and analysed using a calibration ranging from 40 to 300 ng for Glc, 238–1900 ng for Mal, and 471–2352 ng for Mal3. Outliers were determined via the interquartile range method with a cut-off at ± 1.5. The precision of each released saccharide was calculated as percentage relative standard deviation (% RSD).

Recovery was studied at 50%, 100%, and 150% Glc as well as 20%, 40%, and 60% Mal. Therefore, soluble starch samples were spiked with 36, 72, and 108 ng Glc as well as 98, 196, and 391 ng Mal. The wheat 405 samples were spiked with 79, 158, and 237 ng Glc as well as 179, 359, and 717 ng Mal. Spiked and unspiked soluble starch and hydrothermally treated wheat 405 samples were applied in triplicate, digested on-surface, and analysed. Calibration ranged from 25 to 500 ng/band for Glc and 285–2375 ng/band for Mal. The recovery rate (%) was calculated by dividing the mean of the spiked sample by the mean of the unspiked samples plus the added saccharide amount and multiplying by 100.

3. Results and discussion

The recently introduced all-in-one nanoGIT$^{+active}$ system showed a novel enzymatic or metabolic on-surface reaction with subsequent separation and analysis of the formed products on the same surface (Morlock et al., 2021). However, the suitability for quantitative analysis still needed to be clarified. As an example, the digestion of starch and flour by α-amylase, contained in the oral and intestinal phases, was selected. Flour presented a particular challenge in terms of its poor solubility and handling as a suspension.

3.1. Hydrothermal treatment of flour as sample preparation

The ten different commercial flour samples (Table S1) contained high amounts of free saccharides due to an intrinsic amylolysis (Fig. S3A). These native interferences must be removed before the study of their digestibility. Considering the high water solubility of saccharides, a simple washing procedure was performed. Flours were washed twice with bi-distilled water, each followed by centrifugation. Unexpectedly, this procedure was not sufficient to remove all native saccharides. A not negligible amount of saccharides was still present in the samples (Fig. S3B). Liu and Rochfort (2015) reported a cooking step as extraction for trisaccharides, causing the gelatinization of starch and thereby their release. Combining the cooking step and washing procedure, all saccharides were removed (Fig. S3C). Cooking for 15 min was sufficient (Fig. S4). The gelatinization process broke up the strongly ordered polymeric structure of starch, thus releasing the trapped saccharides. Additionally, the heat during the cooking inactivated the native α-amylases which also helps to stop the intrinsic amylolysis of flour samples. Gelatinization also better represents reality, since flour is usually not used as a raw product, but is hydrothermally processed, as in the case of bread, pastries, or biscuits. The gelatinized starch was expected to have higher accessibility for added α-amylase (Tahir et al., 2011; Slaughter et al., 2001). Thus, the usage of gelatinized starch in these digestive experiments is more reasonable than examining raw flour. Stability tests showed that the hydrothermally treated flour samples were not stable when stored in an aqueous environment (Fig. S5). Thus, the flour samples had to be freshly prepared daily.

3.2. Adjustments for a quantitative method

Various factors of influence (Fig. 1) afforded standardization as far as possible. Different method conditions were investigated to ensure a reproducible and quantitative enzyme reaction on the surface. Our previous mobile phase system consisting of ethyl acetate/2-propanol/water 3:3:1 (Morlock et al., 2021) was optimized to be acetonitrile/2-propanol/water/acetone 12:3:4:1 (*V/V/V/V*). It led to a better zone resolution between Lac (extender compound in Panc), Mal, and Mal3. A removal of the extender Lac from the Panc via a centrifugation filtration (3 kDa molecular weight cut-off, which was the smallest filter available) caused a loss of activity (Fig. S6). However, since the used acetone was very volatile, which impaired good reproducibility of the separation, it was omitted later, and the mixture was finally adjusted to acetonitrile/2-propanol/water 3:1:1 (*V/V/V*).

To equalize the activity of the plate due to the daily variation in relative humidity of the surrounding air. The plate was placed horizontally in a plastic box filled with saturated sodium carbonate solution (Fig. S1A) and pre-conditioned for 30 min prior to the wetting treatment. This pre-treatment of the plate prevented or mitigated the drying of the wet plate during incubation. In particular, the enzyme activity strongly depended on the humid atmosphere prevailing during incubation. Therefore, plate wetting had to be standardized. The wetting treatment for the enzymatic reaction (at the application zone) should not affect the subsequent separation and good zone resolution. When all needed solutions were piezoelectrically sprayed onto the whole plate, the zone resolution was worse (Fig. S7). Hence, only the lower plate part, where the enzymatic reaction took place, was wetted with 0.1 M sodium chloride solution. However, to prevent rapid drying out of this small wetted part of the plate, the remaining upper part of the plate was covered by a second smaller plate, which was truncated according to the width of the reaction area (Fig. S2). This uncovered part width should only show the application zone, whereas the saccharide at the lowest hR_F in the later separation should already be covered by the second plate. Both plates were packed together during the wetting treatment so that both were wetted with the sodium chloride solution (to maintain the humidity during the following incubation). Subsequently, this plate package was incubated in a humid plastic box at 37 °C (Fig. S1B). The

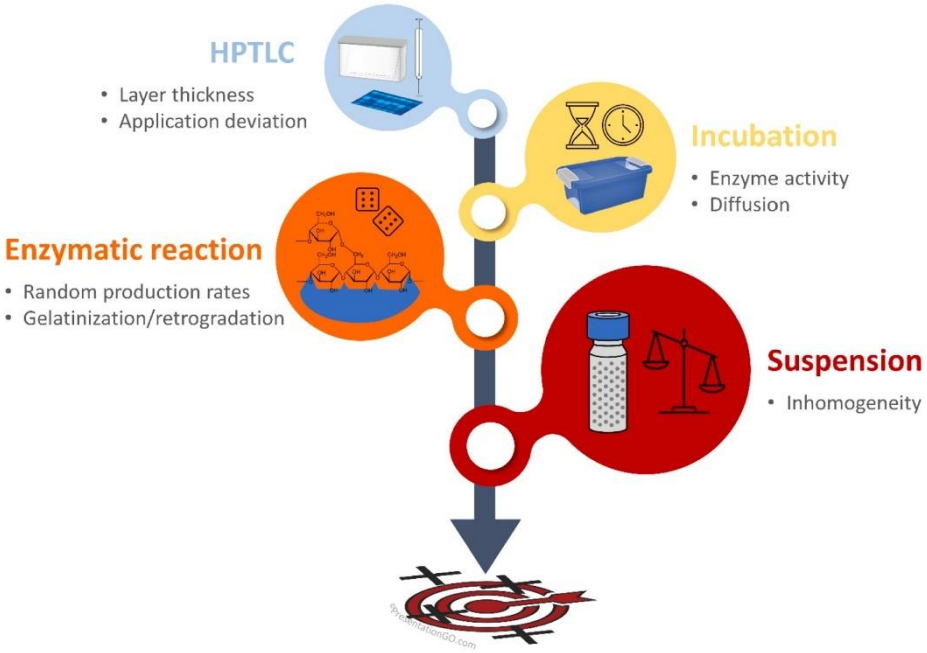

Fig. 1. Factors of influence increasing in importance on the performance of the HPTLC–nanoGIT–FLD method for salivary or pancreatic amylolysis.

enzyme reaction area should still be visibly wet after the incubation (Fig. S8). Furthermore, the right balance between not too much (restricted by the maximal water adsorption capacity of the plate) and sufficient wetting for optimal and reproducible enzyme activity had to be found. Too much adsorbed water resulted in a massive loss of sensitivity due to zone diffusion, whereas not enough adsorbed water led to drying out of the reaction zones and thus fluctuations. This balance was also dependent on the plate size and layer thickness. Smaller and thinner plates were prone to dry out faster. A wetting volume of 2.5–3.0 mL was considered satisfactory (Fig. S8).

Once it was demonstrated that the on-surface reaction of the enzyme was reproducible, the metabolic reaction itself was adjusted. The optimal enzyme to substrate (E/S) ratio was determined regarding two different substrates, *i.e.* soluble starch and hydrothermally treated wheat 405. It is recommended to choose as low enzyme amounts as possible and an excess of the substrate. Panc was lowered from 20 to 10 TAME mU and HSA from 750 to 75 mU. The amount of substrate was 20 μg for hydrothermally treated wheat 405, whereas it was decreased from 5 to 2 μg for soluble starch (which was still an excess). By this, the E/S ratio was reduced for soluble starch (from 4:1 to 5:1 for Panc and from 150:1 to 38:1 for HSA). Since the flour samples were suspensions and a syringe-dosed application of several samples may lead to increased sedimentation for the last samples to be applied, this influence was studied in more detail. To ensure the same filling level in every sample vial, ten individual hydrothermally treated wheat 405 sample suspensions were applied, on-surface digested, and analysed. The evaluation of the obtained saccharide amounts of all samples showed a downward trend from the first to the last sample applied (Fig. S9). Nevertheless, the obtained precisions (%RSD of 14–18) of successive application of up to ten suspension samples were found to be acceptable, given for the handling of inhomogeneous flour suspensions. To avoid a downward trend in the future, the sample (substrate) could be applied gradually by shaking the sample vials in between.

3.3. Validation of the HPTLC–nanoGIT–FLD method

The workflow optimized for quantification (Fig. 2) was validated according to ICH guidelines (ICH, 1995/2005). The simulated intestinal phase, which was more complex than the oral phase, was selected as an example. The increased zone diffusion during the longer incubation (60 min *versus* 2 min) and the more complex enzyme mixture (Panc *versus* HSA) of the selected intestinal phase example made the validation more challenging.

3.3.1. LOD/LOQ and working ranges

The saccharide standards were applied at different amounts and the whole workflow (pre-conditioning, wetting, on-surface incubation, and separation) was performed to simulate all influences. The high relative humidity of the pre-conditioning and wetting processes resulted in increased zone diffusion with increasing incubation time (60 min). In contrast, such zone diffusion did not occur during the short oral phase incubation (2 min). LODs ($S/N \geq 3$) were determined to be 5 ng/band (S/N 7) for Glc, 38 ng/band (S/N 4) for Mal, and 47 ng/band (S/N 4) for Mal3 (Fig. S10). The LOD of Glc (S/N 7) is actually lower, but no lower standard level was studied experimentally. Morlock et al. (2014) showed a LOD of 1 ng for lactose, which showed similar sensitivity as Glc. LOQs ($S/N \geq 10$) for Glc, Mal, and Mal3 were determined as 10, 48, and 188 ng/band, respectively (Fig. S10). In particular, the LOD/LOQ for Glc is exceptionally low, highlighting the great potential of HPTLC in carbohydrate analysis due to the high sensitivity of the used derivatization reagent, *i.e.* the *p*-aminobenzoic acid reagent. Glc and Mal, the most stable products of amylolysis, were more sensitively detected at low amounts. The lower the number of monomeric units in the molecule, the better the detectability. As a reagent sequence, the subsequent derivatization with either the diphenylamine aniline *o*-phosphoric acid reagent or β-naphthol reagent, which are more sensitive for long-chain carbohydrates, can be applied to improve the detection of Mal3, if needed.

Wide working ranges via quadratic regression functions for all three

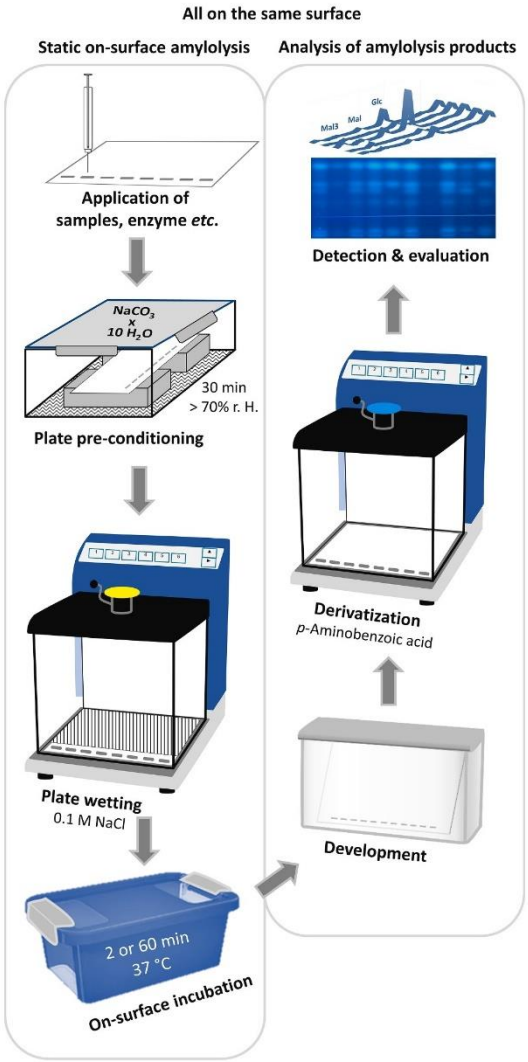

Fig. 2. Workflow scheme of the validated HPTLC–nanoGIT–FLD method for salivary or pancreatic on-surface amylolysis.

saccharides highlighted the good suitability of the method. The working range for Glc ranged from 5 to 800 ng/band with a %RSD of 4.4 and a correlation coefficient (R) of 0.9989. For Mal, the lower range for LOD/LOQ evaluation was 10–950 ng/band (%RSD of 2.6, R of 0.9991), whereas the working range was 285–2375 ng/band (%RSD of 4.7, R of 0.9962). For Mal3, the lower range for LOD/LOQ evaluation was 47–565 ng/band (%RSD of 7.9, R of 0.9898), whereas the working range was 471–2635 ng/band (%RSD of 2.2, R of 0.9980).

3.3.2. Interday and intraday precisions

Hydrothermally treated wheat 405 and soluble starch samples were applied fivefold, digested (amylolysis via Panc), and analysed on three different days (Fig. S11). Both interday and intraday precisions showed better results for the soluble starch than flour samples (Table 1), explained by the homogenous starch solution in contrast to the comparatively more inhomogeneous flour suspension. For soluble starch, all intraday precisions were $\leq$ 16%, except one measurement for Mal3 (22%). Using the interquartile range method, one outlier was revealed in each third set of Mal and Mal3 (Table S2). The amount of Glc was also increased for this track but was still within the range of uncertainty. This was explained by application errors or the metabolic reaction itself as only one track was affected in this measurement set. The outlier-corrected interday precisions for soluble starch for all saccharides were $\leq$ 10%. Comparing interday with intraday precisions for soluble starch, all measurement sets showed good precision and acceptable repeatability for all saccharides.

As a challenging worst-case scenario due to poor solubility, hydrothermally treated wheat 405 suspensions were studied next. Eliminating all outliers (Table S3), intraday and interday precisions were improved to $\leq$ 24% and $\leq$ 25%, respectively, which was higher but acceptable considering the complex method including the digestion and analysis. Although the flour suspension was finely distributed and the application settings were selected to ensure proper representative sample application, it was difficult to control the actual amount of suspension applied on the plate (small amount taken out of the suspension). This was underlined by the number of outliers. For Glc and Mal, the third measurement set showed three out of five data points are outliers (Table S3), whereas all values were within the range of uncertainty for Mal3. The highest %RSD of 25 for the interday precision of Mal3 can also be explained by the signal responses close to the upper limit of the working range. The application of a lower concentrated suspension could improve the precision in the future.

3.3.3. Recovery

The recovery was investigated via the analysis of a spiked and unspiked sample each. Initial experiments showed that Mal3 had the ability to be further converted by α-amylase, and thus was not considered. Both, soluble starch and hydrothermally wheat 405 were spiked with defined amounts of the stable products Glc and Mal. Since the working range of Glc was rather wide, the spiking levels were set to +50%, +100%, and +150%. Due to the high amount of Mal in wheat 405, the spiking levels were set to +20%, +40%, and +60% to not exceed the upper limit of the working range. All levels were analysed as triplicates. For soluble starch, the calculated mean recoveries (n = 3) across all levels ranged between 111 and 112% for Glc and 106–115% for Mal (Table S4). For wheat 405, the mean recoveries across all levels ranged between 80 and 98% for Glc and 62–94% for Mal. A trend was observed where the lowest spike level showed better recovery results than the highest spike level (Table S4) which was explained by their signal responses close to the upper limit of the working range. The application of a lower concentrated suspension and respective lower spike levels could improve the precision in the future. Overall, the accuracy of the method was found acceptable.

3.3.4. Future adjustments

The accurate dosing of the substrate (inhomogeneous flour suspension) was difficult. In the future, the process of flour preparation could be optimized by grinding the flour finer to create a more homogeneous and finer suspension which tends to float longer and sediment slower. However, finer starchy powders tend to agglomerate more during gelatinization, and the optimal compromise has to be studied for better dosing of suspensions. For Mal, the use of lower concentrated suspensions and lower spike levels could improve precision and recovery, as mentioned. A future reduction of the 60-min incubation time (Morlock et al., 2021) would help reduce start zone diffusion but must first be evaluated for compatibility with the standardized protocol. Since the hydrothermal treatment of the flour suspensions initiated a continuous process, analysis refers always to a certain time point only. To better understand such continuous processes the effect of retrogradation of a suspension over time should be investigated.

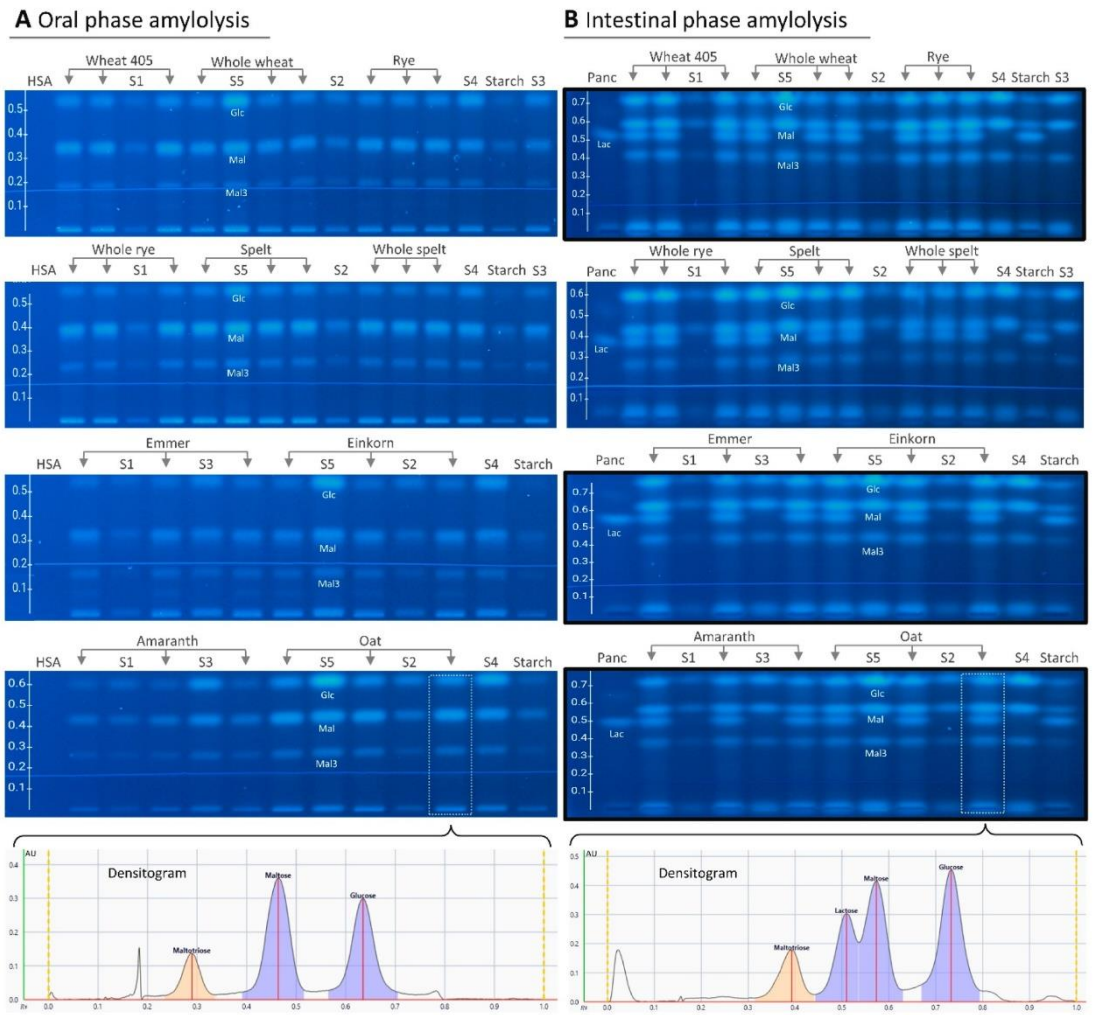

Fig. 3. Application of the validated method to flour samples: HPTLC–nanoGIT–FLD chromatograms and exemplarily densitograms of the saccharide release from ten different hydrothermally treated flour suspensions (10 mg/mL) after on-surface digestion via (**A**) human salivary α-amylase (HSA,75 mU/band) and (**B**) pancreatin (Panc, 10 TAME mU/band) along with calibration standards S1–S5 (471–2832 ng for Mal3, 475–2660 ng for Mal, and 40–400 ng for Glc) on HPTLC plates silica gel 60 developed up to 70 mm either with acetonitrile/water/2–propanol/acetone 12:3:4:1 (*V/V/V/V*) or acetonitrile/water/2–propanol 3:1:1 (*V/V/V*; framed) and detected at FLD 366 nm after derivatization with the *p*-aminobenzoic acid reagent.

3.4. Oral and intestinal amylolysis of ten flour samples and analysis of their products

The validated method was applied to ten hydrothermally treated flours to study their differences in the saccharide release during amylolysis. Flours were especially challenging concerning their varying molecular composition and solubility. Ten different flours were selected being either botanically different or differently processed, *i.e.* refined and whole flour from wheat, spelt, and rye as well as flour from einkorn, amaranth, emmer, and oat. All flours were hydrothermally treated and digested on-surface via human salivary α-amylase or pancreatin as specified. The methodology opens a new field in analysing the specific products released during amylolysis. Comparison with sum value analysis methods was challenging and was done as best as possible since most literature reported a decrease only in the total starch content (no saccharide differentiation) or information about the digestion rate (content of rapid and slow digestible starch).

3.4.1. Oral (salivary) amylolysis

Each flour sample was digested and analysed in triplicate (Table S5 and Fig. 3A). The mean amounts of the three saccharides released (Table 2) showed a common trend, *i.e.* amaranth, emmer, and einkorn showed the lowest overall saccharide release, whereas spelt had the highest. These results were in agreement with the literature including also *in vivo* data (Capriles, Coelho, Guerra-Matias, & Arêas, 2008; Mohan & Malleshi, 2006; Dhanavath & Prasada Rao, 2017; Nakov, Brandolini, Ivanova, Dimov, & Stamatovska, 2018; Barone et al., 2018; Bakhøj, Flint, Holst, & Tetens, 2003; Skrabanja et al., 2001; Leinonen,

Table 1
Validation data: calculated mean amounts with intraday and interday precisions of released saccharides from soluble starch and hydrothermally treated wheat 405 after pancreatic amylolysis.

	Soluble starch			Wheat 405		
Saccharide	Intraday %RSD (n = 4–5)	Interday %RSD (n = 14–15)	Mean amount [ng/band] ± standard deviation [ng/band] (n = 14–15)	Intraday %RSD (n = 2–5)	Interday %RSD (n = 12–15)	Mean amount [ng/band] ± standard deviation [ng/band] (n = 12–15)
Glucose	7	10	81 ± 8	15	21*	152 ± 30*
	14			9		
	9			20*		
Maltose	7	10*	636 ± 63*	17	16*	1086 ± 171*
	12			7		
	16*			24*		
Maltotriose	10	10*	650 ± 66*	20	25	1555 ± 385
	10			7		
	22*			22		

*Outlier-corrected values using the interquartile range method with a cut-off of ±1.5 (full datasets in Tables S2 and S3).
%RSD = percentage relative standard deviation.

Table 2
Comparison of the mean saccharide release (n = 3) ascending in amount after salivary amylolysis for ten hydrothermally treated flours (full dataset in Table S5).

Type of flour	Amount Glc[ng/band]	Type of flour	Amount Mal[ng/band]	Type of flour	Amount Mal3[ng/band]
Amaranth	26	Amaranth	711	Amaranth	668
Emmer	71	Emmer	1571	Emmer	1743
Einkorn	73	Einkorn	1801	Whole spelt	1813
Whole wheat	132	Whole wheat	2009	Einkorn	1835
Oat	140	Whole spelt	2027	Whole rye	1836
Rye	144	Whole rye	2118	Whole wheat	1852
Wheat 405	163	Wheat 405	2221	Spelt	2041
Whole spelt	164	Rye	2290	Rye	2156
Whole rye	168	Spelt	2451	Oat	2230
Spelt	217	Oat	2532	Wheat 405	2581

Glc = Glucose, Mal = Maltose, Mal3 = Maltotriose.

Liukkonen, Poutanen, Uusitupa, & Mykkänen, 1999; Pentikäinen et al., 2014), whereby most literature compared wheat with other cereals. The matching of the evaluated data in this study with *in vitro* and *in vivo* (only for einkorn) data highlighted the reliability of the results, despite using a totally different approach to investigate the amylolysis. The cited *in vivo* data (Bakhøj et al., 2003; Barone et al., 2018) dealt with the glycaemic and insulinemic response and their conclusions could be confirmed in our study with the approach of investigating the saccharide release. So not only the comparison of *in vitro* hydrolysis rates or the decrease of total starch content but also physiological data are comparable with our study. The Glc and Mal amount released from wheat 405 were in the upper-middle range of all evaluated cereals, whereas the Mal3 amount was the highest. Comparing the other refined flours with wheat 405, only spelt showed a consistently higher saccharide release, while oat and rye gave varying results, especially for Glc. Thus, they are not suitable as an alternative for a low GI value diet. Emmer, einkorn, and especially amaranth showed significantly low saccharide amounts, comparatively suitable for an adjusted diet for diabetics and obese people. The evaluated amounts for amaranth are surprisingly low. It was observed that only the centrifuged amaranth sample showed a slight mist on top of the flour sediment, which was removed together with the supernatant containing the native saccharides. This mist was considered soluble dietary fibre and was increased in amaranth compared to wheat (Lamothe, Srichuwong, Reuhs, & Hamaker, 2015). However, no mist was observed for oat which soluble dietary fibres are also reported to be increased (Manthey, Hareland, & Huseby, 1999). Other evaluated flours differed a lot, thus no trend was evident. The variation of the released saccharides was explained by the hydrolysis of starch as a random enzymatic reaction. The very short incubation time of only 2 min could be a major factor of influence, even though the saccharide amounts in the middle amount range did not differ significantly from each other. Most of the studies reported much longer hydrolysis periods, and to the best of our knowledge, no literature was available for the short hydrolysis time of salivary amylolysis. The hypothesis that whole grains are slower or just partially digested than refined flour (Slavin et al., 2001; Hallfrisch et al., 2000) could be confirmed by our observations made. However, an exception was rye, for which the whole grain flour showed higher saccharide amounts than the refined one, excluding Mal.

3.4.2. Intestinal (pancreatic) amylolysis

For comparison, the ten hydrothermally treated flours were also analysed in triplicate for pancreatic amylolysis (Table S6 and Fig. 3B). The released mean saccharide amounts (Table 3) differed from the results of salivary amylolysis. Remarkable is the increase of Glc, which was explained by the significantly longer incubation time (60 min instead of 2 min), resulting in longer digestion of starch and thus higher Glc release. This observation corresponds to the common understanding about the digestive process, where the salivary α-amylase briefly predigests the consumed carbohydrates into smaller units, consequentially resulting in low amounts of the smallest unit, *i.e.* Glc. It also highlights the importance of following standardized protocols when

Table 3
Comparison of the mean saccharide release (n = 3) ascending in amount after pancreatic amylolysis for ten hydrothermally treated flours (full dataset in Table S6).

Type of flour	Amount Glc [ng/band]	Type of flour	Amount Mal [ng/band]	Type of flour	Amount Mal3 [ng/band]
Whole wheat	115	Amaranth	1313	Whole wheat	1441
Amaranth	128	Whole wheat	1420	Amaranth	1597
Wheat 405	163	Whole spelt	1599	Whole spelt	1805
Whole spelt	173	Wheat 405	1728	Wheat 405	2031
Rye	174	Oat	1985	Oat	2039
Oat	178	Emmer	2134	Emmer	2305
Emmer	191	Rye	2155	Einkorn	2476
Einkorn	219	Einkorn	2297	Spelt	2547
Spelt	297	Whole rye	2299	Whole rye	2585
Whole rye	306	Spelt	2303	Rye	≫

Glc = Glucose, Mal = Maltose, Mal3 = Maltotriose.

studying a time-dependent enzyme-substrate reaction. Nevertheless, salivary and pancreatic α-amylase are two different enzymes coded by different genes, but less is known about their difference in activity because salivary α-amylase is often neglected in digestion studies. The developed methodology could be the first step to investigate enzymatic interactions in a simple and cost-effective way to gather more information. The amount of Mal3 for refined rye was too high and thus out of the calibration range. Wheat 405, in contrast to all other refined flours and to the results of salivary amylolysis, released rather low saccharide amounts. If the digestion of common wheat products, especially those out of whole grain wheat flour, had the lowest saccharide release in pancreatic amylolysis, there is no nutritional reason to discredit them as unhealthy. But the saccharide release itself is not the only parameter for a nutritional recommendation. Additionally, emmer and einkorn showed higher amounts of saccharides, much higher than for oat, which is not in agreement with the literature (Mohan & Malleshi, 2006; Dhanavath & Prasada Rao, 2017; Nakov et al., 2018; Barone et al., 2018; Bakhøj et al., 2003; Kim & White, 2012; Kaur, Gill, & Karwasra, 2018). However, Kulathunga (2020) evaluated a higher hydrolysis index for emmer > einkorn > spelt compared to hard red spring wheat, which supports our results. The prolonged hydrolysis period of 60 min made a significant difference in the saccharide release for those ancient grains. They were more accessible for amylolysis with higher incubation times, maybe due to their different starch granule structure.

3.4.3. *Amylolyses in comparison*

In general, less saccharide release was reported for whole grain flours (Slavin et al., 2001; Hallfrisch et al., 2000), which supported our results. Both amylolyses highlight the possible benefit of whole grain products for almost all flours due to their lower saccharide release, with special attention to rye with predominantly contrary observations. The evaluated saccharide amounts of both amylolyses for whole rye were mainly higher and with a higher variation (%RSD = 6–16) than those of rye (% RSD = 2–5). Whole rye had the second highest precisions of all analysed flours beside amaranth (only during salivary amylolysis). Investigating the specific data sets for whole rye and amaranth (Tables S5 and S6) an ascending trend could be observed (application of starch particles increased during the suspension application), however, was judged as arbitrarily. Nevertheless, the determined saccharide values for whole rye should be considered with reservation. In general, an explanation for a lower saccharide release of whole grains is the starch weighing since coarse components of the whole grain flour contribute to the total weight. Consequently, a lower amount of starch is weighed in compared to refined flour. Amaranth released the lowest whereas spelt the highest amount of saccharides for both amylolyses. Based on pancreatic amylolysis, amaranth, whole wheat, wheat 405, and whole spelt could be nutrition recommendations for a low GI value diet, whereas the saccharide amounts for wheat 405 were significantly higher for salivary amylolysis. Considering both amylolyses, amaranth is leading among the studied flours, followed by whole wheat and whole spelt as nutrition recommendations for a low GI value diet. In contrast, spelt, rye, and whole rye are not recommended since, despite the quite different incubation times, both amylolyses nearly resulted in a similar saccharide release. This can be explained by a rapid enzyme-substrate reaction, which is nevertheless time-dependent. The partially decreasing activity of salivary amylase due to the pH rise on its way from the oral cavity to the stomach (Freitas, Le Feunteun, Panouillé, & Souchon, 2018) as a dynamic process is also an important factor of influence on digestion, which complexity could not be simulated in this more simple static on-surface digestion study. The enzyme activity of both amylolyses could not be matched since the exact α-amylase activity in Panc was not available. For a better understanding, the enzyme activity and hydrolysis process over time could be studied via this validated HPTLC–nanoGIT–FLD method.

In literature, only a few studies compared different types of cereals with each other, mostly wheat as a reference grain compared to several other grains. The available information about amaranth, einkorn, and emmer has been very poor. Cooked amaranth (Capriles et al., 2008), isolated starch from emmer (Mohan & Malleshi, 2006; Dhanavath & Prasada Rao, 2017), rye bread (Leinonen et al., 1999; Pentikäinen et al., 2014) and einkorn products (Nakov et al., 2018; Barone et al., 2018; Bakhøj et al., 2003) as well as cooked oat flours (Kim & White, 2012) showed a slower or equal digestion rate than wheat flours, starches or products. Refined spelt wheat flour products (Skrabanja et al., 2001) and cooked isolated oat starch (Kim & White, 2012; Kaur et al., 2018) showed a significantly higher digestibility than wheat bread. In comparison with the HPTLC–nanoGIT–FLD results, a lower saccharide release for amaranth and a higher for spelt were confirmed.

4. Conclusions

The HPTLC–nanoGIT–FLD methodology had the great advantage of performing all relevant steps (such as digestion and analysis of the degradation products) on the same surface. Hence, no analytes were lost during the biotechnological–analytical workflow. It is cost-effective (0.4 €/sample; calculated for 19 samples per plate) and time-effective with about 15 min/sample for the intestinal phase and 12 min/sample for the oral phase. The developed quantitative HPTLC–nanoGIT–FLD method was successfully validated for salivary and pancreatic amylolysis for the first time. Considering the complexity of the enzymatic and chromatographic all-in-one system, the sensitivity, accuracy, and precision values for the saccharides Glc, Mal, and Mal3 released from soluble starch and hydrothermally treated flour were acceptable. The application of the validated HPTLC–nanoGIT–FLD method to ten hydrothermally treated flours revealed important differences but also similarities in salivary and pancreatic amylolysis. Evaluating the saccharide release, a good estimation for nutrition recommendations for especially diabetics and obese people can be made but further investigations are needed. In the future, the temporal enzymatic saccharide release can be studied with the developed quantitative HPTLC–nanoGIT–FLD method.

CRediT authorship contribution statement

Isabel Müller: Conceptualization, Methodology, Data curation, Validation, Writing – original draft. **Gertrud E. Morlock:** Conceptualization, Methodology, Supervision, Writing – review & editing.

Declaration of Competing Interest

The authors declare that they have no known competing financial interests or personal relationships that could have appeared to influence the work reported in this paper.

Data availability

Data will be made available on request.

Acknowledgements

Thank is owed to Jessica Richardson for the performance of the initial experiments. Instrumentation was partially funded by the Deutsche Forschungsgemeinschaft (DFG, German Research Foundation) - INST 162/536-1 FUGG.

Appendix A. Supplementary data

Supplementary data to this article can be found online at https://doi.org/10.1016/j.foodchem.2023.137145.

References

Ahluwalia, N., Herrick, K. A., Terry, A. L., & Hughes, J. P. (2019). *Contribution of whole grains to total grains intake among adults aged 20 and over: United States, 2013–2016*. Hyattsville, MD.

Astrup, A., & Finer, N. (2000). Redefining type 2 diabetes: 'diabesity' or 'obesity dependent diabetes mellitus'? *Obesity Reviews, 1*, 57–59.

Aune, D., Keum, N., Giovannucci, E., Fadnes, L. T., Boffetta, P., Greenwood, D. C., … Norat, T. (2016). Whole grain consumption and risk of cardiovascular disease, cancer, and all cause and cause specific mortality: Systematic review and dose-response meta-analysis of prospective studies. *BMJ, 353*, Article i2716.

Bakhøj, S., Flint, A., Holst, J. J., & Tetens, I. (2003). Lower glucose-dependent insulinotropic polypeptide (GIP) response but similar glucagon-like peptide 1 (GLP-1), glycaemic, and insulinaemic response to ancient wheat compared to modern wheat depends on processing. *European Journal of Clinical Nutrition, 57*, 1254–1261.

Barone, F., Laghi, L., Gianotti, A., Ventrella, D., Saa, D. L. T., Bordoni, A., Forni, M., Brigidi, P., Bacci, M. L., & Turroni, S. (2018). In Vivo Effects of Einkorn Wheat (Triticum monococcum) Bread on the Intestinal Microbiota, Metabolome, and on the Glycemic and Insulinemic Response in the Pig Model. *Nutrients, 11*.

Bird, A. R., Lopez-Rubio, A., Shrestha, A. K., & Gidley, M. J. (2009). Resistant Starch in Vitro and in Vivo. In S. Kasapis (Ed.), *Modern biopolymer science: Bridging the divide between fundamental treatise and industrial application* (pp. 449–510). Amsterdam: Elsevier/AP.

Capriles, V. D., Coelho, K. D., Guerra-Matias, A. C., & Arêas, J. A. G. (2008). Effects of processing methods on amaranth starch digestibility and predicted glycemic index. *Journal of Food Science, 73*, H160–H164.

Chung, H.-J., Lim, H. S., & Lim, S.-T. (2006). Effect of partial gelatinization and retrogradation on the enzymatic digestion of waxy rice starch. *Journal of Cereal Science, 43*, 353–359.

Dhanavath, S., & Prasada Rao, U. J. S. (2017). Nutritional and Nutraceutical Properties of Triticum dicoccum Wheat and Its Health Benefits: An Overview. *Journal of Food Science, 82*, 2243–2250.

Dhital, S., Warren, F. J., Butterworth, P. J., Ellis, P. R., & Gidley, M. J. (2017). Mechanisms of starch digestion by α -amylase—Structural basis for kinetic properties. *Critical Reviews in Food Science and Nutrition, 57*, 875–892.

Edwards, C. H., Veerabahu, A. S., Mason, A. J., Butterworth, P. J., & Ellis, P. R. (2021). α-Amylase action on starch in chickpea flour following hydrothermal processing and different drying, cooling and storage conditions. *Carbohydrate Polymers, 259*, Article 117738.

Freitas, D., Le Feunteun, S., Panouillé, M., & Souchon, I. (2018). The important role of salivary α-amylase in the gastric digestion of wheat bread starch. *Food & Function, 9*, 200–208.

Hallfrisch, J., Facn, & Behall, K. M. (2000). Mechanisms of the effects of grains on insulin and glucose responses. *Journal of the American College of Nutrition, 19*, 320S-325S.

Han, T. S., Richmond, P., Avenell, A., & Lean, M. E. (1997). Waist circumference reduction and cardiovascular benefits during weight loss in women. *International Journal of Obesity, 21*, 127–134.

ICH. (1995/2005). *Q 2(R1): Validation of Analytical Procedures: Text and Methodology*. International Council for Harmonisation.

Jenkins, D. J. A., Kendall, C. W. C., Augustin, L. S. A., Franceschi, S., Hamidi, M., Marchie, A., … Axelsen, M. (2002). Glycemic index: Overview of implications in health and disease. *American Journal of Clinical Nutrition, 76*, 266S–S273.

Kaur, H., Gill, B. S., & Karwasra, B. L. (2018). In vitro digestibility, pasting, and structural properties of starches from different cereals. *International Journal of Food Properties, 21*, 70–85.

Kelly, S. am, Hartley, L., Loveman, E., Colquitt, J. L., Jones, H. M., Al-Khudairy, L., Clar, C., Germanò, R., Lunn, H. R., Frost, G., & Rees, K. (2017). Whole grain cereals for the primary or secondary prevention of cardiovascular disease. *The Cochrane Database of Systematic Reviews, 8*, CD005051.

Kim, H. J., & White, P. J. (2012). In vitro digestion rate and estimated glycemic index of oat flours from typical and high β-glucan oat lines. *Journal of Agricultural and Food Chemistry, 60*, 5237–5242.

Kulathunga, J. (2020). Comparative Study on Hulled Wheats: Kernel, Flour, Dough Quality and Dietary Fiber Variation. Fargo, ND, USA.

Lamothe, L. M., Srichuwong, S., Reuhs, B. L., & Hamaker, B. R. (2015). Quinoa (Chenopodium quinoa W.) and amaranth (Amaranthus caudatus L.) provide dietary fibres high in pectic substances and xyloglucans. *Food Chemistry, 167*, 490–496.

Leinonen, K., Liukkonen, K., Poutanen, K., Uusitupa, M., & Mykkänen, H. (1999). Rye bread decreases postprandial insulin response but does not alter glucose response in healthy Finnish subjects. *European Journal of Clinical Nutrition, 53*, 262–267.

Liu, Z., & Rochfort, S. (2015). Identification and quantitative analysis of oligosaccharides in wheat flour using LC–MS. *Journal of Cereal Science, 63*, 128–133.

Manthey, F. A., Hareland, G. A., & Huseby, D. J. (1999). Soluble and Insoluble Dietary Fiber Content and Composition in Oat. *Cereal Chemistry Journal, 76*, 417–420.

Minekus, M., Alminger, M., Alvito, P., Ballance, S., Bohn, T., Bourlieu, C., … Brodkorb, A. (2014). A standardised static in vitro digestion method suitable for food - an international consensus. *Food & Function, 5*, 1113–1124.

Mohan, B. H., & Malleshi, N. G. (2006). Characteristics of native and enzymatically hydrolyzed common wheat (Triticum aestivum) and dicoccum wheat (Triticum dicoccum) starches. *European Food Research and Technology, 223*, 355–361.

Morlock, G. E., Drotleff, L., & Brinkmann, S. (2021). Miniaturized all-in-one nanoGIT+ active system for on-surface metabolization, separation and effect imaging. *Analytica Chimica Acta, 1154*, Article 338307.

Morlock, G. E., Morlock, L. P., & Lemo, C. (2014). Streamlined analysis of lactose-free dairy products. *Journal of Chromatography A, 1324*, 215–223.

Nakov, G., Brandolini, A., Ivanova, N., Dimov, I., & Stamatovska, V. (2018). The effect of einkorn (Triticum monococcum L.) whole meal flour addition on physico-chemical characteristics, biological active compounds and in vitro starch digestion of cookies. *Journal of Cereal Science, 83*, 116–122.

Pentikäinen, S., Sozer, N., Närväinen, J., Ylätalo, S., Teppola, P., Jurvelin, J., … Poutanen, K. (2014). Effects of wheat and rye bread structure on mastication process and bolus properties. *Food Research International, 66*, 356–364.

Skrabanja, V., Kovac, B., Golob, T., Liljeberg Elmståhl, H. G., Björck, I. M., & Kreft, I. (2001). Effect of spelt wheat flour and kernel on bread composition and nutritional characteristics. *Journal of Agricultural and Food Chemistry, 49*, 497–500.

Slaughter, S. L., Ellis, P. R., & Butterworth, P. J. (2001). An investigation of the action of porcine pancreatic α-amylase on native and gelatinised starches. *Biochimica et Biophysica Acta (BBA) - General Subjects, 1525*, 29–36.

Slavin, J. L., Jacobs, D., Marquart, L. E., & Wiemer, K. (2001). The Role of Whole Grains in Disease Prevention. *Journal of the American Dietetic Association, 101*, 780–785.

Swaminathan, S., Dehghan, M., Raj, J. M., Thomas, T., Rangarajan, S., Jenkins, D., … Yusuf, S. (2021). Associations of cereal grains intake with cardiovascular disease and mortality across 21 countries in Prospective Urban and Rural Epidemiology study: Prospective cohort study. *BMJ, 372*, Article m4948.

Tahir, R., Ellis, P. R., Bogracheva, T. Y., Meares-Taylor, C., & Butterworth, P. J. (2011). Study of the structure and properties of native and hydrothermally processed wild-type, lam and r variant pea starches that affect amylolysis of these starches. *Biomacromolecules, 12*, 123–133.

Vega-López, S., Venn, B. J., & Slavin, J. L. (2018). Relevance of the Glycemic Index and Glycemic Load for Body Weight, Diabetes, and Cardiovascular Disease. *Nutrients, 10*, 1361.

Ye, E. Q., Chacko, S. A., Chou, E. L., Kugizaki, M., & Liu, S. (2012). Greater whole-grain intake is associated with lower risk of type 2 diabetes, cardiovascular disease, and weight gain. *The Journal of Nutrition, 142*, 1304–1313.

Zafar, M. I., Mills, K. E., Zheng, J., Regmi, A., Hu, S. Q., Gou, L., & Chen, L.-L. (2019). Low-glycemic index diets as an intervention for diabetes: A systematic review and meta-analysis. *The American Journal of Clinical Nutrition, 110*, 891–902.

Supplementary Information

Quantitative saccharide release of hydrothermally treated flours by validated salivary/pancreatic on-surface amylolysis (nanoGIT) and high-performance thin-layer chromatography

Isabel Müller, Gertrud E. Morlock[#,*]

Institute of Nutritional Science, Chair of Food Science, and Interdisciplinary Research Centre for Biosystems, Land Use and Nutrition, Justus Liebig University Giessen, Heinrich-Buff-Ring 26−32, 35392 Giessen, Germany

[#]Dedicated to the 85th birthday of Dr. Fred Rabel, ChromHELP, Woodbury, NJ, USA

*Corresponding authors: Prof. Dr. Gertrud Morlock, phone: +49-641-9939141; fax +49-641-99-39149, email: gertrud.morlock@uni-giessen.de

Table of Contents (short titles)

Table S1
List of the studied samples purchased on the market, *i.e.* ten different flours and soluble starch.

Sample	Type	Cultivation (brand)	Supplier or producer
Amaranth	Whole grain	Controlled organic cultivation	Govinda Natur, Neustadt, Germany
Einkorn	Whole grain	Organic, Demeter	Spielberger, Brackenheim, Germany
Emmer	Whole grain	Organic, Demeter	Spielberger, Brackenheim, Germany
Oat		Conventional	The Hut.com (Myprotein), Northwich, England
Rye	Type 997	Conventional	Wieler Hausermühle, Wetzlar, Germany
Rye	Whole grain	Conventional	Wieler Hausermühle, Wetzlar, Germany
Spelt wheat	Type 630	Conventional (Gut und Günstig)	Edeka Zentrale, Hamburg, Germany
Spelt wheat	Whole grain	Organic	Rewe, Aalen, Germany
Wheat	Type 405	Conventional (Belbake, Lidl)	Friesinger Mühle, Bad Wimpfen, Germany
Wheat	Whole grain	Organic (Rewe Bio)	Friesinger Mühle, Bad Wimpfen, Germany
Soluble starch	Potato		Riedel-de Haen, Seelze, Germany

Table S2
Evaluated amounts of the precision measurement of soluble starch.

Saccharide	Measurement	Amount [ng/band]	Outlier	Intraday %RSD	Interday %RSD
Glucose	1_1	86		7	10
	1_2	91			
	1_3	89			
	1_4	85			
	1_5	76			
	2_1	86		14	
	2_2	86			
	2_3	83			
	2_4	73			
	2_5	61			
	3_1	91		9	
	3_2	74			
	3_3	76			
	3_4	78			
	3_5	77			
Maltose	1_1	607		7	10
	1_2	656			
	1_3	635			
	1_4	602			
	1_5	539			
	2_1	757		12	
	2_2	744			
	2_3	695			
	2_4	617			
	2_5	565			
	3_1	853	X	16	
	3_2	670			
	3_3	606			
	3_4	606			
	3_5	596			
Maltotriose	1_1	679		10	10
	1_2	728			
	1_3	708			
	1_4	618			
	1_5	573			
	2_1	764		10	
	2_2	659			
	2_3	599			
	2_4	602			
	2_5	650			
	3_1	933	X	22	
	3_2	708			
	3_3	584			
	3_4	540			
	3_5	687			

Table S3

Evaluated amounts of the precision measurement of wheat 405.

Saccharide	Measurement	Amount [ng/band]	Outlier	Intraday %RSD	Interday %RSD
Glucose	1_1	114		15	21
	1_2	148			
	1_3	130			
	1_4	105			
	1_5	145			
	2_1	180		9	
	2_2	159			
	2_3	142			
	2_4	151			
	2_5	153			
	3_1	201		20	
	3_2	200			
	3_3	293	X		
	3_4	288	X		
	3_5	293	X		
Maltose	1_1	854		17	16
	1_2	1073			
	1_3	917			
	1_4	746			
	1_5	1135			
	2_1	1225		7	
	2_2	1142			
	2_3	1051			
	2_4	1234			
	2_5	1257			
	3_1	1096		24	
	3_2	1297			
	3_3	1772	X		
	3_4	1866	X		
	3_5	1956	X		
Maltotriose	1_1	924		20	25
	1_2	1306			
	1_3	1184			
	1_4	920			
	1_5	1426			
	2_1	1873		7	
	2_2	1778			
	2_3	1556			
	2_4	1786			
	2_5	1715			
	3_1	1327		22	
	3_2	1375			
	3_3	2048			
	3_4	2038			
	3_5	2072			

Table S4
Evaluated recoveries for soluble starch and wheat 405.

Saccharide	Level	Amount [ng/band]	Recovery (%)	Mean recovery (%) (*n* = 3)
Starch				
Glucose	0	47		
	0	75		
	0	47		
	+50%	111	121	112
	+50%	97	105	
	+50%	101	110	
	+100%	149	116	112
	+100%	128	100	
	+100%	154	120	
	+150%	185	113	111
	+150%	184	112	
	+150%	180	109	
Maltose	0	599		
	0	951		
	0	615		
	+20%	981	120	115
	+20%	929	113	
	+20%	925	113	
	+40%	1085	118	114
	+40%	996	109	
	+40%	1063	116	
	+60%	1225	110	106
	+60%	1243	112	
	+60%	1068	97	
Wheat 405				
Glucose	0	156		
	0	219		
	0	142		
	+50%	258	103	98
	+50%	221	88	
	+50%	260	104	
	+100%	272	82	82
	+100%	239	72	
	+100%	298	90	
	+150%	324	79	80
	+150%	346	85	
	+150%	309	76	
Maltose	0	1177		
	0	1855		
	0	1317		
	+20%	1489	91	94
	+20%	1376	84	
	+20%	1712	105	
	+40%	1267	70	71
	+40%	1146	63	
	+40%	1417	78	
	+60%	1318	61	62
	+60%	1462	67	
	+60%	1255	58	

Table S5
Evaluated saccharide amounts for all ten hydrothermally treated flour samples digested by human salivary α-amylase.

Type of flour	Saccharide	Amount [ng/band]	Mean amount [ng/band] (*n* = 2–3)	%RSD
Amaranth	Maltose	577	711	17
		746		
		809		
	Maltotriose	548	668	19
		662		
		794		
	Glucose	23	26	15
		28		
Einkorn	Maltose	1720	1801	4
		1838		
		1845		
	Maltotriose	1757	1835	5
		1800		
		1948		
	Glucose	69	73	7
		72		
		79		
Emmer	Maltose	1517	1571	6
		1686		
		1510		
	Maltotriose	1678	1743	5
		1842		
		1709		
	Glucose	72	71	1
		71		
		71		
Oat	Maltose	2580	2532	5
		2397		
		2620		
	Maltotriose	2227	2230	3
		2170		
		2293		
	Glucose	142	140	1
		139		
		139		
Rye	Maltose	2310	2290	2
		2247		
		2314		
	Maltotriose	2240	2156	4
		2085		
		2144		
	Glucose	141	144	3
		141		
		150		
Whole rye	Maltose	1818	2118	16
		2063		
		2474		
	Maltotriose	1623	1836	13
		1782		
		2103		
	Glucose	146	168	15
		161		
		196		

Type of flour	Saccharide	Amount [ng/band]	Mean amount [ng/band] (n = 2–3)	%RSD
Spelt wheat	Maltose	2565	2451	7
		2336		
		2381		
	Maltotriose	2161	2041	5
		1954		
		2009		
	Glucose	223	217	3
		210		
		217		
Whole spelt wheat	Maltose	2075	2027	2
		1987		
		2020		
	Maltotriose	1824	1813	1
		1786		
		1830		
	Glucose	175	164	5
		159		
		159		
Wheat 405	Maltose	2168	2221	3
		2274		
	Maltotriose	2459	2581	9
		2434		
		2850		
	Glucose	151	163	11
		155		
		184		
Whole wheat	Maltose	2090	2009	4
		1954		
		1984		
	Maltotriose	1947	1852	5
		1781		
		1828		
	Glucose	141	132	7
		122		
		134		

Table S6
Evaluated saccharide amounts for all ten hydrothermally treated flour samples digested by pancreatin.

Type of flour	Saccharide	Amount [ng/band]	Mean amount [ng/band] (n = 3)	%RSD
Amaranth	Maltose	1389	1313	8
		1354		
		1196		
	Maltotriose	1605	1597	9
		1741		
		1444		
	Glucose	128	128	2
		131		
		126		
Einkorn	Maltose	2536	2297	11
		2038		
		2317		
	Maltotriose	2496	2476	5
		2342		
		2589		
	Glucose	233	219	6
		205		
		220		
Emmer	Maltose	2413	2134	14
		1822		
		2166		
	Maltotriose	2356	2305	5
		2161		
		2398		
	Glucose	218	191	19
		151		
		204		
Oat	Maltose	1819	1985	11
		1913		
		2223		
	Maltotriose	1951	2039	9
		1921		
		2246		
	Glucose	175	179	2
		176		
		182		
Rye	Maltose	2209	2155	3
		2157		
		2099		
	Glucose	182.6	174	5
		174.3		
		166.2		
Whole rye	Maltose	2035	2299	12
		2289		
		2573		
	Maltotriose	2252	2585	13
		2582		
		2920		
	Glucose	286	306	6
		309		
		323		

Type of flour	Saccharide	Amount [ng/band]	Mean amount [ng/band] (n = 3)	%RSD
Spelt wheat	Maltose	2573	2303	10
		2191		
		2144		
	Maltotriose	2793	2547	8
		2425		
		2424		
	Glucose	325	297	8
		282		
		283		
Whole spelt wheat	Maltose	1698	1599	6
		1515		
		1584		
	Maltotriose	1968	1805	8
		1677		
		1770		
	Glucose	171	173	10
		156		
		191		
Wheat 405	Maltose	1587	1728	9
		1890		
		1706		
	Maltotriose	1768	2031	13
		2310		
		2015		
	Glucose	163	163	12
		182		
		143		
Whole wheat	Maltose	1414	1420	8
		1313		
		1534		
	Maltotriose	1372	1441	10
		1345		
		1605		
	Glucose	107	115	9
		111		
		127		

S-10

Fig. S1. Standardization of the plate humidity: (**A**) Plastic box for pre-conditioning filled with 200 mL saturated sodium carbonate and (**B**) a smaller plastic box for incubation at 37 °C lined with wet filter paper and filled with 70 mL water.

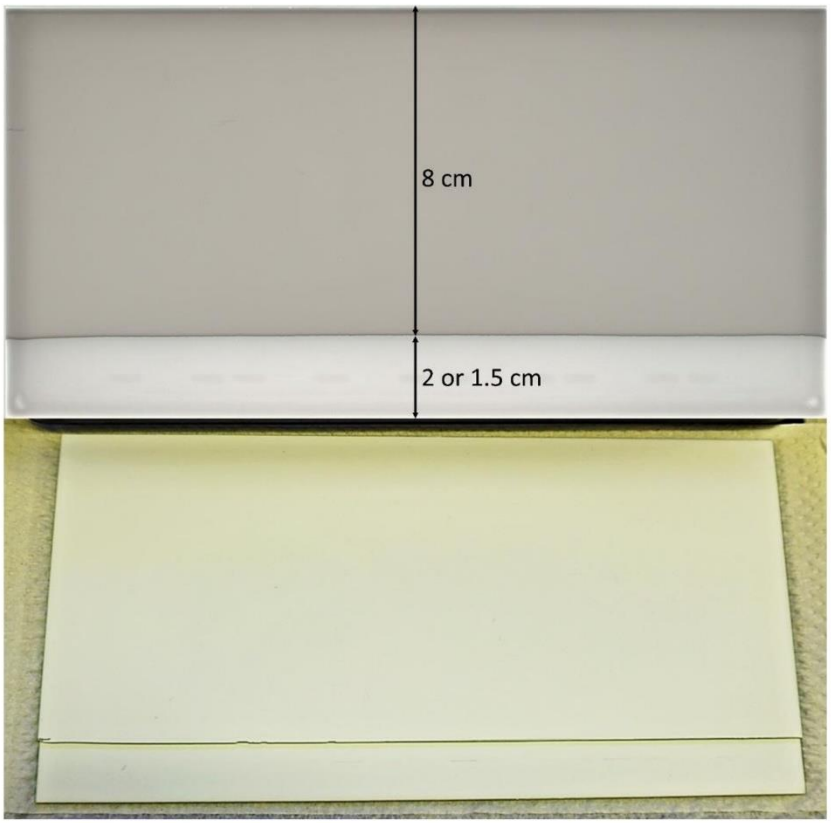

Fig. S2. Start of amylolysis by wetting of the reaction zone of the HPTLC plate silica gel 60 (2 or 1.5 cm) after sample application; the upper dry part (8 cm) was covered by a cut HPTLC silica gel plate (20 cm × 8–8.5 cm) to maintain the humidity and avoid drying out during the incubation (Fig. S1B). The plate and cover plate were both together wetted with 2.5 mL 0.1 M sodium chloride solution via piezoelectrically spraying.

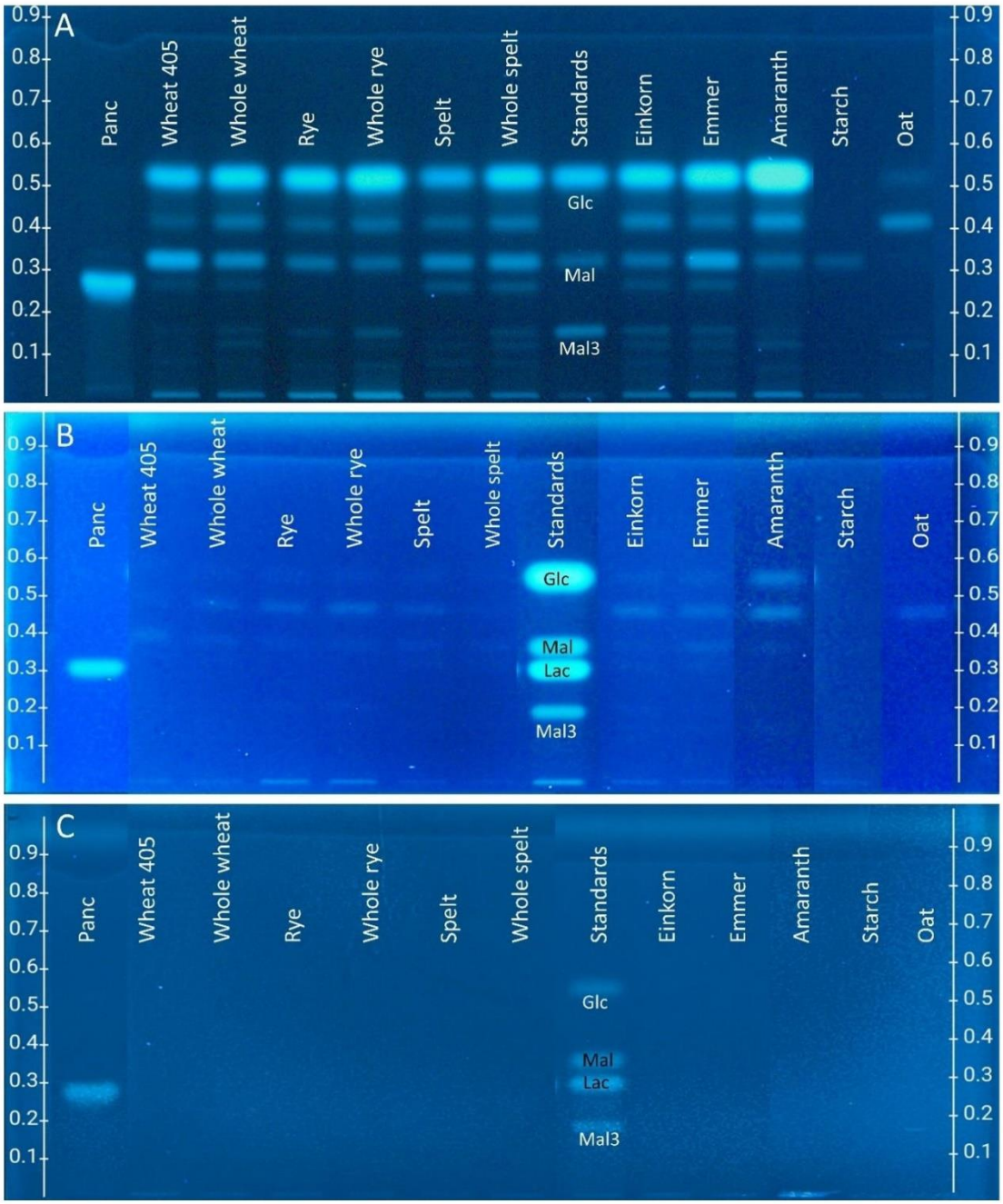

Fig. S3. HPTLC−FLD chromatograms showing the removal of native saccharides from ten different undigested flour samples via different preparation methods, *i.e.* (**A**) flours resuspended in bi-distilled water (unfortunately here, starch was contaminated with Mal), (**B**) flours washed twice with bi-distilled water, centrifuged in-between for 10 min at 9.000 × g, resuspended in bi-distilled water or (**C**) flours cooked for 30 min in boiling water, washed twice with bi-distilled water, centrifuged in-between for 10 min at 9.000 × g and resuspended in bi-distilled water. Flour samples (2 µL each, 10 mg/mL), pancreatin (1 µL, 10 TAME mU/µL), starch (2 µL, 1 mg/mL) and Glc, Mal, Lac and Mal3 (different amounts) were applied onto the HPTLC plate silica gel 60, separated with acetonitrile/2-propanol/water/acetone 12:4:3:1 (*V*/*V*/*V*/*V*) up to 70 mm, detected at FLD 366 nm after derivatization with the *p*-aminobenzoic acid reagent and depicted as image collages for comparison.

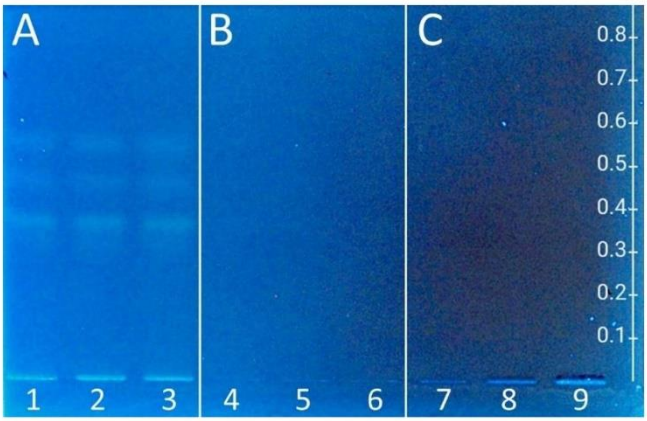

Fig. S4. HPTLC−FLD chromatograms showing the removal of native saccharides after different cooking times, *i.e.* 15 min (tracks 1, 4, and 7), 30 min (tracks 2, 5, and 8) and 45 min (tracks 3, 6 and 9). The supernatants of wheat 405 (10 mg/mL, 5 µL/band each) after (**A**) one or (**B**) two centrifugation cycles (9.000 × g for 10 min, resuspended with bi-distilled water) were applied beside (**C**) wheat 405 (10 mg/mL, 5 µL/band each) after two centrifugation cycles. Separation on HPTLC plates silica gel 60 with acetonitrile/2-propanol/water/acetone 12:4:3:1 (*V*/*V*/*V*/*V*) up to 70 mm and detected at FLD 366 nm after derivatization with the *p*-amino-benzoic acid reagent.

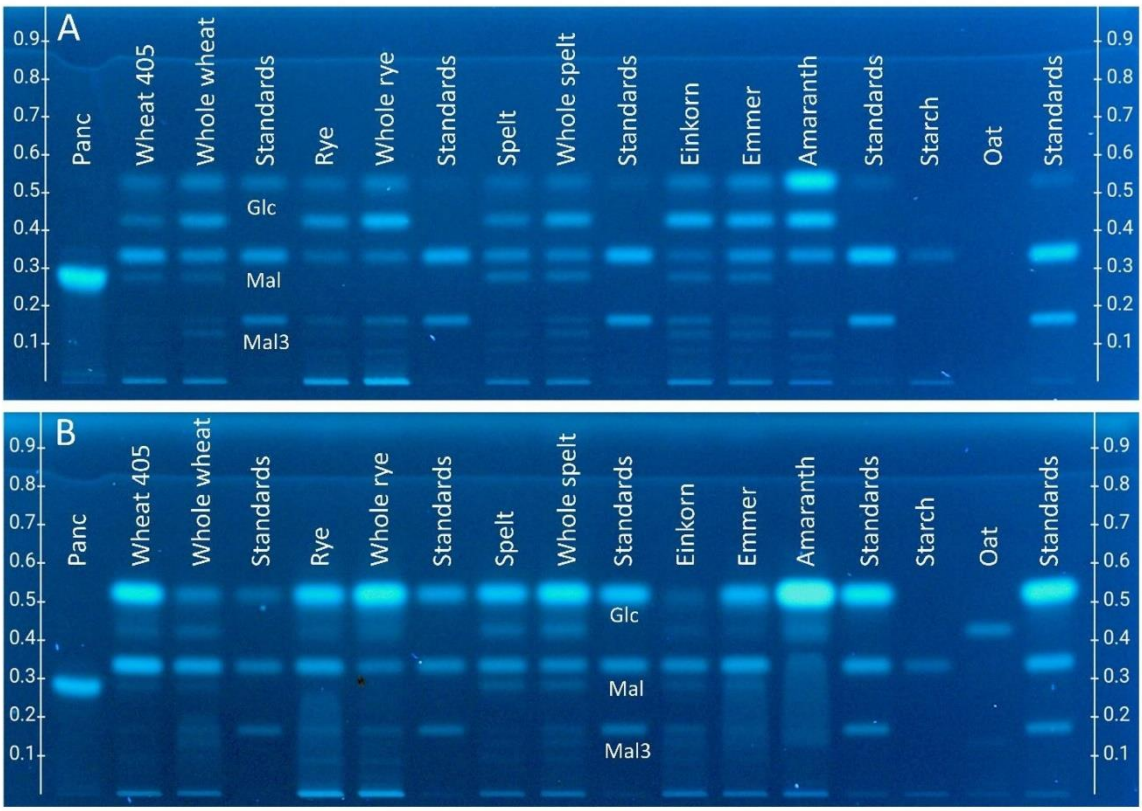

Fig. S5. HPTLC−FLD chromatograms showing the instability of undigested flour suspensions, resuspended in bi-distilled water and analysed (**A**) directly after preparation and (**B**) after 24 h. Flour samples (2 µL each, 10 mg/mL), pancreatin (1 µL, 10 TAME mU/µL), starch (2 µL, 1 mg/mL, contaminated with Mal) and Glc, Mal, Lac, and Mal3 (different amounts) were applied onto HPTLC plates silica gel 60, developed with acetonitrile/2-propanol/water/acetone 12:4:3:1 (*V*/*V*/*V*/*V*) up to 70 mm and detected at FLD 366 nm after derivatization with the *p*-amino-benzoic acid reagent.

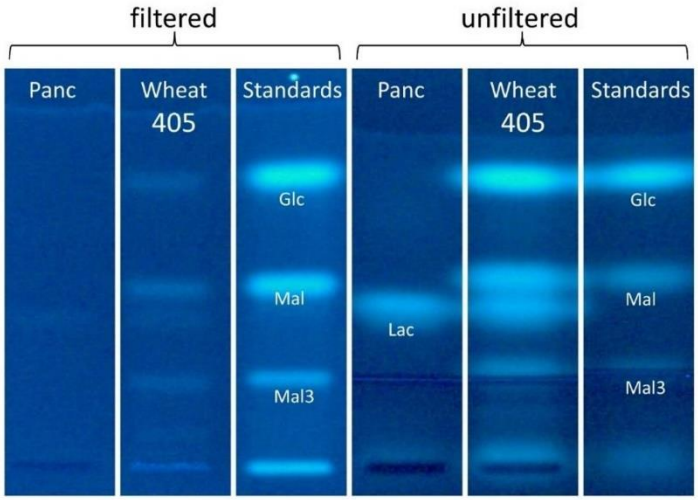

Fig. S6. HPTLC−nanoGIT−FLD chromatograms showing the influence of centrifugation filtration using a 3 kDa Amicon Ultra-0,5 filter (Merck, Darmstadt, Germany) on the enzyme activity of pancreatin (Panc), exemplarily tested on the pancreatic amylolysis of wheat 405 on HPTLC silica gel 60 plates. Hydrothermally treated wheat 405 (2 µL of 10 mg/mL) were digested via Panc (1 µL, 10 TAME mU/µL), and as standards Glc, Mal and Mal3 (1 µg/band) were applied, separated with acetonitrile/2-propanol/water/acetone 12:4:3:1 (*V*/*V*/*V*/*V*) up to 70 mm and detected at FLD 366 nm after derivatization with the *p*-aminobenzoic acid reagent.

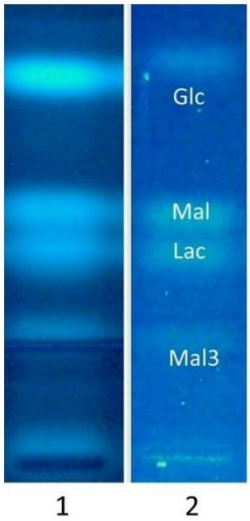

Fig. S7. HPTLC−nanoGIT−FLD chromatograms comparing the plate wetting treatment with (**1**) and without (**2**) a cut cover plate (20 cm × 8.5 cm) to ensure the wetting of only the enzymatic reaction area (application area) for the prevention of zone diffusion. Hydrothermally treated wheat 405 (2 µL of 10 mg/mL) were digested via pancreatin (1 µL, 10 TAME mU/µL) on HPTLC plates silica gel 60, developed with acetonitrile/2-propanol/water/acetone 12:4:3:1 (*V*/*V*/*V*/*V*) up to 70 mm and detected at FLD 366 nm after derivatization with the *p*-aminobenzoic acid reagent.

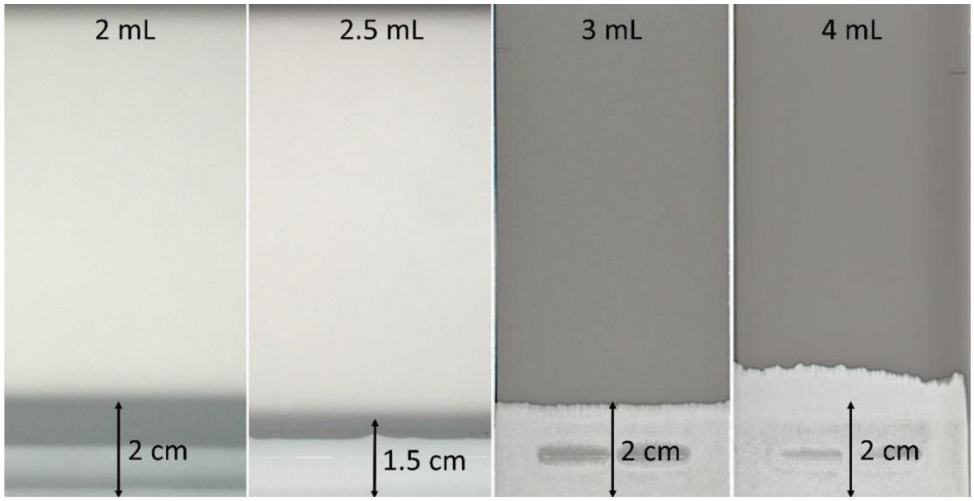

Fig. S8. Influence on HPTLC plates silica gel 60 of different wetting volumes (0.1 M sodium chloride solution, piezoelectrically sprayed) on diffusion/drying out of the wetted enzymatic reaction zone (1.5–2 cm) during incubation at 37 °C for 60 min. Wet zones appear bright and dried-out zones appear dark. The enzymatic reaction zone was still visibly wet after incubation with a wetting volume of 2.5 mL, too much dried out with 2 mL, and too wet with 3–4 mL. Plates were documented under white light illumination in transmission mode.

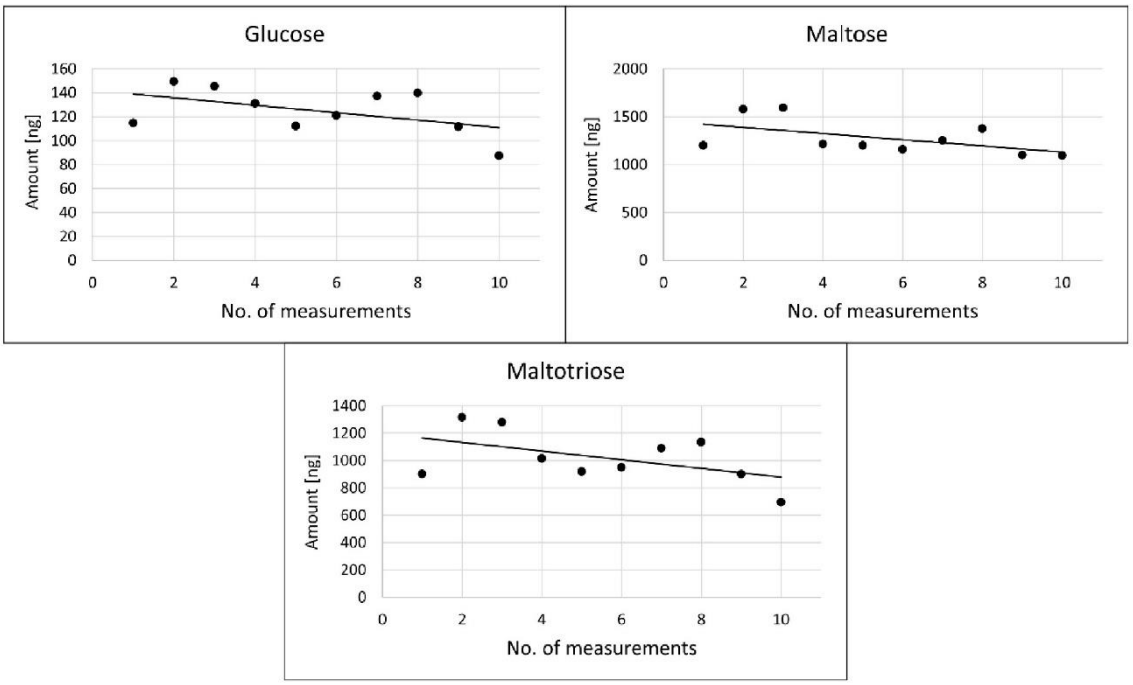

Fig. S9. Study of a sedimentation trend for wheat 405: Plotted number of measurements (n = 10) against each measured saccharide amount showing the linear trendline with a slight downward trend, which was found to be still acceptable (%RSD of 14–18%).

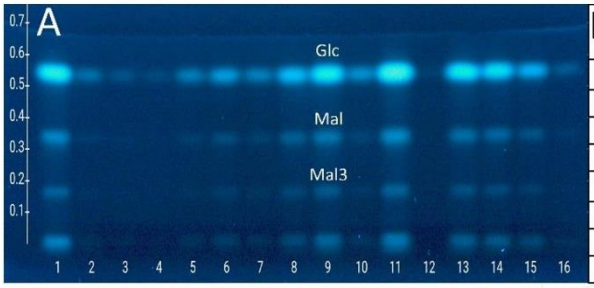

B Saccharide	S/N Height	Amount [ng]	Track
	LOD		
Glucose	0.0171/0.0023 = 7	5	12
Maltose	0.0092/0.0022 = 4	38	16
Maltotriose	0.0042/0.0011 = 4	47	4
	LOQ		
Glucose	0.0178/0.0015 = 12	10	4
Maltose	0.0113/0.0011 = 10	48	2
Maltotriose	0.0124/0.0012 = 10	188	6

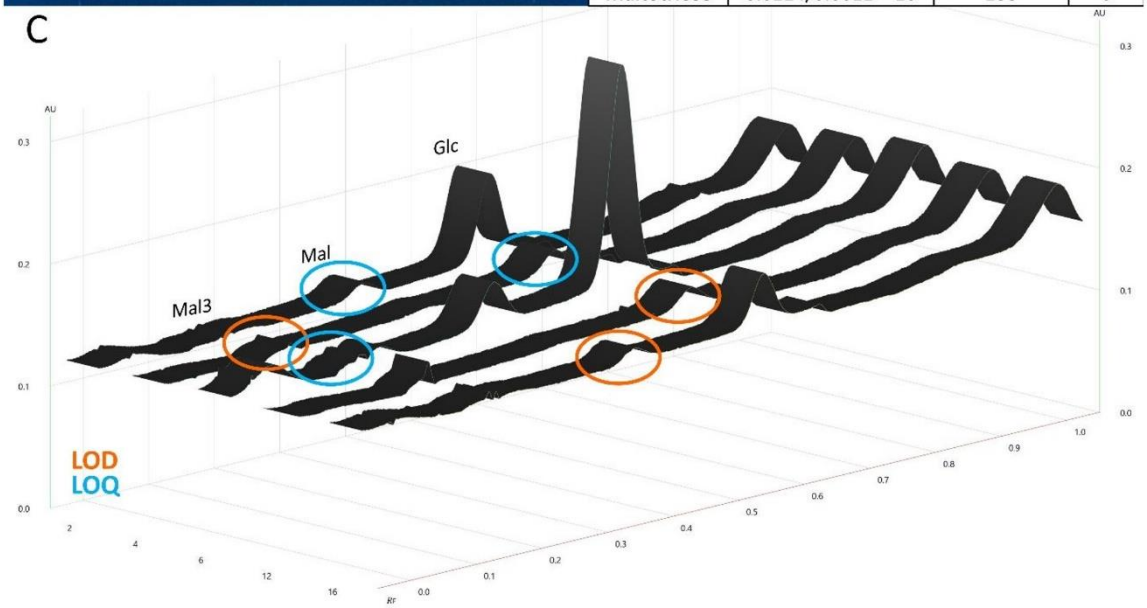

Fig. S10. Determination of limits of detection and quantification (LOD/LOQ): (**A**) HPTLC−nanoGIT−FLD chromatogram showing 16 levels (unsorted in order) of Glc 5–800 ng/band, Mal 10–950 ng/band, and Mal3 47–1129 ng/band on a pre-treated HPTLC plate silica gel 60 separated with acetonitrile/2-propanol/water/acetone 12:4:3:1 (*V*/*V*/*V*/*V*) up to 70 mm, and detected at FLD 366 nm after derivatization with the *p*-aminobenzoic acid reagent; (**B**) signal-to-noise ratio (S/N) and LOD/LOQ calculated via peak height; and (**C**) 3D densitogram of fluorescence measurement at 366/>400 nm.

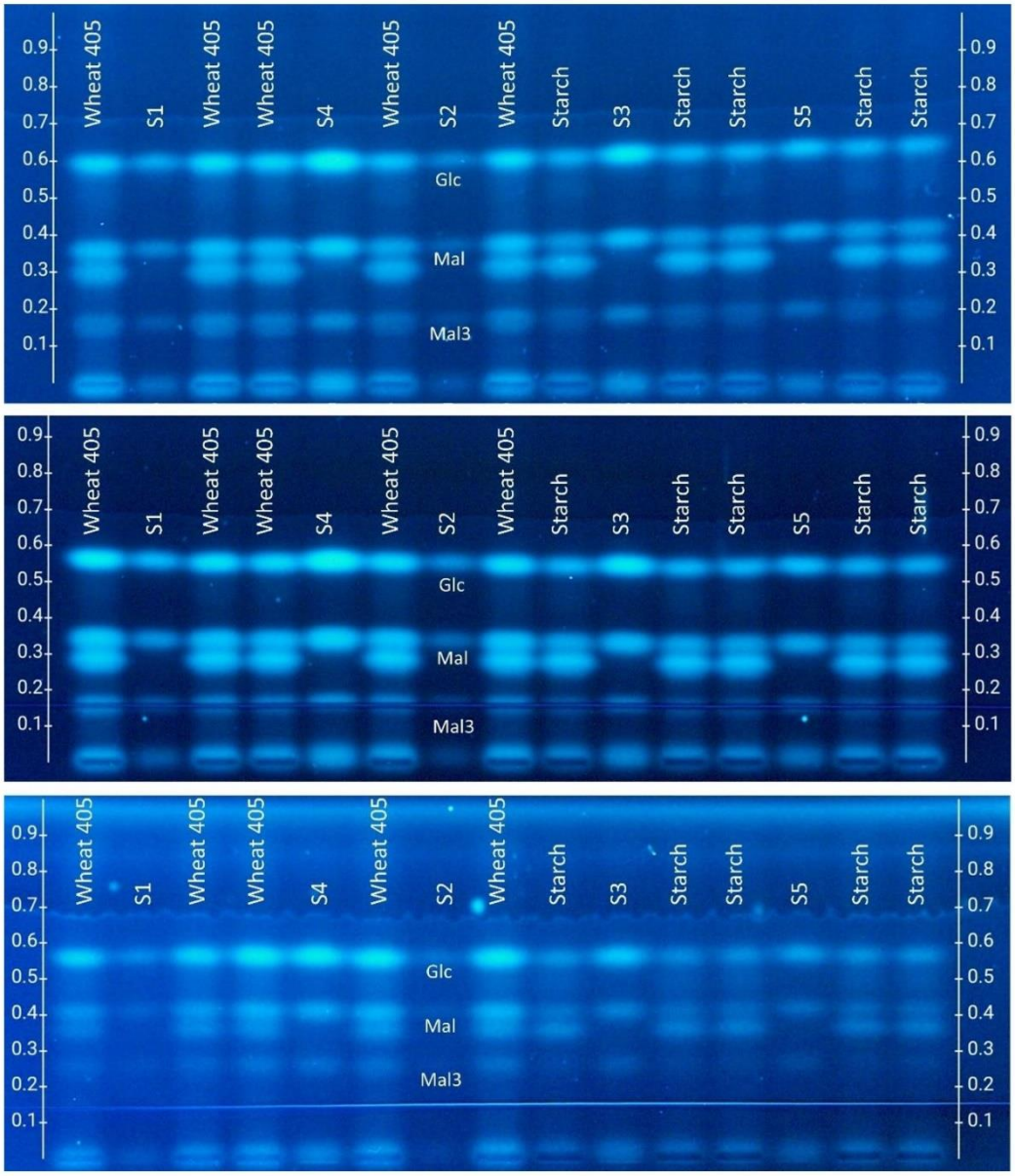

Fig. S11. HPTLC−nanoGIT−FLD chromatograms on three days/plates (n = 3) for determination of the precision of wheat 405 and soluble starch (n = 5 each) digested by 10 TAME mU/band Panc along with calibration levels (S1–S5) ranged 471–2352 ng for Mal3, 238–1900 ng for Mal, and 50–300 ng for Glc, separated on pre-treated HPTLC plates silica gel 60 with acetonitrile/2-propanol/water/acetone 12:4:3:1 (*V*/*V*/*V*/*V*) up to 70 mm and detected at 366 nm after derivatization with the *p*-aminobenzoic acid reagent.

File S1. visionCATS method file for salivary amylolysis

File S2. visionCATS method file for pancreatic amylolysis

Publication II

Bioactive profiles of edible vegetable oils determined using 10D hyphenated comprehensive high-performance thin-layer chromatography (HPTLC × HPTLC) with on-surface metabolism (nanoGIT) and planar bioassays

Isabel Müller, Alexander Gulde, Gertrud E. Morlock

Published in Frontiers in Nutrition

Received 23rd May 2023, Accepted 4th August 2023, Published 22nd September 2023

frontiers | Frontiers in Nutrition

TYPE Original Research
PUBLISHED 22 September 2023
DOI 10.3389/fnut.2023.1227546

OPEN ACCESS

EDITED BY
Yisheng Chen,
Shanxi Agricultural University, China

REVIEWED BY
Zhenfeng Wu,
Jiangxi University of Traditional Chinese Medicine, China
Petar Ristivojevic,
University of Belgrade, Serbia
Laura Barp,
University of Udine, Italy

*CORRESPONDENCE
Gertrud E. Morlock
✉ gertrud.morlock@uni-giessen.de

†Member of the More than One Constituent Substances (MOCS) Initiative, www.vielstoffgemische.de

RECEIVED 23 May 2023
ACCEPTED 04 August 2023
PUBLISHED 22 September 2023

CITATION
Müller I, Gulde A and Morlock GE (2023) Bioactive profiles of edible vegetable oils determined using 10D hyphenated comprehensive high-performance thin-layer chromatography (HPTLC×HPTLC) with on-surface metabolism (nanoGIT) and planar bioassays. *Front. Nutr.* 10:1227546. doi: 10.3389/fnut.2023.1227546

Bioactive profiles of edible vegetable oils determined using 10D hyphenated comprehensive high-performance thin-layer chromatography (HPTLC×HPTLC) with on-surface metabolism (nanoGIT) and planar bioassays

Isabel Müller [1], Alexander Gulde[1] and Gertrud E. Morlock [1,2*†]

[1]Institute of Nutritional Science, Chair of Food Science, as well as Interdisciplinary Research Centre for Biosystems, Land Use and Nutrition, Justus Liebig University Giessen, Giessen, Germany, [2]Center for Sustainable Food Systems, Justus Liebig University Giessen, Giessen, Germany

Introduction: Vegetable oils rich in unsaturated fatty acids are assumed to be safe and even healthy for consumers though lipid compositions of foods vary naturally and are complex considering the wealth of minor compounds down to the trace level.

Methods: The developed comprehensive high-performance thin-layer chromatography (HPTLC×HPTLC) method including the on-surface metabolization (nanoGIT) and bioassay detection combined all steps on the same planar surface. The pancreatic lipolysis (intestinal phase) experiment and the subsequent analysis of the fatty acid composition including its effect-directed detection using a planar bioassay was performed without elaborate sample preparation or fractionation to ensure sample integrity. Thus, no sample part was lost, and the whole sample was studied on a single surface regarding all aspects. This made the methodology as well as technology miniaturized, lean, all-in-one, and very sustainable.

Results and discussion: To prioritize important active compounds including their metabolism products in the complex oil samples, the nanoGIT method was used to examine the pancreatic lipolysis of nine different vegetable oils commonly used in the kitchen and food industry, e.g., canola oil, flaxseed oil, hemp oil, walnut oil, soybean oil, sunflower oil, olive oil, coconut oil, and palm oil. The digested oils revealed antibacterial and genotoxic effects, which were assigned to fatty acids and oxidized species via high-resolution tandem mass spectrometry (HRMS/MS). This finding reinforces the importance of adding powerful techniques to current analytical tools. The 10D hyphenated nanoGIT-HPTLC×HPTLC-Vis/FLD-bioassay-heart cut-RP-HPLC-DAD-HESI-HRMS/MS has the potential to detect any potential hazard due to digestion/metabolism, improving food safety and understanding on the impact of complex samples.

KEYWORDS

all-in-one digestion analysis system, on-surface metabolization, lipolysis, effect-directed analysis, intestinal phase, comprehensive high-performance thin-layer chromatography, plant oils, sustainability transition

10.3389/fnut.2023.1227546

1. Introduction

Lipids are one of the three important macronutrients in the human diet, and fat has the highest energy density of all nutrients. It is recommended that not more than 30%−35% of the energy intake should be in the form of fat (1, 2). The fatty acid (FA) composition of dietary fats can influence body weight (3, 4). High intake of saturated or monounsaturated fats causes an increase in weight gain and waist circumference, a factor for adiposity, whereas polyunsaturated fatty acids (PUFAs) show no increase. Among other aspects, saturated fatty acids (SFAs) such as lauric acid (C12:0), myristic acid (C14:0), and palmitic acid (C16:0) are associated with a higher risk of cardiovascular disease (5, 6). Replacing SFA-rich fats with PUFA-rich oils showed a lower risk of cardiovascular disease but no effect on adiposity (7), as mentioned earlier. Therefore, a deeper knowledge of the FA composition of food and its impact is of the utmost interest since the biological activity of FAs may influence not only cell and tissue metabolism and signaling pathways (8) but also our microbiome (9) and health (10). To achieve a low-fat diet, foods of plant origin are preferred to those of animal origin (1). Such plant-based foods contain less total fat and a more favorable FA composition, such as more essential FAs, namely α-linolenic acid (C18:3, *n*-3) and linoleic acid (C18:2, *n*-6), whereby *n*-6 to *n*-3 FA ratios of 1–5:1 are preferred (4, 11, 12); however, the ratio alone is not decisive for a diet recommendation (13, 14). Therefore, edible vegetable oils are the most commonly used fats in the kitchen and for the preparation and processing of foods (15, 16). They mainly consist of triacylglycerols (TAGs), in addition to a few percent of diacylglycerols (DAGs), monoacylglycerols (MAGs), and free FAs, as well as further lipophilic minor compounds in the per mille range down to the trace level (17–19).

The simulation of *in vitro* digestion is important to provide insights into the digestion mechanisms of fats and oils. After partial hydrolysis of TAGs by gastric lipases, the nutrients entering the small intestine are emulsified by bile salts and further digested enzymatically by pancreatic lipases in the intestinal phase (20). Both lipases cleave TAGs mainly into 2-MAGs and free FAs. However, while the main hydrolysis takes place in the intestine, it should not be neglected that gastric and pancreatic lipases act as complementary enzymes (21). The rate of lipolysis of TAGs is dependent on the FA chain length and degree of saturation (22–24). Research is currently being conducted on various simulated digestion models to study the digestibility of isolated nutrients in foods or the food itself, not ignoring the influence of the food matrix (25, 26). Due to the sensitivity of simulated digestion systems to altering enzymatic parameters and environmental conditions, Minekus et al. (27) designed an internationally harmonized protocol for static *in vitro* digestion via oral, gastric, and intestinal phases. Morlock et al. (28) showed the successful transfer of the internationally harmonized protocol for *in vitro* assays to high-performance thin-layer chromatography (HPTLC–UV/Vis/FLD), and moreover, they created an all-in-one digestion and analysis system for on-surface digestion at the nanomolar level (nanoGIT), followed by the analysis of the food samples, including the resulting metabolism products, all on the same surface. The optional hyphenation with post-chromatographic derivatization reagents, planar bioassays, and high-resolution tandem mass spectrometry (HRMS/MS) makes the lean all-in-one methodology very flexible, fast, and sustainable. In contrast, all current methods require elaborate sample preparation after the simulated lipolysis and the subsequent analysis of the metabolized food samples. Mostly, spectrophotometric assay kits or titration methods, such as the pH-stat method, are used for the determination of the sum of hydrolyzed FAs and thus lipolysis rate (26, 29, 30). Gas chromatography and high-performance liquid chromatography methods are performed rarely (23, 31), although Helbig et al. (29) showed the necessity of examining the detailed FA composition.

In this study, an all-in-one 10D hyphenated nanoGIT–HPTLC×HPTLC–Vis/FLD–bioassay–heart cut–RP-HPLC–DAD–HESI-HRMS/MS methodology was created and studied for the first time. The nanoGIT system was used to examine the pancreatic lipolysis of nine different vegetable oils commonly used in the kitchen and food industry, i.e., canola oil, flaxseed oil, hemp oil, walnut oil, soybean oil, sunflower oil, olive oil, coconut oil, and palm oil. A two-dimensional (2D) separation with orthogonal selectivity was developed for the differentiation of the lipids, resulting in a comprehensive HPTLC×HPTLC method. The entire sample separated in the first dimension was transferred to the second orthogonal separation dimension by a simple 90° plate turn. After the on-surface nanoGIT digestion, the first dimension was separated based on functional groups such as TAGs, DAGs, MAGs, and FAs. In the second separation dimension, the FAs were separated according to lipophilicity, and the approximate FA composition was determined. Antibacterial and genotoxic properties of the lipids were detected via respective bioassays and assigned to molecules via automated heart cuts of the active zones of interest to RP-HPLC–DAD–HESI-HRMS/MS. No information or sample part was lost since the whole workflow was performed on the same planar surface.

2. Materials and methods

2.1. Chemicals and materials

3-(4,5-Dimethylthiazol-2-yl)-2,5-diphenyltetrazolium bromide (MTT, ≥98%), acetone (≥99.9%), formic acid (≥99.9%), acetic acid (100%), dipotassium phosphate trihydrate (≥99.9%), glycerol (86%), monopotassium phosphate (≥99%), magnesium chloride (≥98.5%), sodium chloride (≥99.8%), monosodium phosphate monohydrate (≥98%), *n*-hexane (≥98%), sulfuric acid (96%, *p. a.*), decanoic acid (C10:0, >98%), octanoic acid (C8:0, >99%), oleic acid (C18:1, >99%), stearic acid (C18:0, >98%), sodium hydroxide (≥98%), 4-methylumbelliferyl-β-D-galactopyranoside (≥99%, for biochemistry), dimethylsulfoxide (≥99.8%), and molecular sieve 3 Å (0.3 nm, type 564, beads) were purchased from Carl Roth (Karlsruhe, Germany). Acetonitrile (≥99.9%), disodium phosphate (≥99%), sodium bicarbonate (≥99.7%), pancreatin from porcine pancreas (8 × USP specifications), bile extract porcine, dioleoylglycerol (diolein, >99%, mixture of 1,3- and 1,2-isomers), glyceryl trioleate (triolein, ≥99%), 1-oleoyl-*rac*-glycerol (monoolein, >99%; 2-monoolein was rarely available and six times more expensive), caffeine (>99%),

linoleic acid (C18:2, 60%−74%), myristic acid (C14:0, >99%), palmitic acid (C16:0, >99%), dodecanoic acid (C12:0, 98%), peptone from casein (for microbiology), Müller–Hinton broth (for microbiology), D-(+)-glucose (99.5%), ampicillin sodium salt, and lysogeny broth (LB) powder (including 5 g/L of sodium chloride) were purchased from Fluka-Sigma-Aldrich (Steinheim, Germany). Methanol (99.9%) was supplied by VWR International (Darmstadt, Germany). Magnesium sulfate heptahydrate (99.5%), potassium chloride (≥99.5%), citric acid monohydrate (≥99.5%), HPTLC plates silica gel 60 RP-18 W, HPTLC plates silica gel 60 RP-18, and HPTLC plates silica gel 60 as cover plates (all 20 cm × 10 cm), and *Bacillus subtilis* subsp. *spizizenii* spore suspension (DSM 618) were purchased from Merck (Darmstadt, Germany). Diammonium phosphate (≥99%), diethyl ether (≥99%), and linolenic acid (C18:3, 99%) were purchased from Acros Organics (Morris Plains, NJ, USA). Yeast extract powder (for microbiology), ethyl acetate (≥99.8%), *o*-phosphoric acid (85%), ethanol (≥99.9%), and dichloromethane (≥99.9%, stabilized with amylene) were purchased from Th. Geyer (Renningen, Germany). Copper(II) sulfate pentahydrate (p. a.) was purchased from Honeywell International (Morristown, NJ, USA). Calcium chloride dihydrate (≥99.9%) was supplied by Bernd Kraft (Duisburg, Germany). The luminescent marine *Aliivibrio fischeri* (DSM 7151) bacteria were purchased from the DSMZ Leibnitz Institut (Berlin, Germany). Tetracycline hydrochloride (research grade, USP) was purchased from Serva Electrophoresis (Heidelberg, Germany). Bidistilled water was produced by a Heraeus Destamat B-18E (Thermo Fisher Scientific, Dreieich, Germany). Rhodamine 6G (100% ± 3%) was purchased from Alfa Aesar (Kandel, Germany). *Salmonella typhimurium* bacteria strain TA1535, modified to contain the plasmid pSK1002 (PTM *S. typhimurium* TA1535/pSK1002, cryostock), was purchased from Trinova Biochem (Giessen, Germany). 4-Nitroquinoline-1-oxide (98%) was purchased from TCI (Eschborn, Germany). Edible vegetable oils (Supplementary Table S1) were purchased from local supermarkets.

2.2. Pre-treatment of the HPTLC RP-18 W plate

For on-surface metabolic reactions, the HPTLC RP-18 W plate was pre-treated as follows. The plate was heated at 120°C for 60 min (TLC Plate Heater III, CAMAG, Muttenz, Switzerland; to fix the binder for the current plate batches used) and pre-washed by development first with methanol and then, after plate drying, with ethyl acetate, both up to 90 mm in a twin-trough chamber. To ensure the pancreatin reaction in the application zone, the acidic plate pH (ca. pH 4.2) was neutralized via piezoelectrical spraying (2.8 ml, ultra-yellow nozzle, level 3, Derivatizer, CAMAG) with phosphate-citrate buffer (6 g/L of citric acid and 10 g/L of disodium hydrogen phosphate, adjusted to pH 12 by sodium hydroxide). Therefore, except for the application zone, the plate was covered by a cut HPTLC plate silica gel 60, with the layer facing upward (Supplementary Figure S1). Then, the plates were dried at 120°C for 10 min.

2.3. Preparation of solutions for the enzyme, calcium chloride, standards, and samples

The digestion fluid stock solution was prepared as described by Minekus et al. (27). The pancreatin solution (200 TAME mU/µl) and the corresponding calcium chloride solution (6 pmol/µl) were prepared according to Morlock et al. (28). Monoolein, diolein, triolein, fatty acids (reference compounds were applied via overspraying to obtain the mixture on the start zone), and samples were weighed via a pipette and dissolved in *n*-hexane (all 1 mg/ml each), whereby solid fats (i.e., palm oil and coconut oil) were slightly warmed to the melting point before pipetting. All solutions were stored in solvent-tight vials in the dark at 4°C.

2.4. Initial triacylglycerol separation on HPTLC plate RP-18

Oil sample and FA standard solutions (10 µl/band each; 1 mg/ml) were applied as 8-mm bands, unless stated otherwise, as follows: a track distance of 10 mm, distance from the lower edge of 10 mm and left edge of 10 mm, dosage speed of 150 nl/s, filling speed of 15 µl/s, filling vacuum time of 0 s, and syringe volume of 25 µl (Automatic TLC Sampler ATS 4, CAMAG). The plate was developed with dichloromethane/acetic acid/acetone 2:4:5 (*V*/*V*/*V*) (32) in a twin-trough chamber (20 cm × 10 cm) up to 80 mm. The plate was subjected to a derivatization reagent sequence performed via dipping (immersion time 8 s, immersion speed 3 cm/s, Chromatogram Immersion Device 3, CAMAG), i.e., first in rhodamine 6G reagent solution (0.1% in ethanol) and, after plate drying and detection at FLD 366 nm (TLC Visualizer 2, CAMAG), then in copper sulfate phosphoric acid reagent (25 g copper sulfate pentahydrate in 250 ml *o*-phosphoric acid/water 4:41, *V*/*V*), followed by heating at 150°C for 20 min (TLC Plate Heater III, CAMAG) and detection at FLD 366 nm and white light illumination.

2.5. On-surface lipolysis and separation systems on HPTLC plate RP-18 W

The following workflow was adapted from the nanoGIT$^{+active}$ methodology (28, 33). The application was performed as mentioned, except for a band length of 6 mm, a track distance of 9 mm, and a distance from the left edge of 14.5 mm. Reference standard mixtures were applied via overspraying. Since the previous solutions were in *n*-hexane, the cleaning unit of the ATS 4 had to be rinsed with bi-distilled water once and the syringe twice before pancreatin application. The applied sample bands were first oversprayed with pancreatin solution (5 µl/band, 200 TAME mU/µl) and then with calcium chloride solution (1 µl/band, 6 pmol/µl) using a dosage speed of 50 nl/s and a filling speed of 8 µl/s. The application zone of the plate was wetted with 2.5 ml of 0.1 M sodium chloride solution by piezoelectrical spraying (yellow nozzle, level 6, Derivatizer), whereby the plate area for chromatographic separation was covered with a cut HPTLC plate

silica gel 60 (Supplementary Figure S2A) (33) to avoid the salt load on this adsorbent area and ensure good zone resolution during the later separation. This plate package was incubated at 37°C in a humid plastic box (26.5 × 16 × 10 cm, ABM, Wolframs-Eschenbach, Germany) for 60 min. After plate drying (120°C, 10 min), the lipids were focused twice by front elution with acetone up to 25 mm in a twin-trough chamber (10 min before, the second trough of the twin-trough chamber was filled up to half with molecular sieve 0.3 nm), and the lower part of the plate was cut off at 15 mm (Supplementary Figure S3) to reduce the influence of the pancreatin matrix on the chromatographic separation. The plate was developed from the cut edge side with either *n*-hexane/diethyl ether/formic acid 90:25:2 (*V*/*V*/*V*) (34) up to 60 mm for the separation of acylglycerols or acetonitrile/water 4:1 (*V*/*V*) up to 50 mm for the separation of FAs in the twin-trough chamber filled with molecular sieve as mentioned. Chromatograms were derivatized via the reagent sequence, whereby the cut 15-mm plate strip was stuck together with adhesive tape on the glass side of the HPTLC plate and detected as mentioned.

2.6. On-surface lipolysis and HPTLC × HPTLC analysis on HPTLC plate RP-18 W

As mentioned in the previous subsection, one oil sample per plate (10 cm × 10 cm) was applied as a 3-mm band, except for setting the distance from the left edge to 9 mm and using cover plates that covered everything but the applied sample band (Supplementary Figures S1B, S2B). The applied sample was treated with pancreatin and calcium chloride, wetted, incubated, focused (but no plate cut), developed two-dimensionally, detected via a bioassay as follows, or derivatized optionally via the reagent sequence, and detected as mentioned. For 2D development, the apolar mobile phase for acylglycerol separation was chosen as the first dimension, and the polar mobile phase for FAs separation as the second dimension. In between, the plate was dried at 120°C (TLC Plate Heater III) for 10 min and rotated by 90° (Supplementary Figure S4). Before the bioassay application, the plate was freed from residuals of the mobile phase via heating at 120°C for 10 min (TLC Plate Heater III) and neutralization with 2.5% sodium bicarbonate solution (2.8 ml, yellow nozzle, level 3, Derivatizer) followed by drying at 120°C for 10 min.

2.6.1. Gram-negative *Aliivibrio fischeri* bioassay

The bacterial cryostock solution (200 µl) was suspended in 20 ml of medium according to DIN EN ISO 11348-1, Section 5 (35), and the cultivation was performed overnight (18–24 h) in a 100-ml baffled flask in room temperature by shaking at 120 rpm (KMCO2, Edmund Bühler, Hechingen, Germany). As soon as the culture showed brilliant turquoise bioluminescence when shaken in the dark, it was ready for use. The bacterial suspension was piezoelectrically sprayed onto the plate (3.5 ml, blue nozzle, level 6, Derivatizer) (36, 37), and the instant bioluminescence was recorded from the wet plate over a 30-min period (time interval 3 min, exposure time 100 s, BioLuminizer 2, CAMAG). Antibacterials and cytotoxins were detected as dark zones, whereas metabolism-enhancing substances appeared as bright zones on the bioluminescent background, depicted as a grayscale image. The positive control was caffeine (1–7 µl/band, 1 mg/ml in methanol).

2.6.2. Gram-positive *Bacillus subtilis* bioassay

The bacterial stock solution (80 µl) was suspended in 20 ml of Müller–Hinton broth and incubated overnight at 37°C and 120 rpm. The culture was ready to use at an optical density measured at 600 nm (OD_{600}) between 0.7 and 1.1 (Spectrophotometer M501, CamSpec, Garforth, UK). The bacterial suspension was piezoelectrically sprayed onto the plate (3.0 ml, red nozzle, level 6, Derivatizer) and incubated at 37°C for 2 h in a humid plastic box (38). Subsequently, the plate was sprayed with a 0.2% phosphate-buffered saline MTT solution (0.75 ml, blue nozzle, level 6, Derivatizer), incubated for 5 h (until an appropriate purple plate background coloring was achieved), and heated at 50°C for 10 min (TLC Plate Heater III). The positive control was tetracycline (1–7 µl/band, 10 ng/µl in ethanol). Antibacterials and cytotoxins appeared colorless (i.e., white) on a formazan-purple plate background under white light illumination.

2.6.3. Planar SOS-Umu-C genotoxicity bioassay

The *S. typhimurium* TA1535/pSK1002 bacterial cryostock (25 µl) was suspended in 35 ml of LB medium (20 g/L), containing 0.1063 mg/ml of ampicillin sodium salt and 1 mg/ml of glucose, and cultivated at 37°C in a 125-ml plastic baffled flask with an aeration filter at 120 rpm for 16 h. The culture was 1:10 diluted to adjust to an OD_{660} of 0.2. The bacterial suspension was piezoelectrically sprayed onto the plate (2.8 ml, red nozzle, level 6, Derivatizer). After incubation at 37°C in a humid plastic box for 3 h, the plate was dried for 4 min in a cold air stream. The 4-methylumbelliferyl-β-D-galactopyranoside substrate (2 mg in 100 µl of dimethylsulfoxide added to 3 ml of phosphate-citrate buffer of pH 12) was piezoelectrically sprayed onto the plate (2.5 ml yellow nozzle, level 3, Derivatizer), followed by incubation at 37°C for 1 h. 4-Nitroquinoline-1-oxide (0.2–1.0 µl/band, 1 µg/ml in methanol) was used as a positive control. Genotoxins appeared as 4-methylumbelliferone-blue fluorescent zones on a dark bluish background at FLD 366 nm.

2.6.4. HRMS/MS recording of active substance zones

After the bioassay, HPTLC–UV/Vis/FLD–bioassay–heart cut–RP-HPLC–DAD–HESI-HRMS/MS (39) equipped with an autoTLC interface (40) was used to analyze zones of interest directly from the bioautogram. HRMS/MS signals were recorded via the polarity switching full-scan data-dependent MS2 (ddMS2) mode. Ionization settings were equal for all MS acquisition methods: sheath gas of 20 AU, aux gas of 10 AU, a spray voltage of 3.5 kV, capillary temperature of 320°C, probe heater temperature of 350°C, and S-lens RF level 50 AU. The full-scan settings were a mass range of *m*/*z* 100–1,100, a resolving power of 70,000 (at *m*/*z* 200, full width at half-maximum, FWHM), and automatic gain control (AGC) target 3e6. Fragmentation scans followed

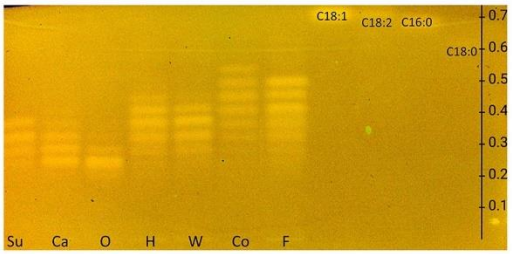

FIGURE 1
HPTLC RP-18 chromatogram of triacylglycerols in sunflower (**Su**), canola (**Ca**), olive (**O**), hemp (**H**), walnut (**W**), coconut (**Co**), and flaxseed (**F**) oils and fatty acid standards of oleic acid (C18:1), linoleic acid (C18:2), palmitic acid (C16:0), and stearic acid (C18:0), all 10 μg/band each, developed with dichloromethane/acetic acid/acetone 2:4:5 (*V*/*V*/*V*) up to 80 mm, detected at FLD 366 nm after the application of the rhodamine 6G reagent and copper sulfate phosphoric acid reagent (for comparison in Supplementary Figure S5, chromatogram with rhodamine 6G reagent only).

in Top5 ddMS2 acquisition mode at a mass range of *m*/*z* 80–1,000, resolution of 17,500 FWHM, AGC target 1e6, and stepped normalized collision energies of 20, 40, and 60 eV. The HRMS/MS fragmentation data were optionally evaluated. Substances were eluted from the plate using methanol/water 1:1 (*V*/*V*). During the study, the binary pump (HPG-3200SD) of the Dionex Ultimate HPLC system (Dionex Softron, Germering, Germany) was changed to a quaternary pump (LPG-3400RS), which caused a retention time shift.

3. Results and discussion

3.1. Development of the on-surface lipolysis and both orthogonal one-dimensional separations

The European Pharmacopeia Chapter 2.3.2 method on HPTLC RP-18 plates (32) was tested first and extended to include FAs. Differently, the plate was derivatized with the rhodamine 6G reagent. The resulting FLD 366 nm chromatogram showed bands, although weak, only for FAs but not for TAGs (Supplementary Figure S5). Therefore, by exploiting the reagent sequence technique, the plate was subsequently derivatized with copper sulfate phosphoric acid reagent, and in the study, both TAG and FA zones appeared in the HPTLC RP-18 chromatogram at FLD 366 nm (Figure 1), but no charring reaction could be observed on the HPTLC RP-18 plate at white light illumination as intended for this reagent. The currently revealed fluorescence of the rhodamine 6G reagent was explained by the pH dependence of the rhodamine 6G fluorescence and the needed acidic pH for proper visualization, here provided via the copper sulfate phosphoric acid reagent (36).

Next, the plate type had to be changed from RP-18 to a wettable reversed-phase (RP-18 W), and thus, the mobile phase system had to be changed as well since the desired aim for this study was on-surface digestion via the nanoGIT method (28). Before on-surface digestion, the intrinsic acidic pH of the RP-18 W plate (ca. pH 4.2) needed to be neutralized in the application zone with a phosphate-citrate buffer of pH 12. Unfortunately, the buffer salts interfered with derivatization via the rhodamine 6G reagent (Supplementary Figure S6); therefore, everything except the application zone had to be covered as narrowly as possible (Supplementary Figure S1). Unification of the wetting and neutralization processes (after the application) to only one neutralizing wetting step is recommended, as we established in another study. The pancreatin matrix interfered during development by causing a retardation shift in contrast to the reference standards. Thus, it had to be removed by focusing the lipids twice by front-elution with acetone after the lipolysis and cutting off the lower plate part containing the remaining pancreatin matrix. Since the focusing result with acetone was strongly dependent on the relative humidity of the laboratory environment, the second trough was half-filled with a molecular sieve of 0.3 nm within 10 min prior to focusing. When a dry environment (<15% relative humidity) in the twin-trough chamber was reached, acetone was filled in the opposite trough, and the plate was placed inside as fast as possible for development. The dry conditions during focusing as well as the (second) polar mobile phase development showed reproducibly good zone resolutions.

Due to the amphiphilic properties of the RP-18 W phase (apolar C18 chains and residual silanol groups), two orthogonal mobile phase systems were developed, i.e., one apolar to separate acylglycerols and one polar to separate FAs. Both resulting nanoGIT–HPTLC RP-18 W chromatograms (Figures 2A, C) proved the orthogonality of the mobile phases. Surprisingly, the derivatization with rhodamine 6G directly showed all lipophilic compounds. This variation in the fluorescence response was explained by different initial plate pHs and proven by additional experiments, in which the rhodamine 6G fluorescence showed a strong plate batch dependence due to different plate pHs. Fortunately, the current plate batch pH supported the required acidic milieu for the rhodamine 6G fluorescence (41). To exploit a reagent sequence, the subsequent derivatization of the same plate with copper sulfate phosphoric acid reagent (Figures 2B, D) led to a charring reaction of all unsaturated lipophilic compounds detected as black zones. The combination of both derivatization reagents on the same plate surface made it possible to first visualize all lipophilic compounds and then differentiate saturated and unsaturated zones.

As observed for the standard mixture (Figures 2A, B, **St**), the separation of acylglycerols according to polarity in TAGs, DAGs, and MAGs was successful, but all the reference FAs were eluting as one unseparated diffuse zone (hR_F 37–57). This system also allowed the separation of both DAG isomers (hR_F 19 and 26) and TAG isomers, as observed for flaxseed oil (**F**, hR_F 80 and 86). Comparing the side-by-side separated undigested and digested ($^+$) samples, a massive increase in the FAs and decrease in the TAGs amount/signal was observed, indicating the successful simulation of the lipolysis. The undigested samples showed two bands at the DAG zone; however, after the lipolysis, only one band remained, which was caused by the pancreatin enzyme blank (**EB**). Two further interferences were observed from the pancreatin blank, one intense zone was just below the MAGs, and another weaker

10.3389/fnut.2023.1227546

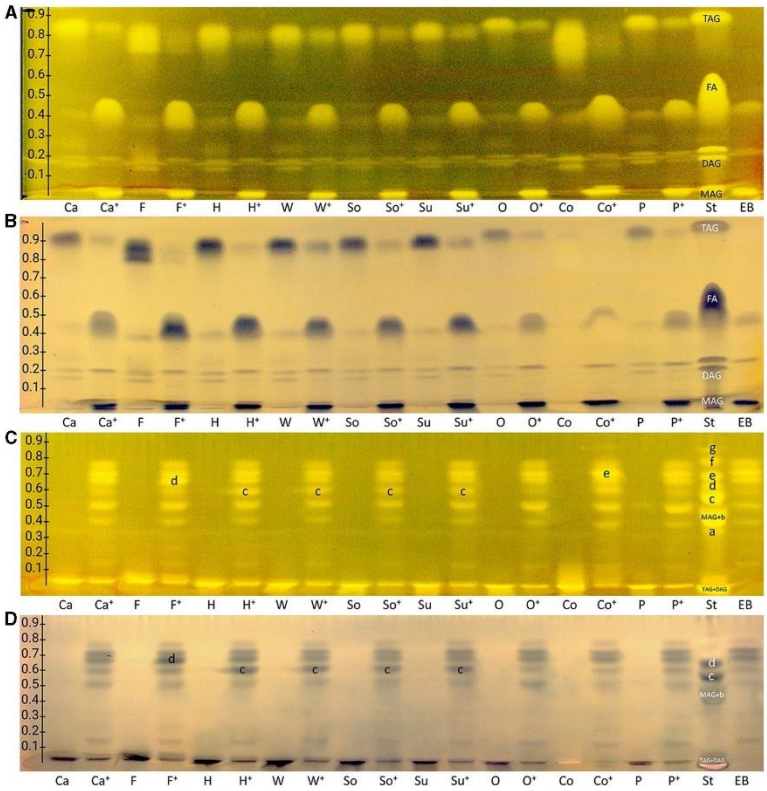

FIGURE 2
nanoGIT–HPTLC RP-18 W chromatograms of **(A, B)** acylglycerols and **(C, D)** fatty acids (**FAs**) in canola (**Ca**), flaxseed (**F**), hemp (**H**), walnut (**W**), soybean (**So**), sunflower (**Su**), olive (**O**), coconut (**Co**), and palm (**P**) oil (all 10 µg/band each) before and after (+) lipolysis via overspraying of pancreatin (each 1 TAME U/band), focused twice with acetone and, after plate cut off at 15 mm, developed (from the cut edge) with **(A, B)** *n*-hexane/diethyl ether/formic acid 90:25:2 (*V*/*V*/*V*) up to 60 mm, or **(C, D)** acetonitrile/water 4:1 (*V*/*V*, with molecular sieve) up to 50 mm, derivatized as reagent sequence on the same plate **(A, C)** first with rhodamine 6G reagent detected at FLD 366 nm, **(B, D)** followed by copper sulfate phosphoric acid reagent detected at white light illumination (in remission); for comparison, standards (**St**) triolein (**TAG**), diolein (**DAG**), monoolein (**MAG**), stearic acid (C18:0, **a**), palmitic acid (C16:0, **b**), oleic acid (C18:1, **b**), linoleic acid (C18:2, **c**), myristic acid (C14:0, **c**), linolenic acid (C18:3, **d**), lauric acid (C12:0, **e**), capric acid (C10:0, **f**), and caprylic acid (C8:0, **g**) and enzyme blank (**EB**, 1 TAME U/band of pancreatin).

zone was at the FAs position (assigned to triterpenoid acids as discussed later), which complicated the evaluation of those in the sample. Nevertheless, the comparison of both derivatization reagents supported the literature-known oil composition of all samples. Oils with a variety of FAs, such as flaxseed, hemp, and coconut oils, showed broader TAG and FA zones, whereas olive oil (mainly containing C18:1) showed comparatively compact zones. Concentrating on the unsaturated FAs in the copper sulfate phosphoric acid chromatogram (Figure 2B), the most intense zones for flaxseed oil (mainly PUFAs) and, in contrast, almost no zones for coconut oil (containing comparatively much more SFAs) confirmed the oil compositions as well.

The orthogonal selectivity selected for the separation of FAs according to lipophilicity showed a successful qualitative separation of nearly all FA reference standards (Figures 2C, D, **St**). In this system, TAGs and DAGs were retained at the application zone, whereas the MAGs were eluted. Due to their similar lipophilicity, C18:1, C16:0, and MAGs co-eluted as well as C18:2 and C14:0, which was proven in another experiment (Figure 3, framed). In the nanoGIT–HPTLC RP-18 W chromatogram (Figures 2C, D), the undigested samples did not show any noticeable FA zones, but the digested samples did. Thus, the lipolysis of TAGs into FAs was successful. High FA amounts as in the reference track (Figures 2C, D, **St**) and pancreatin matrix effects on the sample tracks led to a retardation shift; thus, the zone matching between the samples and reference compounds was challenging but nevertheless possible. With the aid of the copper sulfate phosphoric acid reagent chromatogram, C18:2 and C18:3 could be identified as intense black zones. The rhodamine 6G reagent chromatogram helped identify C8:0, C10:0, and C12:0. Due to this assigned pattern of the FAs and the literature data (37, 38), the FAs in the samples could be identified successfully via pattern recognition based on their main components. Intense zones for C18:3 (zone **d**) in flaxseed oil, C18:2 (zone **c**) in hemp, walnut, soybean, and

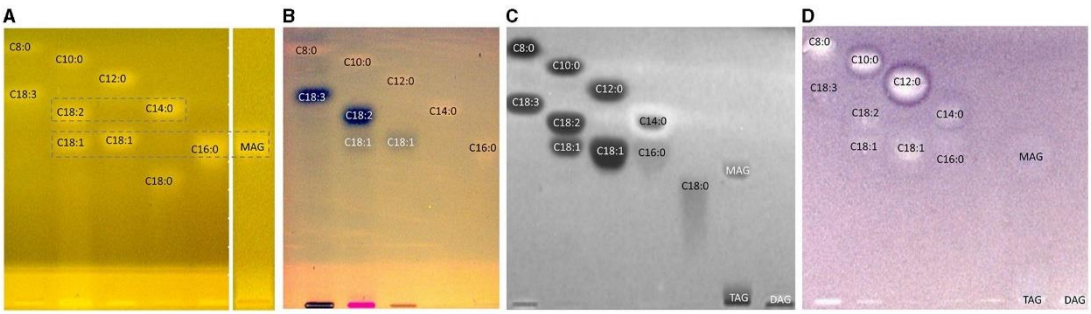

FIGURE 3
HPTLC RP-18 W chromatograms **(A, B)** and bioautograms **(C, D)** of fatty acids (**C8:0**–**C18:3**) and acylglycerols (**MAG**, **TAG**, and **DAG**), 10 μg/band each, separated with acetonitrile/water 4:1 (*V*/*V*, with molecular sieve) up to 50 mm, detected **(A)** at FLD 366 nm after derivatization with rhodamine 6G reagent, and a white light illumination (in remission) after **(B)** derivatization as reagent sequence first with rhodamine 6G reagent followed by copper sulfate phosphoric acid reagent, **(C)** Gram-negative *Aliivibrio fischeri* bioassay (bioluminescence depicted as a greyscale image), and **(D)** Gram-positive *Bacillus subtilis* bioassay.

sunflower oils, and C14:0 (zone **e**) in coconut oil were determined after digestion via pancreatin (Figures 2C, D).

As mentioned for the separation of acylglycerols, polar impurities of the pancreatin co-eluting with the FAs hindered their assignment and could also lead to false-positive interpretations. Using automated heart-cut elution of the interesting zones to RP-HPLC–DAD–HESI-HRMS/MS (39), these impurities were assigned as the bile acids ursodeoxycholic acid (UDCA), hyodeoxycholic acid (HDCA), (cheno)deoxycholic acid (CDCA/DCA), and cholenic acid (Figure 4 and Supplementary Table S2). The isomers UDCA, HDCA, and (C)DCA were identified in the negative ionization mode ($HESI^-$) in two separate peaks at retention times of 8.11 min and 8.45 min with $[M-H]^-$ at *m/z* 391.2858 and 391.2860, respectively. The $HESI^-$ and respective positive ionization mode ($HESI^+$) revealed the presence of their dimers ($[2M-H]^-$ at *m/z* 783.5791 and $[2M+H]^+$ at *m/z* 785.5927, Figure 4), identified via fragmentation (Supplementary Figure S7), as well as their tetramer ($[4M+2H]^+$ at *m/z* 785.5909 with its corresponding isotopic pattern, Supplementary Figure S8). Cholenic acid could only be assigned via $HESI^+$ as $[M+H]^+$ at *m/z* 375.2885. Since bile acids also show antibacterial properties (40), false-positive results should be considered and, when necessary, confirmed/excluded via HRMS. Fortunately, the following comprehensive separation system solved this coelution issue.

3.2. Development and proof of the nanoGIT–HPTLC×HPTLC–FLD on RP-18 W plates

The one-dimensional separation systems showed some limits, such as interferences with the pancreatin used and no separation of acylglycerols and FAs at once, which could not be overcome by method optimization or modification. Hence, the combination of both orthogonal separation systems into a comprehensive HPTLC method (HPTLC×HPTLC) was evaluated (Figure 5). The normal phase separation mechanism separating according to polarity (apolar acylglycerol-separating mobile phase) was chosen to be the first dimension, whereas the reversed-phase separation mechanism separating according to lipophilicity (polar FA-separating mobile phase) was selected as the second dimension. The orthogonality was given by the very different selectivity of the first dimension in contrast to the second dimension. The orthogonal separation was first tested with reference standards (Figure 6A), and successful separation of acylglycerols and FAs could be achieved, in particular the separation of the previously co-eluted MAGs and FAs. The zone assignment of the FAs in the nanoGIT–HPTLC×HPTLC–FLD chromatogram was more difficult than via one-dimensional separation. Using the co-development of reference standards for each dimension on a separate plate (Supplementary Figure S4), a retardation shift could be observed for the FA zones. Since both mobile phases were prone to changes in relative humidity, the co-development of reference standards on the same plate was recommended to verify a retardation shift and proper assignment. The dominance of the C18:2 and C18:3 fatty acids (zones **c** and **d**, respectively) was also helpful for proper assignment.

Next, the on-surface digestion of an oil sample and the subsequent lipid separation of its lipolysis products on the same surface were demonstrated (Figure 6B). Therefore, flaxseed oil rich in C18:3 and C18:2 was selected for the proof of principle. A retardation shift was observed between reference standards (Figure 6A) and samples (Figure 6B). Using automated heart cuts to RP-HPLC–DAD–HESI-HRMS/MS (39), the highest eluting FAs (Figure 6B, zone **d**) were identified as C18:3, C18:2, C16:0, and C18:1 (Supplementary Figure S9, zone **d**, Supplementary Table S3). The most intense signal for this zone was from C18:3. Since it was stamped perpendicular to the band due to an accidentally 90°-rotated plate (positioned incorrectly) in the autoTLC interface (42), several FA signals were derived from and assigned to the neighboring bands. Some additional FAs were identified that could not be associated with the flaxseed oil sample: in zones **c** and **d**, oxidized C9:0 and oxidized C12:1 were identified, which could be explained as degradation products of linoleic acid and linolenic

10.3389/fnut.2023.1227546

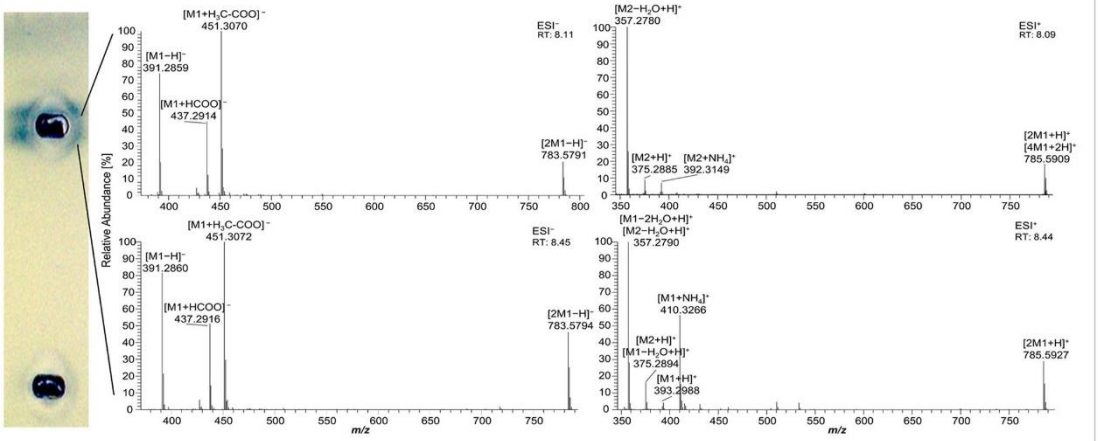

FIGURE 4
High-resolution mass spectra and corresponding ion species in the negative and positive ionization mode after nanoGIT–HPTLC –Vis/FLD–heart cut–RP-HPLC–DAD–HESI-HRMS/MS analysis of pancreatin developed with acetonitrile/water 4:1 (*V*/*V*) and molecular sieve (3 Å) up to 50 mm. **M1** = ursodeoxycholic acid, hyodeoxycholic acid, (cheno)deoxycholic acid, **M2** = cholenic acid; after the transfer of the interesting zones to the HRMS, the stamped plate was derivatized using the copper sulfate phosphoric acid reagent to check whether the elution head was properly positioned on the zones of interest.

acid, respectively. In zone **d**, C14:0, and zone **e**, C10:0, C11:0, and C12:0 were found. No fragmentation pattern was evident via HRMS/MS recording. The previously interfering pancreatin matrix was presently successfully separated from the FAs since most pancreatin impurities did not elute in the first dimension (in contrast, the FAs did) but did elute first in the second dimension. Thus, the FAs could be identified easily, in contrast to the one-dimensional separation of the reference standards (Figure 6B). Additionally, the eluted FA zones were fully separated from the bile acids, and their mass signals were not detected in the HRMS spectra anymore. By doing so, the nanoGIT–HPTLC×HPTLC–FLD method was proven to be successful in its application to real-life samples and in the detailed study of the lipolysis of complex samples. The whole sample was studied in all aspects on the same surface, and no sample part was lost.

3.3. Antibacterial profiles via nanoGIT–HPTLC×HPTLC–vis/FLD–bioassay–heart cut–RP-HPLC–DAD–HESI-HRMS/MS

After a successful proof of principle and implementation of the nanoGIT–HPTLC×HPTLC–FLD hyphenation, it was extended to bioassays to evaluate the antibacterial activity of the lipolysis products of digested flaxseed oil (Figures 7A, B) and coconut oil (Figure 7C) against Gram-negative *A. fischeri* and Gram-positive *B. subtilis* bacteria. The *A. fischeri* bioautogram revealed antibacterial effects for all seven FA reference standard zones as well as for the MAG, DAG (both isomers of diolein), and TAG reference standard zones (Figure 7A). In the *B. subtilis* bioautogram, the antibacterial detection was comparable, apart from the weaker response for two FA reference zones (**d** and **g**, Figure 7B), which was proven and confirmed in another experiment (Figure 5). These findings of antibacterial activity were consistent with the literature, which confirmed the antibacterial effect of FAs and MAGs (8, 41, 43, 44) and DAGs (9) against Gram-negative and Gram-positive bacteria. Usually, no antibacterial effect for TAGs (three ester groups but optionally double bonds) would be expected due to the lack of reactive functional groups (41, 45). However, the studied TAG, DAG, and MAG had one double bond in each acyl chain, which could induce a genotoxic or cytotoxic effect, as discussed later.

A separate study of all reference standards (Figure 3) showed in more detail the differences in their antibacterial effects against both Gram-negative and Gram-positive bacteria. The FAs C18:0 and C16:0 showed only a very light antibacterial response, whereas a metabolism-enhancing effect (detected as a halo surrounding an antibacterial effect in the center) was detected for C14:0. If co-eluted with C18:2 as in the standard track, this enhancing effect was weakened since the antibacterial effect of C18:2 was stronger (Figure 7, zone **c**). Compared to previous bioautograms on HPTLC plates silica gel 60 (39, 46), C16:0 showed no metabolism-enhancing effect on RP-18 W plates, which was explained by the doubled amount (10 µg/band vs. 5 µg/band) since such enhancing effects are dose-dependent and, in addition, also time-dependent (bioluminescence images monitored for 30 min). The antibacterial response for C8:0–12:0 was very intense against both Gram-negative *A. fischeri* and Gram-positive *B. subtilis* bacteria (Figure 3). In the *A. fischeri* bioautogram, a strong antibacterial effect of unsaturated FAs (C18:1–C18:3) against *A. fischeri* was observed, whereas an increase in the antibacterial effect with increasing double bonds was not observed. In the *B. subtilis* bioautogram, the antibacterial effect of unsaturated FAs against Gram-positive bacteria was weaker, which was directly evident since the same

10.3389/fnut.2023.1227546

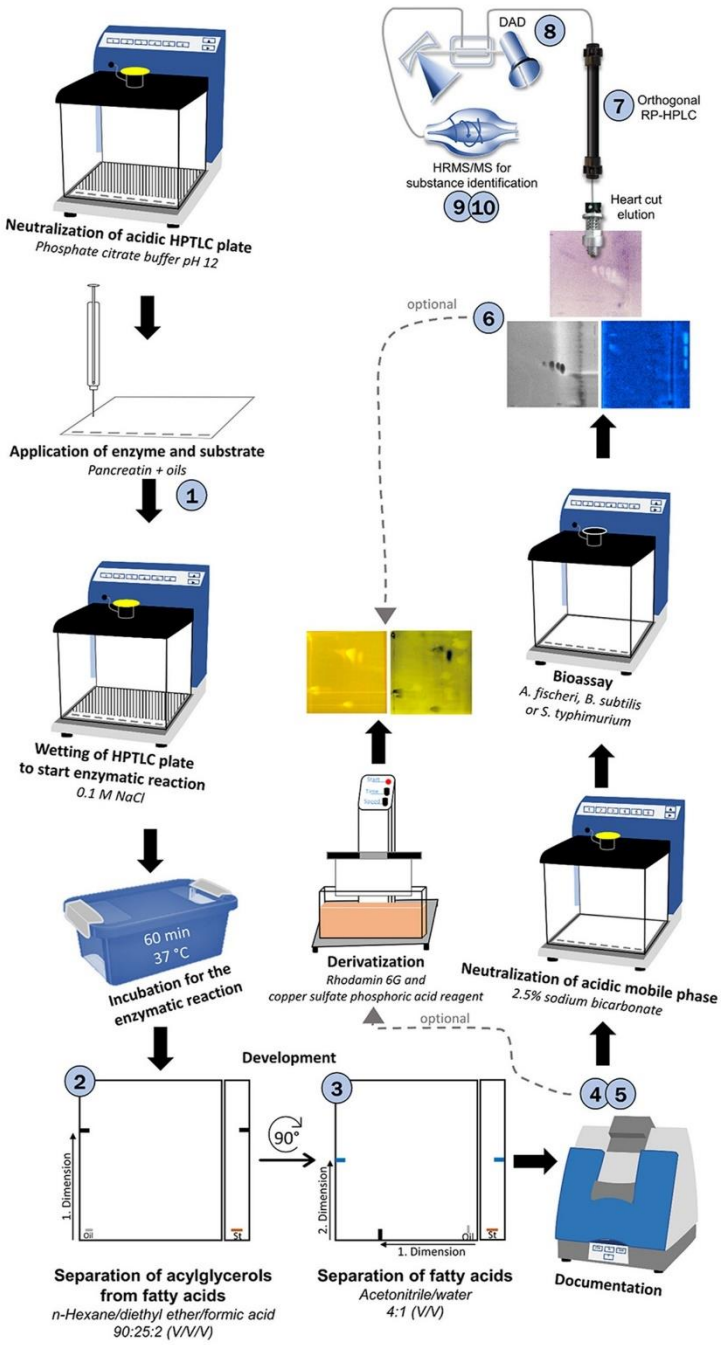

FIGURE 5
Schematic workflow of the developed 10D hyphenation, combining lipolysis with analysis and effect-detection on the same surface: nanoGIT–HPTLC×HPTLC–Vis/FLD–bioassay–heart cut–RP-HPLC–DAD–HESI-HRMS/MS.

10.3389/fnut.2023.1227546

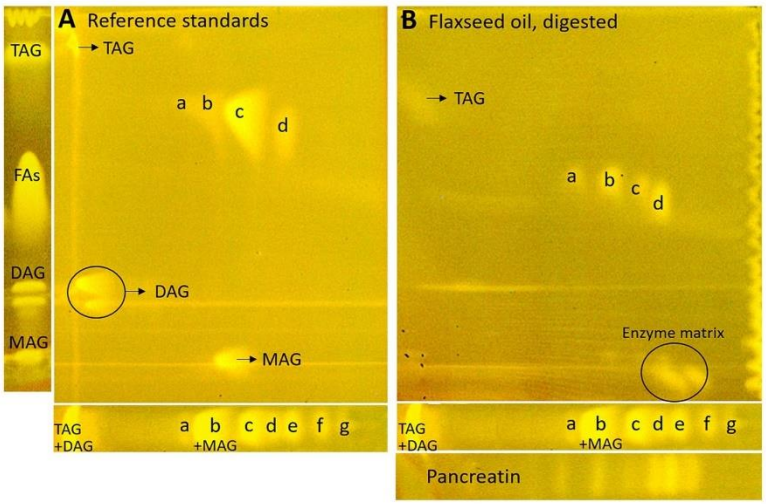

FIGURE 6
nanoGIT–HPTLC×HPTLC–FLD chromatograms of **(A)** the reference sample mixture (undigested) and **(B)** flaxseed oil (all 10 μg/band each) after lipolysis via overspraying of pancreatin (1 TAME U/band) on HPTLC RP-18 W plate, focused twice with acetone and, after a plate cut off at 15 mm, developed (from the cut edge) first with *n*-hexane/diethyl ether/formic acid 90:25:2 (*V*/*V*/*V*) up to 60 mm and, after 90°-plate turn, then with acetonitrile/water 4:1 (*V*/*V*, with a molecular sieve) up to 50 mm, derivatized with rhodamine 6G reagent, and detected at FLD 366 nm; for comparison respective one-dimensionally separated references, i.e., acylglycerols (**MAG**, **TAG**, and **DAG**) and fatty acids (**FAs**) such as stearic acid (C18:0, **a**), palmitic acid (C16:0, **b**), oleic acid (C18:1, **b**), linoleic acid (C18:2, **c**), myristic acid (C14:0, **c**), linolenic acid (C18:3, **d**), lauric acid (C12:0, **e**), capric acid (C10:0, **f**), and caprylic acid (C8:0, **g**), all 10 μg/band each.

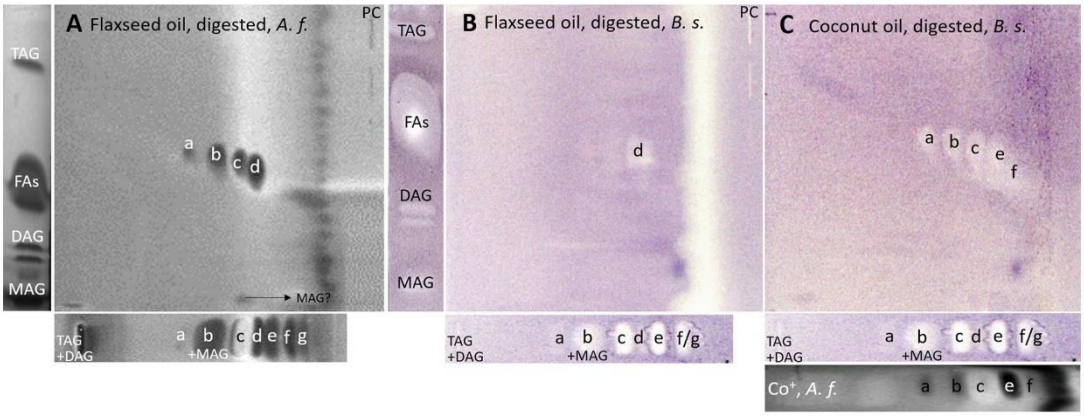

FIGURE 7
nanoGIT–HPTLC×HPTLC–bacterial bioassay–FLD/bioluminescence: Gram-negative *Aliivibrio fischeri* and Gram-positive *Bacillus subtilis* bioautograms showing the antibacterial activity (dark or colorless zones, respectively) of **(A, B)** digested flaxseed oil and **(C)** digested coconut oil (10 μg/band each) analyzed as in Figure 5, detected **(A)** via the bioluminescence (depicted as a grayscale image) after the *A. fischeri* bioassay and **(B, C)** at white light illumination (in remission) after the *B. subtilis* bioassay; positive controls (**PCs**) were 10–70 μg/band caffeine for *A. fischeri* bioassay or 10–70 ng/band tetracycline for *Bacillus subtilis* bioassay.

reference standard amounts were applied. Further research is needed to understand the mechanism of the observed biological responses of the FAs and acylglycerols. On the one hand, the biological response may derive from the acid head group and/or altered membrane permeability and thus be an antibacterial effect (as one example of the many different antibacterial mechanisms). On the other hand, the biological effect may derive from trace impurities (e.g., co-eluting epoxidized longer-chain fatty acids, Figure 3) in the reference standards (only up to 99% pure) or oxidative degradation and thus be a cytotoxic effect.

Unfortunately, the separation power of HPTLC is too weak to chromatographically differentiate all of them. Nevertheless, the powerful hyphenation with the bioassay provides the first evidence of harmful compounds present.

Using automated heart cuts of the interesting zones to RP-HPLC–DAD–HESI-HRMS/MS, the Gram-positive antibacterial zones of the reference standard track (Figure 7B) could be identified as the corresponding FAs (Figure 8, Supplementary Table S4). The assignments for zones **a** (C18:0) and **b** (C16:0/C18:1) were reached through pattern recognition. The latter assignments were more challenging since these FAs can also be HRMS system signals, which must be excluded first. Zones **c** and **e** were the most intense, containing co-eluting C14:0/C18:2 and C12:0/C18:3 (from adjacent zone **d**), respectively. Zone **d** (C18:3) was too close to the surrounding zones for an elution head-based analysis (too narrow for an additional elution head imprint). The C8:0 (zone **g**) was not separated in the 2D bioautogram but co-eluted with the C10:0 (zone **f**).

Considering the information obtained about the antibacterial behavior of the reference standards, the assignment of the lipolysis products of flaxseed oil was possible. Flaxseed oil, which mainly consists of C18:3, C18:1, and C18:2 and small amounts of C16:0 and C18:0 (38), showed after on-surface digestion and effect-directed analysis of four zones in the 2D *A. fischeri* bioautogram but only one zone in the 2D *B. subtilis* bioautogram (Figures 7A, B). The four zones in the 2D *A. fischeri* bioautogram were identified as C18:0 (zone **a**), C18:1/C16:0 (zone **b**), C18:2 (zone **c**), and C18:3 (zone **d**) in comparison to corresponding reference standards. No metabolism-enhancing effect was detected, and thus, the presence of C14:0 was excluded, which could have co-eluted with C18:2. The antibacterial zone **d** in the *B. subtilis* bioautogram (Figure 7B) was not so clear in the assignment, and thus identified via HRMS as C18:3 ($[M–H]^-$, *m/z* 277.2175, Δ ppm −0.71) and *trans*-4,5-epoxy-(*E*)-2-decenal ($C_{10}H_{16}O_2$, $[M–H]^-$, *m/z* 167.1078, Δ ppm −0.28). The latter is a typical genotoxic marker of linoleic acid oxidation (47–49).

As a further example, coconut oil was digested on-surface and analyzed for any antibacterial effects (Figure 7B). Coconut oil was selected as a quite different oil sample compared to flaxseed oil since it consists of comparatively much more SFAs of shorter chain lengths (C8:0–14:0, mostly C12:0 and C14:0) (37, 45). In contrast to the flaxseed oil (one antibacterial zone), the 2D *B. subtilis* bioautogram showed five antibacterial zones. Using the standard track, the FAs were identified as C18:0 (zone **a**), C18:1/C16:0 (zone **b**), C18:2/C14:0 (zone **c**), C12:0 (zone **e**), and C10:0 (zone **f**); however, C18:3 (zone **d**) was not present. The zone was heart-cut eluted to RP-HPLC–DAD–HESI-HRMS/MS (Figure 9, Supplementary Table S5) and revealed C14:0, C12:0, and C10:0 signals for the zones **c**, **e**, and **f**, respectively, but no significant signals for C18:0 and C18:1/C16:0. The *A. fischeri* bioautogram of the on-surface digested coconut oil (Figure 7C, Co^+) was used to confirm zone **c** to be C14:0 via its metabolism-enhancing effect as further proof.

3.4. Genotoxicity profiles via nanoGIT–HPTLC x HPTLC–vis/FLD–bioassay–heart cut–RP-HPLC–DAD–HESI-HRMS/MS

On-surface digested flaxseed oil revealed four genotoxic substance zones in the 2D bioautogram after the genotoxicity bioassay using the *S. typhimurium* TA1535/pSK1002 strain (Figure 10A). Two genotoxic substance zones did not migrate/elute at all in the second dimension, indicating apolar substances. One zone was assigned as TAGs via comparison with the standard track, and the second more apolar compound (marked* close to the solvent front of the first dimension) could be a genotoxic aromatic mineral oil contaminant; however, the latter assumption still needs proof. The genotoxic effect of TAGs was explained by the epoxidized fatty acid bond in the TAG molecule. Only two weak signals for the FAs were detected in the flaxseed oil and reference standard mixture (second dimension), which were assigned to C18:2/C14:0 and C18:3/C12:0 or C10:0. The digestion of the TAGs did not eliminate genotoxicity but showed that the FAs produced have strongly different genotoxic potentials. Both FAs were not natively fluorescent, which was expected (Figure 10B); however, native blue fluorescence was observed for the genotoxic TAGs zone of flaxseed oil, which indicated any impurities, e.g., of aromatic structure, as mentioned.

For adequate signal intensity via the genotoxicity bioassay, the amount of flaxseed oil was doubled (20 µg/band). In contrast to our previous very sensitive screening method (10), the amount of oil needed to be increased 200-fold due to the (I) enzymatic metabolization with a 60-min on-surface incubation known to lead to diffusion at the application zone (33), (II) interference by the buffer salts (Supplementary Figure S6), (III) 2D separation known to cause signal loss (50) by the 2-fold diffusion of the substances (as for C18:0, Figure 3), (IV) usage of RP-18 W plates known to be possibly less sensitive in the response, though dependent on the molecule, compared to silica gel 60 plates (51, 52), and (V) purchased oils opened just before analysis (assumedly, comparatively fewer oxidized degradation products). These reasons also explained why HRMS analysis was challenging since oxidized species present at the trace level were not found. In contrast to Morlock and Meyer (19), in which a six-fold concentrated genotoxic compound zone was directly transferred to the HRMS, only one weaker genotoxic compound zone was eluted from the 2D bioautogram, passed through an HPLC column via a prior desalting unit and diode-array detector, and finally reached the HRMS. The presence of highly potent genotoxic FA in oxidized and epoxidized forms at the trace level in various plant oils (10, 49, 53), and its potential sources, such as the unsaturated FAs C18:2 (54) and C18:3 (54, 55), were already reported. If safely delivered to a healthy liver, detoxification may be expected, as was recently shown via simulated on-surface S9 liver metabolization (10, 56). Furthermore, synergistic effects can occur (57), which can be detected and studied via the latest multiplex planar assays (51).

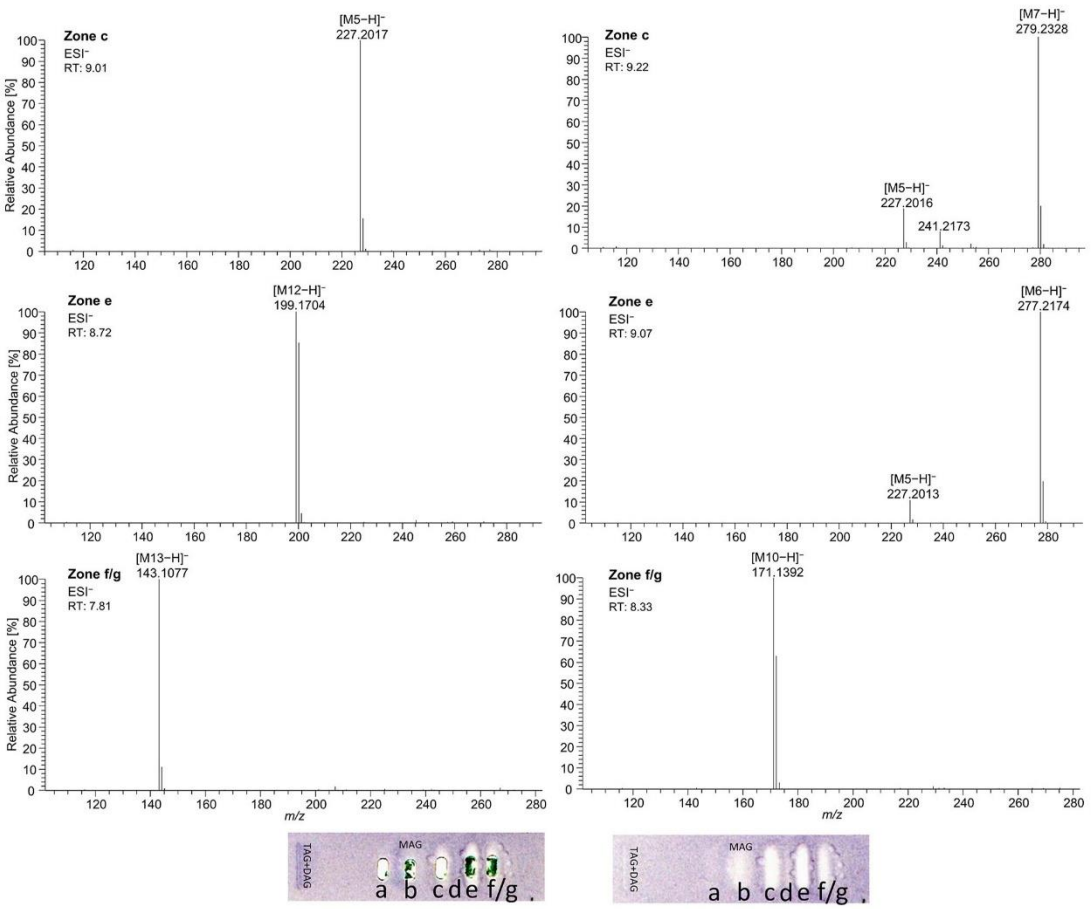

FIGURE 8
High-resolution mass spectra and corresponding ion species in the negative ionization mode after HPTLC–Vis–bioassay–heart cut–RP-HPLC–DAD–HESI-HRMS/MS analysis on HPTLC RP-18 W plates of all identified fatty acids of the standard reference track after the *Bacillus subtilis* bioassay, which was developed with acetonitrile/water 4:1 (*V*/*V*, with molecular sieve) up to 50 mm; **M5** = C14:0, **M6** = C18:3, **M7** = C18:2, **M10** = C10:0, **M12** = C12:0, and **M13** = C8:0.

The advantages and disadvantages of this quite new methodology against reported conventional methods (Supplementary Table S6) (58, 59), including the further ability of an effect-directed analysis after separation, strongly highlight the ability to illuminate every facet of the sample.

4. Conclusion

The on-surface simulated digestion on the RP-18 W plate, followed by comprehensive orthogonal HPTLC×HPTLC separation and effect-directed bioassay detection, successfully demonstrated a sustainable all-in-one digestion and analysis system. It allowed the analysis of the digestion during the intestinal phase itself and the resulting products as well as their biological effects via antibacterial and genotoxic bioassays. Since the developed method included a 2D development, the sample throughput was limited to only one sample per plate, but two sample plates could be processed at the same time with the HPTLC system used. The low solvent consumption (max. 16 ml per analysis/two plates) and rather short analysis time (5 h per analysis/two plates including bioassay and MS) endorsed the application as a multi-faceted analysis system. The developed 10D hyphenated nanoGIT–HPTLC×HPTLC–Vis/FLD–bioassay–heart cut–RP-HPLC–DAD–HESI-HRMS/MS methodology is a new tool that contributes to the understanding of complex samples and their harmful or beneficial metabolism/digestion products. Advantageously, no sample part was lost, and the whole sample was studied without any elaborate sample preparation. Digestion of the oils did not eliminate antibacterial effects or genotoxicity but showed that the metabolism products as well as a genotoxic contaminant may have harmful potential, which requires further investigation and consideration, or even reconsideration of

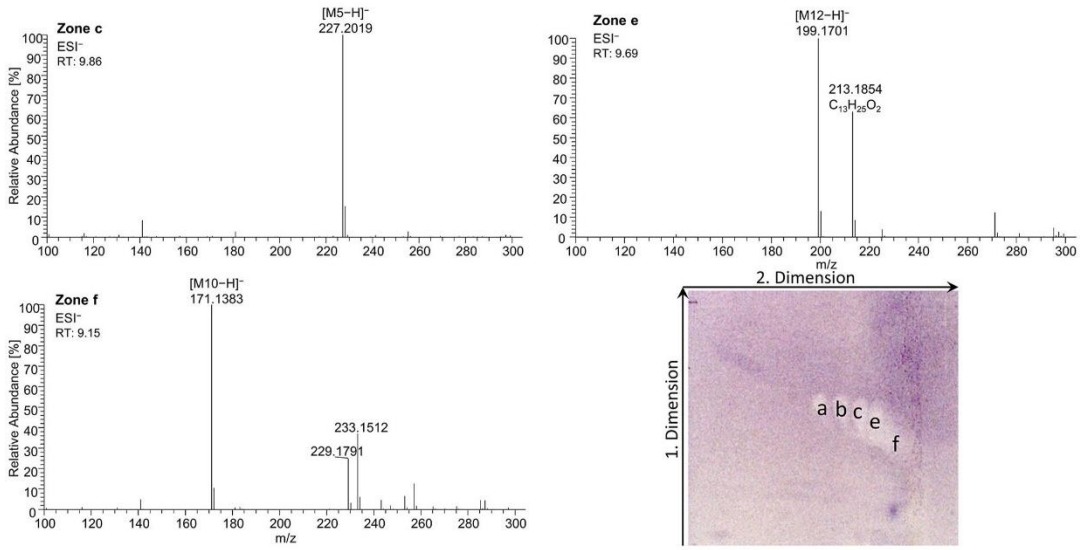

FIGURE 9
High-resolution mass spectra and corresponding ion species in the negative ionization mode after the nanoGIT–HPTLC×HPTLC–Vis–bioassay–heart cut–RP-HPLC–DAD–HESI-HRMS/MS analysis of all identified fatty acids of digested coconut oil after the *Bacillus subtilis* bioassay on HPTLC RP-18 W plates, where the plates were focused twice with acetone and cut at 15 mm, developed (from the cut edge) first with *n*-hexane/diethyl ether/formic acid 90:25:2 (*V*/*V*/*V*) up to 60 mm, after 90° plate turn, and then with acetonitrile/water 4:1 (*V*/*V*, with molecular sieve) up to 50 mm; retention time shift due to HPLC pump exchange; **M5** = C14:0, **M10** = C10:0, and **M12** = C12:0.

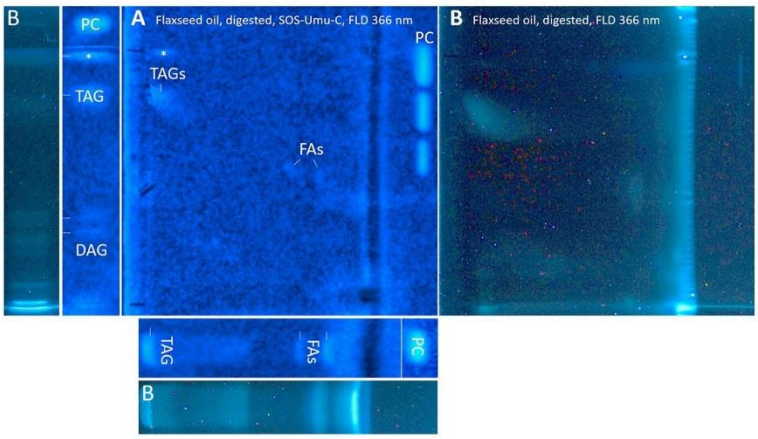

FIGURE 10
nanoGIT–HPTLC×HPTLC–FLD–SOS-Umu-C bioassay–FLD: genotoxicity bioautogram (using *Salmonella typhimurium* TA1535/pSK1002) of digested flaxseed oil (20 µg/band) analyzed as in Figure 5, detected at FLD 366 nm **(A)** after the genotoxicity bioassay, showing genotoxic (blue fluorescent) TAGs, DAGs, FAs, and an unknown apolar genotoxic substance zone (*, e.g., mineral oil aromatic hydrocarbons); **(B)** comparative chromatogram before the bioassay; 0.2–1.0 ng/band 4-nitroquinoline-1-oxide as a positive control (**PC**).

the current risk assessment. Literature about the potential of edible vegetable oils as next-generation antimicrobial agents was confirmed, whereas the observed genotoxic potential remaining after metabolic digestion needs further attention regarding food safety.

Data availability statement

The original contributions presented in the study are included in the article/Supplementary material, further inquiries can be directed to the corresponding author.

Author contributions

IM: conceptualization, methodology, experimental analysis, data analysis, and writing—original draft. AG: experimental analysis and data analysis. GM: conceptualization, methodology, supervision, and writing—review and editing. All authors contributed to the article and approved the submitted version.

Funding

Instrumentation was partially funded by the Deutsche Forschungsgemeinschaft (DFG, German Research Foundation)—INST 162/536-1 FUGG and INST 162/471-1 FUGG.

Acknowledgments

The authors would like to thank Lisa-Marie Niemeier for support.

Dedication

Dedicated to the lifework of Prof. Dr. Colin Poole, Wayne State University, Detroit, USA.

Conflict of interest

The authors declare that the research was conducted in the absence of any commercial or financial relationships that could be construed as a potential conflict of interest.

The reviewer PR declared a past co-authorship with the author GM to the handling editor.

Publisher's note

Supplementary material

The Supplementary Material for this article can be found online at: https://www.frontiersin.org/articles/10.3389/fnut.2023.1227546/full#supplementary-material

References

1. Wolfram G, Bechthold A, Boeing H, Ellinger S, Hauner H, Kroke A, et al. Evidence-based guideline of the German Nutrition Society: fat intake and prevention of selected nutrition-related diseases. *Ann Nutr Metab.* (2015) 67:141–204. doi: 10.1159/000437243

2. *Deutsche Gesellschaft für Ernährung, Österreichische Gesellschaft für Ernährung, Schweizerische Gesellschaft für Ernährung.* D-A-CH-Referenzwerte für die Nährstoffzufuhr. Bonn (2018).

3. Doucet E, Alméras N, White MD, Després JP, Bouchard C, Tremblay A. Dietary fat composition and human adiposity. *Eur J Clin Nutr.* (1998) 52:2–6. doi: 10.1038/sj.ejcn.1600500

4. Simopoulos AP. An increase in the omega-6/omega-3 fatty acid ratio increases the risk for obesity. *Nutrients.* (2016) 8:128. doi: 10.3390/nu8030128

5. Keys A, Mickelsen O, Miller EVO, Chapman CB. The relation in man between cholesterol levels in the diet and in the blood. *Science.* (1950) 112:79–81. doi: 10.1126/science.112.2899.79

6. Hooper L, Martin N, Jimoh OF, Kirk C, Foster E, Abdelhamid AS. Reduction in saturated fat intake for cardiovascular disease. *Cochrane Database Syst Rev.* (2020) 5:CD011737. doi: 10.1002/14651858.CD011737.pub2

7. Abdelhamid AS, Martin N, Bridges C, Brainard JS, Wang X, Brown TJ, et al. Polyunsaturated fatty acids for the primary and secondary prevention of cardiovascular disease. *Cochrane Database Syst Rev.* (2018) 11:CD012345. doi: 10.1002/14651858.CD012345.pub3

8. Casillas-Vargas G, Ocasio-Malavé C, Medina S, Morales-Guzmán C, Del Valle RG, Carballeira NM, et al. Antibacterial fatty acids: an update of possible mechanisms of action and implications in the development of the next-generation of antibacterial agents. *Prog Lipid Res.* (2021) 82:101093. doi: 10.1016/j.plipres.2021.101093

9. Mehl A, Morlock GE. Strong antibacterial effects in animal-derived food detected via non-target planar bioassays. *Food Chem Adv.* (2023). doi: 10.1016/j.focha.2023.100283

10. Morlock GE, Meyer D. Designed genotoxicity profiling detects genotoxic compounds in staple food such as healthy oils. *Food Chem.* (2023) 408:135253. doi: 10.1016/j.foodchem.2022.135253

11. Russo GL. Dietary n-6 and n-3 polyunsaturated fatty acids: from biochemistry to clinical implications in cardiovascular prevention. *Biochem Pharmacol.* (2009) 77:937–46. doi: 10.1016/j.bcp.2008.10.020

12. Simopoulos AP. The importance of the ratio of omega-6/omega-3 essential fatty acids. *Biomed Pharmacother.* (2002) 56:365–79. doi: 10.1016/S0753-3322(02)00253-6

13. Czernichow S, Thomas D, Bruckert E. n-6 Fatty acids and cardiovascular health: a review of the evidence for dietary intake recommendations. *Br J Nutr.* (2010) 104:788–96. doi: 10.1017/S0007114510002096

14. Salter AM. Dietary fatty acids and cardiovascular disease. *Animal.* (2013) 7(Suppl 1):163–71. doi: 10.1017/S1751731111002023

15. Bundesministerium für Ernährung und Landwirtschaft. *Konsum von Ölen und Fetten in Deutschland in den Jahren 2008 bis 2019 (in 1.000 Tonnen Reinfett): [Graph].* Deutschland (2021).

16. Bundesministerium für Ernährung und Landwirtschaft. *Konsum von pflanzlichen Ölen und Fetten in Deutschland nach Art in den Jahren 2007 bis 2019 (in 1.000 Tonnen Reinfett): [Graph].* Deutschland (2021).

17. Fedeli E, Jacini G. Lipid composition of vegetable oils. *Adv Lipid Res.* (1971) 9:335–82. doi: 10.1016/B978-0-12-024909-1.50014-4

18. Fronimaki P, Spyros A, Christophoridou S, Dais P. Determination of the diglyceride content in greek virgin olive oils and some commercial olive oils by employing (31)P NMR spectroscopy. *J Agric Food Chem.* (2002) 50:2207–13. doi: 10.1021/jf011380q

19. Bosque-Sendra JM, Cuadros-Rodríguez L, Ruiz-Samblás C, de La Mata AP. Combining chromatography and chemometrics for the characterization and authentication of fats and oils from triacylglycerol compositional data–a review. *Anal Chim Acta.* (2012) 724:1–11. doi: 10.1016/j.aca.2012.02.041

20. Carlier H, Bernard A, Caselli C. Digestion and absorption of polyunsaturated fatty acids. *Reprod Nutr Dev.* (1991) 31:475–500. doi: 10.1051/rnd:19910501

21. Carriere F, Barrowman JA, Verger R, René L. Secretion and contribution to lipolysis of gastric and pancreatic lipases during a test meal in humans. *Gastroenterology.* (1993) 105:876–88. doi: 10.1016/0016-5085(93)90908-U

22. Desnuelle P, Savary P. Specificities of lipases. *J Lipid Res.* (1963) 4:369–84. doi: 10.1016/S0022-2275(20)40278-0

23. Giang TM, Gaucel S, Brestaz P, Anton M, Meynier A, Trelea IC, et al. Dynamic modeling of *in vitro* lipid digestion: individual fatty acid release and bioaccessibility kinetics. *Food Chem.* (2016) 194:1180–8. doi: 10.1016/j.foodchem.2015.08.125

24. Yang LY, Kuksis A, Myher JJ. Lipolysis of menhaden oil triacylglycerols and the corresponding fatty acid alkyl esters by pancreatic lipase *in vitro*: a reexamination. *J Lipid Res.* (1990) 31:137–47. doi: 10.1016/S0022-2275(20)42768-3

25. McClements DJ Li Y. Review of *in vitro* digestion models for rapid screening of emulsion-based systems. *Food Funct.* (2010) 1:32–59. doi: 10.1039/c0fo00111b

26. Calvo-Lerma J, Fornés-Ferrer V, Heredia A, Andrés A. *In vitro* digestion of lipids in real foods: influence of lipid organization within the food matrix and interactions with nonlipid components. *J Food Sci.* (2018) 83:2629–37. doi: 10.1111/1750-3841.14343

27. Minekus M, Alminger M, Alvito P, Ballance S, Bohn T, Bourlieu C, et al. A standardised static *in vitro* digestion method suitable for food - an international consensus. *Food Funct.* (2014) 5:1113–24. doi: 10.1039/C3FO60702J

28. Morlock GE, Drotleff L, Brinkmann S. Miniaturized all-in-one nanoGIT+active system for on-surface metabolization, separation and effect imaging. *Anal Chim Acta.* (2021) 1154:338307. doi: 10.1016/j.aca.2021.338307

29. Helbig A, Silletti E, Timmerman E, Hamer RJ, Gruppen H. *In vitro* study of intestinal lipolysis using pH-stat and gas chromatography. *Food Hydrocoll.* (2012) 28:10–9. doi: 10.1016/j.foodhyd.2011.11.007

30. Mat DJ, Le Feunteun S, Michon C, Souchon I. *In vitro* digestion of foods using pH-stat and the INFOGEST protocol: impact of matrix structure on digestion kinetics of macronutrients, proteins and lipids. *Food Res Int.* (2016) 88:226–33. doi: 10.1016/j.foodres.2015.12.002

31. Janssen H-G, Hrnciník K, Szórádi A, Leijten M. An improved method for sn-2 position analysis of triacylglycerols in edible oils and fats based on immobilised lipase D (*Rhizopus delemar*). *J Chromatogr A.* (2006) 1112:141–7. doi: 10.1016/j.chroma.2005.11.097

32. *European Pharmacopoeia: Amtliche deutsche Ausgabe.* Stuttgart: Deutscher Apotheker Verlag (2017), p. 5858.

33. Müller I, Morlock GE. Quantitative saccharide release of hydrothermally treated flours by validated salivary/pancreatic on-surface amylolysis (nanoGIT) and high-performance thin-layer chromatography. *Food Chem.* (2023) (in press). doi: 10.1016/j.foodchem.2023.137145

34. Schwertner HA, Mosser EL. Comparison of lipid fatty acids on a concentration basis vs weight percentage basis in patients with and without coronary artery disease or diabetes. *Clin Chem.* (1993) 39:659–63. doi: 10.1093/clinchem/39.4.659

35. European Committee for Standardization. *Water Quality - Determination of the Inhibitory Effect of Water Samples on the Light Emission of Vibrio Fischeri (Luminescent Bacteria Test): Part 1: Method Using Freshly Prepared Bacteria* (2009).

36. Vult von Steyern F, Josefsson JO, Tågerud S. Rhodamine B, a fluorescent probe for acidic organelles in denervated skeletal muscle. *J Histochem Cytochem.* (1996) 44:267–74. doi: 10.1177/44.3.8648087

37. Orsavova J, Misurcova L, Ambrozova JV, Vicha R, Mlcek J. Fatty acids composition of vegetable oils and its contribution to dietary energy intake and dependence of cardiovascular mortality on dietary intake of fatty acids. *Int J Mol Sci.* (2015) 16:12871–90. doi: 10.3390/ijms160612871

38. Silska G. Walkowiak M. Comparative analysis of fatty acid composition in 84 accessions of flax (*Linum usitatissimum* L). *J Pre Clin Clin Res.* (2019) 13:118–29. doi: 10.26444/jpccr/111889

39. Schreiner T, Eggerstorfer NM, Morlock GE. Ten-dimensional hyphenation including simulated static gastro-intestinal digestion on the adsorbent surface, planar assays, and bioactivity evaluation for meal replacement products. *Food Funct.* (2023) 14:344–53. doi: 10.1039/D2FO02610D

40. Urdaneta V, Casadesús J. Interactions between bacteria and bile salts in the gastrointestinal and hepatobiliary tracts. *Front Med.* (2017) 4:163. doi: 10.3389/fmed.2017.00163

41. Desbois AP, Smith VJ. Antibacterial free fatty acids: activities, mechanisms of action and biotechnological potential. *Appl Microbiol Biotechnol.* (2010) 85:1629–42. doi: 10.1007/s00253-009-2355-3

42. Mehl A, Schwack W, Morlock GE. On-surface autosampling for liquid chromatography-mass spectrometry. *J Chromatogr A.* (2021) 1651:462334. doi: 10.1016/j.chroma.2021.462334

43. Kabara JJ, Swieczkowski DM, Conley AJ, Truant JP. Fatty acids and derivatives as antimicrobial agents. *Antimicrob Agents Chemother.* (1972) 2:23–8. doi: 10.1128/AAC.2.1.23

44. Churchward CP, Alany RG, Snyder LAS. Alternative antimicrobials: the properties of fatty acids and monoglycerides. *Crit Rev Microbiol.* (2018) 44:561–70. doi: 10.1080/1040841X.2018.1467875

45. Silalahi J, Permata YM, de lux putra E. Antibacterial activity of hydrolyzed virgin coconut oil. *Asian J Pharm Clin Res.* (2014) 7:90–4. Available online at: https://journals.innovareacademics.in/index.php/ajpcr/article/view/1042

46. Chandana NGASS, Morlock GE. Eight different bioactivity profiles of 40 cinnamons by multi-imaging planar chromatography hyphenated with effect-directed assays and high-resolution mass spectrometry. *Food Chem.* (2021) 357:129135. doi: 10.1016/j.foodchem.2021.129135

47. Gassenmeier K, Schieberle P. Formation of the intense flavor compound trans-4,5-epoxy-(E)-2-decenal in thermally treated fats. *J Am Oil Chem Soc.* (1994) 71:1315–9. doi: 10.1007/BF02541347

48. Nieva-Echevarría B, Goicoechea E, Guillén MD. Effect of adding alpha-tocopherol on the oxidation advance during *in vitro* gastrointestinal digestion of sunflower and flaxseed oils. *Food Res Int.* (2019) 125:108558. doi: 10.1016/j.foodres.2019.108558

49. Silano V, Bolognesi C, Castle L, Cravedi J-P, Engel K-H, Fowler P. et al. Scientific Opinion on Flavouring Group Evaluation 226 Revision 1 (FGE226Rev1): consideration of genotoxicity data on one α,β-unsaturated aldehyde from chemical subgroup 111(b) of FGE19. *EFSA J.* (2017) 15:e04847. doi: 10.2903/j.efsa.2017.4847

50. Stütz L, Schulz W, Winzenbacher R. Identification of acetylcholinesterase inhibitors in water by combining two-dimensional thin-layer chromatography and high-resolution mass spectrometry. *J Chromatogr A.* (2020) 1624:461239. doi: 10.1016/j.chroma.2020.461239

51. Ronzheimer A, Schreiner T, Morlock GE. Multiplex planar bioassay detecting estrogens, antiestrogens, false-positives and synergists as sharp zones on normal phase. *Phytomedicine.* (2022) 103:154230. doi: 10.1016/j.phymed.2022.154230

52. Klingelhöfer I, Morlock GE. Sharp-bounded zones link to the effect in planar chromatography-bioassay-mass spectrometry. *J Chromatogr A.* (2014) 1360:288–95. doi: 10.1016/j.chroma.2014.07.083

53. Guillen MD, Goicoechea E. Formation of oxygenated α,β-unsaturated aldehydes and other toxic compounds in sunflower oil oxidation at room temperature in closed receptacles. *Food Chem.* (2008) 111:157–64. doi: 10.1016/j.foodchem.2008.03.052

54. Rojas-Molina M, Campos-Sánchez J, Analla M, Muñoz-Serrano A, Alonso-Moraga A. Genotoxicity of vegetable cooking oils in the *Drosophila* wing spot test. *Environ Mol Mutagen.* (2005) 45:90–5. doi: 10.1002/em.20078

55. Anter J, Campos-Sánchez J, Hamss RE, Rojas-Molina M, Muñoz-Serrano A, Analla M, et al. Modulation of genotoxicity by extra-virgin olive oil and some of its distinctive components assessed by use of the *Drosophila* wing-spot test. *Mutat Res.* (2010) 703:137–42. doi: 10.1016/j.mrgentox.2010.08.012

56. Kiwamoto R, Spenkelink A, Rietjens IMCM, Punt A. A physiologically based in silico model for trans-2-hexenal detoxification and DNA adduct formation in human including interindividual variation indicates efficient detoxification and a negligible genotoxicity risk. *Arch Toxicol.* (2013) 87:1725–37. doi: 10.1007/s00204-013-1091-8

57. Beeharry N, Lowe JE, Hernandez AR, Chambers JA, Fucassi F, Cragg PJ, et al. Linoleic acid and antioxidants protect against DNA damage and apoptosis induced by palmitic acid. *Mutat Res.* (2003) 530:27–33. doi: 10.1016/S0027-5107(03)00134-9

58. Clinical and Laboratory Standards Institute. *Performance Standards for Antimicrobial Disk Susceptibility Tests*. Wayne, PA: CLSI Standard M02 Clinical and Laboratory Standards Institute (2018).

59. Clinical and Laboratory Standards Institute. *Performance Standards for Dilution Antimicrobial Susceptibility Tests for Bacteria that Grow Aerobically*. Wayne, PA: CLSI Standard M07 Clinical and Laboratory Standards Institute (2018).

frontiers

Supplementary Material

Bioactive profiles of edible vegetable oils determined using 10D hyphenated comprehensive high-performance thin-layer chromatography (HPTLC×HPTLC) with on-surface metabolism (nanoGIT) and planar bioassays

Isabel Müller[1], Alexander Gulde[1], Gertrud E. Morlock[1,2,#,*]

[1]Institute of Nutritional Science, Chair of Food Science, as well as Interdisciplinary Research Centre for Biosystems, Land Use and Nutrition, Justus Liebig University Giessen, Heinrich-Buff-Ring 26-32, 35392 Giessen, Germany

[2]Center for Sustainable Food Systems, Justus Liebig University Giessen, Senckenbergstr. 3, 35390 Giessen, Germany

[#]Member of the More than One Constituent Substances (MOCS) Initiative, www.vielstoffgemische.de

Dedicated to the lifework of Prof. Dr. Colin Poole, Wayne State University, Detroit, USA

*Corresponding authors: Prof. Dr. Gertrud Morlock, phone: +49-641-9939141; fax +49-641-99-39149, email: gertrud.morlock@uni-giessen.de

Supplementary Material

Table of contents

Table S2

Supplier information of all investigated oil samples.

Vegetable oil	Supplier or producer (brand)	Best before	Production type
Flaxseed oil	dm Bio, Karlsruhe, Germany	09.2021	Organic
Palm oil	Ölmühle Solling, Boffzen, Germany	10.2022	Organic, red
Hemp oil	Ölmühle Solling, Boffzen, Germany	12.2021	Conventional
Sunflower oil	Huilerie Bio Occitane, Bram, France (Rewe Bio)	06.2022	Organic
Walnut oil	bio Zentrale, Wittibreut, Germany	02.2022	Organic
Coconut oil	Palmin, Elmshorn, Germany	Expired	Conventional
Olive oil	El. Renieris & Co., Kissamos/Crete, Greece (Lidl, Eridanous)	01.2022	Conventional, extra native
Canola oil	Mazola, Elmshorn, Germany	Expired	Conventional
Soybean oil	Heuschen & Schrouff, Landgraaf, Netherlands	05.2022	Conventional

Table S3

Evaluated masses, substances, and ion species of enzyme interferences via nanoGIT−HPTLC −Vis/FLD−heart cut−RP-HPLC−DAD− HESI-HRMS/MS (Fig. S7).

RT [min]	Substance	*m/z*	Mass error [Δ ppm]	Ion species
8.09 (ESI^+) 8.11 (ESI^-)	UDCA, HDCA, CDCA, DCA	391.2858	−2.57	$[M1-H]^-$
		437.2913	−2.28	$[M1+HCOO]^-$
		451.3070	−2.36	$[M1+CH_3\text{-}COO]^-$
		783.5791	−2.02	$[2M1-H]^-$
		785.5909	2.18	$[2M1+H]^+$ $[4M1+2H]^+$
	Cholenic acid	357.2780	2.20	$[M2-H_2O+H]^+$
		375.2885	2.45	$[M2+H]^+$
		392.3149	2.57	$[M2+NH_4]^+$
8.45	UDCA, HDCA, CDCA, DCA	391.2860	−3.05	$[M1-H]^-$
		437.2916	−1.61	$[M1+HCOO]^-$
		451.3072	−1.48	$[M1+CH_3\text{-}COO]^-$
		783.5794	-1.73	$[2M1-H]^-$
		393.2988	2.91	$[M1+H]^+$
		410.3266	−0.35	$[M1+NH_4]^+$
		785.5927	−0.15	$[2M1+H]^+$
	UDCA, HDCA, CDCA, DCA, Cholenic acid	357.2790	−0.40	$[M1-2H_2O+H]^+$
				$[M2-H_2O+H]^+$
		375.2894	−0.05	$[M1-H_2O+H]^+$
				$[M2+H]^+$

M1 = UDCA, HDCA, CDCA, DCA; **M2** = Cholenic acid; **UDCA**: Ursodeoxycholic acid; **HDCA**: Hyodeoxycholic acid; **(C)DCA**: (Cheno)deoxycholic acid

Table S4

Evaluated masses, substances, sum formula and ion species of identified fatty acids after the on-surface digestion of flaxseed oil via nanoGIT−HPTLC×HPTLC−Vis/FLD−heart cut−RP-HPLC−DAD−HESI-HRMS/MS (Fig. S10).

Zone	RT [min]	Substance	Sum formula	*m/z*	Mass error [Δ ppm]	Ion species
c	6.71	Oxidized C9:0	C9 H15 O3	171.1028	−0.77	$[M3-H]^-$
	7.49	Oxidized C12:1	C12 H19 O3	211.1340	−0.15	$[M4-H]^-$
d	6.71	Oxidized C9:0	C9 H15 O3	171.1028	−0.77	$[M3-H]^-$
	7.49	Oxidized C12:1	C12 H19 O3	211.1340	−0.15	$[M4-H]^-$
	9.03	C14:0	C14 H27 O2	227.2018	−0.64	$[M5-H]^-$
		C18:3	C18 H29 O2	277.2175	−0.71	$[M6-H]^-$
	9.24	C18:2	C18 H31 O2	279.2334	−1.60	$[M7-H]^-$
	9.38	C16:0	C16 H31 O2	255.2334	−1.75	$[M8-H]^-$
	9.49	C18:1	C18 H33 O2	281.2489	−1.05	$[M9-H]^-$
e	8.29	C10:0	C10 H19 O2	171.1391	−0.27	$[M10-H]^-$
	8.51	C11:0	C11 H21 O2	185.1546	0.56	$[M11-H]^-$
	8.68	C12:0	C12 H23 O2	199.1707	−1.74	$[M12-H]^-$

M3 = oxidized C9:0, **M4** = oxidized C12:1, **M5** = C14:0, **M6** = C18:3, **M7** = C18:2, **M8** = C16:0, **M9** = C18:1, **M10** = C10:0, **M11** = C11:0, **M12** = C12:0

Table S5

Evaluated masses, substances, sum formula and ion species of identified fatty acids of the standard reference track after subsequent *B. subtilis* assay via HPTLC−Vis/FLD−bioassay−heart cut−RP-HPLC−DAD−HESI-HRMS/MS (Fig. S11).

Zone	RT [min]	Substance	Sum formula	*m/z*	Mass error [Δ ppm]	Ion species
c	9.01	C14:0	C14 H27 O2	227.2017	−0.07	$[M5-H]^-$
	9.22	C18:2	C18 H31 O2	279.2328	0.55	$[M7-H]^-$
e	8.72	C12:0	C12 H23 O2	199.1702	0.77	$[M12-H]^-$
	9.07	C18:3	C18 H29 O2	277.2174	−0.35	$[M6-H]^-$
f	7.81	C8:0	C8 H15 O2	143.1077	0.38	$[M13-H]^-$
	8.33	C10:0	C10 H19 O2	171.1392	−0.85	$[M10-H]^-$

M5 = C14:0, **M6** = C18:3, **M7** = C18:2, **M10** = C10:0, **M12** = C12:0, **M13** = C8:0

Table S6

Evaluated masses, substances, sum formula and ion species of identified fatty acids after the on-surface digestion of coconut oil and subsequent *B. subtilis* assay via nanoGIT−HPTLC×HPTLC−Vis/FLD−bioassay−heart cut−RP-HPLC−DAD−HESI-HRMS/MS (Fig. S12). Retention time shift due to HPLC pump exchange.

Zone	RT [min]	Substance	Sum formula	*m/z*	Mass error [Δ ppm]	Ion species
c	9.86	C14:0	C14 H27 O2	227.2019	−0.95	$[M5-H]^-$
e	9.69	C12:0	C12 H23 O2	199.1703	0.42	$[M12-H]^-$
f	9.15	C10:0	C10 H19 O2	171.1389	0.96	$[M10-H]^-$

M5 = C14:0, **M10** = C10:0, **M12** = C12:0

Table S7

Advantages and disadvantages of the developed nanoGIT−HPTLC×HPTLC−Vis/FLD−bioassay−heart cut−RP-HPLC−DAD−HESI-HRMS/MS method in comparison with literature

Method highlights	**Compared method**	**Advantages**	**Disadvantages**
All-in-one system (metabolization + analysis)	<u>TAG analysis</u> GC-FID (29) <u>Fatty acid analysis</u> - HPLC-ELSD (23) - GC-FID (23, 29) <u>Sum parameter value</u> - Spectrophotometric assay kit (26) - pH-stat titration (29) - GC-FID (29)	- No sample loss - No sample preparation after metabolization - Miniaturized approach (less amounts, more sustainable, faster metabolization)	
Analysis of detailed acylglycerol composition with subsequent detailed fatty acid composition		- Separation of TAGs, DAGs, MAGs, and FAs in one run - No sample loss - No fatty acid methyl esters needed - No pre-chromatographic derivatization step - Evaluation of sum parameter values possible if calibration on plate - Subsequent detailed FA analysis possible	- No detailed TAG composition
Application of bioassays and hyphenation with HRMS/MS	Disk diffusion (58) Broth microdilution (59)	- No sample loss - Detailed analysis and identification of the individual bioactive substance in the food matrix - Identification of signal-responsible substances after the bioassay	

GC-FID = gas chromatography with flame ionization detector, HPLC-ELSD = high-performance liquid chromatography with evaporative light scattering detector, TAG = triacylglycerol, DAG = diacylglycerol, MAG = monoacylglycerol, FA = fatty acid

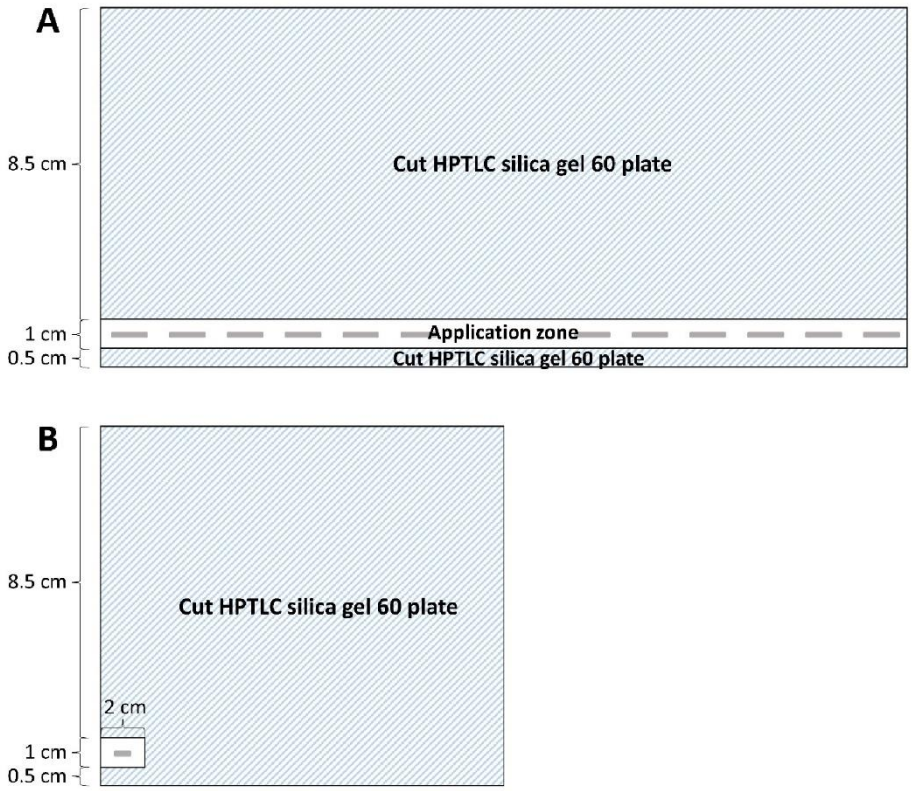

Figure S1: Schemes of the cover plates (HPTLC silica gel 60, layer faced upward) used for neutralization of the HPTLC RP-18 W plates before the application for (**A**) one-dimensional development and (**B**) two-dimensional development.

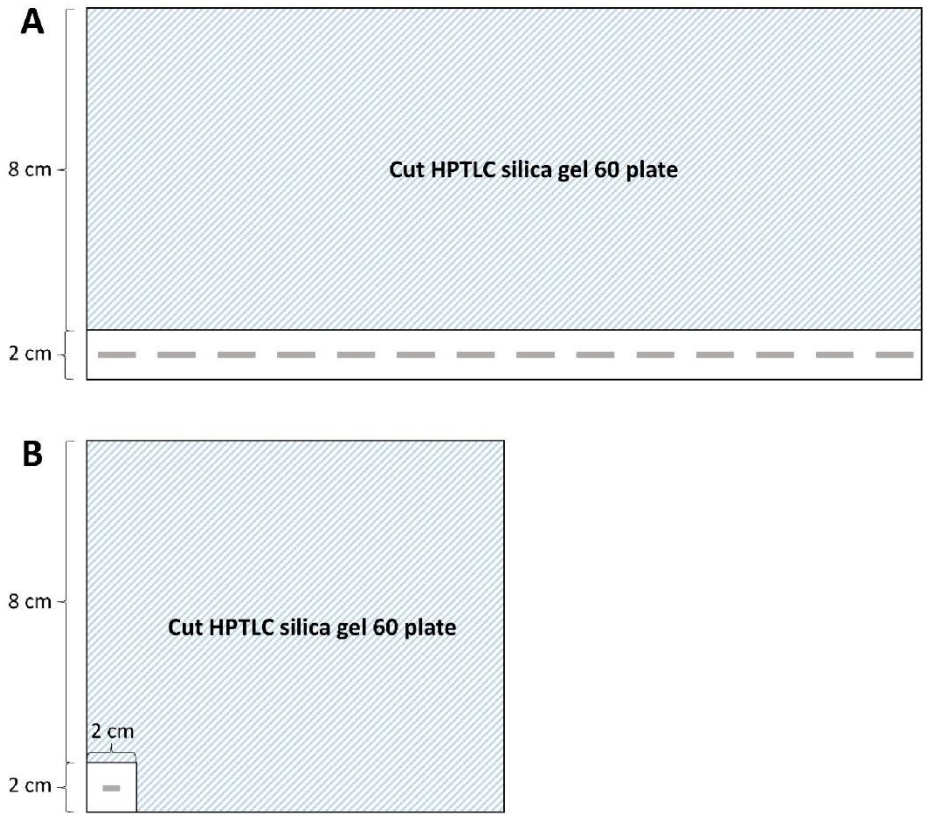

Figure S2: Schemes of the cover plates (HPTLC silica gel 60, layer faced upward) used for wetting of the HPTLC RP-18 W plates before the incubation for (**A**) one-dimensional development and (**B**) two-dimensional development.

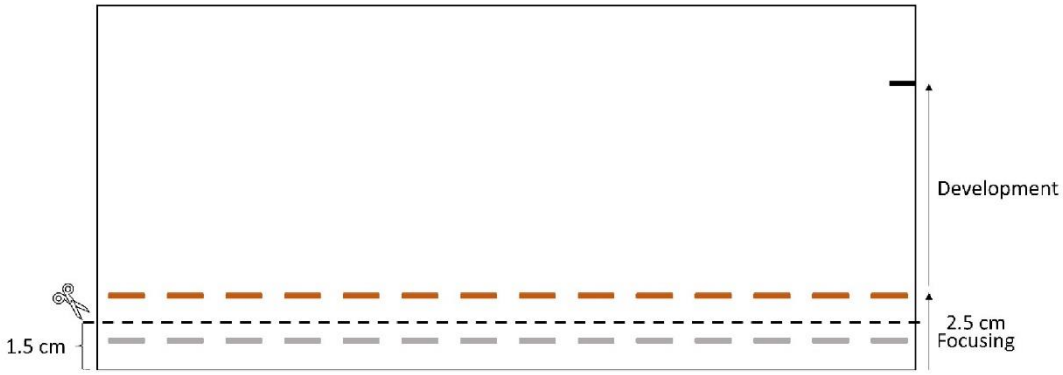

Figure S3: Scheme of the focusing process to remove enzyme interferences for the one-dimensional development.

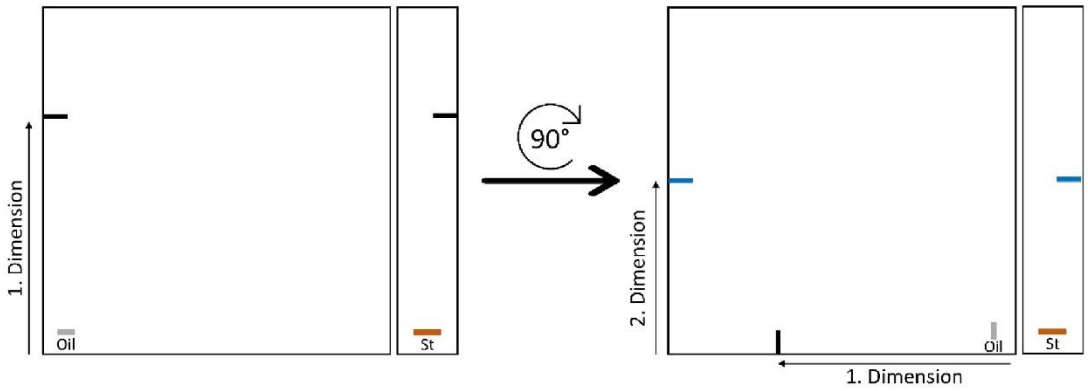

Figure S4: Scheme and orientation of the two-dimensional development on a 10 cm × 10 cm plate with additional co-development of the standards on a separate plate.

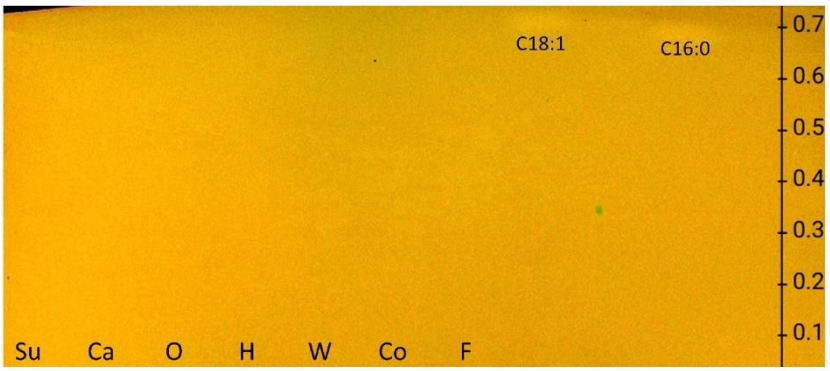

Figure S5: HPTLC RP-18 chromatogram of triacylglycerols in sunflower (Su), canola (Ca), olive (O), hemp (H), walnut (W), coconut (Co), and flaxseed (F) oil and fatty acid standards of oleic acid (C18:1) and palmitic acid (C16:0), all 10 µg/band each, developed with dichloromethane/acetic acid/acetone 2:4:5 (*V/V/V*) up to 80 mm, detected at FLD 366 nm after application of the rhodamine 6G reagent (for comparison in Fig. 2, chromatogram with rhodamine 6G reagent and copper sulfate phosphoric acid reagent).

Figure S6: Influence of the phosphate-citrate buffer pH 12 on HPTLC RP-18 W plates after the derivatization with rhodamine 6G reagent, detected at FLD 366 nm.

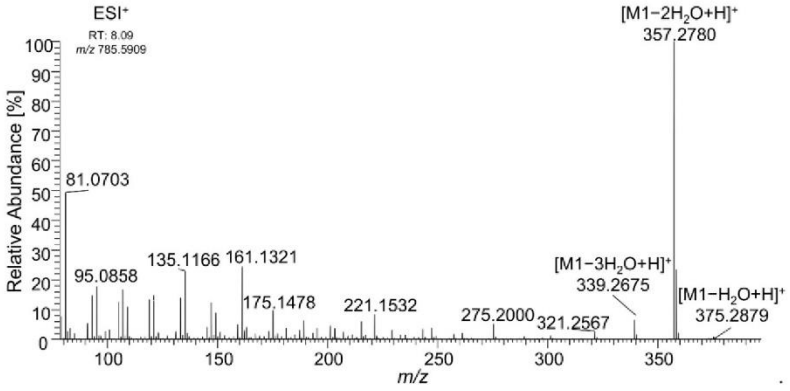

Figure S7: High-resolution mass spectra of the fragmentation of *m/z* 785.5909 and corresponding ion species in the positive ionization mode after nanoGIT−HPTLC −Vis/FLD−heart cut−RP-HPLC−DAD− HESI-HRMS/MS analysis. **M1** = Ursodeoxycholic acid, hyodeoxycholic acid, (cheno)deoxycholic acid

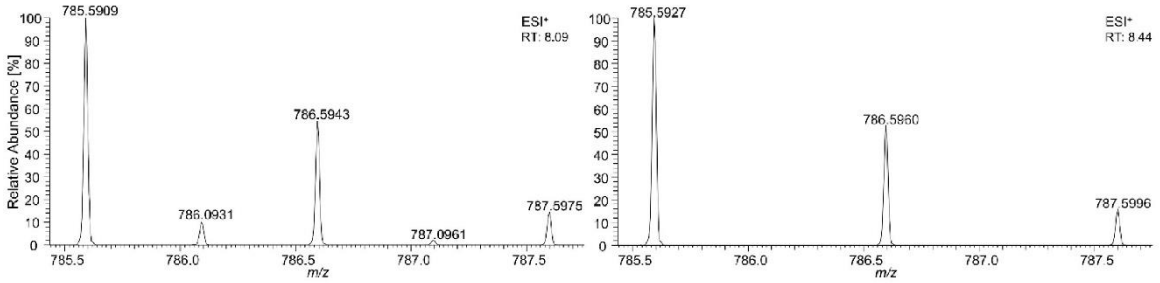

Figure S8: Isotopic pattern of the ion species *m/z* 785.5909 in the positive ionization mode after nanoGIT−HPTLC −Vis/FLD−heart cut−RP-HPLC−DAD− HESI-HRMS/MS analysis revealed a tetramer $[4M+2H]^+$ and/or dimer $[2M1+H]^+$ at retention time 8.09 min and a dimer $[2M1+H]^+$ at retention time 8.44 min. **M1** = Ursodeoxycholic acid, hyodeoxycholic acid, (cheno)deoxycholic acid

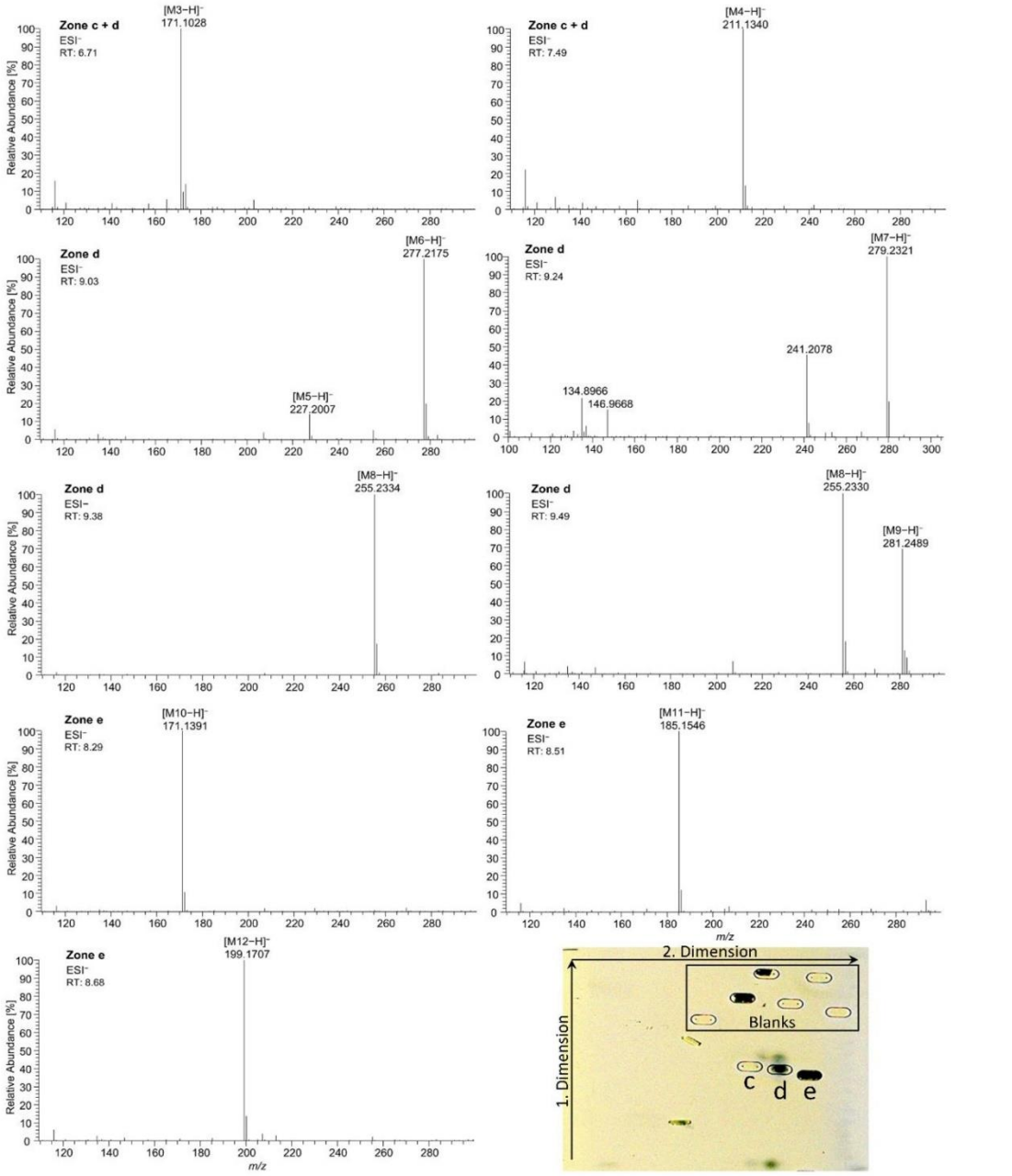

Figure S9: High-resolution mass spectra and corresponding ion species in the negative ionization mode after nanoGIT−HPTLC×HPTLC−Vis/FLD−heart cut−RP-HPLC−DAD− HESI-HRMS/MS analysis of all identified fatty acids found in zones **c**, **d** and **e** of digested flaxseed oil on HPTLC RP-18 W plates. Plate focused twice with acetone and cut at 15 mm and developed first with *n*-hexane/diethyl ether/formic acid 90:25:2 (*V*/*V*/*V*) up to 60 mm from cut edge, then turned 90° and developed with acetonitrile/water 4:1 (*V*/*V*) and molecular sieve (3 Å) up to 50 mm; after the transfer of the interesting zones to the HRMS, the stamped plate was derivatized using the copper sulfate phosphoric acid reagent to check whether the elution head was properly positioned on the zones of interest. **M3** = oxidized C9:0, **M4** = oxidized C12:1, **M5** = C14:0, **M6** = C18:3, **M7** = C18:2, **M8** = C16:0, **M9** = C18:1, **M10** = C10:0, **M11** = C11:0, **M12** = C12:0

Publication III

Screening of α-amylase/trypsin inhibitor activity in wheat, spelt and einkorn by high-performance thin-layer chromatography

Isabel Müller, Bianca Schmid, Loredana Bosa, Gertrud E. Morlock

Published in Analytical Methods

Received 4th March 2024, Accepted and published 25th April 2024

Analytical Methods

ROYAL SOCIETY OF CHEMISTRY

PAPER

View Article Online
View Journal | View Issue

Cite this: *Anal. Methods*, 2024, **16**, 2997

Screening of α-amylase/trypsin inhibitor activity in wheat, spelt and einkorn by high-performance thin-layer chromatography†

Isabel Müller, Bianca Schmid, Loredana Bosa and Gertrud Elisabeth Morlock *

α-Amylase/trypsin inhibitor proteins (ATI) are discussed as possible triggers for non-celiac gluten sensitivity. The potential of high-performance thin-layer chromatography (HPTLC) was studied for the first time to analyse the inhibitory properties of ATIs from flour of wheat, spelt, and einkorn. Inhibition by each flour of the digestive enzymes trypsin or α-amylase was determined by the reduction of released metabolisation products in comparison to non-digested flour, and positive (acarbose) and negative (water) controls. Firstly, amylolysis was carried out in miniaturized form on the HPTLC surface (HPTLC-nanoGIT) after in-vial pre-incubation of the amylase with the inhibitors from flour. α-Amylase inhibition was evident *via* the reduction of released saccharides, as analysed by normal phase HPTLC. A strong influence of the flour matrix on the assay results (individual saccharides) was evident, caused by an increased amylolysis of further polysaccharides present, making HPTLC analysis more reliable than currently used spectrophotometric sum value assays. The detection and visualization of such matrix influence helps to understand the problems associated with spectrophotometric assays. Only maltotriose was identified as a reliable marker of the amylolysis. The highest α-amylase inhibition and thus the lowest saccharide response was detected for maltotriose in refined spelt, whereas the lowest α-amylase inhibition and thus the highest saccharide response was detected for maltotriose in refined wheat. A comparison of refined and whole grain flours showed no clear trend in the responses. Secondly, trypsin inhibition and proteolysis were performed in-vial, and any inhibition was evident *via* the reduction of released peptides, analysed by reversed-phase HPTLC. Based on the product pattern of the proteolysis, einkorn and whole wheat showed the highest trypsin inhibition, whereas refined wheat and refined spelt showed the lowest inhibition. Advantageously, HPTLC analysis provided important information on changes in individual saccharides or peptides, which was more reliable and sustainable than spectrophotometric *in-vial* assays (only sum value) or liquid column chromatography analysis (targeting only the ATI proteins).

Received 4th March 2024
Accepted 25th April 2024

DOI: 10.1039/d4ay00402g

rsc.li/methods

Introduction

Digestive problems concerning the consumption of especially wheat (*Triticum aestivum*) as a carbohydrate diet source have increased in recent decades.[1] Studies have shown that complicated dietary adjustments are needed, if possible, to distinguish gastrointestinal disorders,[2] such as celiac and inflammatory bowel disease, irritable bowel syndrome, wheat allergy, and non-celiac gluten sensitivity (NCGS). Among these, NCGS is the least studied and has the highest but also varying prevalence (0.5–15%).[2–4] To ensure a safe and conclusive diagnosis, analysts tend to identify causative compounds. The ongoing discussion on NCGS involves identifying the specific compound classes that serve as triggers, and multiple approaches have been explored to narrow down and comprehend a diverse range of triggers. Under suspicion are gluten-related gliadins, α-amylase/trypsin inhibitors (ATIs) and/or fermentable oligosaccharides, disaccharides, monosaccharides, and polyols (FODMAPs).[5] Gliadins and ATIs are cereal-derived compounds, whereas FODMAPs are widely distributed among foods. Since gluten and its components have been well studied, the focus has shifted to the evaluation of the exact role of ATIs and FODMAPs in the diagnosis of NCGS.[2,3]

The ATI proteins with two different binding sites act as bifunctional inhibitors to the digestive enzymes trypsin and α-amylase.[6] Originally, this function represents their role in the plant defence mechanism to protect the grain from parasites and pests by inhibiting only their digestive enzymes and not those of the cereals themselves.[7] This inhibitory ability could

Chair of Food Science, Institute of Nutritional Science, Interdisciplinary Research Centre for Biosystems, Land Use and Nutrition, Justus Liebig University Giessen, Heinrich-Buff-Ring 26-32, 35392 Giessen, Germany. E-mail: gertrud.morlock@uni-giessen.de; Fax: +49-641-99-39149; Tel: +49-641-9939141

† Electronic supplementary information (ESI) available. See DOI: https://doi.org/10.1039/d4ay00402g

play an important role considering the potential accumulation of digestion-resistant gluten peptides, which are the cause of an immunogenic reaction in patients with gastrointestinal disorders.[6,8] Another possible mechanism of action of these inhibitors is the activation of Toll-like receptor 4 complex (TLR4–MD2–CD14) and with it, the release of proinflammatory cytokines in cells.[9,10] At least 19 ATIs in their monomeric, dimeric or tetrameric form were reported, which account for 2–4% of the total proteins in wheat.[11,12] These low molecular weight proteins (12–15 kDa) are part of the water-soluble fraction and can be extracted according to the Osborne fractionation with the aid of aqueous salt buffers.[2] They are known to be heat resistant and thus survive food processing like baking, which implies they still could be bioactive in processed food like pasta, bread or biscuits.[5,13] However, there are also contrary studies that mainly focus on α-amylase activity, suggesting a decrease in inhibition after heat treatment.[14,15] Such contradictory studies highlight the difficulties in understanding such complex diseases and the problems encountered in interpreting results from *in vitro* experiments, not to mention the relevance of *in vivo* data.

Two approaches were pursued for the evaluation of ATI. One was the tandem mass spectrometric analysis of known ATIs to identify/quantify their amounts in cereal products.[16–25] The other approach was the screening of the ATI inhibitory potency *via* enzymatic assays followed by non-selective spectrophotometric detection.[7,23,24,26] However, mass spectrometry and enzymatic assays were rarely combined for an ideal matching, difficult to interpret,[24] and recently no correlation between ATI amount and inhibition potential was found.[26]

Because there is only a choice between expensive tandem mass spectrometry (targeting only the ATI proteins) and cheap, non-selective spectrophotometric assay screening (providing only a sum value), this study exploited the potential of high-performance thin-layer chromatography (HPTLC). HPTLC has the advantage of reducing any interfering matrix effects *via* its planar separation, thus detecting individual saccharides or peptides. The miniaturised, sustainable nano gastrointestinal tract (nanoGIT) HPTLC methods dealing with digestive products of amylolysis[27,28] and proteolysis,[27] as well as TLC/HPTLC methods for α-amylase[29,30] and trypsin[31] inhibition, served as motivation. It was hypothesised that changes in enzyme activity caused by ATIs and, thus, in the saccharide or peptide profiles can be measured. It was expected that fewer digestion products would be released due to the inhibition of amylolysis or proteolysis. As samples, ATI-containing flour extracts from wheat (refined and whole), spelt (refined and whole) and einkorn were selected.

Materials and methods

Chemicals and materials

Acarbose (≥95%), D-(+)-glucose (≥99.5%, Glc), maltotriose hydrate (97%, Mal3), 4-aminobenzoic acid (≥99%), D-(+)-maltose monohydrate (≥99%, Mal), trypsin inhibitor from *Glycine max* (90%), triethylamine (>99.5%), casein from bovine milk (technical grade), aniline (≥99.5%), diphenylamine (≥99%), pyridine (≥99%), ammonium hydroxide solution (25%, p. a.), peptone/tryptone from casein (tryptic digested, suitable for microbiology), α-amylase from hog pancreas (45.5 U mg^{-1}) and trypsin from bovine pancreas (97%; 10 000 BAEE U per mg protein) were purchased from Sigma Aldrich Fluka (Steinheim, Germany). *o*-Phosphoric acid (85%, *purissimum*) and dichloromethane (≥99.9%) were from Th. Geyer (Renningen, Germany). 2-Propanol (≥99.8%), calcium chloride dihydrate (≥98%), formic acid (≥98.0%), sodium dihydrogen phosphate monohydrate (≥98%), disodium hydrogen phosphate (≥99%), albumin fraction V (BSA, ≥98%), hydrogen chloride (37%, p. a.), sodium hydroxide (≥99%) and citric acid monohydrate (≥99.5%) were from Carl Roth (Karlsruhe, Germany). Acetic acid (99–100%), acetonitrile (≥99.9%), starch soluble (analytical grade) and potassium iodide (Puriss, p. a. grade) were from Riedel-de Haen (Seelze, Germany). Acetone (≥99.9%) and sodium chloride (≥99%) were purchased from VWR International (Darmstadt, Germany). *n*-Hexane (≥96%), iodine (p. a.), ninhydrin (analytical grade), HPTLC plates silica gel 60 (NP) and silica gel 60 RP-18 W (both 20 × 10 cm), and 3 kDa Amicon Ultra-0.5 mL centrifugal filters (low-binding regenerated cellulose) were purchased from Millipore (Merck, Darmstadt, Germany). Fluorescamine was supplied by abcr (Karlsruhe, Germany). 2-Butanol (99%) was purchased from Alfa Aesar (Kandel, Germany). Ethanol (≥99.8%) was supplied by Thermo Fisher Scientific (Geel, Belgium). Bi-distilled water was produced using Heraeus Destamat B-18E (Thermo Fisher Scientific, Dreieich, Germany).

Five flour samples were purchased from supermarkets. Refined, but not bleached wheat flour type 405 (Lidl Belbake) and organic whole wheat flour (Rewe Bio), both produced by Friesinger Mühle, Bad Wimpfen, Germany, refined, but not bleached spelt flour type 630 (Gut und Günstig, Edeka Zentrale, Hamburg, Germany), organic whole spelt flour (Rewe Bio), produced by BioKorn, Aalen, Germany, and organic whole einkorn flour (Spielberger, Brackenheim, Germany).

Defatting and buffered extraction of ATI

According to a protocol for defatting and ATI extraction,[24] flour (1 g) was weighed into a 15 mL reaction tube, defatted twice using 10 mL *n*-hexane and in-between it was centrifuged at 3000×*g* for 1 min. Excessive *n*-hexane was evaporated using a flow of nitrogen (TH 26, HLC BioTech, Bovenden, Germany). Extraction buffer (5 mL, 150 mM sodium chloride in 1.3 mM phosphate buffer pH 7) was added to each defatted flour sample, which was then vortexed for 10 min using a multi-tube holder (Vortex Genie 2, Scientific Industries, New York City, NY, USA). The supernatant was collected after centrifugation at 3000×*g* for 10 min. The buffer extraction was repeated, both turbid supernatants were combined, centrifuged for 30 s, and the resulting supernatant was filtered through a sterile 0.45 μm cellulose acetate membrane syringe filter (VWR International), resulting in clear ATI-containing flour extracts (*i.e.*, 0.1 g flour per mL buffer). These should be analysed within few weeks, as it was observed that turbidity occurred and increased for longer storage.

Removal of saccharides by centrifugal membrane filtration

Each ATI-containing flour extract (50 μL) was diluted 1 : 10 with extraction buffer pre-cooled to 4 °C (to reduce potential protein denaturation during long centrifugation periods in an uncooled centrifuge). The 500 μL aliquot was filtered twice *via* the 3 kDa Amicon filter by centrifugation at 14 000×*g* for 30 min, whereby the first remaining 48 μL concentrate (remaining inside the filter insert) was filled with 452 μL cooled extraction buffer and filter-centrifuged again. To collect the clear twice-membrane-filtered concentrate (48 μL), the filter was inserted upside down into a clean tube and centrifuged at 1000×*g* for 2 min. Both saccharide-containing filtrates were discarded.

HPTLC-nanoGIT (amylolysis)-FLD/Vis screening of saccharides after in-vial α-amylase inhibition by the flour extracts

The in-vial pre-incubation at 37 °C without rotation for 30 min was performed in 1.5 mL sample vials with 0.2 mL conical inserts. In each insert, 5 μL (2.5 μg, 114 mU) of the α-amylase solution (0.5 mg mL^{-1}, 22.8 U mL^{-1} in water) was pipetted and mixed with 6 μL either membrane-filtered flour extract (equivalent to 600 μg flour) or bi-distilled water as negative control (NC) or aqueous acarbose solution as positive controls (PC1 10 ng μL^{-1}: 60 ng; PC2 5 ng μL^{-1}: 30 ng).

If not stated otherwise, HPTLC instrumentation (CAMAG, Muttenz, Switzerland) was operated under VisionCATS software version 3.1. NP-HPTLC plates were pre-washed by front elution up to 90 mm with acetonitrile, followed by drying for 10 min. The entire pre-incubated enzyme–inhibitor mixture (11 μL per band) was applied onto the NP-HPTLC plate and oversprayed with 2 μL per band soluble starch substrate solution (1 mg mL^{-1}) using the following ATS 4 settings: band length 7 mm, track distance 11 mm, distance from lower and left edge 10 mm, dosage speed 50 nL s^{-1}, filling speed 8 μL s^{-1}, filling vacuum time 0 s, syringe volume 25 μL and the option *fill only programmed volume*.

As references, the corresponding membrane-filtered flour extracts (6 μL per band) as well as saccharide standards (each 1 mg mL^{-1}) of glucose (Glc, 0.5 μL per band), maltose (Mal, 1 μL per band), and maltotriose (Mal3, 1 μL per band), soluble starch (2 μL per band, 1 mg mL^{-1}), α-amylase (5 μL per band, 0.5 mg mL^{-1}, 22.8 U mL^{-1}) and acarbose (6 μL per band, 10 ng μL^{-1}) were applied.

The plate was instantly wetted with 2.5 mL sodium chloride solution (0.1 M) by piezoelectrical spraying (yellow nozzle, level 6, Derivatizer), whereby only the application zone was wetted because the residual adsorbent area was covered by an NP-HPTLC plate cut to 8.5 cm × 20 cm, layer faced upwards.[28] The still-covered plate was incubated for 60 min at 37 °C in a humid plastic box (26.5 × 16 × 10 cm, ABM, Wolframs-Eschenbach, Germany) lined with wet filter paper and filled with 70 mL water. The enzymatic on-surface reaction was stopped by heating the plate (120 °C, 10 min, TLC Plate Heater).

After chamber saturation for 5 min, the plate was developed with 8 mL acetonitrile/water/2-propanol/acetone 6 : 1.5 : 2 : 0.5 (V/V/V/V) up to 70 mm (Twin-Trough Chamber), and sprayed piezoelectrically as mentioned with the *p*-aminobenzoic acid reagent (4 mL, 2 g *p*-aminobenzoic acid in 252 mL glacial acetic acid/water/acetone/*o*-phosphoric acid 1 : 1 : 3 : 0.04, V/V/V/V), followed by heating (140 °C, 5 min) and detection at 366 nm (TLC Visualizer 2). To perform a reagent sequence on the same plate, the latter was automated dipped (immersion time 2 s, immersion speed 3 cm s^{-1}, Chromatogram Immersion Device 3) in the diphenylamine aniline *o*-phosphoric acid reagent (diphenylamine/aniline/2-propanol/water/*o*-phosphoric acid 0.1 : 0.1 : 8 : 1 : 1, w/V/V/V/V), followed by heating at 120 °C for 5–10 min, documentation under white light illumination (TLC Visualizer 2), and densitometric detection at 370 nm (absorbance measurement, deuterium/tungsten lamp, slit 5.0 mm × 0.2 mm, TLC Scanner 4).

Calculation of the relative α-amylase inhibition

After densitometric measurement, the signal height intensity (Int) of an individual saccharide in the flour extract was subtracted from the signal in the corresponding amylolysed flour extract and divided by the signal of the NC (bi-distilled water; amylolysis without inhibitor). This corrected relative signal was subtracted from 1 and multiplied by 100 for calculation of the percentage inhibition as follows:

$$\text{Inhibition}(\%) = 1 - \frac{\text{Int(amylolysed flour extract)} - \text{Int(flour extract)}}{\text{Int(NC)}} \times 100$$

RP-HPTLC-FLD screening of peptides after in-vial trypsin inhibition by the flour extracts

The pre-incubation and proteolysis were performed in 1.5 mL sample vials with 0.2 mL conical inserts. An aliquot of 200 μL trypsin solution (0.33 mg mL^{-1}, 3300 BAEE U mL^{-1} in 5 M calcium chloride monohydrate solution, pH 4)[24] was deacidified by adding 2 μL sodium hydroxide solution (1 M) and then adjusted to pH 8 before use. For the enzyme–inhibitor reaction, 3 μL (1 μg) trypsin solution (0.33 mg mL^{-1}, pH 8) was mixed in each vial with either 7 or 17 μL unfiltered flour extract (equivalent to 0.7 or 1.7 mg flour, 100 mg mL^{-1}) or 3 μL (0.9 μg) trypsin inhibitor solution (0.3 mg mL^{-1}) used as PC or 17 μL bi-distilled water used as NC. As references, 17 μL of the corresponding unfiltered flour extract was filled in vials (without trypsin, no proteolysis). All vials were filled to 20 μL with bi-distilled water and incubated at 37 °C without rotation for 30 min. For the enzyme–substrate reaction, 100 μL (100 μg) of casein substrate solution (1 mg mL^{-1}) was added, followed by further incubation for 120 min. The final assay volume was 120 μL. The enzyme-to-substrate ratio was 1 : 100.

The HPTLC RP-18 W plate was dipped (immersion time 8 s, immersion speed 3 cm s^{-1}, Chromatogram Immersion Device 3) in phosphate–citrate buffer (6 g per L citric acid and 10 g per L di-sodium hydrogen phosphate, adjusted to pH 12 by sodium hydroxide powder). After plate drying (5 min, 100 °C), an aliquot of 10 μL of each trypsin assay solution (resulting in 80 ng trypsin, ATI-containing extract from 60 or 140 μg flour, 80 ng

trypsin inhibitor, and 8 μg casein per band) was applied (with the ATS 4 settings as mentioned, but band length 8 mm and distance from left edge 9 mm) on the buffered plate, which was developed with 8 mL 2-propanol/formic acid/acetonitrile 10 : 1 : 5 (V/V/V) up to 60 mm (Twin-Trough Chamber).

For derivatisation, the plate was dipped (immersion time 2 s, immersion speed 3 cm s^{-1}, Chromatogram Immersion Device 3) in fluorescamine reagent (10% w/V in acetone), followed by plate drying (1 min). For fluorescence enhancement/stabilisation, the plate was dipped subsequently in a triethylamine solution (10% V/V in dichloromethane), followed by plate drying (5 min at 20 °C, room temperature). The fluorescent peptide signals were detected at FLD 366 nm in enhanced mode (TLC Visualizer 2). Alternatively, the plate was derivatised with the ninhydrin reagent (ninhydrin/ethanol/glacial acetic acid 0.2 : 92 : 8, w/V/V).

Results and discussion

After flour defatting, the ATIs were extracted with a sodium chloride-containing phosphate buffer according to Call *et al.*[24] and the inhibitory potential towards α-amylase and trypsin was evaluated. Two approaches were pursued for the evaluation of the flour extracts. The first was the HPTLC α-amylase inhibition assay, in which inhibition by ATIs was detected at the end of analysis after separation. However, this approach was critical, as it probably caused the denaturation of ATI proteins by organic solvents during chromatographic separation, and thus loss of the ability to inhibit α-amylase in the final assay detection. The second approach was the HPTLC-nanoGIT (amylolysis)-FLD/Vis method. Amylolysis was performed in the starting zone prior to chromatographic separation. This approach seemed promising as a combined in-vial/on-surface incubation method. Both approaches were discussed in detail as follows.

HPTLC-α-amylase inhibition assay (caused denaturation of ATI)

Initial experiments followed the HPTLC-α-amylase inhibition assay.[29–31] The assay was performed after separation to detect ATIs, here α-amylase inhibitors, in the flour extracts. The unfiltered ATI extracts were applied onto an NP-HPTLC plate and separated with 2-butanol/pyridine/ammonia/water 19 : 5 : 17 : 6 (V/V/V/V) up to 65 mm. The optimised mobile phase mixture (Fig. S1†) differed in the solvent ratios compared to the peptide separations by Pasilis *et al.*[32] (39 : 34 : 10 : 26, V/V/V/V) and Biller *et al.*[33] (39 : 20 : 10 : 31, V/V/V/V). The α-amylase inhibition assay was performed *via* piezoelectrical spraying.[34] First, the amylase solution, followed by 30 min incubation, then the soluble starch substrate solution, followed by 20 min incubation, and finally, for the detection, the derivatisation reagent iodine/potassium iodide solution[30] was sprayed, or iodine vapour[29] was used (Fig. S2†). The α-amylase-inhibiting zones should be visible as deep-purple zones on a less purple background. However, no purple inhibitor zones were revealed. Only an unstable white zone (vanished with longer incubation time) was observed and characterised as a saccharide *via* selective derivatisation with the diphenylamine aniline reagent (Fig. S2†). However, ATIs are proteins, and selective derivatisation with the ninhydrin reagent showed several zones in the separated ATI extract, these zones did not show any inhibition response, as mentioned. The assumption was that the ATIs were denatured during separation with the highly organic mobile phase and were no longer active. Therefore, purple inhibitor zones were not observed.

Removal of initial saccharides in flour by membrane filtration and NP-HPTLC-nanoGIT (amylolysis)-FLD/Vis method development

The next experiments studied the on-surface metabolization in the start zone (nanoGIT), followed by the analysis of the released metabolization products on the same surface, as developed by Morlock *et al.*[27] As predominant amylolysis products, the released saccharides glucose (Glc), maltose (Mal) and maltotriose (Mal3) were separated, previously shown to be detected quantitatively.[28] Nevertheless, the five flour extract samples contained a high amount of native saccharides (Fig. S3†), which had to be removed before the analysis of the reduction in saccharide release. Therefore, each flour extract was cleaned *via* a 3 kDa centrifugal membrane filter. This ensured no loss of ATIs (mainly > 15 kDa), but the passage of saccharides (≤0.5 kDa), much smaller than the membrane cut-off. Simultaneous with centrifugal membrane filtration, the ATI extract was 10-fold concentrated (from 500 μL to 48 μL). To avoid concentration of the extract and subsequent protein precipitation, the sample was previously diluted 1 : 10 to maintain a consistent concentration. Two 30 min centrifugation steps were sufficient to remove all native saccharides (Fig. S3†).

First, the inhibition of α-amylase by ATI and the substrate reaction with soluble starch were performed in the same start zone. The design of experiment included two separate on-surface incubations: a 30 min pre-incubation of the enzyme with ATI-containing flour extract (to guarantee proper interaction), followed by a 60 min substrate incubation.[24,27] The known α-amylase inhibitor acarbose was used as PC for proof of the inhibition of amylolysis and bi-distilled water as NC. However, the approach to perform all steps on the same HPTLC surface failed because of the two incubation steps and the associated diffusion of the inhibitor, enzyme, and substrate on the start zone (Fig. S4†). To reduce the number of incubations on the HPTLC plate, a 30 min pre-incubation was performed in a sample vial (in-vial pre-incubation), whereas the following enzyme–substrate reaction remained on the NP-HPTLC plate surface (on-surface incubation/metabolization, Fig. 1A).

The in-vial pre-incubation volume was selected as small as possible. Enzyme–inhibitor mass ratios (E/I) of 25 : 100 and 124 : 100 in 25 μL were evaluated, whereof only 11 μL was applied onto the plate. The enzyme–substrate mass ratio (E/S) for on-surface incubation was set to 1 : 2. Co-application of the NC (bi-distilled water) proved that the α-amylase activity was retained after pre-incubation, whereas co-application of the PC (acarbose) inhibited α-amylase (Fig. S5†). The combination of

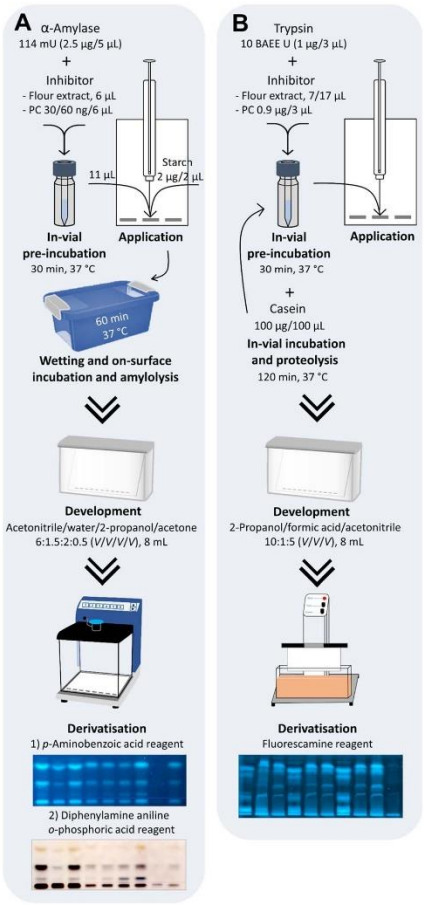

Fig. 1 Workflow for screening (A) α-amylase inhibitory potential using in-vial pre-incubation, followed by NP-HPTLC-nanoGIT (amylolysis)-FLD/Vis, and (B) trypsin inhibitory potential using in-vial pre-incubation and in-vial proteolysis, followed by RP-HPTLC-FLD.

in-vial pre-incubation (for enzyme–inhibitor reaction) and on-surface incubation (for enzyme–substrate reaction) was successful. The nanoGIT chromatograms showed total α-amylase inhibition at a higher E/I of 25 : 100 and 124 : 100. Total inhibition was not of interest, as the signals should be in a dynamic response range. In addition, no signals could not exclude a failed enzymatic reaction. Consequently, the E/I was optimised to 83 : 1, and the total pre-incubation volume was reduced to 11 µL and entirely applied onto the HPTLC plate. The E/S (1 : 2) was changed to 2.5 : 2. Thus, for the PC acarbose, the favoured moderate inhibition was detected, being strongest for Mal3, weakest for Mal, and absent for Glc (Fig. S5†).

Derivatisation with the *p*-aminobenzoic acid reagent detected monosaccharides more sensitively than polysaccharides at FLD 366 nm.[28,34] To improve polysaccharide detection, a second derivatisation with the diphenylamine aniline *o*-phosphoric acid reagent, followed by detection under white light illumination, was performed as a reagent sequence on the same plate. The final amounts and ratios used for in-vial incubation were 2.5 µg α-amylase (114 mU) and ATI-containing extract from 600 µg flour or PC acarbose (60 ng as PC1, 30 ng as PC2). For subsequent on-surface amylolysis, 2 µg soluble starch substrate was applied. Calculated for the PC, this corresponded to an E/I of 42 : 1–83 : 1 and an E/S of 2.5 : 2. Unfortunately, these conditions could not be compared with published studies, since either α-amylase activity was not reported, a common inaccuracy in studies on enzymatic activities, or other substrates (synthesised chromogenic starch-like substances) were used.

NP-HPTLC-nanoGIT (amylolysis)-FLD/Vis screening of α-amylase inhibitor activity of flours

After successful demonstration of α-amylase inhibition using the PC acarbose, the developed NP-HPTLC-nanoGIT (amylolysis)-FLD/Vis method was used for screening and comparing the five membrane-filtered ATI extracts from flours of wheat (refined and whole), einkorn, and spelt (refined and whole). The resulting nanoGIT chromatograms after derivatisation with the *p*-aminobenzoic acid reagent (Fig. 2A), followed by the diphenylamine aniline *o*-phosphoric acid reagent (Fig. 2B), showed amylolytic products. The absorbance of each saccharide was measured using densitometry after the second reagent, which detected the Mal3 zones more sensitively (Fig. 2B). A great advantage of the developed NP-HPTLC-nanoGIT-FLD/Vis method was the selective detection of individual saccharides. This allowed to investigate the correlation between the inhibition of amylolysis and the release of individual saccharides.

In contrast, current in vial assays detect only the overall saccharide release as a sum value, which can be influenced by matrix effects as discussed in the following. A disproportionate increase in Mal was revealed for the flour extracts. This was explained by the long-chain polysaccharides (visible at the start zone), which were retained due to membrane filtration in the clear extracts and were co-metabolised by α-amylase in addition to the starch substrate. A cheaper but not time-saving alternative would be dialysis, which was investigated in a separate study.[35] Such individual increases in released saccharides would not be detected in spectrophotometric (sum value) assays. When subtracting the respective not amylolysed flour extract, such unexpected co-metabolization would result in underestimated relative inhibition or negative absorbance (as the inhibitory reaction released a higher amount of detected product).

As expected, and as a successful proof, the NC (bi-distilled water) revealed three amylolysis products. However, saccharide impurities (Glc and Mal) in the purchased enzyme, which was co-applied as α-amylase reference, were detected. Such impurities did not influence the calculation of the relative

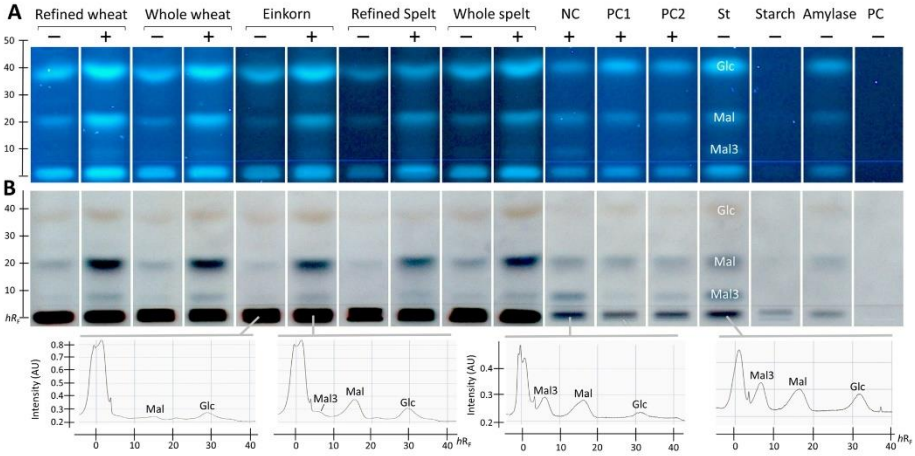

Fig. 2 Screening of the α-amylase inhibitory potential: NP-HPTLC-nanoGIT (amylolysis)-FLD/Vis chromatograms of the in-vial pre-incubated (30 min) flour extracts (600 μg flour per band) of wheat (refined/whole), einkorn, and spelt (refined/whole), negative control (NC, bi-distilled water) and positive control acarbose (PC1 60 ng per band, PC2 30 ng per band), all 11 μL per band as with (+) α-amylase solution (114 mU per band) *versus* flour extracts, 6 μL per band, as without (–) α-amylase solution. As references, saccharide standards (St) glucose (Glc, 0.5 μg per band), maltose (Mal) and maltotriose (Mal3, each 1 μg per band), soluble starch (2 μg per band), α-amylase (2.5 μg per band, 114 mU per band) and PC acarbose (60 ng per band) were applied. All were oversprayed with soluble starch substrate (2 μg per band) and incubated on-surface (60 min). The HPTLC silica gel 60 plate was developed with acetonitrile/water/2-propanol/acetone 6 : 1.5 : 2 : 0.5 (V/V/V/V) up to 70 mm, derivatised with (A) *p*-aminobenzoic acid reagent, followed by detection at FLD 366 nm and, as reagent sequence, with (B) diphenylamine aniline phosphoric acid reagent, detected under white light illumination (remission-transmission mode): for the latter, example densitograms *via* absorbance measurement at 370 nm are illustrated.

inhibition but were still problematic regarding the detector limits, which can be exceeded more quickly and falsify the results of the inhibition assay. For this reason, the α-amylase impurities were not subtracted, as they were present in both the flour extract and the NC.

Additionally, the flour extracts contained saccharide impurities despite prior purification (membrane filtration) of the extracts. Hence, the absorbance of individual saccharides in the amylolysed flour extract was corrected by subtracting the absorbance of the flour extract and then calculating the relative α-amylase inhibition with reference to the NC (Fig. 3 and Table S1†).

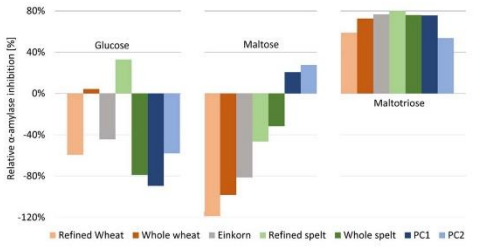

Fig. 3 Relative α-amylase inhibition by the flour extracts and positive control acarbose at two different amounts (PC1 60 ng per band, PC2 30 ng per band) calculated for the three saccharides released (full dataset in Table S1†).

The relative inhibition was only single determined as first proof of the quantification of α-amylase inhibition and for comparison with other methods.

For Glc and Mal, the relative inhibition values were mainly negative for the flour extracts, that is, more Glc and Mal products were released and detected in the amylolysed flour extracts than in the NC without any inhibitor. As mentioned, the higher absorbance values for Mal were explained by the co-metabolization of the matrix during amylolysis, which could also be the case for Glc. Nevertheless, the whole wheat (4%) and refined spelt extract (33%) showed positive inhibition values regarding Glc (Fig. 3), where whole wheat released more Glc than refined spelt, resulting in lower inhibition. No trend regarding their whole grain or refined counterparts was observed. Thus, the evaluation of the release of Mal and Glc for the calculation of the relative inhibition was classified as critical without any further purification of the extracts. However, the reduction in Mal3 release led to positive relative inhibition values for all amylolysed flour extracts, with the strongest inhibition observed for refined spelt and the lowest inhibition observed for refined wheat.

According to Geisslitz *et al.*,[19] einkorn contained the lowest amount of ATIs compared to wheat, spelt, and emmer, resulting in the lowest α-amylase inhibition, as confirmed by Simonetti *et al.*[36] Our results did not support this hypothesis. The flour extract of einkorn showed no significantly lower inhibition than all other investigated flours, keeping in mind the possible

presence of other α-amylase inhibitors, the affinity of the enzyme regarding its origin (human or animal),[26] the different analytical approaches, and the natural variety of the flour composition. Other studies on α-amylase inhibition[26,36] have also reported moderate to high standard deviations. Calculating the overall inhibition (Table S1†) as a simulation of values obtained by spectrophotometric assays, refined spelt (15%) showed the strongest inhibition, and refined wheat the lowest (−40%). Interestingly, the inhibition was only positive for refined and whole spelt, whereas the other extracts resulted in negative inhibition (not evaluable in a spectrophotometric assay). Repeatedly, the investigation of the Mal3 release evaluated the same trend as the overall inhibition, but with consistently positive inhibition values and thus more reliable results. In conclusion, the influence of the flour matrix plays an important but often neglected role in determining the inhibitory potential, which was uncovered with the developed NP-HPTLC-nanoGIT (amylolysis)-FLD/Vis method. The comparison of refined and whole grain flours regarding Mal3-release showed contrary results; whole wheat showed a higher and whole spelt a lower inhibition than its corresponding refined types. ATIs are predominantly present in the starchy endosperm of the grain,[37,38] and to a lesser extent in the outer aleurone layer. The latter is removed in refined flour together with the cereal bran. In contrast, whole grain flour contains an aleurone layer and other components that influence the weight distribution. Consequently, the ATI amount was expected to be enriched in refined flour.

Saccharide release should be reduced by increasing the amount of the α-amylase inhibitor. However, the addition of more PC (PC1 60 ng acarbose > PC2 30 ng acarbose) led to unexpected increases in Glc and Mal release (Fig. 2, Table S1†). Especially, Glc was released in a higher amount than in the NC, resulting in negative inhibition (Fig. 3). The acarbose reference standard showed no impurities, but acarbose is a pseudo-tetrasaccharide that may fit into the active centre of α-amylase and become partially digested, which explains the additional and thus higher Glc release. In conclusion, acarbose may not be the first choice as PC, which was further investigated in another study.[35] All in all, only a decrease in Mal3 was observed with increasing acarbose amount, confirming the reduction in the Mal3 release as a suitable mechanism for the screening of the inhibitory potential of ATI in flours.

Comparing the overall inhibition (Table S1†) of PC1 and PC2, they revealed the same inhibitory potential (25% and 26%, respectively, despite differing amounts) as consequence of the higher Glc release with higher acarbose amounts masking the lower Mal3 release. Hence, in a spectrophotometric assay, doubling the amount of PC would result in an underestimated inhibition for acarbose. This highlights the better reliability of the developed NP-HPTLC-nanoGIT (amylolysis)-FLD/Vis method in contrast to the spectrophotometric (sum value) assays.

Method development to measure the trypsin inhibition by ATI

ATIs are bi-functional inhibitors for α-amylase and trypsin. After successful inhibition of α-amylase, it was necessary to also prove trypsin inhibition. First, the nanoGIT on-surface incubation/metabolization was attempted. The zone diffusion on the NP-HPTLC plate was expected to be less (compared to the α-amylase inhibition study) because of the higher molecular weights of trypsin (24 kDa) and casein (25 kDa). First, the enzyme–substrate reaction was optimised with trypsin and tryptone (tryptic-digested casein) by evaluating different E/S from 2 : 100 to 1 : 1 (Fig. S6†). The in-vial proteolytic products were separated with 2-butanol/ammonia/pyridine/water 19 : 5 : 17 : 13 (V/V/V/V) and detected under white light illumination after derivatisation with the ninhydrin reagent. The resulting NP-HPTLC-nanoGIT (proteolysis)-Vis chromatogram showed that the separation was increasingly impaired (*i.e.*, peptides were pushed upwards) the more trypsin was applied on the plate. The interferences were assumed to be caused by the associated high-molar (5 M) calcium chloride solution. Only the lowest E/S of 2 : 100 showed no interferences but also no peptide increase, so the amounts were considered too low.

Next, the stationary phase was switched from polar NP to more apolar RP-18 W plates. The water-wettable RP-18 W adsorbent is more polar than RP-18 but rather apolar in contrast to NP.[39] Due to its acidic pH (pH ≈ 4), the RP-18 W plate was buffered with citrate–phosphate buffer (pH 12) to neutral pH. A mobile phase for peptide separation was developed, resulting in 2-propanol/formic acid/acetonitrile 10 : 1 : 5 (V/V/V). Peptide separation worked better on buffered *versus* non-buffered plates, as observed in the RP-HPTLC-nanoGIT (proteolysis)-Vis chromatograms (Fig. S7†). As expected, the acidic mobile phase caused an acid gradient with the lowest pH at the bottom and the highest pH at the top, which was confirmed *via* planar pH electrode measurement and by the background colour gradient formed after derivatisation with the ninhydrin reagent. By replacing formic acid in the mobile phase with ammonia (25%), no gradient in the coloured background was observed, but the separation was too low in elution strength and would require further optimisation. Proteolysis on RP-18 W plates still showed no increase in peptide zones (Fig. S7†); as tryptone is a tryptically pre-digested casein, further proteolytic products could be marginal and thus undetectable. Hence, the in-vial proteolysis was performed with casein to ensure sufficient enzymatic degradation. The fluorescamine derivatisation reagent was tested as an alternative to the ninhydrin reagent (Fig. 1B). Proteolysis products were detected more sensitively as blue fluorescent zones in the RP-HPTLC chromatogram at FLD 366 nm. An incubation time of 2 h with an E/S of 1 : 100 and an application volume of 10 μL was considered sufficient (Fig. S8†). Again, a higher E/S interfered with the separation, caused by trypsin in its high-molar calcium chloride solution. To prove the inhibition of proteolysis, the trypsin inhibitor from *Glycine max* was used as PC and bi-distilled water as NC. Different E/I and pre-incubation periods were evaluated for the PC and the flour extract of refined wheat (Fig. S9†). For the PC, an E/I of 11 : 10 showed already a complete inhibition after 15 min. A lower E/I was preferred to prevent false-positive results if the enzyme assay did not work. A pre-incubation time of 30 min was chosen for the enzyme–inhibitor reaction. For wheat, the best results were achieved by adding 7 μL (60 μg flour) or 17 μL (140 μg flour)

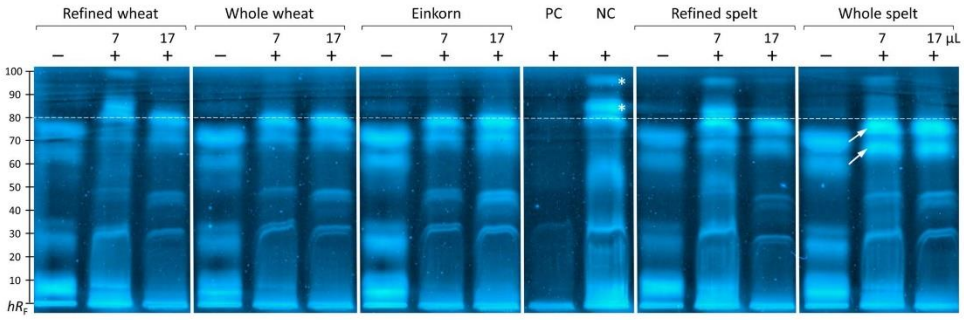

Fig. 4 Screening of the trypsin inhibitor activity: RP-HPTLC-FLD chromatogram of 7 µL (60 µg per band) and 17 µL (140 µg per band) proteolysed (0.08 µg per band trypsin) flour extracts of refined/whole wheat, einkorn, and refined/whole spelt, along with the positive control (PC, trypsin inhibitor, 0.08 µg per band) and the negative control (NC, bi-distilled water), all 10 µL per band (marked +) *versus* flour extracts without trypsin solution (140 µg flour per band, marked −), separated on HPTLC RP-18 W plates with 2-propanol/formic acid/acetonitrile 10 : 1 : 5 (V/V/V) up to 65 mm, derivatised with the fluorescamine reagent and detected at FLD 366 nm (enhanced mode). Zones ≥ hR_F 80 (marked *) were well-suited for evaluation. Calcium chloride load pushed zones together towards a higher hR_F (marked by arrows).

of the flour extract (Fig. S9†), whereas higher volumes (27 µL) resulted in excessive inhibition, potentially leading to false-positive results that are more challenging to recognise.

RP-HPTLC screening of trypsin inhibitor activity of flours

The inhibition of the proteolysis was effective for all samples. The PC (*Glycine max* trypsin inhibitor) showed strong inhibition, whereas the NC (bi-distilled water) did not (Fig. 4). Screening of the five unfiltered flour extracts of wheat (refined and whole), einkorn, and spelt (refined and whole) showed satisfactory trypsin inhibition in the chromatogram in comparison to the NC and their non-proteolyzed counterparts. In particular, the zones with a retardation factor times 100 (hR_F) ≥ 80 (Fig. 4, marked *) were well-suited for evaluating the inhibition of the proteolysis. Zones in the proteolyzed unfiltered flour extracts containing trypsin in 5 M calcium chloride solution (Fig. 4, marked +) were eluted and pushed together towards a higher hR_F (Fig. 4, marked by arrows) owing to the comparatively higher elution power caused by the calcium chloride load on the start zone. Only the extracts of 60 µg refined flours of wheat and spelt suggested at hR_F 81 and 91 peptide zone responses equivalent to the NC. Indicating, that nearly all extracts inhibited zones ≥ hR_F 80 and showed trypsin inhibitory properties. With comparable intensity, the extracts from the flours of einkorn and whole wheat inhibited trypsin most strongly.

These results were consistent with the findings of Simonetti *et al.*,[36] which evaluated the highest trypsin inhibition for einkorn samples; however, contrary to the results of Geisslitz *et al.*,[19] where einkorn had the lowest ATI amount. Unfortunately, the assay conditions were not comparable to those of other studies[24,36] since they used chromogenic substrates, which have a different affinity to trypsin compared to the used casein.

Qualitative screening and visual evaluation of the chromatogram was performed. The current separation was not suited for densitometric measurement and calculation of the relative trypsin inhibition. In future, firstly, the elution strength of the mobile phase could be reduced to better separate the upper chromatogram part, where clear differences were observed. Secondly, the salt load could be reduced to overcome the interference caused by high trypsin-associated calcium chloride load on the start zone. Thirdly, the transfer from in-vial to on-surface incubation with shorter incubation periods (to reduce the diffusion of reactants in the start zone) could be tested.

Conclusions

Two screening methods were successfully developed to evaluate the α-amylase and trypsin inhibitory properties of extracts from five different flours. Analysis of the α-amylase inhibitory potential consisted of in-vial pre-incubation, followed by NP-HPTLC-nanoGIT (amylolysis)-FLD/Vis, whereas analysis of the trypsin inhibition used in-vial pre-incubation and proteolysis, followed by RP-HPTLC-FLD. In contrast to spectrophotometric assays, the developed HPTLC screening methods detected individual saccharides or peptides, and the inhibitory potential of flours was determined *via* the reduction of released saccharides during amylolysis or proteolysis, respectively. A strong influence of the flour matrix on the assay results (individual saccharides) was observed, explained by an increased amylolysis of further polysaccharides. The visualization of such matrix influence made HPTLC analysis a more reliable and information-rich method than currently used spectrophotometric sum value assays and helped to understand the problems associated with spectrophotometric assays (matrix effects depending on the chromogenic substrate used). HPTLC screening was not only more reliable and sustainable than conventional in-vial assays but also than liquid column chromatography analysis targeting only the ATI proteins. In comparison, up to 17

samples can be analysed all at once in HPTLC, consuming far less materials. Organic solvents were needed in the HPTLC workflow for conclusive results, but there is potential to use solvents of renewable sources for improvements regarding green chemistry.

In the future, the workflow of both methods could be optimised using a full on-surface digestion strategy. Further purification of the flour extracts *via* fractionation and ensuring their stability over time could improve the accuracy. Additional effect-directed detection on the planar surface could provide new information about further non-proteinogenic inhibitors of the flour extracts. The results of both the α-amylase and trypsin inhibition assays need to be validated and verified by an independent method. Additionally, an investigation of consumer products such as bread would reveal the remaining activity of ATIs after exposure to high temperatures and provide more comprehensive diet information.

Author contributions

Isabel Müller: conceptualization, methodology, experimental analysis, data analysis, writing – original draft. Loredana Bosa: experimental analysis, data analysis. Bianca Schmid: experimental analysis, data analysis. Gertrud E. Morlock: conceptualization, methodology, supervision, writing – original draft, writing – review and editing.

Conflicts of interest

The authors declare that they have no known competing financial interests or personal relationships that could have influenced the work reported in this study.

Acknowledgements

Instrumentation was partially funded by the Deutsche Forschungsgemeinschaft (DFG, German Research Foundation) – INST 162/536-1 FUGG and INST 162/471-1 FUGG.

References

1 A. Sapone, J. C. Bai, C. Ciacci, J. Dolinsek, P. H. R. Green, M. Hadjivassiliou, K. Kaukinen, K. Rostami, D. S. Sanders, M. Schumann, R. Ullrich, D. Villalta, U. Volta, C. Catassi and A. Fasano, Spectrum of gluten-related disorders: consensus on new nomenclature and classification, *BMC Med.*, 2012, **10**, 13.

2 S. Geisslitz, P. Shewry, F. Brouns, A. H. P. America, G. P. I. Caio, M. Daly, S. D'Amico, R. de Giorgio, L. Gilissen, H. Grausgruber, X. Huang, D. Jonkers, D. Keszthelyi, C. Larré, S. Masci, C. Mills, M. S. Møller, M. E. Sorrells, B. Svensson, V. F. Zevallos and P. L. Weegels, Wheat ATIs: Characteristics and Role in Human Disease, *Front. Nutr.*, 2021, **8**, 667370.

3 F. I. Cárdenas-Torres, F. Cabrera-Chávez, O. G. Figueroa-Salcido and N. Ontiveros, Non-Celiac Gluten Sensitivity: An Update, *Medicina*, 2021, **57**(6), 526.

4 C. Catassi, J. C. Bai, B. Bonaz, G. Bouma, A. Calabrò, A. Carroccio, G. Castillejo, C. Ciacci, F. Cristofori, J. Dolinsek, R. Francavilla, L. Elli, P. Green, W. Holtmeier, P. Koehler, S. Koletzko, C. Meinhold, D. Sanders, M. Schumann, D. Schuppan, R. Ullrich, A. Vécsei, U. Volta, V. Zevallos, A. Sapone and A. Fasano, Non-Celiac Gluten sensitivity: the new frontier of gluten related disorders, *Nutrients*, 2013, **5**, 3839–3853.

5 M. G. Mumolo, F. Rettura, S. Melissari, F. Costa, A. Ricchiuti, L. Ceccarelli, N. de Bortoli, S. Marchi and M. Bellini, Is Gluten the Only Culprit for Non-Celiac Gluten/Wheat Sensitivity?, *Nutrients*, 2020, **12**, 3785.

6 M. Cuccioloni, M. Mozzicafreddo, I. Ali, L. Bonfili, V. Cecarini, A. M. Eleuteri and M. Angeletti, Interaction between wheat alpha-amylase/trypsin bi-functional inhibitor and mammalian digestive enzymes: Kinetic, equilibrium and structural characterization of binding, *Food Chem.*, 2016, **213**, 571–578.

7 S. Priya, S. Kumar, N. Kaur and A. K. Gupta, Specificity of α-amylase and trypsin inhibitor proteins in wheat against insect pests, *N. Z. J. Crop Hortic. Sci.*, 2013, **41**, 49–56.

8 L. Shan, Ø. Molberg, I. Parrot, F. Hausch, F. Filiz, G. M. Gray, L. M. Sollid and C. Khosla, Structural basis for gluten intolerance in celiac sprue, *Science*, 2002, **297**, 2275–2279.

9 Y. Junker, S. Zeissig, S.-J. Kim, D. Barisani, H. Wieser, D. A. Leffler, V. Zevallos, T. A. Libermann, S. Dillon, T. L. Freitag, C. P. Kelly and D. Schuppan, Wheat amylase trypsin inhibitors drive intestinal inflammation via activation of toll-like receptor 4, *J. Exp. Med.*, 2012, **209**, 2395–2408.

10 V. F. Zevallos, V. Raker, S. Tenzer, C. Jimenez-Calvente, M. Ashfaq-Khan, N. Rüssel, G. Pickert, H. Schild, K. Steinbrink and D. Schuppan, Nutritional Wheat Amylase-Trypsin Inhibitors Promote Intestinal Inflammation via Activation of Myeloid Cells, *Gastroenterology*, 2017, **152**, 1100–1113.e12.

11 S. B. Altenbach, W. H. Vensel and F. M. Dupont, The spectrum of low molecular weight alpha-amylase/protease inhibitor genes expressed in the US bread wheat cultivar Butte 86, *BMC Res. Notes*, 2011, **4**, 242.

12 F. M. Dupont, W. H. Vensel, C. K. Tanaka, W. J. Hurkman and S. B. Altenbach, Deciphering the complexities of the wheat flour proteome using quantitative two-dimensional electrophoresis, three proteases and tandem mass spectrometry, *Proteome Sci.*, 2011, **9**, 10.

13 M. Kostekli and S. Karakaya, Protease inhibitors in various flours and breads: Effect of fermentation, baking and in vitro digestion on trypsin and chymotrypsin inhibitory activities, *Food Chem.*, 2017, **224**, 62–68.

14 P. E. Granum, Studies on α-amylase inhibitors in foods, *Food Chem.*, 1979, **4**, 173–178.

15 P. Gélinas, C. McKinnon and F. Gagnon, Inhibitory activity towards human α-amylase in cereal foods, *LWT–Food Sci. Technol.*, 2018, **93**, 268–273.

16 U. Bose, K. Byrne, C. A. Howitt and M. L. Colgrave, Targeted proteomics to monitor the extraction efficiency and levels of barley α-amylase trypsin inhibitors that are implicated in

non-coeliac gluten sensitivity, *J. Chromatogr. A*, 2019, **1600**, 55–64.
17 U. Bose, A. Juhász, J. A. Broadbent, K. Byrne, C. A. Howitt and M. L. Colgrave, Identification and Quantitation of Amylase Trypsin Inhibitors Across Cultivars Representing the Diversity of Bread Wheat, *J. Proteome Res.*, 2020, **19**, 2136–2148.
18 S. Geisslitz, C. F. H. Longin, P. Koehler and K. A. Scherf, Comparative quantitative LC-MS/MS analysis of 13 amylase/trypsin inhibitors in ancient and modern Triticum species, *Sci. Rep.*, 2020, **10**, 14570.
19 S. Geisslitz, C. Ludwig, K. A. Scherf and P. Koehler, Targeted LC-MS/MS Reveals Similar Contents of α-Amylase/Trypsin-Inhibitors as Putative Triggers of Nonceliac Gluten Sensitivity in All Wheat Species except Einkorn, *J. Agric. Food Chem.*, 2018, **66**, 12395–12403.
20 S. Tchewonpi Sagu, E. Landgräber, M. Rackiewicz, G. Huschek and H. Rawel, Relative Abundance of Alpha-Amylase/Trypsin Inhibitors in Selected Sorghum Cultivars, *Molecules*, 2020, **25**, 5982.
21 S. Tchewonpi Sagu, L. Zimmermann, E. Landgräber, T. Homann, G. Huschek, H. Özpinar, F. J. Schweigert and H. M. Rawel, Comprehensive Characterization and Relative Quantification of α-Amylase/Trypsin Inhibitors from Wheat Cultivars by Targeted HPLC-MS/MS, *Foods*, 2020, **9**(10), 1448.
22 B. Prandi, A. Faccini, T. Tedeschi, G. Galaverna and S. Sforza, LC/MS analysis of proteolytic peptides in wheat extracts for determining the content of the allergen amylase/trypsin inhibitor CM3: influence of growing area and variety, *Food Chem.*, 2013, **140**, 141–146.
23 S. Tchewonpi Sagu, G. Huschek, J. Bönick, T. Homann and H. M. Rawel, A New Approach of Extraction of α-Amylase/trypsin Inhibitors from Wheat (Triticum aestivum L.), Based on Optimization Using Plackett-Burman and Box-Behnken Designs, *Molecules*, 2019, **24**(19), 3589.
24 L. Call, E. V. Reiter, G. Wenger-Oehn, I. Strnad, H. Grausgruber, R. Schoenlechner and S. D'Amico, Development of an enzymatic assay for the quantitative determination of trypsin inhibitory activity in wheat, *Food Chem.*, 2019, **299**, 125038.
25 L. Call, E. Haider, S. D'Amico, E. Reiter and H. Grausgruber, Synthesis and accumulation of amylase-trypsin inhibitors and changes in carbohydrate profile during grain development of bread wheat (Triticum aestivum L.), *BMC Plant Biol.*, 2021, **21**, 113.
26 N. Jahn, C. F. H. Longin, K. A. Scherf and S. Geisslitz, No correlation between amylase/trypsin-inhibitor content and amylase inhibitory activity in hexaploid and tetraploid wheat species, *Curr. Res. Food Sci.*, 2023, **7**, 100542.
27 G. E. Morlock, L. Drotleff and S. Brinkmann, Miniaturized all-in-one nanoGIT+active system for on-surface metabolization, separation and effect imaging, *Anal. Chim. Acta*, 2021, **1154**, 338307.
28 I. Müller and G. E. Morlock, Quantitative saccharide release of hydrothermally treated flours by validated salivary/pancreatic on-surface amylolysis (nanoGIT) and high-performance thin-layer chromatography, *Food Chem.*, 2023, **432**, 137145.
29 V. Sonkamble, G. Zore and L. Kamble, A simple method to screen amylase inhibitors using thin layer chromatography, *Sci. Res. Rep.*, 2014, **4**, 85–88.
30 S. Agatonovic-Kustrin and D. W. Morton, HPTLC – bioautographic methods for selective detection of the antioxidant and α-amylase inhibitory activity in plant extracts, *MethodsX*, 2018, **5**, 797–802.
31 P. Houghton, M. Simmonds and S. Larssen, Detection of trypsin inhibition and antioxidant effects on TLC, *Planta Med.*, 2010, **76**(12), DOI: **10.1055/s-0030-1264254**.
32 S. P. Pasilis, V. Kertesz, G. J. van Berkel, M. Schulz and S. Schorcht, Using HPTLC/DESI-MS for peptide identification in 1D separations of tryptic protein digests, *Anal. Bioanal. Chem.*, 2008, **391**, 317–324.
33 J. Biller, L. Morschheuser, M. Riedner and S. Rohn, Development of optimized mobile phases for protein separation by high performance thin layer chromatography, *J. Chromatogr. A*, 2015, **1415**, 146–154.
34 G. E. Morlock, L. P. Morlock and C. Lemo, Streamlined analysis of lactose-free dairy products, *J. Chromatogr. A*, 2014, **1324**, 215–223.
35 I. Müller, I. Scheibelhut and G. E. Morlock, Study of the quantitative α-amylase or trypsin inhibition by refined and whole wheat and einkorn using high-performance thin-layer chromatography–nanoGIT *versus* conventional spectrophotometry, in submission.
36 E. Simonetti, S. Bosi, L. Negri and G. Dinelli, Amylase Trypsin Inhibitors (ATIs) in a Selection of Ancient and Modern Wheat: Effect of Genotype and Growing Environment on Inhibitory Activities, *Plants*, 2022, **11**(23), 3268.
37 C. Finnie, S. Melchior, P. Roepstorff and B. Svensson, Proteome analysis of grain filling and seed maturation in barley, *Plant Physiol.*, 2002, **129**, 1308–1319.
38 G. Guo, D. Lv, X. Yan, S. Subburaj, P. Ge, X. Li, Y. Hu and Y. Yan, Proteome characterization of developing grains in bread wheat cultivars (Triticum aestivum L.), *BMC Plant Biol.*, 2012, **12**, 147.
39 I. Klingelhöfer and G. E. Morlock, Sharp-bounded zones link to the effect in planar chromatography-bioassay-mass spectrometry, *J. Chromatogr. A*, 2014, **1360**, 288–295.

Electronic Supplementary Material (ESI) for Analytical Methods.

Supplementary Information

Screening of α-amylase/trypsin inhibitor activity in wheat, spelt and einkorn by high-performance thin-layer chromatography

Isabel Müller, Bianca Schmid, Loredana Bosa, Gertrud Elisabeth Morlock*

Chair of Food Science, Institute of Nutritional Science, and Interdisciplinary Research Centre for Biosystems, Land Use and Nutrition, Justus Liebig University Giessen, Heinrich-Buff-Ring 26-32, 35392 Giessen, Germany

*Corresponding author: Prof. Dr. Gertrud Morlock, phone: +49-641-9939141; fax +49-641-99-39149, email: gertrud.morlock@uni-giessen.de

Table of contents

	(**124:100**) or acarbose (2.7 ng/µL) + α-amylase (10.3 mU/µL) in 11 µL (**83:1**). The negative control (**NC**) was α-amylase (113.8 mU/band) + bi-distilled water. All samples were overspotted with soluble starch (2 µg/band). For comparison, reference standards of glucose (Glc) 0.5 µg/band, maltose (Mal) and maltotriose (Mal3) each 1 µg/band were applied on HPTLC silica gel 60 plates, developed with acetonitrile/water/2-propanol/acetone 6:1.5:2:0.5 (*V*/*V*/*V*/*V*) up to 70 mm, derivatized with the *p*-aminobenzoic acid reagent and documented at FLD 366 nm.	
Fig. S6	NP-HPTLC-nanoGIT (proteolysis)-Vis chromatogram of different ratios of trypsin to tryptone (**1:1**–**2:100**), trypsin (3 µg/band) and tryptone (5 µg/band). For the trypsin assay, tryptone (5 µg/band) was overspotted with different volumes (0.4–18.5 µL) of 0.27 µg/µL trypsin. The HPTLC silica gel 60 plate was developed with 2-butanol/ammonia (25%)/pyridine/water 19:5:17:13 (*V*/*V*/*V*/*V*) up to 70 mm, derivatized with the ninhydrin reagent and documented at white light illumination in remission-transmission mode.	S10
Fig. S7	RP-HPTLC-nanoGIT (proteolysis)-Vis chromatogram of the influence on the peptide separation and derivatization of an acidic or basic mobile phase on HPTLC RP-18 W plates (non-)buffered with citrate-phosphate buffer (pH 12). The trypsin assay (5 µL/band, tryptone overspotted with trypsin) were applied with a trypsin/tryptone ratio of 1:20 (**c**$_1$) or 1:100 (**c**$_2$). Tryptone (**a,** 5 µg/band) and trypsin (**b,** 0.25 µg/band) were applied beside. The plates were developed with 2-propanol/formic acid/acetonitrile 10:1:5 (*V*/*V*/*V*) or 2-propanol/ammonia (25%)/acetonitrile 10:1:5 (*V*/*V*/*V*) up to 65 mm, derivatized with the ninhydrin reagent and documented at white light illumination in remission-transmission mode.	S11
Fig. S8	RP-HPTLC-nanoGIT (proteolysis)-FLD chromatogram showing the influence of the enzyme-substrate ratio (**1:20** or **1:100**) and incubation time (**2** or **18 h**) on the in-vial trypsin-casein assay and the application volume (**5** or **10** µL) on the peptide separation on HPTLC RP-18 W plates. The in-vial trypsin-casein assay was 100 µL casein (1 µg/µL) with trypsin (0.33 µg/µL) in the ratio of 1:20 or 1:100. The plate was developed with 2-propanol/formic acid/acetonitrile 10:1:5 (*V*/*V*/*V*) up to 65 mm, derivatized with the fluorescamine reagent and documented at FLD 366 nm in enhanced mode.	S12
Fig. S9	RP-HPTLC-nanoGIT (proteolysis)-FLD chromatogram of the influence of pre-incubation times of 15 min (**a**) or 30 min (**b**) with different volumes of wheat extract (7, 17 and 27 µL) or a trypsin inhibitor as positive control (**PC**) on the in-vial trypsin inhibition assay. Application of 10 µL/band of each wheat assay, the PC and the negative control (**NC**, trypsin-casein assay (1:100) and a wheat extract blank (27 µL) on HPTLC RP-18 W plates. The plate was developed with 2-propanol/formic acid/acetonitrile 10:1:5 (*V*/*V*/*V*) up to 65 mm, derivatized with the fluorescamine reagent and documented at FLD 366 nm in enhanced mode.	S13

Table S1
Absorbance values of the three saccharides released after the amylolysis for the different flour extracts (n = 1), the positive controls (PC1/PC2, acarbose) and the negative control (NC, bi-distilled water) as well as the corrected absorbance (flour extract impurities subtracted), relative inhibition regarding each saccharide and the overall inhibition referred to the NC.

	Saccharide	Absorbance	Corrected absorbance	Inhibition [%]	Overall inhibition [%]
Wheat extract blank	Glucose	0.05654444	Blank		
	Maltose	0.06809270			
	Maltotriose	0.00841666			
Wheat extract assay	Glucose	0.09134534	0.034800903	−59	−40
	Maltose	0.21398657	0.145893872	−119	
	Maltotriose	0.03206499	0.023648334	59	
Whole wheat extract blank	Glucose	0.04721251	Blank		
	Maltose	0.05110990			
	Maltotriose	0.00931743			
Whole wheat extract assay	Glucose	0.06811189	0.020899378	4	−16
	Maltose	0.18340296	0.132293060	−98	
	Maltotriose	0.02511425	0.015796815	73	
Einkorn extract blank	Glucose	0.05547531	Blank		
	Maltose	0.02432215			
Einkorn extract assay	Glucose	0.08699152	0.031516217	−44	−14
	Maltose	0.14527881	0.120956658	−81	
	Maltotriose	0.01343024	-	77	
Spelt extract blank	Glucose	0.02496919	Blank		
	Maltose	0.02618494			
Spelt extract assay	Glucose	0.03958507	0.014615879	33	15
	Maltose	0.12393922	0.097754274	−47	
	Maltotriose	0.01138892	-	80	
Whole spelt extract blank	Glucose	0.07248845	Blank		
	Maltose	0.06095526			
	Maltotriose	0.01227069			
Whole spelt extract assay	Glucose	0.11157182	0.039083369	−79	4
	Maltose	0.14874004	0.087784777	−32	
	Maltotriose	0.02603717	0.013766482	76	
PC1	Glucose	0.04139276		−90	25
	Maltose	0.05287774		21	
	Maltotriose	0.01401116		76	
PC2	Glucose	0.03449744		−58	26
	Maltose	0.04826322		28	
	Maltotriose	0.02665399		54	
NC	Glucose	0.02183936	Reference		0
	Maltose	0.06669746			
	Maltotriose	0.05745075			
Amylase	Glucose	0.03121545			
	Maltose	0.03433898			

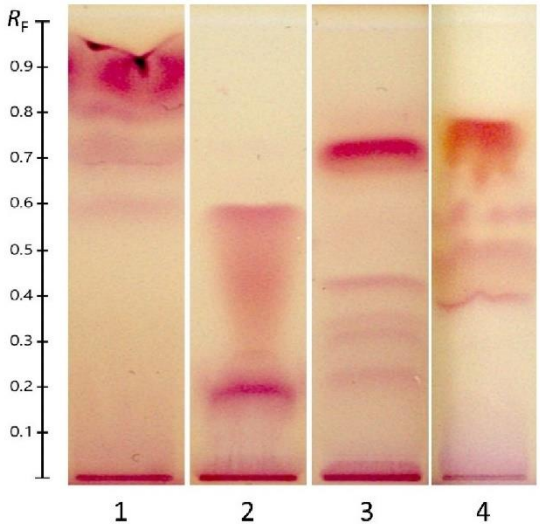

Fig. S1 HPTLC-Vis chromatograms for mobile phase optimization with different ratios of 2-butanol/ammonia (25%)/pyridine/water: (**1**) 10:5:17:13, (**2**) 19:5:8:13, (**3**) 19:5:17:6, and (**4**) 19:5:17:13 (all *V*/*V*/*V*/*V*); HPTLC silica gel 60 plate derivatized with the ninhydrin reagent and detected at white light illumination (remission and transmission mode).

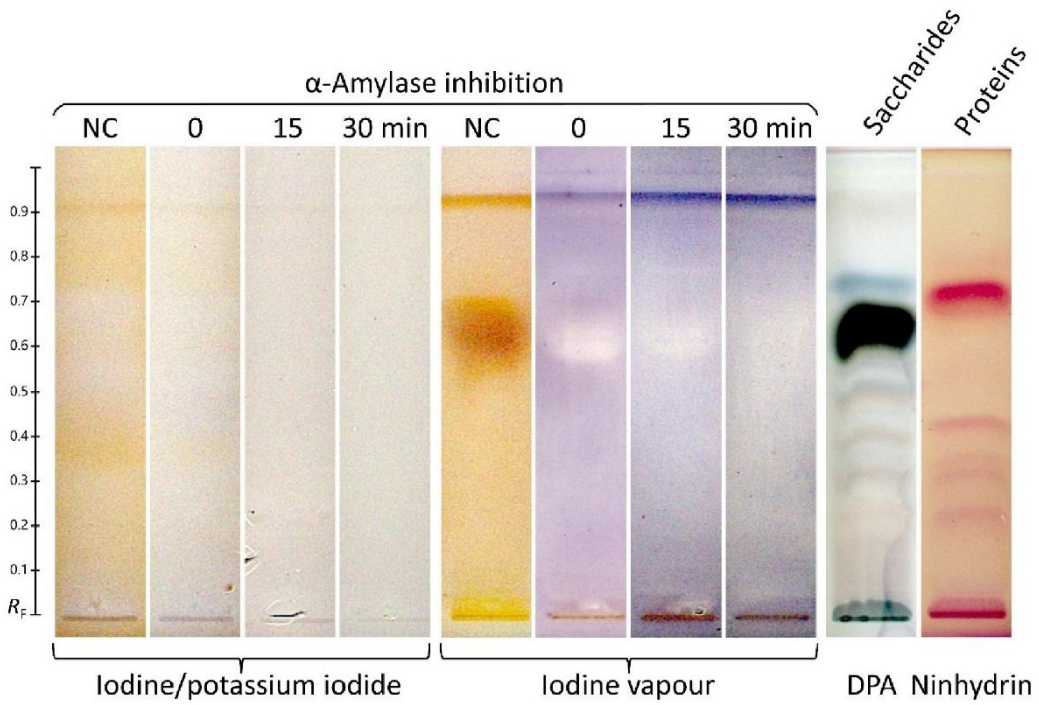

Fig. S2 HPTLC-Vis chromatograms showing separated refined wheat extract (5 µL/band) with different incubation times (0–30 min) of the amylolysis using either iodine/potassium iodide or iodine vapour as derivatization for detection of α-amylase inhibition in comparison with derivatization with the ninhydrin reagent for proteins and the diphenylamine aniline phosphoric acid reagent (**DPA**) for saccharides. As a negative control (**NC**), the assay was performed without enzyme. HPTLC silica gel 60 plates developed with 2-butanol/ammonia (25%)/pyridine/water 19:5:17:6 (*V*/*V*/*V*/*V*) up to 65 mm and documented at white light illumination (remission and transmission mode).

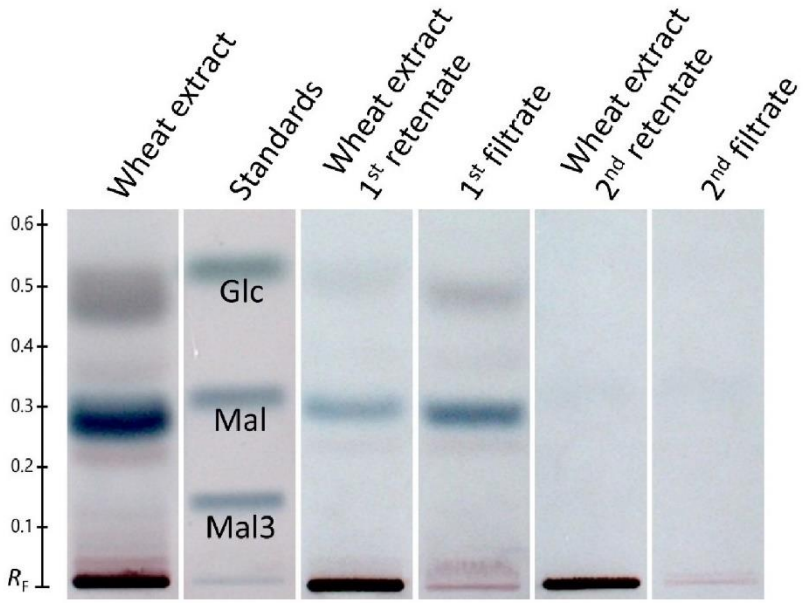

Fig. S3 HPTLC-Vis chromatograms showing saccharide evaluation of the crude and filtered refined wheat extract (5 µL/band) and the corresponding filtrate (10 µL/band). The wheat extract was filtered once or twice for 30 min with a 3k Da Amicon Ultra-0,5 filter. For comparison, reference standards (1 µg/band) glucose (Glc), maltose (Mal) and maltotriose (Mal3) were applied on HPTLC silica gel 60 plate, developed with acetonitrile/water/ 2-propanol/acetone 6:1.5:2:0.5 (*V*/*V*/*V*/*V*) up to 70 mm, derivatized with the diphenylamine aniline phosphoric acid reagent and documented at white light illumination (remission and transmission mode).

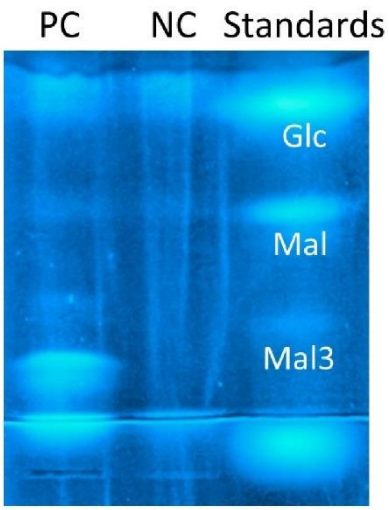

Fig. S4 NP-HPTLC-nanoGIT chromatogram (amylolysis with 45.5 mU/band α-amylase + 2 µg/band soluble starch) after both on-surface pre- and main incubation of the positive control acarbose (**PC**, 5 µg/band) and the negative control bi-distilled water (**NC**). For comparison, reference standards (1 µg/band) of glucose (Glc), maltose (Mal) and maltotriose (Mal3) were applied on HPTLC silica gel 60 plates, developed with acetonitrile/water/2 propanol/acetone 6:1.5:2:0.5 (V/V/V/V) up to 70 mm, derivatized with the *p*-aminobenzoic acid reagent and documented at FLD 366 nm.

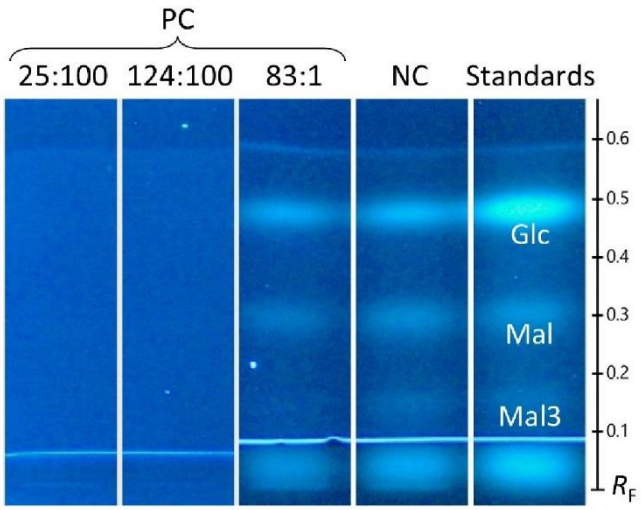

Fig. S5 Evaluation of an appropriate acarbose concentration as the positive control (**PC**) with an in-vial pre-incubation (30 min) and on-surface incubation (60 min). The pre-incubated enzyme-inhibitor mixture (11 µL/band) contained either acarbose (0.4 µg/µL) + α-amylase (4.5 mU/µL) in 25.1 µL (**25:100**), acarbose (80 ng/µL) + α-amylase (4.5 mU/µL) in 25.1 µL (**124:100**) or acarbose (2.7 ng/µL) + α-amylase (10.3 mU/µL) in 11 µL (**83:1**). The negative control (**NC**) was α-amylase (113.8 mU/band) + bi-distilled water. All samples were overspotted with soluble starch (2 µg/band). For comparison, reference standards of glucose (Glc) 0.5 µg/band, maltose (Mal) and maltotriose (Mal3) each 1 µg/band were applied on HPTLC silica gel 60 plates developed with acetonitrile/water/2-propanol/acetone 6:1.5:2:0.5 (*V*/*V*/*V*/*V*) up to 70 mm, derivatized with the *p*-aminobenzoic acid reagent and documented at FLD 366 nm.

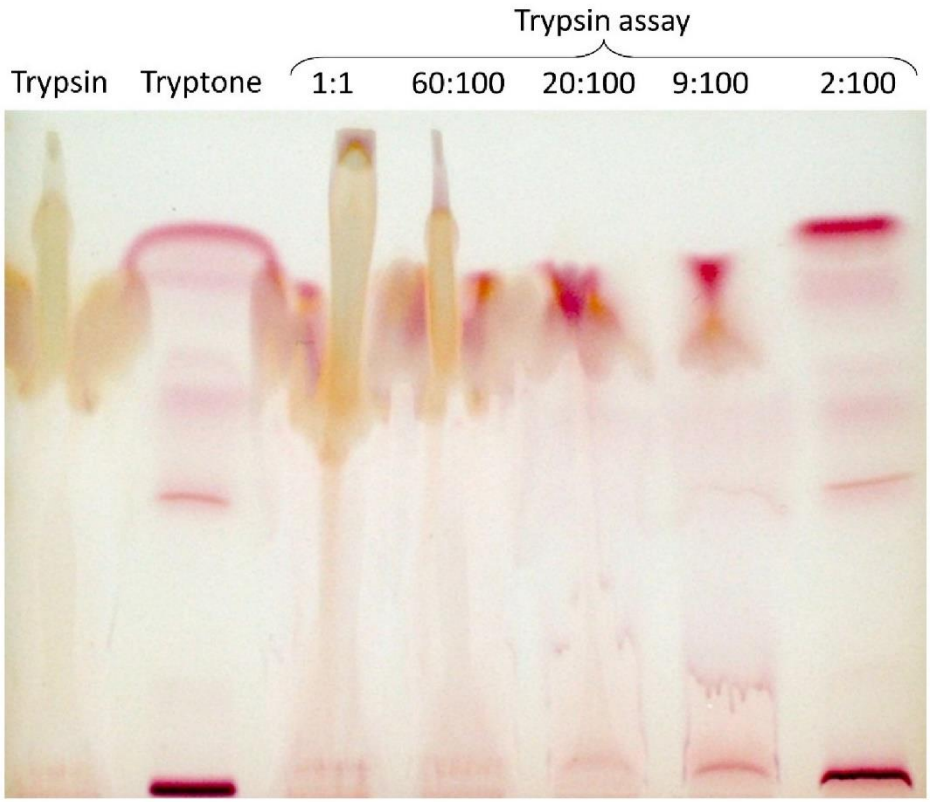

Fig. S6 NP-HPTLC-nanoGIT (proteolysis)-Vis chromatogram of different ratios of trypsin to tryptone (**1:1**–**2:100**), trypsin (3 µg/band) and tryptone (5 µg/band). For the trypsin assay, tryptone (5 µg/band) was overspotted with different volumes (0.4–18.5 µL) of 0.27 µg/µL trypsin. The HPTLC silica gel 60 plate was developed with 2-butanol/ammonia (25%)/pyridine/water 19:5:17:13 (*V*/*V*/*V*/*V*) up to 70 mm, derivatized with the ninhydrin reagent and documented at white light illumination (remission and transmission mode).

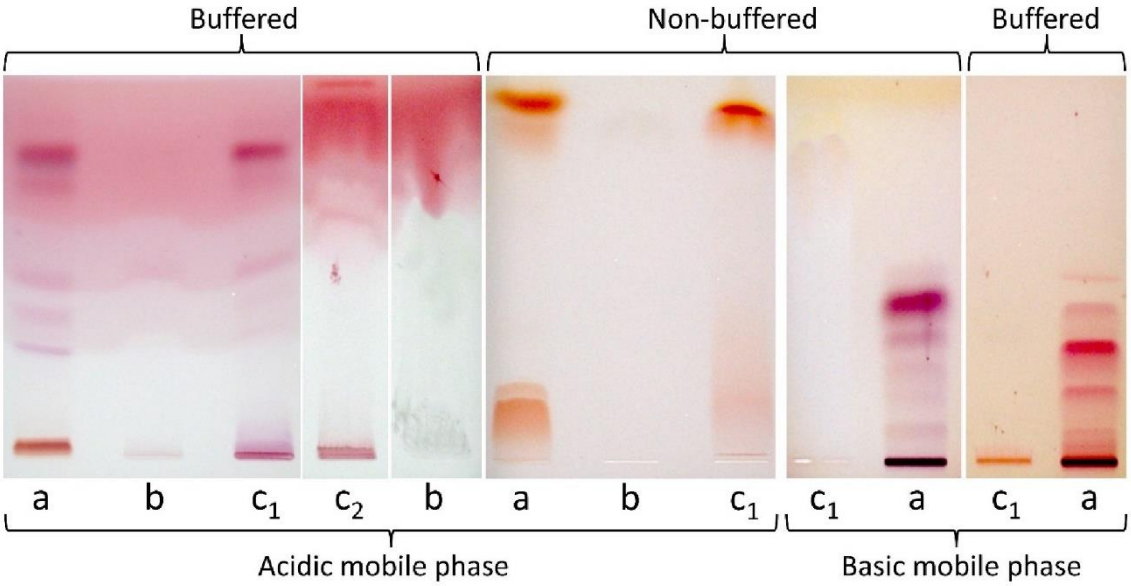

Fig. S7 RP-HPTLC-nanoGIT (proteolysis)-Vis chromatogram of the influence on the peptide separation and derivatization of an acidic or basic mobile phase on HPTLC RP-18 W plates (non-)buffered with citrate-phosphate buffer (pH 12). The trypsin assay (5 µL/band, tryptone overspotted with trypsin) were applied with a trypsin/tryptone ratio of 1:20 (**c_1**) or 1:100 (**c_2**). Tryptone (**a,** 5 µg/band) and trypsin (**b,** 0.25 µg/band) were applied beside. The plates were developed with 2-propanol/formic acid/acetonitrile 10:1:5 (*V*/*V*/*V*) or 2-propanol/ammonia (25%)/acetonitrile 10:1:5 (*V*/*V*/*V*) up to 65 mm, derivatized with the ninhydrin reagent and documented at white light illumination (remission and transmission mode).

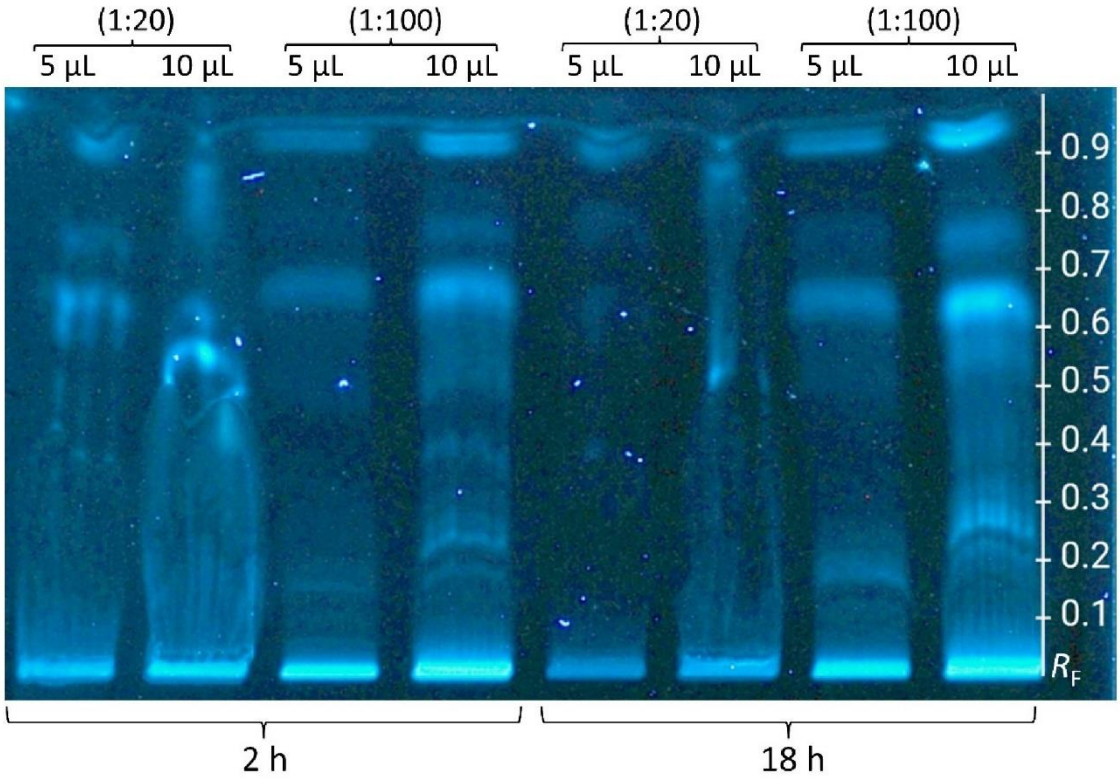

Fig. S8 RP-HPTLC-nanoGIT (proteolysis)-FLD chromatogram showing the influence of the enzyme-substrate ratio (**1:20** or **1:100**) and incubation time (**2** or **18 h**) on the in-vial trypsin-casein assay and the application volume (**5** or **10** µL) on the peptide separation on HPTLC RP-18 W plates. The in-vial trypsin-casein assay was 100 µL casein (1 µg/µL) with trypsin (0.33 µg/µL) in the ratio of 1:20 or 1:100. The plate was developed with 2-propanol/formic acid/acetonitrile 10:1:5 (*V*/*V*/*V*) up to 65 mm, derivatized with the fluorescamine reagent and documented at FLD 366 nm (enhanced mode).

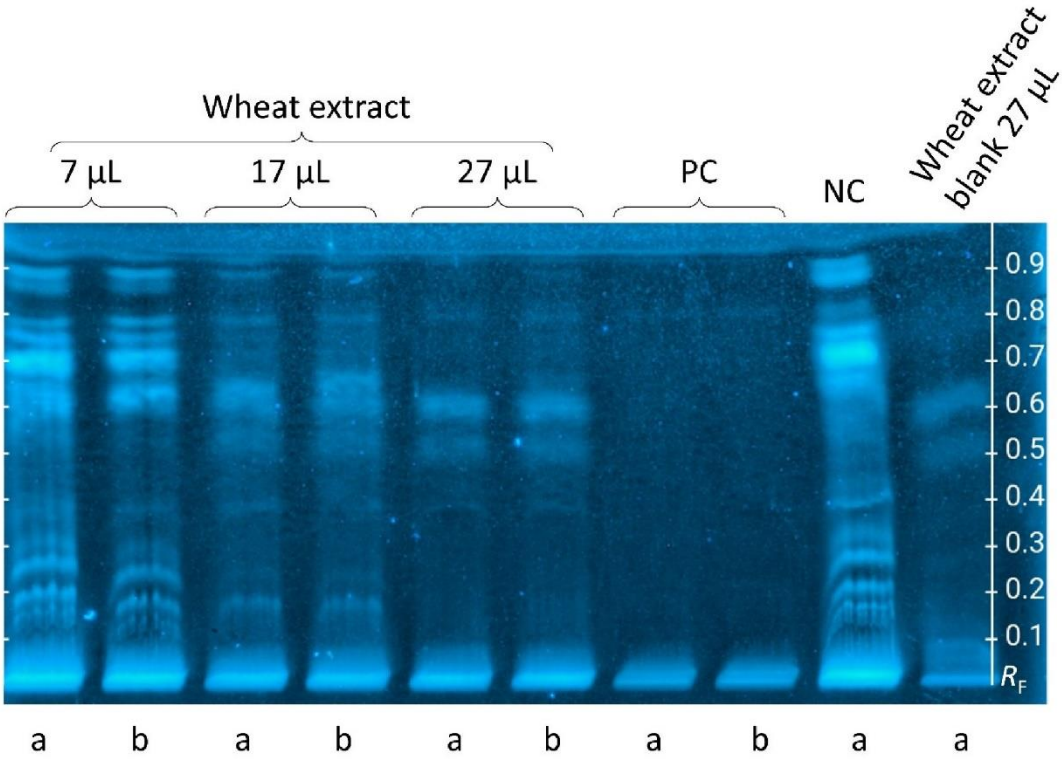

Fig. S9 RP-HPTLC-nanoGIT (proteolysis)-FLD chromatogram of the influence of pre-incubation times of 15 min (**a**) or 30 min (**b**) with different volumes of wheat extract (7, 17 and 27 µL) or a trypsin inhibitor as positive control (**PC**) on the in-vial trypsin inhibition assay. Application of 10 µL/band of each wheat assay, the PC and the negative control (**NC**, trypsin-casein assay (1:100) and a wheat extract blank (27 µL) on HPTLC RP-18 W plates. The plate was developed with 2-propanol/formic acid/acetonitrile 10:1:5 (*V*/*V*/*V*) up to 65 mm, derivatized with the fluorescamine reagent and documented at FLD 366 nm (enhanced mode).

Publication IV

Study of the quantitative α-amylase or trypsin inhibition by refined and whole wheat and einkorn using high-performance thin-layer chromatography–nanoGIT versus conventional spectrophotometry

Isabel Müller, Ilka Scheibelhut, Gertrud E. Morlock

In preparation for submission

Study of the quantitative α-amylase or trypsin inhibition by refined and whole wheat and einkorn using high-performance thin-layer chromatography–nanoGIT *versus* conventional spectrophotometry

Isabel Müller, Ilka Scheibelhut, Gertrud E. Morlock*

Chair of Food Science, Institute of Nutritional Science, and Interdisciplinary Research Centre for Biosystems, Land Use and Nutrition, Justus Liebig University Giessen, Heinrich-Buff-Ring 26-32, 35392 Giessen, Germany

*Corresponding authors: Prof. Dr. Gertrud Morlock, phone: +49-641-9939141; fax +49-641-99-39149, email: gertrud.morlock@uni-giessen.de

Abstract

The investigation of α-amylase/trypsin inhibitors (ATI) is complicated due to a lack of a link between inhibition potential and inhibitors. Two on-surface assays (nanoGIT) for α-amylase and trypsin inhibition were developed, followed by analysis of the metabolisation products via high-performance thin-layer chromatography (HPTLC). ATI-containing extracts from refined and whole wheat and einkorn were digested using porcine pancreatic α-amylase and bovine trypsin. α-Amylase inhibition was quantified by HPTLC–nanoGIT (amylolysis inhibition)–FLD/Vis. The flour extract from einkorn showed lower α-amylase inhibition than that from refined/whole wheat. No differences were observed between refined and whole wheat. Trypsin inhibition analysed via HPTLC–nanoGIT (proteolysis inhibition)–Vis was compared with spectrophotometry. Both on-surface methods made it possible to provide a profile pattern of the released individual metabolisation products and compare them for different inhibitors. They were found a superior alternative to existing spectrophotometric assays and can be used complementarily to estimate the inhibitory potential of ATIs.

Keywords

α-amylase/trypsin inhibitor (ATI); on-surface metabolization; enzyme inhibition assay; non-celiac wheat sensitivity

1. Introduction

α-Amylase/trypsin inhibitors (ATIs) are naturally occurring proteins found in plant seeds and inhibit both digestive enzymes which are essential for breaking down carbohydrates and proteins in the human body.[1] They account for 2–4% of the total proteins in wheat and the 19 ATIs known to date occur in monomeric, dimeric or tetrameric form.[2,3] ATIs have been shown to have a negative impact on digestive health and can contribute to several health issues, such as gastrointestinal distress[1,4] and inflammation.[5,6] In numerous studies, ATIs are discussed as potential triggers of non-celiac gluten sensitivity (NCGS), a disease with a widely spread but also highly varying range of prevalence (0.5–15%).[7–10] The water-soluble low molecular weight proteins could be a concern for consumers, as they are suspected to be heat resistant and could resist food processing such as baking and cooking.[8,10,11] Contrary studies, mainly dealing with only α-amylase activity, state a reduction in activity and thus less inhibition after heat treatment.[12,13] The exact cause of NCGS is not well understood and other triggers such as gluten-related gliadins and/or fermentable oligosaccharides, disaccharides, monosaccharides, and polyols (FODMAPs) are discussed as well.[10] The ATIs and well-studied gliadins are cereal-related, whereas FODMAPs have various origins. Sparse research has led to upcoming interest in ATIs as potential disruptors of the human digestive system.

Several analytical approaches have been studied to identify ATIs in cereals and elucidate their specific roles in gastrointestinal complaints. One is tandem mass spectrometric analysis to identify and/or quantify the content of already known ATIs in cereal products.[14–23] Another is the application of spectrophotometric methods to analyse the inhibition as a sum value[21,22,24]. In our previous study[25], for the first time, the potential of high-performance thin-layer chromatography (HPTLC) for the analysis of matrix-rich cereal extracts containing ATIs was demonstrated and revealed a massively disturbing matrix load after standardised extraction. All these techniques have in common that they identify the inhibitory potential or quantify already known inhibitors, but do not directly link the observed inhibition with specific inhibitors. Very rarely, both techniques were combined[26], assumedly due of their huge effort and costs.

This study aimed to improve the previously developed HPTLC screening[25]. It was hypothesized that the workflow can be performed completely on the surface in one step together (HPTLC–nanoGIT), and that inhibition by ATIs can be analysed quantitatively. This could result in a better alternative method for the assessment of inhibitors besides vulnerable spectrophotometric methods.

2. Materials and Methods

2.1. Chemicals and materials

Acarbose (≥ 95%), D-(+)-glucose (≥ 99.5%), maltotriose hydrate (97%), 4-aminobenzoic

acid (≥ 99%), D-(+)-maltose monohydrate (≥ 99%), trypsin inhibitor from *Glycine max* (90%), casein from bovine milk (technical grade), pyridine (≥ 99%), ammonium hydroxide solution (25%, puriss p. a.), *N*α-benzoyl-L-arginin-4-nitroanilid-hydrochlorid (L-BAPA, ≥ 98%), sodium acetate trihydrate (≥ 99.0%), magnesium chloride hexahydrate (≥ 99.0%), 2-naphthol (> 99%), α-amylase from hog pancreas (45.5 U/mg) and trypsin from bovine pancreas (97%; 10,000 BAEE (*N*α-benzoyl-L-arginine ethyl ester) U/mg protein) were purchased from Sigma Aldrich Fluka (Steinheim, Germany). *o*-Phosphoric acid (85%, p.a.) was from Th. Geyer (Renningen, Germany). 2-Propanol (≥ 99.8%), calcium chloride dihydrate (≥ 98%), sodium dihydrogen phosphate monohydrate (≥ 98%), disodium hydrogen phosphate (≥ 99%), hydrogen chloride (37%, p. a.), sodium hydroxide (≥ 99%), alkali-soluble casein (≥ 95%), dimethyl sulfoxide (≥ 99.8%), molecular sieve (0.3 nm, type 564, beads), sulfuric acid (≥ 95%) and tris(hydroxy-methyl)aminomethane (Tris, ≥ 99.9%) were from Carl Roth (Karlsruhe, Germany). Acetic acid (99–100 %), acetonitrile (≥ 99.9%), potassium iodide (puriss p. a.) and starch soluble (analytical grade) were from Riedel-de Haen (Seelze, Germany). Acetone (≥ 99.9%), sodium chloride (≥ 99%), and 0.45-µm cellulose acetate membrane syringe filters were purchased from VWR International (Darmstadt, Germany). *n*-Hexane (≥ 96%), ninhydrin (analytical grade), HPTLC plates silica gel 60 (20 cm × 10 cm), Novagen D-Tube Dialyzer Mega (10 mL, with molecular weight cutoff MWCO at 3.5 kDa) and iodine (double sublimated, p. a.) were obtained from Merck (Darmstadt, Germany). 2-Butanol (99%) was delivered by Alfa Aesar (Kandel, Germany). Ethanol (≥ 99.8%) was supplied by Thermo Fisher Scientific (Geel, Belgium). Ammonium bicarbonate (99%) was obtained from Acros Organics (Morris Plains, NJ, USA). Bi-distilled water was produced by a Heraeus Destamat B-18E (Thermo Fisher Scientific, Dreieich, Germany).

Flour samples of conventional, unbleached, refined wheat Type 405 (Belbake, Lidl) and organic whole grain wheat (Rewe Bio, Rewe) were both produced by Friesinger Mühle (Bad Wimpfen, Germany) and einkorn were produced by Spielberger (Brackenheim, Germany). All samples were purchased from local supermarkets.

2.2. Preparation of solutions

2.2.1. HPTLC–nanoGIT (amylolysis inhibition)–FLD/Vis

As a positive control (PC), acarbose (1 mg/mL) was dissolved in water. Soluble starch (10 mg/mL) was dissolved in water and heated in a boiling water bath until a clear solution was obtained and used the next day or stored at 4 °C. The solution was warmed up to about 20 °C for analysis, the clarity of the solution was proven, and if needed, reheated to 100°C (MR Hei-Standard, Heidolph Instruments, Schwabach, Germany) before application. α-Amylase (5 mg/mL) was

dissolved in 20 mM sodium acetate trihydrate and 7 mM sodium chloride to obtain a solution of 227.5 U/mL. Sodium chloride-containing phosphate buffer (1.3 mM phosphate buffer pH 7 with 150 mM sodium chloride) was prepared by diluting (1:8 *V*/*V*) a 10 mM phosphate buffer (0.5 mg/mL disodium hydrogen phosphate and 0.9 mg/mL sodium dihydrogen phosphate monohydrate) and adding sodium chloride (0.9 mg/mL). For the *p*-aminobenzoic acid reagent, 2 g of 4-aminobenzoic acid was dissolved in 252 mL acetic acid/water/acetone/*o*-phosphoric acid 1:1:3:0.04 (*V*/*V*/*V*/*V*). For the 2-naphthol reagent, 2 g of 2-naphthol was dissolved in ethanol/50% sulfuric acid 24:1 (*V*/*V*).

2.2.2. Spectrophotometric α-amylase inhibition assay for comparison

20 mM sodium phosphate buffer pH 6.9 (1.1 mg/mL disodium hydrogen phosphate, 1.7 mg/mL sodium dihydrogen phosphate monohydrate and 0.4 mg/mL sodium chloride) were prepared to dissolve α-amylase (0.5 mg/mL, 22.8 U/mL) in water/sodium phosphate buffer pH 6.9 1:1 (*V*/*V*). Iodine/iodide solution (0.3 mg/mL iodine and 0.15 mg/mL potassium iodide in water) was prepared and a soluble starch solution (1 mg/mL) as mentioned.

2.2.3. In-vial trypsin inhibition assay for method development

Trypsin (0.33 mg/mL, i.e. 33,000 BAEE U/mL) was dissolved in 0.6 M calcium chloride pH 3 and adjusted to pH 8 by mixing 100 µL with 1 µL 1 M sodium hydroxide. Trypsin inhibitor (0.05 and 0.5 mg/mL) was dissolved in water. Casein (20 mg/mL) was dissolved in 25 mM ammonium bicarbonate by mixing either alkali-soluble casein or casein from bovine milk dropwise with 1 M sodium hydroxide, followed by ultrasonification (no heat, Sonorex Digiplus, Bandelin, Berlin, Germany) until pH 11 was reached. Alkali-soluble casein dissolved until clarity and needed less sodium hydroxide than casein from bovine milk, which remained turbid. The required pH of 7 was adjusted dropwise using 1 M hydrogen chloride. Below pH 6, casein precipitated and was resolved by adjusting to a basic pH.

2.2.4. HPTLC–nanoGIT (proteolysis inhibition)–Vis

For storage, trypsin (0.2 mg/mL, i.e. 2,000 BAEE U/mL) was dissolved in water, adjusted to pH 3 using 1 M hydrogen chloride, and adjusted prior to analysis to pH 8 using 1 M sodium hydroxide. Trypsin inhibitor (0.5 mg/mL) was dissolved in water and casein (20 mg/mL) as previously mentioned. Saturated solution of magnesium chloride (33% r. H.) was prepared (544 g/L). For the ninhydrin reagent, ninhydrin (2 mg/mL) was dissolved in ethanol/acetic acid 23:2 (*V*/*V*).

2.2.2. Spectrophotometric trypsin inhibition assay for comparison

As stock solution (0.5 mg/mL), L-BAPA (7.5 mg) was dissolved in dimethyl sulfoxide (0.1 mL) and filled up to 15 mL with tris-calcium chloride buffer (50 mM tris + 5 mM calcium

chloride monohydrate, pH 8.2 ± 0.1). After being dissolved in dimethyl sulfoxide, the solution became turbid, but with the addition of tris-calcium chloride buffer, it turned pale yellow. The solution was diluted with tris-calcium chloride buffer to obtain the L-BAPA working solution (0.27 mg/mL). The solution was stable at 4 °C for one day. Trypsin (0.0135 mg/mL) was dissolved in a 5 M calcium chloride solution.

2.3. ATI extraction and membrane-filtration of saccharides

ATI extraction was performed using a modified protocol[25] according to Call et al.[22] Briefly, flour (1 g) was weighed into a 15 mL reaction tube and defatted twice with *n*-hexane (10 mL each) by mixing and in-between centrifugation (3,000 × *g*, 1 min). The supernatant was discarded and the remaining *n*-hexane was removed by a flow of nitrogen (TH 26, HLC BioTech, Bovenden, Germany). To each flour, sodium chloride-containing phosphate buffer (pH 7, 5 mL) was added and vortexed for 10 min using a multi-tube holder (Vortex Genie 2, Scientific Industries, New York City, NY, USA). Extraction with buffer was repeated, and both supernatants were combined after centrifugation each at 3,000 × *g* for 10 min. All extracts (0.1 g flour/mL buffer) were filtered with a 0.45-µm cellulose acetate membrane syringe filter, resulting in clear extracts.

For the removal of the initial saccharides, flour extracts or α-amylase solution (5 mg/mL, *i.e.* 227.5 U/mL) were membrane-filtered (each 5 mL) against stirred water (2 L) using a D-Tube Dialyzer Mega (MWCO 3.5 kDa), prepared as specified by the manufacturer. The conductivity of the permeate was measured continuously (LF92, WTW, Weilheim, Germany) and renewed every 2 h. An aliquot (0.2 mL) of the retentate (flour extract or α-amylase solution) was withdrawn after each cycle as a process control to check the progress until membrane filtration was successful. After every second renewal (every 4 h), the initial salt load of the retentate (20 mM sodium acetate and 7 mM sodium chloride) was restored by adding the corresponding salt amount, taking into account the retentate withdrawal (0.4 mL), as follows:

$$\text{Added salt amount (g)} = \text{salt molarity (mol/L)} * \text{residual retanate volume (L)} * \text{molecular weight of salt (g/mol)}$$

All membrane-filtered solutions were stored at −20 °C.

2.4. Quantification via HPTLC–nanoGIT (amylolysis inhibition)–FLD/Vis

Acarbose solution (5 µL/band, 1 mg/mL) was used as a PC for the inhibition of amylolysis, and each membrane-filtered flour extract (2–11 µL/band) was applied twice onto the HPTLC plate silica gel 60 (20 cm × 10 cm). One was oversprayed onto the membrane-filtered α-amylase solution (5 µL/band, 227.5 U/mL) and the other was used as a reference blank. Soluble starch solution (2 µL/band, 10 mg/mL) were applied were amylolysis where intended. The negative control (NC) did not contain acarbose or the extract for

maximal amylolysis. All substances were applied with the following settings: band length 7 mm, track distance 10 mm, distance from the lower edge 10 mm and left edge 15 mm, dosage speed 50 nL/s, filling speed 8 µL/s, filling vacuum time 4 s, and a syringe volume of 25 µL (Automatic TLC Sampler ATS4, CAMAG, Muttenz, Switzerland). The plate, except the application zone, was covered with a cut HPTLC plate[27] (layer upwards, 20 cm × 8.5 cm) and wetted with a 0.1 M sodium chloride solution by piezoelectrical spraying (2.5 mL, yellow nozzle, level 6, Derivatizer, CAMAG). The covered plate was incubated at 37 °C in a humid plastic box filled with 70 mL water (26.5 cm × 16 cm × 10 cm, ABM, Wolframs-Eschenbach, Germany) for 30 min and then dried at 120 °C for 10 min (TLC Plate Heater III, CAMAG). After development in a twin trough chamber (20 cm × 10 cm) with 8 mL acetonitrile/water/2-propanol 3:1:1 (*V*/*V*/*V*) up to 70 mm (taking 15 min), the plate was piezoelectrically sprayed (4 mL, yellow nozzle, level 6, Derivatizer) with the *p*-aminobenzoic acid reagent, followed by heating (140 °C, 5 min, TLC Plate Heater III). The chromatograms were detected at FLD 366 nm (TLC Visualizer 2, CAMAG) and for densitometric fluorescence measurement at 366/>400 nm (slit 4.0 mm × 0.2 mm, mercury lamp, TLC Scanner 4, CAMAG). Subsequently, as reagent sequence, the same plate was derivatised with 2-naphthol reagent by piezoelectric spraying (4 mL, yellow nozzle, level 6, Derivatizer), followed by heating (120 °C, 5 min). The chromatograms were detected at white light illumination (TLC Visualizer 2) and measured densitometrically at 500 nm (absorbance measurement, slit 4.0 mm × 0.2 mm, deuterium/tungsten lamp, TLC Scanner 4). Instrument operation and data evaluation were performed using visionCATS software (version 3.1, CAMAG).

2.5. Comparison with a spectrophotometric α-amylase inhibition assay

For the iodine/iodide α-amylase inhibition assay,[28] 400 µL of α-amylase (22.8 U/mL, 0.5 mg/mL) and 300 µL PC acarbose (1 mg/mL) or non membrane-filtered flour extract from refined wheat were mixed in a 2 mL reaction tube and pre-incubated at 37 °C for 10 min. Soluble starch (400 µL, 1 mg/mL) was added, and the mixture was incubated at 50 °C for 30 min. For the NC (no flour extract), non-amylolysed acarbose and flour extract as blanks, sodium phosphate buffer (pH 6.9) was added instead. The enzymatic reaction was stopped with 200 µL of 1 M hydrogen chloride solution, and 900 µL iodine/iodide solution was added. Absorbance of the iodine-starch complex was measured at 630 nm using a spectrophotometer (M501, Camspec, Londorf, Germany). As an alternative measurement method, a miniaturised combined handheld cell counter and spectrometer (fluidlab R-300, anvajo, Dresden, Germany) was used.

2.6. In-vial trypsin inhibition assay for method development

The in-vial trypsin inhibition assay[25] was modified. The flour extract (100 and 150 µL) or trypsin inhibitor (168 µL of 0.05 mg/mL and 25 µL of 0.5 mg/mL) was pre-incubated (10 min) with trypsin (12.1 µL, 0.33 mg/mL, pH 8) in a sample vial with 200-µL micro insert followed by the incubation with casein (20 µL, 20 mg/mL) for 30 min. As NC, trypsin and casein were incubated without trypsin inhibitor or extract. Trypsin inhibitor, trypsin, and flour extracts in the mentioned volumes but without proteolysis were used as blanks. If necessary, a final assay volume of 200 µL was achieved by adding 25 mM ammonium bicarbonate. The final trypsin and casein concentrations were 0.02 and 2 mg/mL, respectively. The enzyme-to-substrate ratio (E/S) was 1:100 and the enzyme-to-inhibitor ratio (E/I) was 1:2.1–3.1 for trypsin inhibitor. Trypsin inhibition was evaluated via HPTLC-Vis by application of the proteolyzed samples and blank references (7 µL/band) onto an HPTLC silica gel 60 plate (20 cm × 10 cm) with the same application settings (except for a band length of 8 mm and distance from the left edge of 18 mm) as mentioned for the HPTLC–nanoGIT (amylolysis inhibition)–FLD/Vis. The plate was automatically developed with 10 mL 2-butanol/pyridine/ammonia (25%)/water (10:17:5:13, *V/V/V/V*) up to 50 mm (Automatic Development Chamber 2, ADC2, CAMAG) and derivatised with the ninhydrin reagent (2 mL, yellow nozzle, Derivatizer) and heated afterwards (120 °C, 5 min). The resulting chromatograms were detected under white-light illumination (remission transmission mode).

2.7. Screening via HPTLC–nanoGIT (proteolysis inhibition)–Vis

Trypsin (4 µL/band, 0.2 mg/mL) was applied on the HPTLC plate silica gel 60 (20 cm × 10 cm), where proteolysis was intended. Trypsin inhibitor solution (5 µL/band, 1 mg/mL), used as PC, or flour extract (not membrane-filtered, 2, 4, and 7 µL/band) was applied twice, whereby one was applied on top of the trypsin and the other was used as a reference blank. As NC, the latter two were not applied for maximal proteolysis. Finally, the intended zone was oversprayed with casein (2 µL/band, 20 mg/mL) to induce proteolysis. Additionally, trypsin and casein (volumes as mentioned) were applied as reference blanks. The plate was loaded with solutions (except for a band length of 8 mm and distance from the left edge of 18 mm), covered, wetted, incubated, and dried as described for HPTLC–nanoGIT (amylolysis inhibition)–FLD/Vis. After 10-min plate activation with a saturated solution of magnesium chloride (33% relative humidity) and 10-min plate pre-conditioning with the mobile phase, the plate was automatically developed with 10 mL 2-butanol/pyridine/ammonia (25%)/water (10:17:5:13, *V/V/V/V*) up to 50 mm and molecular sieve (0.3 nm) in the opposite trough (ADC2), taking 50-min all in all and dried afterwards (120 °C, 10 min, TLC Plate Heater III). After derivatisation of the peptides with the ninhydrin reagent as mentioned, the

resulting chromatograms were detected under white-light illumination (remission transmission mode).

2.8. Spectrophotometric trypsin inhibition assay for comparison

For the L-BAPA trypsin inhibition assay[22], flour extract (not membrane-filtered, 3–300 µL) was mixed with trypsin (200 µL, 0.0135 mg/mL), filled to 800 µL with water, and pre-incubated at 37 °C for 10 min. The PC trypsin inhibitor (5–300 µL, 0.05 mg/mL) and NC (water) were used instead of the flour extract. The L-BAPA working solution (1 mL, 0.27 mg/mL) was added and incubated at 37 °C for 20 min. The reaction was stopped by adding 200 µL acetic acid solution (30%). All samples were centrifuged at 17,000 × *g* for 3 min, and the absorbance of the released chromogenic product was measured at 410 nm using either a spectrophotometer (M501) or a combined handheld cell counter and spectrometer (fluidlab R-300). The final trypsin and L-BAPA concentrations in the 1.8 mL assay volume were 0.0015 mg/mL and 0.15 mg/mL, respectively. The corresponding reference blanks were prepared without incubation and were immediately stopped by the addition of acetic acid.

2.9. Calculation of the relative inhibition

After HPTLC–nanoGIT (amylolysis inhibition)–FLD/Vis, the corresponding matrix signal intensity (Int) in the non-amylolyzed flour extract (blank) was subtracted from the saccharide signal in the flour extract subjected to the assay (assay) and divided by the NC. This quotient was subtracted from 1 and multiplied by 100, as follows:

$$\text{Inhibition (\%)} = 1 - \frac{\text{Int (assay)} - \text{Int (blank)}}{\text{Int (NC)}} \times 100$$

After the spectrophotometric α-amylase inhibition assay, the signal intensity of the flour extract subjected to the assay (assay) was corrected by the corresponding signal of the flour extract (blank). The NC was divided by this difference. This quotient was subtracted from 1 and multiplied by 100, as follows:

$$\text{Inhibition (\%)} = 1 - \frac{\text{Int (NC)}}{\text{Int (assay)} - \text{Int (blank)}} \times 100$$

After the spectrophotometric trypsin inhibition assay, the signal intensity of each flour extract subjected to the assay (assay) was corrected by the corresponding signal intensity of the flour extract (blank), divided by that of the NC, subtracted from 1, and multiplied by 100 as follows:

$$\text{Inhibition (\%)} = 1 - \frac{\text{Int (assay)} - \text{Int (blank)}}{\text{Int (NC)}} \times 100$$

3. Results and discussion

3.1. Detection via spectrophotometric α-amylase inhibition assay

The α-amylase inhibition potential can be detected chemically via the iodine/iodide reagent[28] reacting with the remaining starch or the dinitrosalicylic acid reagent[21] reacting with the formed saccharides and enzyme kits using chromogenic substrates releasing *p*-nitrophenol[29] or fluorescent substrates[26,13]. Among these, the iodine/iodide reagent and dinitrosalicylic acid reagent were tested as

cuvette assays; however, the latter did not yield reproducible results because of the high matrix load of polysaccharides in the flour extract reacting with the dinitrosalicylic acid reagent. The iodine/iodide reagent was deployed, which does not assess the released products, but rather the decrease in the initial substrate utilised. Exemplarily the flour extract from refined wheat was subjected to a spectrophotometric α-amylase inhibition assay, in which inhibition of α-amylase resulted in more starch (amylolysis inhibition) compared to the NC (no inhibitor), resulting in higher absorption values. The inhibitor acarbose was used as the PC. Furthermore, a handheld photometer (anvajo fluidlab) was compared to a tabletop photometer (Camspec M501). For both spectrophotometric measurements (Table S1), acarbose inhibited amylolysis by 92%, and non-membrane-filtered flour extract from refined wheat (300 µL) inhibited amylolysis by 71% and 75%, respectively. The extract showed strong α-amylase inhibition, which was almost as strong as that of acarbose, confirming the presence of inhibitors. Consequently, the extract was used to develop a quantitative HPTLC–nanoGIT (amylolysis inhibition)–FLD/Vis method as follows.

3.2. Development of HPTLC–nanoGIT (amylolysis inhibition)–FLD/Vis

A previous approach[25] combined in-vial pre-incubation of α-amylase with ATI-containing flour extract and subsequent on-surface incubation with starch as a substrate. In this study, it was aimed to perform a complete workflow on the same surface in one step. The incubation period for amylolysis was shortened and the process was streamlined, resulting in a faster and more efficient workflow. Because amylolysis resulted in less glucose (Glc) than maltose (Mal) and maltotriose (Mal3)[27], a reagent sequence on the same plate was proven to be advantageous. The *p*-aminobenzoic acid reagent detected monosaccharides, such as Glc, up to a factor of 13 more sensitive[30], whereas the 2-naphthol reagent detected saccharides to the same extent.

For the enzyme-substrate reaction (amylolysis), the incubation time was reduced from 60 min to 10 min (Figure S1). A previous separate on-surface pre-incubation of α-amylase with the flour extract (30 min), followed by the enzyme-substrate reaction (10 min), led to the loss of signals due to the wetting of the plate twice (Figure S1). The blow-drying of the HPTLC plate between both incubation steps (15 min) was insufficient, and the remaining humidity on the plate led to zone diffusion. Therefore, a single incubation step was performed, in which the inhibitor, enzyme, and substrate were incubated together for 30 min to ensure adequate interactions (Figure S2). Successful inhibition by flour extract from refined wheat (non-membrane-filtered) was observed for the released Mal3. After membrane filtration, the remaining polysaccharides in the flour extract[25] (retained in the start zone besides starch) were co-metabolised, leading to an increase in Mal,

whereas no change in intensity was apparent for Glc. Hence, the inhibition of amylolysis in a single incubation step was successfully demonstrated and applied to an appropriate PC.

Our previous observation[25] that the PC acarbose, a tetra-pseudo-saccharide, is metabolised by α-amylase was confirmed (Figure 1). When α-amylase was incubated with acarbose, the Glc and Mal zones increased by 29% and the Mal3 zone increased by 17% compared to the respective saccharide signals for α-amylase (Table S2). However, with increasing amounts of acarbose (Figure 1, 1–5 µg/band), an increase in the inhibition of on-surface amylolysis was detected. The release of Glc (−1 to −24%), Mal (−5 to −26%), and Mal3 (−6 to −24%) was visibly reduced and thus inhibited, whereas the Mal3 release was difficult to evaluate with the *p*-aminobenzoic acid reagent because of its weak signal intensity, which was worsened by zone diffusion. The highly sensitive detection of saccharides clearly revealed a massive impurity of α-amylase with Glc, Mal, and Mal3 (Figure 1).

Our previous removal of saccharides using a 3k-Da Amicon Ultra filter[25] still showed residual saccharides in the flour extracts and α-amylase, but higher-volume filters were not available for purchase. Therefore, another type of membrane filtration was carried out using a D-Tube Dialyser Mega (MWCO 3.5 kDa). Although membrane filtration took longer (12 h instead of 2 h) to remove the saccharides, there was no sample concentration or clogged filters, leading to incomplete saccharide removal.

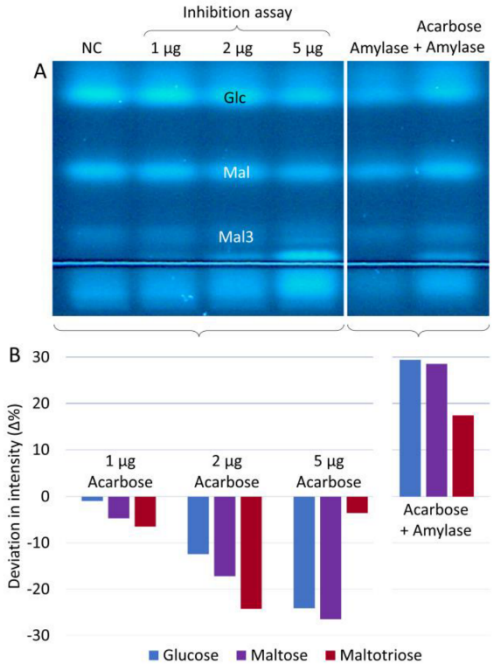

Figure 1. Inhibition of amylolysis by different acarbose amounts (1-5 µg/band): (**A**) HPTLC–nanoGIT (amylolysis inhibition)–FLD chromatogram and (**B**) percentage deviation in intensity (Δ%) of released maltotriose (**Mal3**), maltose (**Mal**) and glucose (**Glc**) in contrast to the NC (α-amylase, 2.5 µg/band and soluble starch, 4 µg/band) and for acarbose (2 µg/band) oversprayed by α-amylase (2.5 µg/band) in contrast to α-amylase (2.5 µg/band). The HPTLC plate silica gel 60 was developed with acetonitrile/water/2-propanol/acetone (12:3:4:1, *V/V/V/V*) up to 70 mm, derivatised with *p*-aminobenzoic acid reagent, detected at FLD 366 nm and densitometrically measured at 366/>400 nm (fluorescence, slit 4.0 mm × 0.2 mm, mercury lamp).

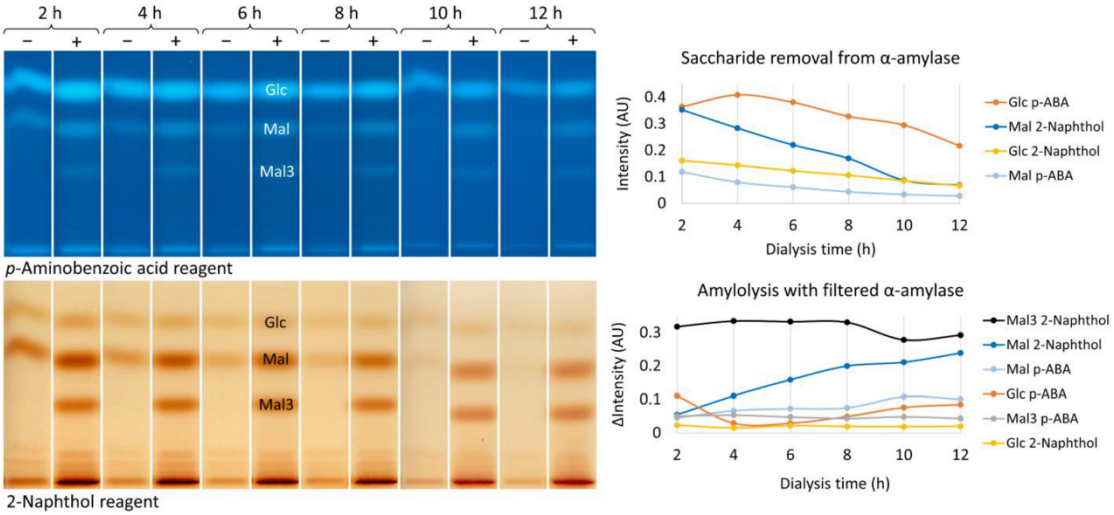

Figure 2. Saccharide removal from α-amylase (5 mg/mL) for membrane-filtration times of 2–12 h: HPTLC–nanoGIT (amylolysis inhibition)–FLD/Vis chromatograms of filtered α-amylase (2.5 µg/band, **−**) overspotted with soluble starch (4 µg/band, **+**) and graphs of respective saccharide removal from α-amylase as well as amylolysis to prove the activity of the membrane-filtered α-amylase. HPTLC plate silica gel 60 developed with acetonitrile/water/2-propanol 3:1:1 (*V*/*V*/*V*) up to 70 mm and derivatised with the *p*-aminobenzoic acid reagent (*p*-ABA), detected at FLD 366 nm and densitometric fluorescence measurement at 366/>400 nm, followed by the 2-naphthol reagent (reagent sequence on the same plate) detected under white-light illumination (remission-transmission) and densitometric absorbance measurement at 500 nm.

Different periods were tested, and a 12-h membrane filtration with salt load renewal after every two cycles (every 4 h) was suitable for the removal of saccharides from α-amylase (Figure 2). After a 2-h membrane filtration, the Mal3 zone was neither detectable with the *p*-aminobenzoic acid reagent nor 2-naphthol reagent. The intensity of the Mal zone (dark blue curve) decreased more with increasing membrane filtration time than that of the Glc zone (orange curve), which was best detectable with the 2-naphthol reagent and *p*-aminobenzoic acid reagent, respectively (Figure 2). The Glc zone was still clearly detectable after a 12-h membrane-filtration, whereas Mal and Mal3 were satisfactorily removed (Figure 2, marked **−**). To ensure proper enzymatic activity of the membrane-filtered α-amylase, on-surface amylolysis was performed (marked **+**), and the zone intensities of the released saccharides, corrected from the saccharides retained in the membrane-filtered α-amylase, were compared with each other (Figure 2). No differences in enzymatic activity were observed over the 12-h membrane-filtration period, although Mal and Mal3 being detected using the 2-naphthol reagent, and Glc being visualized by the *p*-aminobenzoic acid reagent.

Surprisingly, the saccharide release of Mal via the 2-naphthol reagent (dark blue curve) increased constantly with membrane filtration

time, which was not observed to this extent via the *p*-aminobenzoic acid reagent (light blue curve). The lower the amount of Mal present in the sample, the more Mal was released during amylolysis. If Mal acts as a putative inhibitor of amylolysis[31–33], its removal could cause an increase in activity and, thus, higher Mal release; however, no increase in other saccharides was observed. The decrease in the release of Mal3 via the 2-naphthol reagent (black curve) could be an indication of limited α-amylase activity after such a long membrane filtration period, but was not confirmed via derivatisation with the *p*-aminobenzoic acid reagent (grey curve), which, however, is not as sensitive for the detection of polysaccharides. Additionally, the 10-h and 12-h membrane-filtered α-amylase were not applied onto the same HPTLC plate and thus were not derivatised together with the ones collected after 2–8 h, so these intensity signals must be interpreted with caution

The Glc intensity via the *p*-aminobenzoic acid reagent (orange curve) decreased after 4 h of membrane filtration and then slightly increased, which could be due to minor fluctuations in the random enzymatic reaction because the activity was constant via 2-naphthol derivatisation (yellow curve), which, however, is not as sensitive to short-chain saccharides.

As mentioned, native polysaccharides in the flour extract which were co-metabolised in addition to starch by α-amylase led to an increase in the Mal zone after inhibition of amylolysis by these (Figure S2), which is why the flour extracts were also membrane-filtered. The flour extract from whole wheat was selected to evaluate the time required for membrane filtration due to its expected high contents of Glc, Mal, and Mal3 (Figure S3). A 12-h membrane filtration with salt load renewal after every two cycles (every 4 h) was sufficient to remove most of the saccharides. Analogously, the refined wheat and einkorn flour extracts were membrane-filtered for 12 h and used as the corresponding flour extract blanks.

3.3. Quantification of amylolysis inhibition by ATI-containing flour extracts using HPTLC–nanoGIT (amylolysis inhibition)–FLD/Vis

After the successful development of the all-in-one HPTLC–nanoGIT (amylolysis inhibition)–FLD/Vis method, inhibition by ATI-containing membrane-filtered flour extracts from refined wheat, whole wheat, and einkorn was investigated (Figure 3). Two derivatisation reagents were used as reagent sequence (first *p*-aminobenzoic acid reagent and then 2-naphthol reagent) and compared to determine the best detection mode. The PC acarbose was used for comparison (Table S3). As mentioned, the detectability of the released saccharides was different for the two reagents. The difference between both reagents was highest for Glc (16–29%), followed by Mal3 (13–17%), and Mal (3–8%). For three-fold analysis on three different plates, Mal3 (2% and 5%) showed the best and Glc the worst (21% and 23%) interday precisions for the

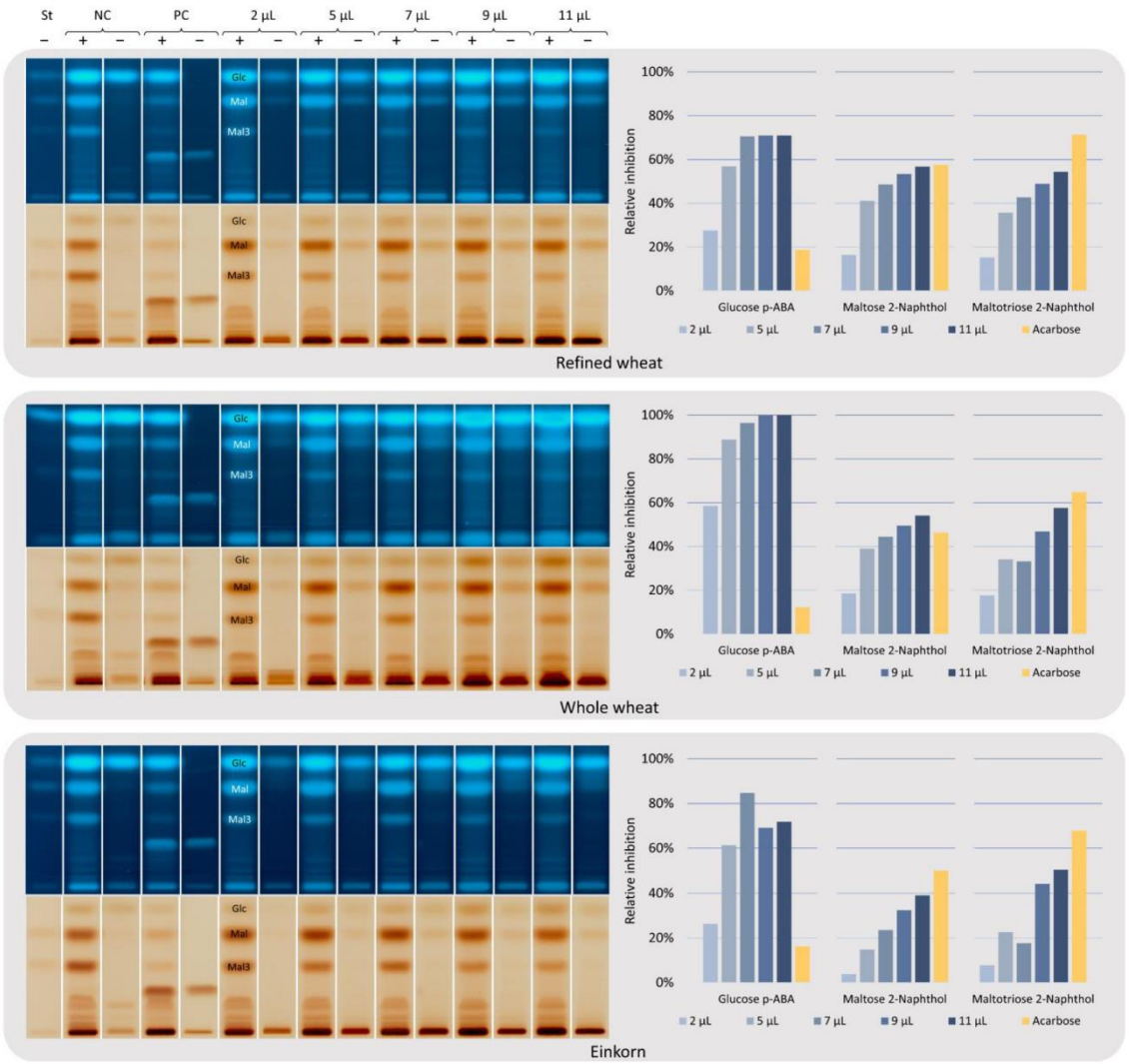

Figure 3. Quantification of the inhibition of the amylolysis by three ATI-containing flour extracts from refined wheat, whole wheat, and einkorn: HPTLC–nanoGIT (amylolysis inhibition)–FLD/Vis chromatograms on HPTLC plates silica gel 60 with different volumes (2–11 µL/band) of 12-h membrane-filtered flour extracts or **NC** (no flour ATI extract applied) or **PC** acarbose (5 µg/band) oversprayed with 12-h membrane-filtered α-amylase (25 µg/band) and soluble starch (20 µg/band) for amylolysis (**+**) *versus* corresponding non-amylolysed (**−**) counterparts and standards (**St**; **Glc** 0.5 µg/band, **Mal** and **Mal3** 1 µg/band). The plates were developed with acetonitrile/water/2-propanol 3:1:1 (*V*/*V*/*V*) up to 70 mm and derivatised as a reagent sequence first with the *p*-aminobenzoic acid reagent (*p*-ABA), detected at FLD 366 nm, followed by densitometric fluorescence measurement at 366/>400 nm, and then with the 2-naphthol reagent detected under white-light illumination (remission-transmission), followed by densitometric absorbance measurement at 500 nm.

p-aminobenzoic acid reagent and 2-naphthol reagent, respectively (Table S3). The *p*-aminobenzoic acid reagent was slightly more precise for all saccharides than the 2-naphthol

reagent (2–21% *versus* 5–23%), and the calculated relative inhibition by acarbose was lower via Glc release and higher via Mal and Mal3 release. In particular, the detection of Glc was challenging. The intensity of Glc using the *p*-aminobenzoic acid reagent was close to the detection limit since it is very sensitive to monosaccharides, and with the 2-naphthol reagent, it was close to the LOD/LOQ due to the low amounts released. A reduction/increase in Glc release alone was not possible because it was limited by amylolysis, releasing all products in specified amounts. The precision values were only worse for those saccharides (Glc and Mal), for which α-amylase was impure. However, the detectability of Glc was better with the *p*-aminobenzoic acid reagent, and of Mal and Mal3 with the 2-naphthol reagent; the inhibition by the flour extracts was evaluated for this detection combination (Figure 3, all in Tables S4–6).

As expected, the relative inhibition of amylolysis (calculated via the reduced release of each saccharide) increased continuously with increasing volume of all ATI-containing flour extracts, except for Glc from the einkorn extract, with a maximum of 85% at 7 µL. The decrease in the relative inhibition at higher volumes could be explained by an inhibitor which tends toward side reactions (dissociation of enzyme-inhibitor complex or creation of inhibitor-substrate or inhibitor-inhibitor complexes)[34] and thus becomes unavailable for further inhibition. This effect was also observed in the spectrophotometric trypsin inhibition assay (2.2.2.), where only einkorn showed a decrease in relative inhibition at higher volumes. Inhibition by flour extracts from refined and whole wheat, with respect to Glc, reached saturation at approximately 70% and 100%, respectively. The relative inhibition of nearly 100% was difficult to evaluate because of the high native amount of Glc in whole wheat. Subtracting this amount, the corrected intensity signal was negative, resulting in inhibition of 100% and 104% for the 9-µL and 11-µL flour extracts, respectively. Comparing the flour extracts from refined and whole wheat, the latter had a higher relative inhibition (based on Glc), but also showed the highest native Glc amount. The reduction in released Mal and Mal3 was slightly higher for the flour extract from refined wheat. Because ATIs are present in the endosperm[35,36], a higher inhibition by the flour extract from refined wheat was assumed. However, the reduced release of Mal and Mal3 indicated a similar α-amylase inhibition. The flour extract from einkorn inhibited α-amylase to a lesser extent than that of refined wheat. This confirmed previous hypotheses.[17,29] Also a correlation between ATI content of different cereals and α-amylase inhibition was not evident, indicating the presence of other inhibitors as well as reduced inhibition of human salivary α-amylase.[26]

Quantification of the inhibition of α-amylase by ATI-containing flour extracts was possible via HPTLC–nanoGIT (amylolysis inhibition)–FLD/Vis. The einkorn extract showed lower inhibition than the refined and whole wheat,

whereas the latter showed no difference. In contrast to our previous study[25], better purification of flour extracts resulted in more differentiated results. Since purification of flour and α-amylase is preferable to subtraction of the respective blank signal intensity, particularly when close to the detection limit (2-naphthol reagent) or signal saturation/detector limit (*p*-aminobenzoic acid reagent), the extracts need to be further purified in the future. Furthermore, different origins of α-amylase[27] should be investigated to clarify their affinities.

3.4. Spectrophotometric trypsin inhibition assay

For comparison, a spectrophotometric trypsin inhibition assay was performed with L-BAPA as a substrate.[22] Again, the tabletop photometer was compared with the handheld photometer and showed no differences in relative inhibition (Figure S4, Table S7). The first experiment, which resulted in no product release, showed that L-BAPA was not interchangeable with DL-BAPA, as suggested by suppliers. Trypsin inhibitor from *Glycine max* was chosen as PC and different final concentrations (0.03–8.33 µg/mL) were used to prove a linear inhibition range and successfully confirmed it (Figure S4A, Table S7). Since a linear increase in inhibition followed by a subsequent decrease at higher flour extract volumes has been reported,[22] trypsin inhibition was investigated for increasing volumes (3–300 µL) of the flour extracts (Figure 4, Table S7). At higher volumes (>80 µL), a decrease at almost 100%

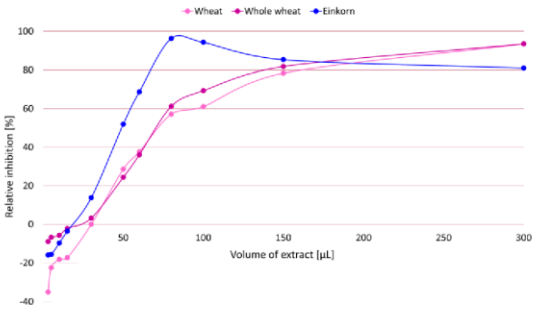

Figure 4. The mean relative inhibition (via tabletop and handheld spectrophotometer, separate relative inhibitions in Figure S4, datasets in Table S7) of trypsin by flour extracts from refined wheat, whole wheat, and einkorn (3–300 µL) in the spectrophotometric trypsin inhibition assay (1.8 mL assay volume, 0.0015 mg/mL trypsin and 0.15 mg/mL L-BAPA.

inhibition was observed only for einkorn, as already discussed for HPTLC–nanoGIT (amylolysis inhibition)–FLD/Vis. The flour extracts from refined and whole wheat showed a nearly linear increase up to 100 µL and then reached a plateau at 100% inhibition, contrary to the results of a previous study[22]. The curve and inhibition potential were very similar for refined and whole wheat. An inhibition of nearly 100% for all three cereal types was observed at high extract volumes. Surprisingly, the assay reproducibly resulted in negative inhibition (increasing trypsin activity) at low extract volumes (3–15 µL) for all three types of cereals. This phenomenon has not been reported thus far, and only assumptions regarding the increase in trypsin activity can be made. The flour ATI-containing extract either contained an activity-increasing co-factor/enzyme, which was suppressed/compensated at higher inhibitor

concentrations, or an L-BAPA-destabilising agent, which suggests higher enzyme activity.

3.5. In-vial trypsin inhibition assay, followed by HPTLC separation

The in-vial trypsin inhibition assay followed by HPTLC separation was performed on wettable reversed-phase HPTLC plates.[25] After several unsuccessful trials of on-surface proteolysis on this batch-dependent plate (data not shown), the plate type was changed to a more batch-robust and cheaper normal phase plate. First, the mobile phase for peptide separation[37] was optimized to ensure good selectivity. The best separation was achieved by 2-butanol/pyridine/ammonia (25%)/water 10:17:5:13 (*V/V/V/V*), which was approximately half of 2-butanol as used before (19.5:17:5:13, *V/V/V/V)*. Before the implementation of the on-surface assay, the best enzyme-inhibitor ratio (E/I) was evaluated via an in-vial trypsin inhibition assay using a trypsin inhibitor from *Glycine max* (TI) as PC and the protein casein as the substrate. An abrupt strong inhibition was observed between an E/I of 1:2.1 and 1:3.1 (Figure S5), which could point to competitive inhibition.[34] To differentiate false positive results for the highest E/I from a failed assay, both E/I were analysed in the following.

First, it was excluded that the protein-containing flour extract was digested by trypsin. The peptides detected for trypsin mixed with flour extract from refined wheat (no casein present) were assigned to the matrix signals from the extract (Figure S6). The optimal incubation period and volume of the flour extracts were also evaluated using an in-vial trypsin inhibition assay (Figure S6). No difference was observed for different pre-incubation times (10–30 min) of the enzyme and inhibitor, and an increase in inhibition of proteolysis by flour extract from refined wheat was only visible between 100 and 150 µL, whereas a further increase in the volume (175 µL) did not increase the inhibition.

Thus, a pre-incubation time of 10 min, an E/I ratio of 1:2–3 for trypsin inhibitor, and flour extract volumes of 100–150 µL were selected for further analysis. The three different types of flours were compared using the in-vial trypsin inhibition assay (Figure 5) with respect to any difference between whole grain and refined flours[35,36] and einkorn as a reported ATI-poor cereal.[38,36,17] For distinct peptide signals (Figure 5, framed), inhibition was observed. The flour extract from refined wheat slightly inhibited proteolysis (marked **+**) compared to that of whole wheat, whereas the evaluation of einkorn was difficult due to high matrix loads. In particular, strong blank signals (marked **−**) were detected for the flour extract from einkorn. A comparison of the PC and flour extracts showed that not the same peptides were inhibited to the same extent, which was most probably caused by different active trypsin centres. With increasing amounts of PC, a clear increase in inhibition was evident (Figure 5), whereas in the repetition of the analysis on the second plate, both E/Is showed complete inhibition (Figure S7). In addition, the NC showed different intensities of the peptide signals on both plates, indicating

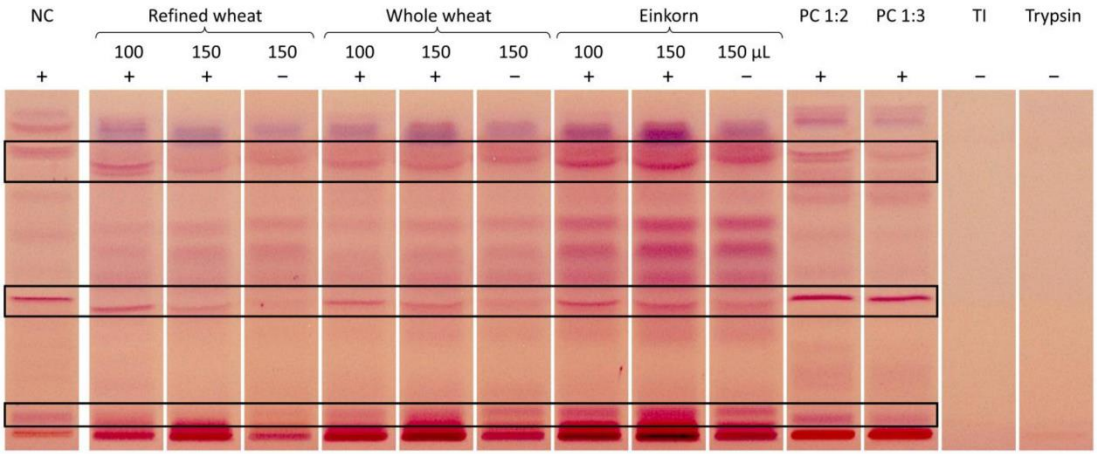

Figure 5. In-vial trypsin inhibition assay (7 µL/band), followed by HPTLC analysis: HPTLC–Vis chromatograms showing inhibition (framed black) of proteolysis (marked **+**) by three flour extracts (100 and 150 µL each) as well as PC trypsin inhibitor (**TI**, 1:2–3) mixed in a vial with trypsin and casein (**NC**, 1:100), pre-incubated (10 min), and incubated (30 min) at 37 °C. Additionally, non-proteolyzed (marked **−**) flour extract, TI, and trypsin were applied and separated on an HPTLC silica gel 60 plate with 2-butanol/pyridine/ammonia (25%)/water 10:17:5:13 (*V/V/V/V*) up to 50 mm, derivatised with ninhydrin reagent, and detected under white-light illumination (remission-transmission).

that the stronger inhibition by the PC could be overlaid by an overall lower signal intensity on the second plate (Figure S7). It was found that the separation was susceptible to relative humidity, which was controlled to be approximately 33% on the plate surface by pre-conditioning with saturated magnesium chloride solution and as dry as possible (< 15%) during development via using a molecular sieve (0.3 nm) in further analyses.

3.6. Development of the on-surface proteolysis inhibition

For full on-surface proteolytic inhibition, the optimal on-surface enzyme-substrate ratio (E/S) was evaluated (Figure S8). Unfortunately, casein showed weak peptide signals in the absence of trypsin. This was explained by the higher absolute amounts analysed, *i.e.* a 50–100-fold higher amount of casein via the on-surface approach (40–80 µg/band) than in the in-vial assay (0.8 µg/band). Standard enzyme assay protocols usually only specify the E/S, so that each user can adapt these ratios to specific applications. However, the evaluation of different absolute amounts of trypsin and casein, but still the same E/S, revealed strong differences in the peptide signals. Nevertheless, the higher the amount of trypsin and casein, the stronger the peptide signals in comparison with casein blanks which proved successful on-surface proteolysis (Figure S8a–d). The casein solution was a difficult substrate due to the presence of casein micelles, which is why highly concentrated solutions were needed to achieve higher amounts with lower volumes. This led to the partial destruction of the plate

at the application zone which impaired the separation (Figure S8d). Thus, 40 µg/band casein (2 µL/band, 20 mg/mL) was the maximum amount that could be applied satisfactorily. After plate drying (blow-drying), the separation of peptides was prone to residual humidity, resulting from the incubation of the plate. Plate heating (120 °C, 10 min) was more effective than blow drying. It did not influence the amount of peptide signals (Figure S8) or lead to denaturation of proteins or false-positive peptide signals. Although an E/S of 1:100 has been recommended[22], the best peptide signals were obtained at a lower E/S of 1:50. The order of the solutions applied/oversprayed on the same start zone was as follows. First, trypsin was applied, followed by the inhibitor, and finally the substrate.

3.7. Comparative inhibition of the proteolysis by ATI-containing flour extracts via HPTLC–nanoGIT (proteolysis inhibition)–Vis

Using the developed HPTLC–nanoGIT (proteolysis inhibition)–Vis, the three flour extracts and PC (TI) were applied on the HPTLC plate via overspotting and incubated for 30 min to ensure optimal interactions (Figure 6). The plate layout did not provide enough space for both E/I ratios of 1:2 and 1:3; thus, an E/I of 1:2.5 was chosen. The PC (E/I 1:2.5) almost completely inhibited proteolysis, and only weak peptide signals were still visible, confirming successful on-surface proteolysis inhibition. Due to the strong native peptide signals of the flour extracts at volumes of 4 µL and 7 µL (Figure 6),

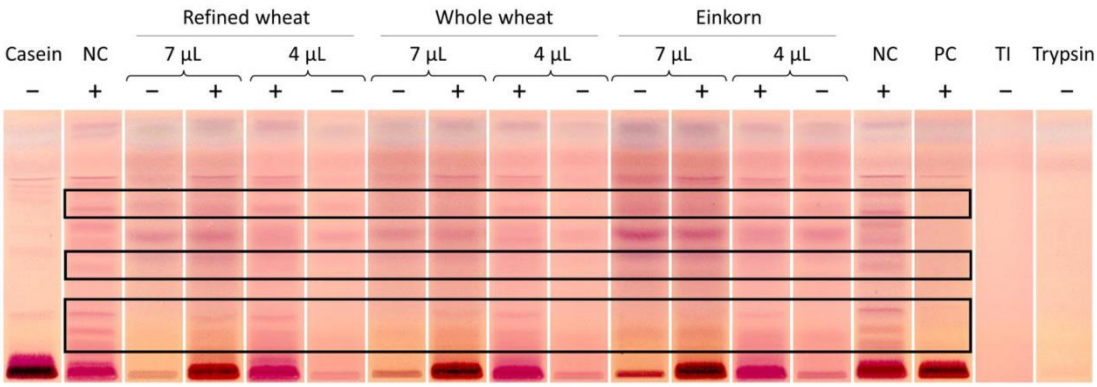

Figure 6 HPTLC–nanoGIT (proteolysis inhibition)–Vis chromatograms showing the inhibition (framed black) of the proteolysis (marked **+**) by three flour extracts (4 and 7 µL/band), trypsin inhibitor (**TI**, 1 µL/band, 0.5 mg/mL) as PC (E/I 1:2.5) and maximal proteolysis (**NC**, E/S 1:50) with trypsin (4 µL/band, 0.2 mg/mL) and casein (2 µL/band, 20 mg/mL) after 30 min incubation at 37 °C. Additionally, non-proteolyzed (marked **−**) flour extracts, TI and trypsin in the mentioned amount was applied and separated on HPTLC silica gel 60 plates with 2-butanol/pyridine/ammonia (25%)/water 10:17:5:13 (*V/V/V/V*) up to 50 mm, derivatised with the ninhydrin reagent, and detected under white-light illumination in remission-transmission.

an additional volume of 2 µL was chosen, and inhibition of proteolysis was still observed (Figure S9). A comparison of different cereal flour extracts and volumes revealed only slight differences in inhibition, except for einkorn at higher volumes (Figure 6, framed).
The flour extract from einkorn showed stronger inhibition of some peptide signals than the refined and whole wheat extracts, which was in accordance with the literature.[29] ATI-containing flour extracts from refined and whole wheat had a similar trypsin inhibitory potential, as a difference was not evident.

Although the native peptides in the extracts hindered easy evaluation of the trypsin inhibition potential, the on-surface assay can successfully be used for studying the inhibition processes. Again, membrane filtration of flour extracts with a higher or even the same molecular weight cut-off as used here could exclude small peptide signals without losing the ATIs. Because it could not be excluded that the flour extracts contained other inhibiting compounds besides the ATIs, pre-fractionation of the extract via HPLC[26] and analysis of the fractions via the developed on-surface method could identify causative substances and reduce matrix signals.

3.8. Comparison of methodologies

The first hypothesis, that the method workflow can be performed completely on the surface in one step together (HPTLC–nanoGIT), was true. The second hypothesis, that inhibition by ATIs can be analysed quantitatively, was true for the inhibition of amylolysis, whereas the inhibition of proteolysis was comparatively evaluated.

A quantitative comparison between the spectrophotometric α-amylase inhibition assay (E/S 1:2) and the HPTLC–nanoGIT (amylolysis inhibition)–FLD/Vis (E/S 1:0.8) was made for the refined wheat flour extract. Since different amounts of enzyme and flour extract were used, a comparison was achieved via E/I, i.e 1:150 and 1:8–44, respectively. For the spectrophotometric assay, an E/I of 1:150 resulted in a mean inhibition of amylolysis of 73%, whereas for the HPTLC approach for the highest E/I of 1:44 an overall inhibition (addition of each corrected saccharide signal) of 62% was calculated according to the mentioned formula (2.9). Both approaches resulted in a difference of 11% in inhibition. Considering the different E/S and E/I ratios, the HPTLC approach provided less substrate (2.5-fold) and inhibitor (3.4-fold) than the spectrophotometric approach, making it difficult to find a clear statement about comparability. Since both approaches used starch as a substrate, excellent comparability could be achieved by reducing the E/I and E/S of the spectrophotometric approach bearing in mind the limit of detection of the iodine/iodide reagent. Nevertheless, the developed HPTLC–nanoGIT (amylolysis inhibition)–FLD/Vis allowed clear and differentiated results regarding the single saccharides released during amylolysis and their interactions with α-amylase. The HPTLC–nanoGIT (proteolysis inhibition)–Vis allowed a comparative evaluation of the inhibition of

proteolysis by different ATI-containing flour extracts but was not suitable for quantification because of the dominant peptide signals in the blank samples. The spectrophotometric trypsin inhibition assay showed nearly 100% inhibition for the three cereal types at higher extract volumes (300 µL), whereas einkorn showed maximum inhibition at 100 µL. Comparability was reached for an E/I of 1:0.7–66 and E/S of 1:100 for the spectrophotometric trypsin inhibition assay and respectively 1:0.6–2 and 1:50 for HPTLC–nanoGIT (proteolysis inhibition)–Vis. Hence, in the overlapping E/I ratio of 1:0.6–2, flour extract volumes were compared (3–100 µL *versus* 2–7 µL). In this E/I range, the curve for the spectrophotometric trypsin inhibition assay (Figure 4) was linear, and thus comparable evaluation was legitimate. At the highest E/I, the inhibition by flour extracts from refined wheat, whole wheat, and refined einkorn was 60%, 70%, and 100%, respectively, and was negative at the lowest E/I. For HPTLC–nanoGIT (proteolysis inhibition)–Vis, a difference of 10% in inhibition between refined and whole wheat was difficult to detect. Total trypsin inhibition by flour extract from einkorn was not observed for any of the peptide signals. The spectrophotometric trypsin inhibition assay showed 100% inhibition for all three types of cereal at higher extract concentrations. In particular, 100% inhibition could only be partially confirmed with the on-surface HPTLC trypsin inhibition assay, where further reduction of the matrix peptide signals is helpful. Nevertheless, matrix reduction is also preferred for spectrophotometric assays to prevent negative relative inhibition values.

In conclusion, for the first time, both on-surface methods were established as reliable, even superior alternatives to existing spectrophotometric inhibitor assays, and can be used complementary to better estimate the inhibition by ATIs. In contrast to mass spectrometric approaches, these methods could be used to identify not only known but also unidentified inhibitors in combination with further purification and effect-directed analysis. Additionally, the inexpensive 2LabsToGo system[39–41] can be utilised to apply the comparatively information-rich and more sustainable on-surface methodology. The power of both developed methods is evident to provide a profile pattern of the released individual metabolisation products and compare these for different inhibitors, thus identifying different modes of inhibition for different inhibitors. Comparatively, more information was obtained which is helpful for understanding the underlying mechanisms.

Funding sources

Instrumentation was partially funded by the Deutsche Forschungsgemeinschaft (DFG, German Research Foundation) - INST 162/536-1 FUGG and INST 162/471-1 FUGG.

Orcid

Gertrud Morlock https://orcid.org/0000-0001-9406-0351

Isabel Müller https://orcid.org/0000-0002-7392-7048

CrediT authorship contribution statement

Isabel Müller: Conceptualization, Methodology, Experimental Analysis, Data Analysis, Writing – Original Draft. **Ilka Scheibelhut**: Experimental Analysis, Data Analysis. **Gertrud E. Morlock**: Conceptualization, Methodology, Supervision, Writing – Review and Editing.

Declaration of interests

The authors declare that they have no known competing financial interests or personal relationships that could have influenced the work reported in this study.

Supporting information

Raw data from the on-surface and spectrophotometric inhibition assays and additional figures of the method optimisation are included in the supplementary information (PDF).

Abbreviations

ATI – α-Amylase/trypsin inhibitors

E/I – Enzyme-to-inhibitor ratio

E/S – Enzyme-to-substrate ratio

FLD – Fluorescence detection

FODMAPS – Fermentable oligosaccharides, disaccharides, monosaccharides, and polyols

Glc – Glucose

HPLC – High-performance liquid chromatography

HPTLC – High-performance thin-layer chromatography

L-BAPA – *N*α-Benzoyl-L-arginin-4-nitroanilid-hydrochlorid

Mal – Maltose

Mal3 – Maltotriose

MWCO – Molecular weight cut-off

nanoGIT – Nano gastrointestinal tract simulation

NC – Negative control

NCGS – Non-celiac gluten sensitivity

PC – Positive control

Tris – Tris(hydroxymethyl)aminomethane

TI – Trypsin inhibitor from *Glycine max*

Vis – Visible light detection

References

(1) Cuccioloni, M.; Mozzicafreddo, M.; Ali, I.; Bonfili, L.; Cecarini, V.; Eleuteri, A. M.; Angeletti, M. Interaction between wheat alpha-amylase/trypsin bi-functional inhibitor and mammalian digestive enzymes: Kinetic, equilibrium and structural characterization of binding, *Food Chem.* **2016**, *213,* 571–578.

(2) Altenbach, S. B.; Vensel, W. H.; Dupont, F. M. The spectrum of low molecular weight alpha-amylase/protease inhibitor genes expressed in the US bread wheat cultivar Butte 86, *BMC Res Notes.* **2011**, *4,* 242.

(3) Dupont, F. M.; Vensel, W. H.; Tanaka, C. K.; Hurkman, W. J.; Altenbach, S. B. Deciphering the complexities of the wheat flour proteome using quantitative two-dimensional electrophoresis, three proteases and tandem mass spectrometry, *Proteome Sci.* **2011**, *9,* 10.

(4) Shan, L.; Molberg, Ø.; Parrot, I.; Hausch, F.; Filiz, F.; Gray, G. M.; Sollid, L. M.; Khosla, C. Structural basis for gluten intolerance in celiac sprue, *Science.* **2002**, *297,* 2275–2279.

(5) Junker, Y.; Zeissig, S.; Kim, S.-J.; Barisani, D.; Wieser, H.; Leffler, D. A.; Zevallos, V.; Libermann, T. A.; Dillon, S.; Freitag, T. L.; Kelly, C. P.; Schuppan, D. Wheat amylase trypsin inhibitors drive intestinal inflammation via activation of toll-like receptor 4, *J. Exp. Med.* **2012**, *209,* 2395–2408.

(6) Zevallos, V. F.; Raker, V.; Tenzer, S.; Jimenez-Calvente, C.; Ashfaq-Khan, M.; Rüssel, N.; Pickert, G.; Schild, H.; Steinbrink, K.; Schuppan, D. Nutritional Wheat Amylase-Trypsin Inhibitors Promote Intestinal Inflammation via Activation of Myeloid Cells, *Gastroenterology.* **2017**, *152,* 1100-1113.e12.

(7) Cárdenas-Torres, F. I.; Cabrera-Chávez, F.; Figueroa-Salcido, O. G.; Ontiveros, N. Non-Celiac Gluten Sensitivity: An Update, *Medicina.* **2021**, *57.*

(8) Geisslitz, S.; Shewry, P.; Brouns, F.; America, A. H. P.; Caio, G. P. I.; Daly, M.; D'Amico, S.; Giorgio, R. de; Gilissen, L.; Grausgruber, H.; Huang, X.; Jonkers, D.; Keszthelyi, D.; Larré, C.; Masci, S.; Mills, C.; Møller, M. S.; Sorrells, M. E.; Svensson, B.; Zevallos, V. F.; Weegels, P. L. Wheat ATIs: Characteristics and Role in Human Disease, *Front. Nutr.* **2021**, *8.*

(9) Catassi, C.; Bai, J. C.; Bonaz, B.; Bouma, G.; Calabrò, A.; Carroccio, A.; Castillejo, G.; Ciacci, C.; Cristofori, F.; Dolinsek, J.; Francavilla, R.; Elli, L.; Green, P.; Holtmeier, W.; Koehler, P.; Koletzko, S.; Meinhold, C.; Sanders, D.; Schumann, M.; Schuppan, D.; Ullrich, R.; Vécsei, A.; Volta, U.; Zevallos, V.; Sapone, A.; Fasano, A. Non-Celiac Gluten sensitivity: the new frontier of gluten related disorders, *Nutrients.* **2013**, *5,* 3839–3853.

(10) Mumolo, M. G.; Rettura, F.; Melissari, S.; Costa, F.; Ricchiuti, A.; Ceccarelli, L.; Bortoli, N. de; Marchi, S.; Bellini, M. Is Gluten the Only Culprit for Non-Celiac Gluten/Wheat Sensitivity?, *Nutrients.* **2020**, *12,* 3785.

(11) Kostekli, M.; Karakaya, S. Protease inhibitors in various flours and breads: Effect of fermentation, baking and in vitro digestion on trypsin and chymotrypsin inhibitory activities, *Food Chem.* **2017**, *224,* 62–68.

(12) Granum, P. E. Studies on α-amylase inhibitors in foods, *Food Chem.* **1979**, *4,* 173–178.

(13) Gélinas, P.; McKinnon, C.; Gagnon, F. Inhibitory activity towards human α-amylase in cereal foods, *LWT Food Sci. Technol.* **2018**, *93,* 268–273.

(14) Bose, U.; Byrne, K.; Howitt, C. A.; Colgrave, M. L. Targeted proteomics to monitor the extraction efficiency and levels of barley α-amylase trypsin inhibitors that are implicated in non-coeliac gluten sensitivity, *J. Chromatogr. A.* **2019**, *1600,* 55–64.

(15) Bose, U.; Juhász, A.; Broadbent, J. A.; Byrne, K.; Howitt, C. A.; Colgrave, M. L. Identification and Quantitation of Amylase Trypsin Inhibitors Across Cultivars Representing the Diversity of Bread Wheat, *J Proteome Res.* **2020**, *19,* 2136–2148.

(16) Geisslitz, S.; Longin, C. F. H.; Koehler, P.; Scherf, K. A. Comparative quantitative LC-MS/MS analysis of 13 amylase/trypsin inhibitors in ancient and modern Triticum species, *Sci Rep.* **2020**, *10,* 14570.

(17) Geisslitz, S.; Ludwig, C.; Scherf, K. A.; Koehler, P. Targeted LC-MS/MS Reveals Similar Contents of α-Amylase/Trypsin-Inhibitors as Putative Triggers of

Nonceliac Gluten Sensitivity in All Wheat Species except Einkorn, *J. Agric. Food. Chem.* **2018**, *66,* 12395–12403.

(18) Tchewonpi Sagu, S.; Landgräber, E.; Rackiewicz, M.; Huschek, G.; Rawel, H. Relative Abundance of Alpha-Amylase/Trypsin Inhibitors in Selected Sorghum Cultivars, *Molecules.* **2020**, *25,* 5982.

(19) Tchewonpi Sagu, S.; Zimmermann, L.; Landgräber, E.; Homann, T.; Huschek, G.; Özpinar, H.; Schweigert, F. J.; Rawel, H. M. Comprehensive Characterization and Relative Quantification of α-Amylase/Trypsin Inhibitors from Wheat Cultivars by Targeted HPLC-MS/MS, *Foods.* **2020**, *9.*

(20) Prandi, B.; Faccini, A.; Tedeschi, T.; Galaverna, G.; Sforza, S. LC/MS analysis of proteolytic peptides in wheat extracts for determining the content of the allergen amylase/trypsin inhibitor CM3: influence of growing area and variety, *Food Chem.* **2013**, *140,* 141–146.

(21) Tchewonpi Sagu, S.; Huschek, G.; Bönick, J.; Homann, T.; Rawel, H. M. A New Approach of Extraction of α-Amylase/trypsin Inhibitors from Wheat (Triticum aestivum L.), Based on Optimization Using Plackett-Burman and Box-Behnken Designs, *Molecules.* **2019**, *24.*

(22) Call, L.; Reiter, E. V.; Wenger-Oehn, G.; Strnad, I.; Grausgruber, H.; Schoenlechner, R.; D'Amico, S. Development of an enzymatic assay for the quantitative determination of trypsin inhibitory activity in wheat, *Food Chem.* **2019**, *299,* 125038.

(23) Call, L.; Haider, E.; D'Amico, S.; Reiter, E.; Grausgruber, H. Synthesis and accumulation of amylase-trypsin inhibitors and changes in carbohydrate profile during grain development of bread wheat (Triticum aestivum L.), *BMC Plant Biol.* **2021**, *21,* 113.

(24) Priya, S.; Kumar, S.; Kaur, N.; Gupta, A. K. Specificity of α-amylase and trypsin inhibitor proteins in wheat against insect pests, *N. Z. J. Crop Hortic. Sci.* **2013**, *41,* 49–56.

(25) Müller, I.; Schmid, B.; Bosa, L.; Morlock, G. E. Screening of α-amylase/trypsin inhibitor activity in wheat, spelt and einkorn by high-performance thin-layer chromatography, *Food Funct.*, *in submission.*

(26) Jahn, N.; Longin, C. F. H.; Scherf, K. A.; Geisslitz, S. No correlation between amylase/trypsin-inhibitor content and amylase inhibitory activity in hexaploid and tetraploid wheat species, *Curr. Res. Food Sci.* **2023**, *7,* 100542.

(27) Müller, I.; Morlock, G. E. Quantitative saccharide release of hydrothermally treated flours by validated salivary/pancreatic on-surface amylolysis (nanoGIT) and high-performance thin-layer chromatography, *Food Chem.* **2023**, *432,* 137145.

(28) Xiao, Z.; Storms, R.; Tsang, A. A quantitative starch-iodine method for measuring alpha-amylase and glucoamylase activities, *Anal. Biochem.* **2006**, *351,* 146–148.

(29) Simonetti, E.; Bosi, S.; Negri, L.; Dinelli, G. Amylase Trypsin Inhibitors (ATIs) in a Selection of Ancient and Modern Wheat: Effect of Genotype and Growing Environment on Inhibitory Activities, *Plants.* **2022**, *11.*

(30) Morlock, G. E.; Morlock, L. P.; Lemo, C. Streamlined analysis of lactose-free dairy products, *J. Chromatogr. A.* **2014**, *1324,* 215–223.

(31) Elödi, P.; Móra, S.; Krysteva, M. Investigation of the active center of porcine-pancreatic amylase, *Eur. J. Biochem.* **1972**, *24,* 577–582.

(32) Tsyrulneva, I.; Alagappan, P.; Liedberg, B. Colorimetric Detection of Salivary α-Amylase Using Maltose as a Noncompetitive Inhibitor for Polysaccharide Cleavage, *ACS Sens.* **2019**, *4,* 865–873.

(33) Warren, F. J.; Butterworth, P. J.; Ellis, P. R. Studies of the effect of maltose on the direct binding of porcine pancreatic α-amylase to maize starch, *Carbohydr. Res.* **2012**, *358,* 67–71.

(34) Howard, D. R.; Herr, J.; Hollister, R. Using Trypsin & Soybean Trypsin Inhibitor To Teach Principles of Enzyme Kinetics, *The American Biology Teacher.* **2006**, *68,* 99–104.

(35) Finnie, C.; Melchior, S.; Roepstorff, P.; Svensson, B. Proteome analysis of grain filling and seed

maturation in barley, *Plant Physiol.* **2002**, *129,* 1308–1319.

(36) Guo, G.; Lv, D.; Yan, X.; Subburaj, S.; Ge, P.; Li, X.; Hu, Y.; Yan, Y. Proteome characterization of developing grains in bread wheat cultivars (Triticum aestivum L.), *BMC Plant Biol.* **2012**, *12,* 147.

(37) Pasilis, S. P.; Kertesz, V.; van Berkel, G. J.; Schulz, M.; Schorcht, S. Using HPTLC/DESI-MS for peptide identification in 1D separations of tryptic protein digests, *Anal. Bioanal.Chem.* **2008**, *391,* 317–324.

(38) Mahalak, K. K.; Firrman, J.; Tomasula, P. M.; Nuñez, A.; Lee, J.-J.; Bittinger, K.; Rinaldi, W.; Liu, L. S. Impact of Steviol Glycosides and Erythritol on the Human and Cebus apella Gut Microbiome, *J. Agric. Food. Chem.* **2020**.

(39) Jakob, K.; Schwack, W.; Morlock, G. E. All-in-one 2LabsToGo system for analysis of ergot alkaloids in whole rye, *in submission.* **2024**.

(40) Morlock, G. E.; Koch, J.; Schwack, W. Miniaturized open-source 2LabsToGo screening of lactose-free dairy products and saccharide-containing foods, *Journal of chromatography. A.* **2023**, *1688,* 463720.

(41) Sing, L.; Schwack, W.; Göttsche, R.; Morlock, G. E. 2LabsToGo—Recipe for Building Your Own Chromatography Equipment Including Biological Assay and Effect Detection, *Anal. Chem.* **2022**, *94,* 14554–14564.

Supplementary information

Study of the quantitative α-amylase or trypsin inhibition by refined and whole wheat and einkorn using high-performance thin-layer chromatography–nanoGIT *versus* conventional spectrophotometry

Isabel Müller, Ilka Scheibelhut, Gertrud E. Morlock*

Chair of Food Science, Institute of Nutritional Science, and Interdisciplinary Research Centre for Biosystems, Land Use and Nutrition, Justus Liebig University Giessen, Heinrich-Buff-Ring 26-32, 35392 Giessen, Germany

*Corresponding authors: Prof. Dr. Gertrud Morlock, phone: +49-641-9939141; fax +49-641-99-39149, email: gertrud.morlock@uni-giessen.de

Table of contents

	acetonitrile/water/2-propanol 3:1:1 (*V/V/V*) up to 70 mm and derivatized with diphenylamine aniline reagent, detected at white-light illumination at remission-transmission.	
Figure S4	Spectrophotometric determination of the inhibitory potential of the positive control trypsin inhibitor (**A**, 0.03–8.3 µg/mL), refined wheat flour extract (**B**, 3–300 µL), whole wheat flour extract (**C**, 3–300 µL) and einkorn flour extract (**D**, 3–300 µL) on the spectrophotometric trypsin assay (0.0015 mg/mL trypsin and 0.15 mg/mL L-BAPA, E/S 1:100). Comparison of the handheld anvajo fluidlab and a tabletop photometer (Camspec M501).	S23
Figure S5	Evaluation of the ideal enzyme-inhibitor ratio (E/I, 1:0.04-3.1) for the positive control trypsin inhibitor (**TI**) in the in-vial trypsin inhibition assay (7 µL/band). As the negative control (**NC**) trypsin (0.02 mg/mL) and casein (2 mg/mL) were used. Additionally, trypsin (0.02 mg/mL), casein (2 mg/mL) and TI (0.01 mg/mL) were applied as blanks (7 µL/band) onto HPTLC plates silica gel 60, developed with 2-butanol/pyridine/ammonia (25%)/water 10:17:5:13 (*V/V/V/V*) up to 50 mm, derivatized with the ninhydrin reagent and detected at white-light illumination in remission-transmission.	S24
Figure S6	Evaluation of the inhibitory potential of different volumes of refined wheat flour extract (100–175 µL) and pre-incubation periods (10-30 min) on in-vial trypsin-casein (**NC**, 1:100) digestion (7 µL/band). Additionally, the digestibility of the refined wheat extract by trypsin was evaluated. All were separated on HPTLC silica gel 60 plates with 2-butanol/pyridine/ammonia (25%)/water 10:17:5:13 (*V/V/V/V*) up to 50 mm, derivatised with the ninhydrin reagent, and detected at white-light illumination in remission-transmission.	S25
Figure S7	Repetition of the in-vial trypsin inhibition assay (7 µL/band), followed by HPTLC analysis: HPTLC–Vis chromatograms showing inhibition (framed black) of proteolysis (marked **+**) by three flour extracts (100 and 150 µL each) as well as PC trypsin inhibitor (**TI**, 1:2–3) mixed in a vial with trypsin and casein (**NC**, 1:100), pre-incubated (10 min), and incubated (30 min) at 37 °C. Additionally, non-proteolyzed (marked **–**) flour extract, TI, and trypsin were applied and separated on an HPTLC silica gel 60 plate with 2-butanol/pyridine/ammonia (25%)/water 10:17:5:13 (*V/V/V/V*) up to 50 mm, derivatised with ninhydrin reagent, and detected under white-light illumination (remission-transmission).	S26
Figure S8	Evaluation of the optimal on-surface enzyme-substrate ratio (E/S, 1:50-100) for the negative control (**NC**) of the HPTLC–nanoGIT (proteolysis inhibition)–Vis on HPTLC silica gel 60 plates with different absolute amounts (in µg/band) of trypsin and casein, respectively: 0.8:40 (**a**), 0.2:20 (**b**), 0.4:40 (**c**), 0.8:80 (**d**). Additionally, a casein blank (40 and 80 µg/band), which was either dried by a plate heater (**Heat**, **a**–**d**) or by a hair dryer (**No heat**) and an **in-vial** NC (7 µL/band, 1:100, 0.02 µg/µL trypsin, 2 µg/µL casein) was applied. All plates were separated with 2-butanol/pyridine/ammonia (25%)/water 10:17:5:13 (*V/V/V/V*) up to 50 mm, derivatised with the ninhydrin reagent and detected at white-light illumination in remission-transmission.	S27
Figure S9	HPTLC–nanoGIT (proteolysis inhibition)–Vis chromatograms showing the repetition of inhibition (framed black) of the proteolysis (marked **+**) by three flour extracts (2, 4 and 7 µL/band), trypsin inhibitor (**TI**, 1 µL/band, 0.5 mg/mL) as PC (E/I 1:2.5) and maximal proteolysis (**NC**,	S28

	E/S 1:50) with trypsin (4 µL/band, 0.2 mg/mL) and casein (2 µL/band, 20 mg/mL) after 30 min incubation at 37 °C. Additionally, non-proteolyzed (marked −) flour extracts, TI and trypsin in the mentioned amount was applied and separated on HPTLC silica gel 60 plates with 2-butanol/pyridine/ammonia (25%)/water 10:17:5:13 (*V*/*V*/*V*/*V*) up to 50 mm, derivatised with the ninhydrin reagent, and detected under white-light illumination in remission-transmission.	

Table S1 Spectrophotometric α-amylase inhibition assay of wheat flour extract and acarbose as positive control evaluated by the handheld anvajo fluidlab and a tabletop photometer (Camspec M501).

Sample	Absorption	Corrected absorption	Inhibition [%]	Absorption	Corrected absorption	Inhibition [%]
	Anvajo fluidlab			Camspec M501		
Amylolysis	0.136			0.121		
Acarbose	1.746	1.669	92	1.591	1.473	92
Acarbose blank	0.077			0.118		
Wheat assay	1.010	0.472	71	1.426	0.479	75
Wheat blank	0.538			0.947		

Table S2 Evaluation of the on-surface α-amylase inhibition by acarbose and its metabolism by α-amylase for each saccharide described as the percentage deviation (Δ%) from amylolysis and α-amylase, respectively.

Substance	Saccharide	Intensity (AU)	Δ%
Inhibition by acarbose			
Acarbose (1 µg)	Glucose	0.5312137	−1
	Maltose	0.3703932	−5
	Maltotriose	0.1202205	−6
Acarbose (2 µg)	Glucose	0.4695306	−12
	Maltose	0.3217580	−17
	Maltotriose	0.0973957	−24
Acarbose (5 µg)	Glucose	0.4070322	−24
	Maltose	0.2856623	−26
	Maltotriose	0.1239826	−4
Amylolysis	Glucose	0.5363443	
	Maltose	0.3886226	
	Maltotriose	0.1285642	
Acarbose metabolization			
Acarbose + amylase	Glucose	0.4016023	29
	Maltose	0.3592573	29
	Maltotriose	0.1228561	17
Amylase	Glucose	0.3103049	
	Maltose	0.2795097	
	Maltotriose	0.1046252	

Table S3 α-Amylase inhibition by acarbose in each HPTLC–nanoGIT (amylolysis inhibition)–FLD/Vis analysis and the difference between the derivatization reagents *p*-aminobenzoic acid and 2-naphthol and the determined precision ($n = 3$) as relative standard deviation (RSD) for each saccharide.

Analysis	Saccharide	*p*-Aminobenzoic acid	2-Naphthol	Difference Δ%
Inhibition by acarbose [%]				
Refined wheat	Glucose	19	35	16
	Maltose	65	58	7
	Maltotriose	85	71	13
Whole wheat	Glucose	12	29	17
	Maltose	50	46	3
	Maltotriose	82	65	17
Einkorn	Glucose	16	45	29
	Maltose	58	50	8
	Maltotriose	84	68	16
Interday precision (RSD) [%] ($n = 3$ plates)				
Acarbose	Glucose	21	23	2
	Maltose	13	11	2
	Maltotriose	2	5	3

Table S4 Determined signal height of each saccharide of the HPTLC–nanoGIT (amylolysis inhibition)–FLD/Vis analysis of refined wheat, corrected signal, and calculated relative inhibition of both derivatisation reagents.

***p*-Aminobenzoic acid**				
Sample	Saccharide	Signal height	Corrected signal	Inhibition [%]
Negative control				
Amylolysis	Glucose	0.52310		
	Maltose	0.25667		
	Maltotriose	0.13955		
Positive control				
Acarbose	Glucose	0.42478		19
	Maltose	0.09105		65
	Maltotriose	0.02110		85
Refined wheat extract				
2 µL	Glucose	0.52325	0.37877	28
	Maltose	0.28431	0.25147	2
	Maltotriose	0.10277	-	26
5 µL	Glucose	0.52354	0.22597	57
	Maltose	0.27168	0.19959	22
	Maltotriose	0.06793	-	51
7 µL	Glucose	0.53331	0.15408	71
	Maltose	0.26659	0.16878	34
	Maltotriose	0.06225	-	55
9 µL	Glucose	0.56442	0.15209	71
	Maltose	0.26778	0.15752	39
	Maltotriose	0.05554	-	60
11 µL	Glucose	0.56595	0.15214	71
	Maltose	0.26313	0.15018	41
	Maltotriose	0.04321	-	69
Refined wheat extract blanks				
2 µL	Glucose	0.14448		
	Maltose	0.03284		
	Maltotriose	-		

Sample	Saccharide	Signal height	Corrected signal	Inhibition [%]
Refined wheat extract blanks				
5 µL	Glucose	0.29757		
	Maltose	0.07209		
	Maltotriose	-		
7 µL	Glucose	0.37923		
	Maltose	0.09781		
	Maltotriose	-		
9 µL	Glucose	0.41233		
	Maltose	0.11026		
	Maltotriose	-		
11 µL	Glucose	0.41380		
	Maltose	0.11296		
	Maltotriose	-		
2-Naphthol				
Negative control				
Amylolysis	Glucose	0.14690		
	Maltose	0.38200		
	Maltotriose	0.36505		
Positive control				
Acarbose	Glucose	0.09571		35
	Maltose	0.16228		58
	Maltotriose	0.10439		71
Refined wheat extract				
2 µL	Glucose	0.12725	0.09062	38
	Maltose	0.42284	0.31913	16
	Maltotriose	0.30935	0.30935	15
5 µL	Glucose	0.14130	0.06248	57
	Maltose	0.40876	0.22485	41
	Maltotriose	0.25208	0.23455	36
7 µL	Glucose	0.15481	0.04752	68
	Maltose	0.40948	0.19625	49
	Maltotriose	0.22709	0.20895	43

Sample	Saccharide	Signal height	Corrected signal	Inhibition [%]
Refined wheat extract				
9 µL	Glucose	0.18953	0.06872	53
	Maltose	0.40767	0.17781	53
	Maltotriose	0.20885	0.18653	49
11 µL	Glucose	0.19999	0.07291	50
	Maltose	0.39942	0.16510	57
	Maltotriose	0.18621	0.16647	54
Refined wheat extract blanks				
2 µL	Glucose	0.03663		
	Maltose	0.10371		
	Maltotriose	-		
5 µL	Glucose	0.07882		
	Maltose	0.18391		
	Maltotriose	0.01752		
7 µL	Glucose	0.10729		
	Maltose	0.21323		
	Maltotriose	0.01815		
9 µL	Glucose	0.12081		
	Maltose	0.22986		
	Maltotriose	0.02232		
11 µL	Glucose	0.12708		
	Maltose	0.23432		
	Maltotriose	0.01974		

Table S5 Determined signal height of each saccharide of the HPTLC–nanoGIT (amylolysis inhibition)–FLD/Vis analysis of whole wheat, corrected signal, and calculated relative inhibition of both derivatisation reagents.

***p*-Aminobenzoic acid**				
Sample	Saccharide	Signal height	Corrected signal	Inhibition [%]
Negative control				
Amylolysis	Glucose	0.55529		
	Maltose	0.27225		
	Maltotriose	0.13754		
Positive control				
Acarbose	Glucose	0.48725		12
	Maltose	0.13686		50
	Maltotriose	0.02518		82
Whole wheat extract				
2 µL	Glucose	0.54721	0.23017	59
	Maltose	0.28660	0.23997	12
	Maltotriose	0.10427	-	24
5 µL	Glucose	0.55389	0.06232	89
	Maltose	0.28537	0.18097	34
	Maltotriose	0.08845	-	36
7 µL	Glucose	0.55766	0.01991	96
	Maltose	0.28671	0.14942	45
	Maltotriose	0.09000	-	35
9 µL	Glucose	0.55900	-0.00170	100
	Maltose	0.27987	0.11943	56
	Maltotriose	0.06958	-	49
11 µL	Glucose	0.53691	-0.01984	104
	Maltose	0.27635	0.08859	67
	Maltotriose	0.05492	0.05492	60
Whole wheat extract blanks				
2 µL	Glucose	0.31704		
	Maltose	0.04663		
	Maltotriose	-		

Sample	Saccharide	Signal height	Corrected signal	Inhibition [%]
Whole wheat extract blanks				
5 µL	Glucose	0.49157		
	Maltose	0.10440		
	Maltotriose	-		
7 µL	Glucose	0.53775		
	Maltose	0.13729		
	Maltotriose	-		
9 µL	Glucose	0.56070		
	Maltose	0.16044		
	Maltotriose	-		
11 µL	Glucose	0.55675		
	Maltose	0.18777		
	Maltotriose	-		
2-Naphthol				
Negative control				
Amylolysis	Glucose	0.16112		
	Maltose	0.39829		
	Maltotriose	0.37627		
Positive control				
Acarbose	Glucose	0.11459		29
	Maltose	0.21362		46
	Maltotriose	0.13236		65
Whole wheat extract				
2 µL	Glucose	0.15302	0.07101	56
	Maltose	0.43147	0.32440	19
	Maltotriose	0.30979	-	18
5 µL	Glucose	0.18604	0.03922	76
	Maltose	0.42666	0.24303	39
	Maltotriose	0.27268	0.24780	34
7 µL	Glucose	0.16725	0.00031	33
	Maltose	0.42592	0.22122	44
	Maltotriose	0.28054	0.25127	100

Sample	Saccharide	Signal height	Corrected signal	Inhibition [%]
Whole wheat extract				
9 µL	Glucose	0.27837	0.08974	44
	Maltose	0.41188	0.20091	50
	Maltotriose	0.23546	0.19990	47
11 µL	Glucose	0.28830	0.09786	39
	Maltose	0.39565	0.18286	54
	Maltotriose	0.19986	0.15969	58
Whole wheat extract blanks				
2 µL	Glucose	0.08201		
	Maltose	0.10707		
	Maltotriose	-		
5 µL	Glucose	0.14682		
	Maltose	0.18364		
	Maltotriose	0.02487		
7 µL	Glucose	0.16695		
	Maltose	0.20469		
	Maltotriose	0.02927		
9 µL	Glucose	0.18863		
	Maltose	0.21098		
	Maltotriose	0.03556		
11 µL	Glucose	0.19044		
	Maltose	0.21279		
	Maltotriose	0.04017		

Table S6 Determined signal height of each saccharide of the HPTLC–nanoGIT (amylolysis inhibition)–FLD/Vis analysis of einkorn, corrected signal, and calculated relative inhibition of both derivatisation reagents.

***p*-Aminobenzoic acid**				
Sample	Saccharide	Signal height	Corrected signal	Inhibition [%]
Negative control				
Amylolysis	Glucose	0.50952		
	Maltose	0.25346		
	Maltotriose	0.14310		
Positive control				
Acarbose	Glucose	0.42674		16
	Maltose	0.10645		58
	Maltotriose	0.02312		84
Einkorn extract				
2 µL	Glucose	0.50709	0.37536	26
	Maltose	0.27218	-	−7
	Maltotriose	0.12567	-	26
5 µL	Glucose	0.50502	0.19698	61
	Maltose	0.27515	0.23137	9
	Maltotriose	0.10163	-	29
7 µL	Glucose	0.49650	0.07770	85
	Maltose	0.27205	0.19956	21
	Maltotriose	0.11246	-	21
9 µL	Glucose	0.54581	0.15739	69
	Maltose	0.26060	0.19528	23
	Maltotriose	0.06772	-	53
11 µL	Glucose	0.54473	0.14338	72
	Maltose	0.24873	0.18413	27
	Maltotriose	0.04981	-	65
Einkorn extract blanks				
2 µL	Glucose	0.13174		
	Maltose	-		
	Maltotriose	-		

Sample	Saccharide	Signal height	Corrected signal	Inhibition [%]
Einkorn extract blanks				
5 µL	Glucose	0.30805		
	Maltose	0.04379		
	Maltotriose	-		
7 µL	Glucose	0.41880		
	Maltose	0.07249		
	Maltotriose	-		
9 µL	Glucose	0.38842		
	Maltose	0.06531		
	Maltotriose	-		
11 µL	Glucose	0.40136		
	Maltose	0.06460		
	Maltotriose	-		
2-Naphthol				
Negative control				
Amylolysis	Glucose	0.16857		
	Maltose	0.41597		
	Maltotriose	0.40387		
Positive control				
Acarbose	Glucose	0.09202		45
	Maltose	0.20803		50
	Maltotriose	0.12999		68
Einkorn extract				
2 µL	Glucose	0.13016	0.09609	43
	Maltose	0.44015	0.39991	4
	Maltotriose	0.37258	-	8
5 µL	Glucose	0.13744	0.06252	63
	Maltose	0.44478	0.35428	15
	Maltotriose	0.32820	0.31253	23
7 µL	Glucose	0.12854	0.01738	90
	Maltose	0.44614	0.31789	24
	Maltotriose	0.35679	0.33245	18

Sample	Saccharide	Signal height	Corrected signal	Inhibition [%]
Einkorn extract				
9 µL	Glucose	0.17582	0.08109	52
	Maltose	0.39746	0.28085	32
	Maltotriose	0.25117	0.22598	44
11 µL	Glucose	0.17398	0.07694	54
	Maltose	0.37629	0.25330	39
	Maltotriose	0.22583	0.20028	50
Einkorn extract blanks				
2 µL	Glucose	0.03407		
	Maltose	0.04023		
	Maltotriose	-		
5 µL	Glucose	0.07492		
	Maltose	0.09050		
	Maltotriose	0.01567		
7 µL	Glucose	0.11116		
	Maltose	0.12825		
	Maltotriose	0.02434		
9 µL	Glucose	0.09473		
	Maltose	0.11661		
	Maltotriose	0.02519		
11 µL	Glucose	0.09704		
	Maltose	0.12300		
	Maltotriose	0.02555		

Table S7 Spectrophotometric trypsin inhibition assay with trypsin inhibitor and flour extracts of refined wheat, whole wheat, and einkorn.

Sample	Absorption	Inhibition [%]	Inhibition/µL	Absorption	Inhibition [%]	Inhibition/µL
	Anvajo fluidlab			Camspec M501		
Trypsin inhibitor #1						
Trypsin blank	0.012			0.015		
Proteolysis	0.127			0.125		
65 µL blank	0.018	84.3	1.3	0.008	83.6	1.3
65 µL	0.036			0.026		
30 µL blank	0.014	47.0	1.6	0.008	36.4	1.2
30 µL	0.075			0.078		
3 µL blank	0.011	9.6	3.2	0.008	5.5	1.8
3 µL	0.115			0.112		
1 µL blank	0.011	10.4	10.4	0.013	8.2	8.2
1 µL	0.114			0.114		
Trypsin inhibitor #2						
Trypsin blank	-0.0400			0.005		
Proteolysis	0.1240			0.292		
300 µL blank	-0.0364			0.014	95.1	0.3
300 µL	-0.0257			0.028		
100 µL blank	-0.0487			0.011	95.8	1.0
100 µL	-0.0170			0.023		
Refined wheat extract						
Trypsin blank	0.020			0.011		
Proteolysis	0.137			0.125		
300 µL blank	0.028	98.3	0.3	0.011	88.6	0.3
300 µL	0.030			0.024		
150 µL blank	0.024	80.3	0.5	0.012	76.3	0.5
150 µL	0.047			0.039		
100 µL blank	0.023	59.8	0.6	0.012	62.3	0.6
100 µL	0.070			0.055		
80 µL blank	0.024	58.1	0.7	0.013	56.1	0.7
80 µL	0.073			0.063		
60 µL blank	0.022	42.7	0.7	0.012	32.5	0.5
60 µL	0.089			0.089		

Sample	Absorption	Inhibition [%]	Inhibition/µL	Absorption	Inhibition [%]	Inhibition/µL
	Anvajo fluidlab			Camspec M501		
50 µL blank	0.023	28.2	0.6	0.013	28.9	0.6
50 µL	0.107			0.094		
30 µL blank	0.021	0.0	0.0	0.016	0.0	0.0
30 µL	0.138			0.130		
15 µL blank	0.021	-15.4	-1.0	0.013	-19.3	-1.3
15 µL	0.156			0.149		
10 µL blank	0.022	-13.7	-1.4	0.012	-22.8	-2.3
10 µL	0.155			0.152		
5 µL blank	0.022	-21.4	-4.3	0.013	-23.7	-4.7
5 µL	0.164			0.154		
3 µL blank	0.021	-36.8	-12.3	0.013	-33.3	-11.1
3 µL	0.181			0.165		
Whole wheat extract						
Trypsin blank	0.017			0.010		
Proteolysis	0.231			0.199		
300 µL blank	0.044	94.4	0.3	0.039	92.6	0.3
300 µL	0.056			0.053		
150 µL blank	0.023	83.6	0.6	0.012	79.9	0.5
150 µL	0.058			0.050		
100 µL blank	0.026	72.0	0.7	0.015	66.7	0.7
100 µL	0.086			0.078		
80 µL blank	0.024	63.1	0.8	0.014	59.3	0.7
80 µL	0.103			0.091		
60 µL blank	0.024	39.3	0.7	0.013	32.8	0.5
60 µL	0.154			0.140		
50 µL blank	0.022	27.1	0.5	0.014	21.7	0.4
50 µL	0.178			0.162		
30 µL blank	0.021	7.0	0.2	0.014	-0.5	0.0
30 µL	0.220			0.204		
15 µL blank	0.020	1.9	0.1	0.010	-6.3	-0.4
15 µL	0.230			0.211		
10 µL blank	0.020	-1.9	-0.2	0.012	-9.5	-1.0

S18

Sample	Absorption	Inhibition [%]	Inhibition/µL	Absorption	Inhibition [%]	Inhibition/µL
	Anvajo fluidlab			Camspec M501		
10 µL	0.238			0.219		
5 µL blank	0.021	-1.9	-0.4	0.010	-11.6	-2.3
5 µL	0.239			0.221		
3 µL blank	0.022	-5.1	-1.7	0.012	-12.7	-4.2
3 µL	0.247			0.225		
Einkorn extract						
Trypsin blank	0.019			0.009		
Proteolysis	0.217			0.194		
300 µL blank	0.062	81.3	0.3	0.053	80.5	0.3
300 µL	0.099			0.089		
150 µL blank	0.039	87.9	0.6	0.028	82.7	0.6
150 µL	0.063			0.060		
100 µL blank	0.043	93.9	0.9	0.031	94.6	0.9
100 µL	0.055			0.041		
80 µL blank	0.049	97.5	1.2	0.031	95.1	1.2
80 µL	0.054			0.04		
60 µL blank	0.027	68.7	1.1	0.016	68.6	1.1
60 µL	0.089			0.074		
50 µL blank	0.028	52.5	1.1	0.015	51.4	1.0
50 µL	0.122			0.105		
30 µL blank	0.023	14.6	0.5	0.015	13.0	0.4
30 µL	0.192			0.176		
15 µL blank	0.020	-5.1	-0.3	0.010	-2.2	-0.1
15 µL	0.228			0.199		
10 µL blank	0.020	-7.6	-0.8	0.009	-11.9	-1.2
10 µL	0.233			0.216		
5 µL blank	0.019	-15.2	-3.0	0.007	-16.2	-3.2
5 µL	0.247			0.222		
3 µL blank	0.017	-15.2	-5.1	0.007	-16.8	-5.6
3 µL	0.245			0.223		

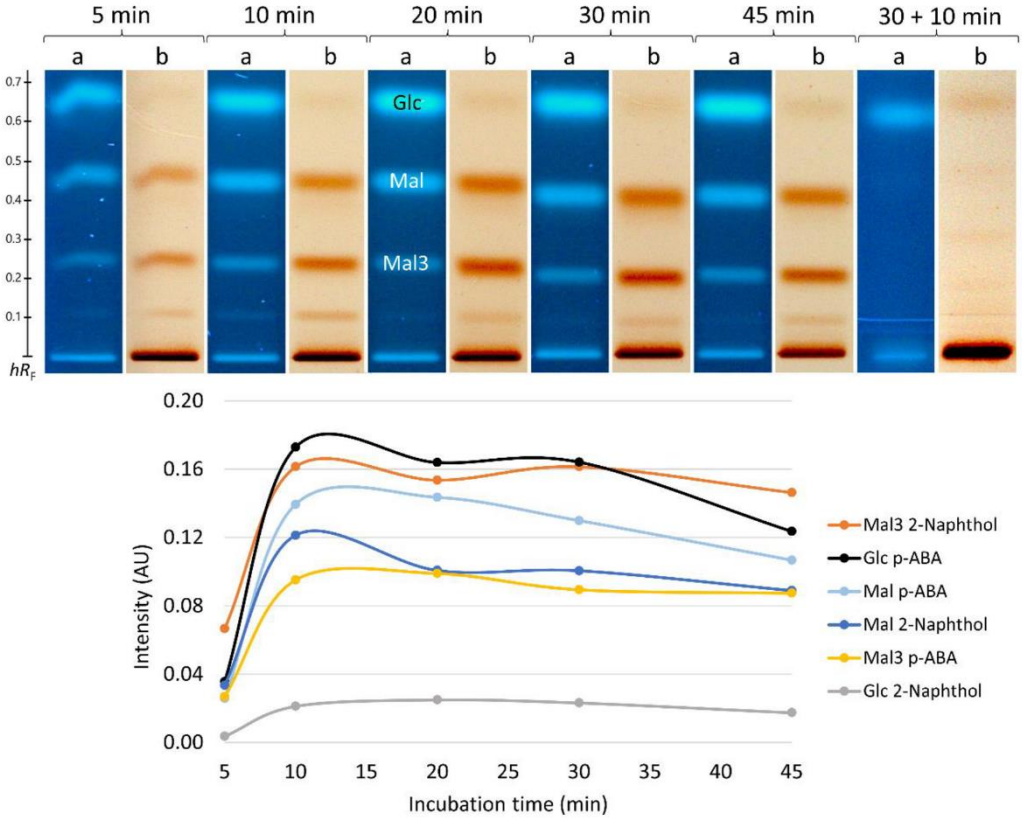

Figure S1 Evaluation of time-dependent (5–45 min) release of glucose (**Glc**), maltose (**Mal**), and maltotriose (**Mal3**) after nanoGIT amylolysis (α-amylase, 5 µg/band and soluble starch solution, 20 µg/band) on HPTLC silica gel 60 plates. Plates were developed with acetonitrile/water/2-propanol (3:1:1 *V*/*V*/*V*) up to 70 mm and derivatized with p-aminobenzoic acid reagent (*p*-ABA, **a**), detected at FLD 366 nm and densitometrically evaluated at 366/>400 nm (fluorescence measurement, slit 4.0 mm × 0.2 mm, mercury lamp) and subsequently with 2-naphthol reagent (**b**), detected at white-light illumination in remission-transmission and densitometrically evaluated at 500 nm (absorbance measurement, slit 4.0 mm × 0.2 mm, deuterium/tungsten lamp).

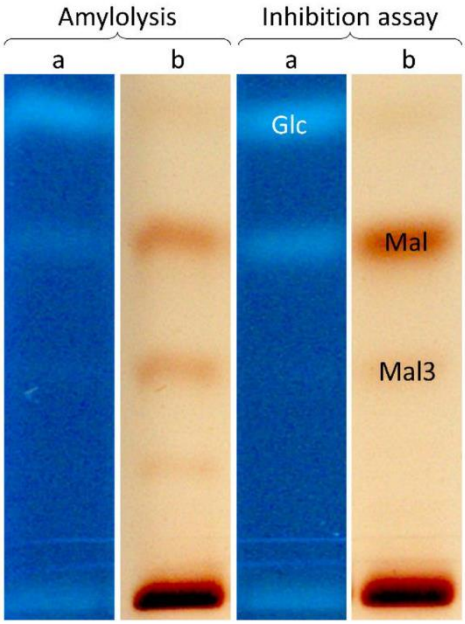

Figure S2 Verification of successful α-amylase inhibition by the ATI-containing refined wheat extract (inhibition assay) on maltotriose (**Mal3**) release via nanoGIT amylolysis (α-amylase, 2.5 µg/band and soluble starch, 20 µg/band) on HPTLC silica gel 60 plates. The addition of flour extract caused an increase in maltose (**Mal**) but no change in glucose (**Glc**). Plates were developed with acetonitrile/water/2-propanol (3:1:1 *V/V/V*) up to 70 mm and derivatised with *p*-aminobenzoic acid reagent (**a**), detected at FLD 366 nm, and subsequently with 2-naphthol reagent (**b**), detected at white-light illumination in remission-transmission.

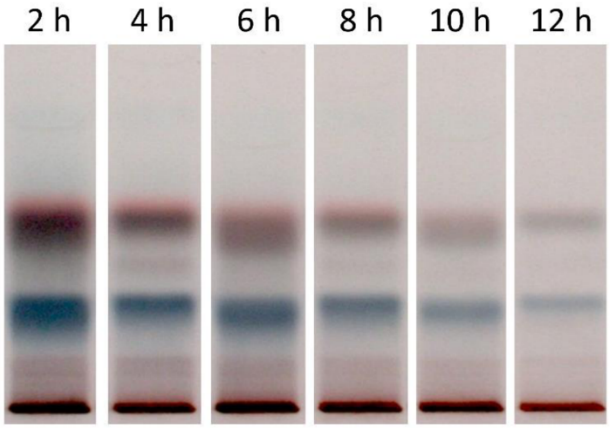

Figure S3 Removal of saccharides from whole wheat flour extract via membrane filtration (2–12 h), separated on HPTLC silica gel 60 plates with acetonitrile/water/2-propanol 3:1:1 (*V/V/V*) up to 70 mm and derivatized with diphenylamine aniline reagent, detected at white-light illumination at remission-transmission.

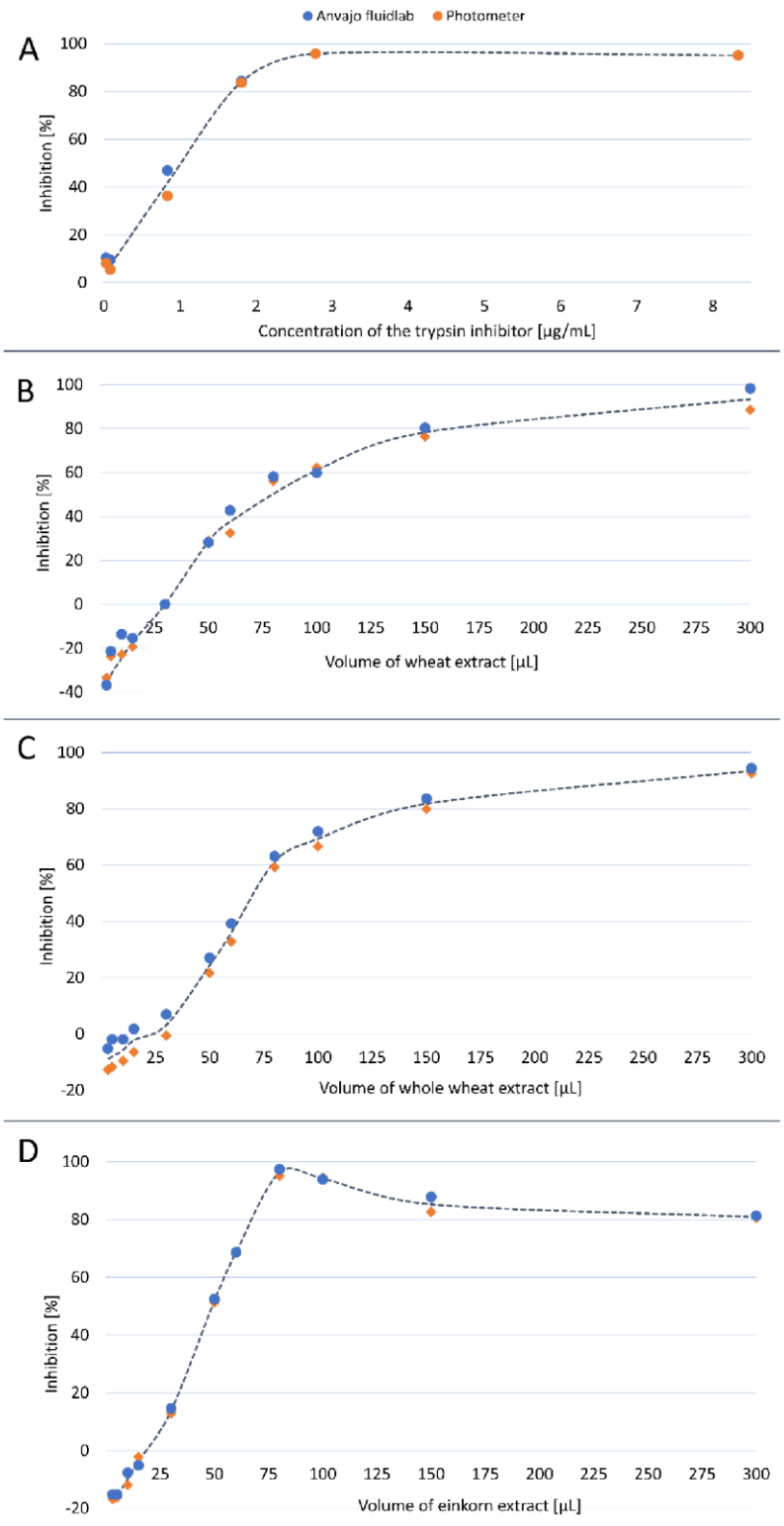

Figure S4 Spectrophotometric determination of the inhibitory potential of the positive control trypsin inhibitor (**A**, 0.03–8.3 µg/mL), refined wheat flour extract (**B**, 3–300 µL), whole wheat flour extract (**C**, 3–300 µL) and einkorn flour extract (**D**, 3–300 µL) on the spectrophotometric trypsin assay (0.0015 mg/mL trypsin and 0.15 mg/mL L-BAPA, E/S 1:100). Comparison of the handheld anvajo fluidlab and a tabletop photometer (Camspec M501).

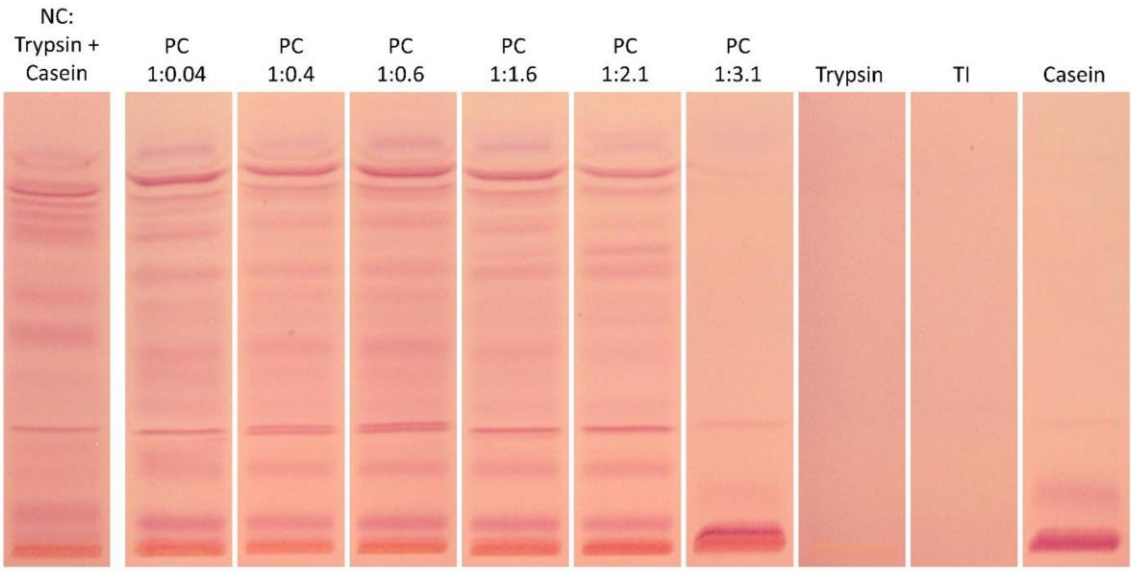

Figure S5 Evaluation of the ideal enzyme-inhibitor ratio (E/I, 1:0.04-3.1) for the positive control trypsin inhibitor (**TI**) in the in-vial trypsin inhibition assay (7 µL/band). As the negative control (**NC**) trypsin (0.02 mg/mL) and casein (2 mg/mL) were used. Additionally, trypsin (0.02 mg/mL), casein (2 mg/mL) and TI (0.01 mg/mL) were applied as blanks (7 µL/band) onto HPTLC plates silica gel 60, developed with 2-butanol/pyridine/ammonia (25%)/water 10:17:5:13 (*V/V/V/V*) up to 50 mm, derivatized with the ninhydrin reagent and detected at white-light illumination in remission-transmission.

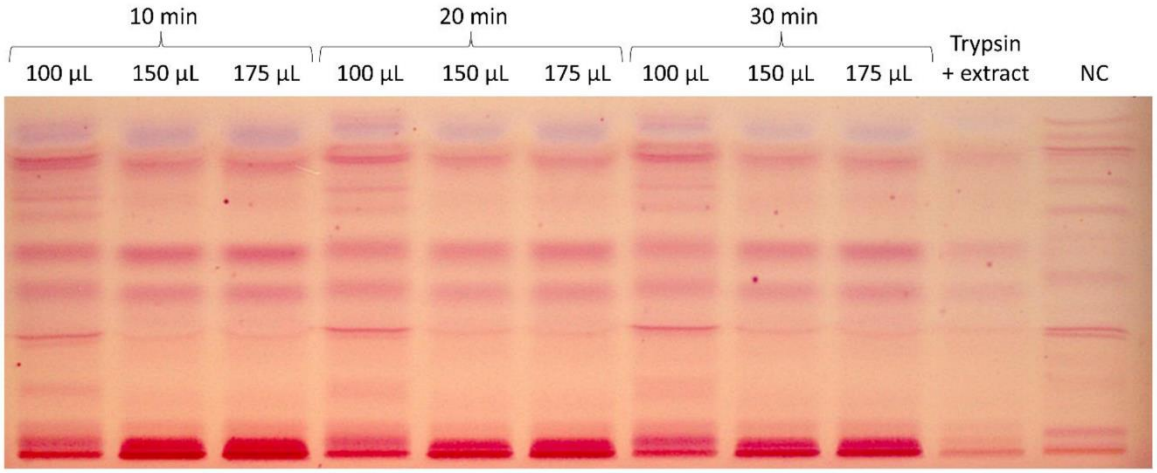

Figure S6 Evaluation of the inhibitory potential of different volumes of refined wheat flour extract (100–175 µL) and pre-incubation periods (10-30 min) on in-vial trypsin-casein (**NC**, 1:100) digestion (7 µL/band). Additionally, the digestibility of the refined wheat extract by trypsin was evaluated. All were separated on HPTLC silica gel 60 plates with 2-butanol/pyridine/ammonia (25%)/water 10:17:5:13 (*V/V/V/V*) up to 50 mm, derivatised with the ninhydrin reagent, and detected at white-light illumination in remission-transmission.

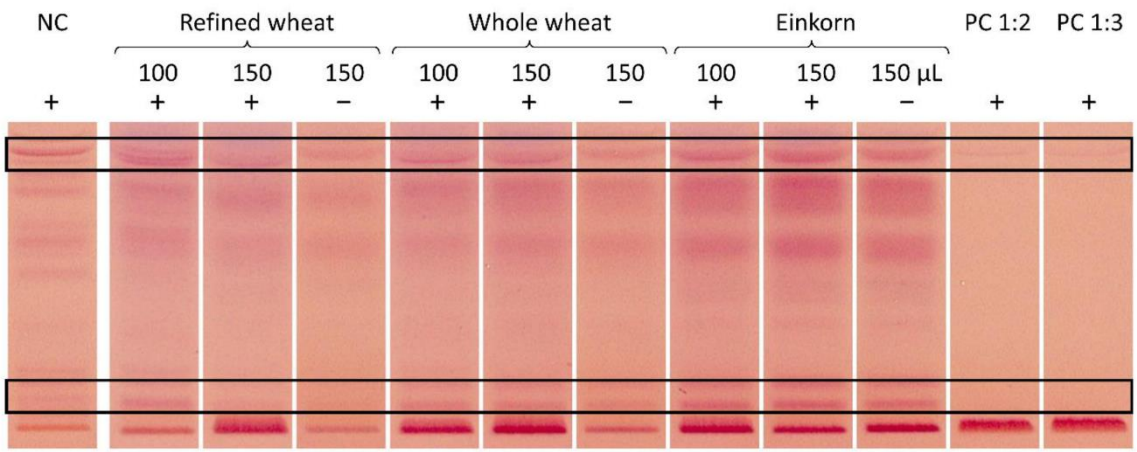

Figure S7 Repetition of the in-vial trypsin inhibition assay (7 µL/band), followed by HPTLC analysis: HPTLC–Vis chromatograms showing inhibition (framed black) of proteolysis (marked **+**) by three flour extracts (100 and 150 µL each) as well as PC trypsin inhibitor (**TI**, 1:2–3) mixed in a vial with trypsin and casein (**NC**, 1:100), pre-incubated (10 min), and incubated (30 min) at 37 °C. Additionally, non-proteolyzed (marked **−**) flour extract, TI, and trypsin were applied and separated on an HPTLC silica gel 60 plate with 2-butanol/pyridine/ammonia (25%)/water 10:17:5:13 (*V*/*V*/*V*/*V*) up to 50 mm, derivatised with ninhydrin reagent, and detected under white-light illumination (remission-transmission).

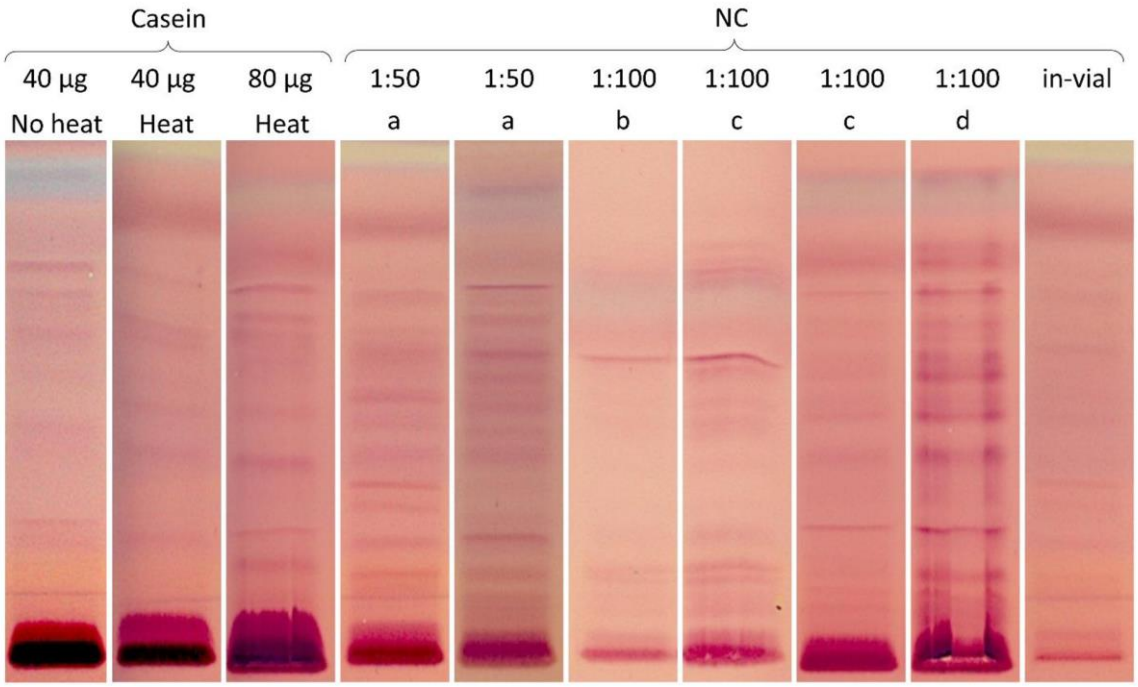

Figure S8 Evaluation of the optimal on-surface enzyme-substrate ratio (E/S, 1:50-100) for the negative control (**NC**) of the HPTLC–nanoGIT (proteolysis inhibition)–Vis on HPTLC silica gel 60 plates with different absolute amounts (in µg/band) of trypsin and casein, respectively: 0.8:40 (**a**), 0.2:20 (**b**), 0.4:40 (**c**), 0.8:80 (**d**). Additionally, a casein blank (40 and 80 µg/band), which was either dried by a plate heater (**Heat**, **a**–**d**) or by a hair dryer (**No heat**) and an **in-vial** NC (7 µL/band, 1:100, 0.02 µg/µL trypsin, 2 µg/µL casein) was applied. All plates were separated with 2-butanol/pyridine/ammonia (25%)/water 10:17:5:13 (*V/V/V/V*) up to 50 mm, derivatised with the ninhydrin reagent and detected at white-light illumination in remission-transmission.

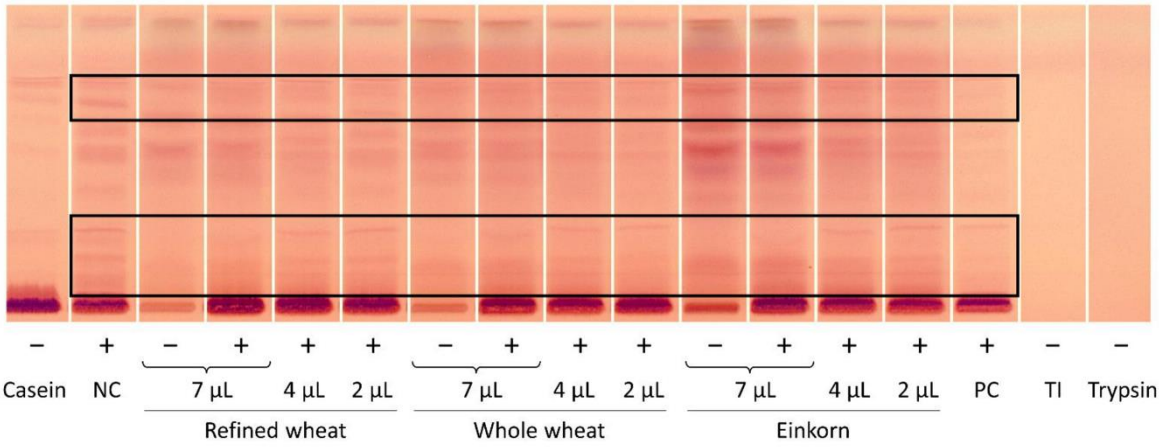

Figure S9 HPTLC–nanoGIT (proteolysis inhibition)–Vis chromatograms showing the repetition of inhibition (framed black) of the proteolysis (marked **+**) by three flour extracts (2, 4 and 7 µL/band), trypsin inhibitor (**TI**, 1 µL/band, 0.5 mg/mL) as PC (E/I 1:2.5) and maximal proteolysis (**NC**, E/S 1:50) with trypsin (4 µL/band, 0.2 mg/mL) and casein (2 µL/band, 20 mg/mL) after 30 min incubation at 37 °C. Additionally, non-proteolyzed (marked **−**) flour extracts, TI and trypsin in the mentioned amount was applied and separated on HPTLC silica gel 60 plates with 2-butanol/pyridine/ammonia (25%)/water 10:17:5:13 (*V/V/V/V*) up to 50 mm, derivatised with the ninhydrin reagent, and detected under white-light illumination in remission-transmission.

Publication V

Feasibility of HPTLC on-surface enzyme assays for the determination of enzyme activity in comparison to spectrophotometric approaches using invertase from *S. cerevisiae*

Isabel Müller, Viktoria H. Englert, Gertrud E. Morlock

In preparation for submission

Feasibility of HPTLC on-surface enzyme assays for the determination of enzyme activity in comparison to spectrophotometric approaches using invertase from *S. cerevisiae*.

Isabel Müller, Viktoria H. Englert, Gertrud E. Morlock*

Chair of Food Science, Institute of Nutritional Science, and Interdisciplinary Research Centre for Biosystems, Land Use and Nutrition, Justus Liebig University Giessen, Heinrich-Buff-Ring 26-32, 35392 Giessen, Germany

*Corresponding authors: Prof. Dr. Gertrud Morlock, phone: +49-641-9939141; fax +49-641-99-39149, email: gertrud.morlock@uni-giessen.de

Abstract

Conventional methods for assessing enzyme activity often rely on spectrophotometric detection techniques. However, high-performance thin-layer chromatography (HPTLC) presents a promising alternative for precise and reliable metabolite quantification. A validated HPTLC invertase nano assay had demonstrated its efficacy in examining the established metabolic reaction of invertase and sucrose, surpassing spectrophotometric assays that operate in the millimolar range. The validated HPTLC approach exhibited remarkable sensitivity, requiring a 12,500-fold lower substrate quantity, while using equivalent enzyme amounts. This enhanced sensitivity could significantly benefit research by enabling the characterisation of minor enzyme quantities. Furthermore, this study offers guidance on managing on-surface assays by addressing their constraints and proposes further methodological enhancements to rival spectrophotometric techniques.

Keywords

Troubleshooting, miniaturised assay, saccharide analysis, method substitution, validation

1. Introduction

The use of enzymes in industry and research has been increasing in recent decades, making it necessary to develop robust and reliable methods for the determination of their activity. Analytical approaches to determine enzyme activity are often limited to spectrophotometric detection methods using chromogenic substrates because of their cost efficiency [1–4]. However, the limitations of spectrophotometric assays are obvious despite their simplicity: determination of sum parameters only, high workload (without automation), high consumption of materials, and matrix-susceptible non-specific reaction mechanisms. These disadvantages can be overcome and the characterisation of enzymes can be improved using high-performance thin-layer chromatography (HTPLC). Previous studies demonstrated the high potential of the all-in-one HPTLC approach by combining metabolic enzyme assays with subsequent separation on the same surface [5–9]. Nevertheless, these methods also have limitations, which is why this study was conducted to better understand the mechanism of action of enzyme reactions on the HPTLC plate. Quantification [5,7] and qualification studies [6,8] demonstrated the pitfalls of biological reactions involving matrix-rich samples. Hence, a detailed analysis of enzyme interactions corresponding to the activity of an enzyme is required, using a substrate of standard purity.

This study characterised invertase and its equimolar conversion of sucrose (Suc) to glucose (Glc) and fructose (Fru). In addition to amylases, invertase is important for industrial processing of sweeteners, sweets, and bakery products [10,11]. Amylase and xylose/glucose isomerase are used to produce corn syrup and glucose-fructose syrup from starch [12], respectively. In contrast, invertase cleaves the glycosidic bond of Suc, resulting in its two monomeric units Glc and Fru [13,14]. Unlike glucose-fructose syrup, which consists of varying amounts of Fru, inverted sugar is an equimolar mixture of Glc and Fru, providing balanced sweetness [10,13]. Inverted sugar is preferably used in the bakery and confectionery industry because of its hygroscopic properties, which support the desired moisture of the products and prevent staling [14,15]. Industrially used acidic invertases are mainly produced by *S. cerevisiae* [16], commonly known as Baker's yeast. In addition to its use in the food industry, invertase is also used as a plasticising agent in cosmetics, the paper industry, and as an enzyme electrode for Suc [15].

Surprisingly, a standard protocol for the determination of invertase activity is difficult to find. In addition to assay kits for invertase activity from named suppliers, a literature review revealed the usage of several substrates and a legally compliant protocol published by the Association of Official Agricultural Chemists (AOAC) dealing with the determination of fructan in animal food [17] and the method of the European Honey Commission [18]. Therefore, an alternative

approach is useful to improve and standardize the determination of the activity of invertase.

A detailed investigation of the enzyme reaction of invertase from Baker's yeast and Suc was performed on-surface using a substance of standard purity and biscuit-extracted Suc, following a comparison and statistical evaluation of the spectrophotometric approach in contrast to the HPTLC approach. Additionally, this study summarizes the limitations of both approaches and provides advice for dealing with on-surface enzyme assays.

2. Materials and methods

2.1. Chemicals

Methanol (≥ 99.9%) was purchased from Fisher Scientific (Schwerte, Germany). Acetone (≥ 99.9%) and glacial acetic acid (≥ 99.8%) were obtained from VWR International (Darmstadt, Germany). *o*-Phosphoric acid (85%) was from Th. Geyer (Renningen, Germany). D-(-)-Fructose (> 99%), D-(+)-glucose (≥ 99.5%), D-(+)-sucrose (≥ 99.5%), acetonitrile (≥ 99.9%), 4-aminobenzoic acid (≥ 99%), potassium sodium tartrate tetrahydrate (99.0%), sodium acetate trihydrate (≥ 99.0%), ammonium acetate (≥ 99.0%), invertase from baker's yeast (Grade VII, ≥ 300 U/mg solid, i. e. 344 U/mg solid) and 4-hydroxybenzoic hydrazide (≥ 97%) were supplied by Sigma Aldrich Fluka (Steinheim, Germany). Sodium carbonate decahydrate (≥ 99%) was from Riedel-de Haen (Seelze, Germany). 3,5-Dinitrosalicylic acid (≥ 98%) and HPTLC silica gel 60 plates (20 × 10 cm) were purchased from Merck (Darmstadt, Germany). Sodium hydroxide (≥ 99%), natural product reagent A (98%), molecular sieve (0.3 nm, type 564) and hydrochloric acid (37%, p. a.) were from Carl Roth (Karlsruhe, Germany). Bi-distilled water was produced using Heraeus Destamat B-18E (Thermo Fisher Scientific, Dreieich, Germany).

Egg biscuits (Eierplätzchen, Ja!, D. Borggreve Zwieback & Keksfabrik, Neuenhaus, Germany) containing wheat flour, sucrose, whole eggs, sodium bicarbonate, natural vanilla flavour, and table salt. The sucrose content was labelled as 40.7 g/100 g biscuit.

2.2. Extraction of sucrose from biscuits

Mortared sucrose-containing egg biscuit (2.5 g) was mixed with 10 mL of 70% aqueous methanol in a 15-mL centrifugation tube, vortexed with a multi-tube holder (Vortex Genie 2, Scientific Industries, New York City, NY, USA) for 5 min, and centrifuged at 4,000 × *g* for 15 min. The supernatant (1 mL) was diluted 1:100 (*V*/*V*) in a two-step dilution series, using 70% aqueous methanol. The final concentration was 2.5 mg biscuit/mL, which corresponded to 1 mg sucrose/mL.

2.3. HPTLC on-surface metabolism of invertase

The HPTLC silica gel 60 plates were pre-washed twice with methanol/water (3:1 *V*/*V*) up to 90 mm, dried in between, and finally dried at 120 °C for 15 min. Invertase stock solution (100 U/mL, i.e. 0.29 mg/mL in water) was freshly prepared and further diluted to

1:10 (*V*/*V*) with water as invertase working solution (10 U/mL).

On an HPTLC plate, sucrose (Suc, 2 µL/band, 1 mg/mL) as standard or extracted from biscuits and on top invertase working solution (0.5–6 µL/band, i. e. 5–60 mU/band, 10 U/mL) were applied via overspraying. Additionally for quantification, glucose (Glc) and fructose (Fru, each 0.5–2.5 µL/band, 0.1 mg/mL and 0.5–1.2 µL/band, 1 mg/mL) were applied as reference standards via overspotting onto the pre-washed HPTLC silica gel 60 plates with the following settings via automatic TLC sampler (ATS4, CAMAG, Muttenz, Switzerland): 7-mm bands, track distance 9 mm, distance from the lower edge 10 mm and left edge 14.5 mm, dosage speed 50 nL/s, filling speed 8 µL/s, filling vacuum time 4 s, 25 µL syringe. After application, the plate was pre-conditioned (30 min) horizontally in a plastic box (365+, 5.2 L, IKEA, Hofheim-Wallau, Germany) filled with 200 mL of saturated sodium carbonate decahydrate solution with a relative humidity of at least 70% [5]. This humid box was kept filled and reused for several months. Alternatively, a twin-trough chamber can be used but must be prepared at least 1 h before pre-conditioning. Next, everything except the application zone was covered with a cut HPTLC silica gel 60 plate (8.5 cm × 20 cm) [5] and wetted with 0.1 M ammonium acetate solution pH 4.5 (2.5 mL, yellow nozzle, Derivatizer, CAMAG). The plate (still covered) was incubated at 50 °C for 15 min in another prior prepared (at least 30 min) plastic box (26.5 cm × 16 cm × 10 cm, ABM, Wolframs-Eschenbach, Germany) filled with 70 mL water and lined with wet filter paper. The HPTLC plate was dried at 120 °C for 10 min (TLC Plate Heater III, CAMAG) and developed with acetonitrile/water 4:1 (*V*/*V*) containing 2 mg/mL natural product reagent A [19] up to 60 mm in a twin-trough chamber (20 cm × 10 cm) filled with molecular sieve (0.3 nm), when a relative humidity of <20% was achieved. For post-chromatographic derivatization the plate was dipped (dipping speed 3 cm/s and dipping time 2 s, Immersion Device II, CAMAG) in *p*-aminobenzoic acid reagent (2 g *p*-aminobenzoic acid in 252 mL glacial acetic acid/water/acetone/*o*-phosphoric acid 1:1:3:0.04, *V*/*V*/*V*/*V*) and heated at 140 °C for 5 min (TLC Plate Heater). The detection was performed at FLD 366 nm (Visualizer 2, CAMAG) and the plate was densitometrically measured at 366/<400 nm (fluorescence mode, mercury lamp, 4 × 0.2 mm slit, 5 mm/s, 25 µm/step, TLC Scanner 4, CAMAG). The peak area was used for the densitometric evaluation. Instrument operation and data evaluation were performed using visionCATS software (version 3.1, CAMAG).

2.4. Validation parameters

All validation parameters were determined according to ICH guidelines [20], and all solutions were applied, incubated, and detected using the aforementioned parameters.

2.4.1. Limit of detection/quantification and working range

The limit of detection/quantification (LOD/LOQ) of the released products Glc and

Fru was determined using the signal-to-noise ratio (S/N). LOD (S/N > 3), LOQ (S/N > 10), and the working range were determined using 18 levels in a mass range of 30–1500 ng/band.

2.4.2. Linear range of the enzymatic reaction

The linear range of the enzymatic reaction of invertase and Suc was evaluated using 14 levels of invertase activity (2–150 mU/band) and a constant amount of Suc (2 µg/band). To calculate the amount of released product, a calibration curve of Glc and Fru (each 100–1500 ng/band) was applied side-by-side. The linear range was determined twice for the statistical evaluation.

2.4.3. Interday and intraday precision

The interday and intraday precision was evaluated on three different days. Each invertase activity (5–60 mU/band) was applied threefold and overspotted with a constant amount of Suc (2 µg/band). To calculate the amount of released product, a calibration curve of Glc and Fru (each 50–1500 ng/band) was applied side-by-side.

2.5. Spectrophotometric invertase assay

First, the dinitrosalicylic acid reagent (50 mL) was prepared by mixing 10 mL potassium sodium tartrate tetrahydrate solution (1.5 mg/mL in 2 M sodium hydroxide solution) and 25 mL dinitrosalicylic acid (22 mg/mL in water) while heating and adding 15 mL water.

Pre-warmed (55 °C, 10 min) Suc (250 µL, 100 mg/mL) was mixed with 30 µL, 40 µL or 50 µL invertase (1 U/mL in sodium acetate pH 4.5, i.e. 2.9 µg/mL), filled to 1 mL with water, and incubated at 55 °C for 15 min without rotation. For the quantification of released product amounts different concentrations of Glc (0.05–0.5 mg/mL in water) were prepared. An aliquot (each 500 µL) was withdrawn, mixed with 1 mL of dinitrosalicylic acid reagent, and heated in a boiling water bath for 5 min. After cooling, absorbance was measured at 540 nm (fluidlab R-300, Anvajo, Dresden, Germany). The blank measurements for invertase and Suc were subtracted from the absorbance of the samples.

2.6. Calculation of invertase activity

One unit of invertase is defined as 1 µmol Suc that was cleaved into 0.5 µmol of Fru and Glc per minute.

For the HPTLC approach, the activity of invertase (mU) was calculated by converting the evaluated amounts (µg) of Glc or Fru of the sample to its amount of substance (µmol) via the corresponding molecular weights (MW) divided by the incubation time (min) and multiplying by 1000.

$$\text{Activity [mU]} = \frac{\text{Amount of Glc/Fru [µg]}}{\text{MW of Glc/Fru } \left[{}^{g}/_{mol}\right] \times \text{ incubation time [min]}} \times 1000$$

For the spectrophotometric assay, the released amount of substance (µmol) of Glc was calculated from the calibration curve of Glc by subtracting the y-intercept of the calibration curve from the measured absorbance of the sample, divided by the slope of the calibration curve.

$$\text{Amount of substance (µmol)} = \frac{\text{Absorbance} - \text{y-intercept}}{\text{Slope}}$$

The activity of invertase (mU) was calculated by dividing the amount of substance (µmol) by the factor of 2 (conversion factor of Suc to Fru and Glc) times the incubation time and multiplied by 1000.

$$\text{Activity [mU]} = \frac{\text{Amount of substance [µmol]}}{2 \times \text{Incubation time [min]}} \times 1000$$

3. Results and discussion

3.1. Spectrophotometric invertase assay

Spectrophotometric methods that use derivatisation reagents to create detectable chromogenic product complexes are commonly used to determine invertase activity. The reagents, *p*-hydroxybenzhydrazide (PAHBAH) [17], dinitrosalicylic acid (DNS) [21], and *p*-aminobenzoic acid (PABA) [22] were tested. The use of a toxic *p*-nitrophenolic substrate (NPG), according to Siegenthaler [2] and as described by the European Honey Commission [18], was avoided. The used invertase from *S. cerevisiae* is categorized as acidic invertase. While the enzyme-substrate reaction took place in an acidic environment (pH 5), the derivatisation reaction with PAHBAH required a basic environment (preparation in 0.5 M sodium hydroxide solution). The altered pH conditions yielded no robust and reproducible results (data not shown). After testing the different derivatisation reagent recipes for PAHBAH, the reagent was substituted. Because PABA is used as the preferred derivatisation reagent for the HPTLC analysis of saccharides [5,23], it was adapted for the spectrophotometric approach. Unfortunately, PABA did not have the same sensitivity in solution than used as a spraying reagent on an HPTLC plate. Therefore, weak colouration was observed for the defined enzyme ranges because of the high dilution effects in solution, regardless of the amount of sucrose (Suc) added. Therefore, DNS was selected as the final derivatisation reagent to quantify the enzyme reaction of invertase and Suc. The enzyme range of invertase in the PAHBAH assay (30–40 mU/assay) was extended to 30–50 mU/assay, and a precision measurement (n = 3) was performed, resulting in a percentage relative standard deviation (RSD%) of 30 in the lower range and 7 in the upper range. A reliable range of 40–50 mU of invertase per assay was set for the DNS reagent.

As for all other reagents, DNS reacts unspecifically with reducing substances such as Glc and keto-enol-capable Fru. Hence, only the sum parameter of all products can be evaluated and considered for the calculation of enzyme activity. Because this study dealt with non-matrix-rich substances of standard purity, the quantification was assumed to be reliable. Overall, these derivatisation reagents should be viewed with concern with regard to selectivity when analysing saccharide-containing matrix-rich samples, as shown previously [7,8]. Instead of using a derivatisation reagent that reacts with the released product, the quantification method used by the European Honey Commission uses a more matrix-robust but toxic

chromogenic substrate. In conclusion, there is potential for a robust, precise, and reliable method for quantification of saccharides, such as HPTLC [5,7,8].

3.2. HPTLC invertase nano assay

The HPTLC nanoGIT methodology [9] was designed as an all-in-one approach to separate metabolism products produced by gastrointestinal enzymes on the same surface. By qualifying [6] or quantifying [5] these products, it is possible to gain more details about the enzyme reaction or its inhibition [7,8]. Previous studies revealed the limitations of this method due to the use of suspensions as substrates [5], the influence of matrix components such as the enzyme mix itself [6], or the strong influence of crude extracts [7,8]. This study was designed to investigate the on-surface enzyme reaction in more detail, using the simple enzyme reaction of invertase and Suc to its equimolar components Glc and Fru. Because invertase is not known as a gastrointestinal enzyme, the suffix *gastrointestinal tract (GIT*) in the established terminology *nanoGIT* is omitted in this publication.

Minimal optimisation was necessary to obtain optimal assay and separation conditions. Wetting (starting of the enzyme reaction) and ideal pH conditions were achieved in one step by only wetting the application zone (to not impair later separation) with ammonium acetate solution (pH 4.5). The omission of the use of high-salt loading buffer solutions for pH adjustment [6] reduced its influence on the enzymatic reaction itself, the separation, and detection. The excellent separation of Suc from Glc and Fru by adding the natural product reagent A to the mobile phase [19] allowed optimal quantification after post-chromatographic derivatisation with the *p*-aminobenzoic acid reagent via densitometry, which is the most sensitive to monosaccharides [5,23]. In contrast to the spectrophotometric assay, the HPTLC invertase nano assay had the advantage of detecting and quantifying Glu and Fru separately, thus eliminating and additionally identifying potential matrix effects by unspecific reduced compounds.

The most reproducible results were achieved by pre-washing the HPTLC plate twice with methanol/water (3:1 *V*/*V*) because it was assumed that invertase is sensitive to metal ions and/or binder residues left on the plate surface. Pre-washing should be carefully evaluated for each enzyme individually, because the enzyme may be sensitive to the impurities left on the plate surface after production or to the residues of organic solvents of the pre-washing procedure. Generally, it is recommended that the plate surface be exposed to as little influence as possible.

However, the HPTLC workflow is more complex than that of the spectrophotometric approach and requires more steps because of the advantageous separation step. It should be emphasised that up to 20 samples could be automatically applied side by side on one HPTLC plate. In contrast, each

spectrophotometric sample had to be prepared and handled individually, which was very time-consuming. Unfortunately, the HPTLC approach cannot be performed without organic solvents (for separation and derivatisation), where the spectrophotometric assay is based on aqueous solutions. However, due to the high variability of the mobile phase and derivatisation reagents, a greener approach could be developed in the future.

3.3. Limit of detection (LOD), limit of quantification (LOQ) and working ranges

Müller and Morlock [5] evaluated the LOD (S/N ≥ 3) and LOQ (S/N ≥ 10) of Glc detected with *p*-aminobenzoic acid reagent as 5 and 10 ng/band, respectively. Because prior method optimisation could influence the detection of Glc, its LOD/LOQ was re-evaluated together with Fru (Figure S1). The determined LOD of Fru was 30 ng/band (S/N 4) and the LOQ was 50 ng/band (S/N 13). As equimolar amounts of Glc and Fru were expected, no more than 30 ng/band Glc was applied, resulting in an S/N of 25. In conclusion, the *p*-aminobenzoic acid reagent was far more sensitive to aldoses (Glc) than to ketoses (Fru). This difference in sensitivity was also reflected in the working ranges. Although the working range of Fru was larger (30–1200 ng/band) than that of Glc (30–800 ng/band), the standard deviation was higher, and the correlation coefficient (R) was lower for Fru (RSD% = 12, R = 0.9925) than for Glc (RSD% = 5, R = 0.9985).

Overall, the detection of both saccharides was far more sensitive using HPTLC (nanomolar range) than all the previously investigated spectrophotometric assays (millimolar range).

3.4. Linear range of the enzyme reaction

The linear range of enzyme activity additionally limits the application of enzyme assays. For the conversion of Suc by invertase to its equimolar components Fru and Glc, the enzyme activity (U) is defined as 1 µmol Suc that was cleaved into 0.5 µmol of Fru and Glc per minute. The release of products of an enzyme reaction and its activity is only proportional if their relationship is linear [24,25]. The linear range of the enzyme reaction of invertase via HPTLC was determined within the limits of 2–150 mU/band (Figure S2). A detailed overview of the linear range and precision of each saccharide (Figure 1 and Table S1) is provided.

For the lowest activity (2 mU/band), Fru was below the LOD and with higher activity (>60 mU/band) the amount of both products reached saturation.

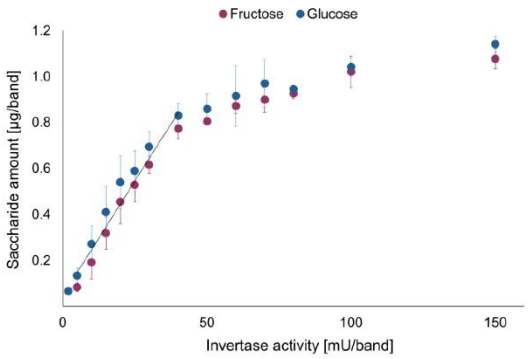

Figure 1 Determination ($n = 2$) of the linear range of the enzyme reaction of invertase and sucrose determined via the released saccharide amount

(µg/band) of glucose and fructose and the corresponding invertase activity (2-150 mU/band) after a constant incubation period of 15 min at 50 °C.

The linear range was determined to be 5–40 mU/band (RSD% = 8, R = 0.9803) for both saccharides, which was a 3.5-times larger range than that specified for the spectrophotometric assay (40–50 mU/band). A broader range simplifies applicability because an unknown enzyme sample can be investigated more effectively and reliably for different activities. The lower linear range showed the potential to determine even small quantities of enzymes. As expected, the precision (n = 2) of the measurements showed the highest fluctuation in the lower range (5–15 mU/band) of the linear range of the enzyme reaction (RSD% = 22–37), and was improved with higher enzyme activities (20–40 mU/band, RSD% = 6–21). For comparability, the precision of the linear range of the spectrophotometric assay (40–50 mU/band) was 7–9%, whereas that of the HPTLC approach was 1–8% in the same range. A saturation plateau arose when limited by the substrate (all active centres were occupied), and the product release was constant, resulting in a lower fluctuation (RSD% = 1–7). Throughout the entire linear range, the RSD% was ≤22 for Fru and ≤27 for Glc, except for the 10 mU/band, where both saccharides had RSD% values of ≥30. It was assumed that the precision became even more accurate with a higher number of repetitions. Keeping in mind the very different environmental conditions of the HPTLC nano assay and the spectrophotometric assay (immobilised but humid vs. aqueous), the precision of both assays in their linear range was comparable.

3.5. Determination of the enzyme activity, intraday and interday precisions

After evaluating the linear range of the enzyme reaction, the intraday and interday precisions in an extended linear range (5–60 mU/band) were determined by three-fold application of each enzyme activity on three different days (Figure 2, Table 1). The intraday precisions for Fru (RSD% = 0.4–14) varied more strongly than those for Glc (RSD% = 1–7), which reflects the previously mentioned differences in sensitivity to the derivatisation reagent. At higher Fru amounts (>800 ng/band, i.e. 60 mU/band), the fluctuation of intraday precision decreased. Unfortunately, this activity was outside the linear range of the enzyme reaction, indicating the complex relationship of all assay parameters. Nevertheless, intraday

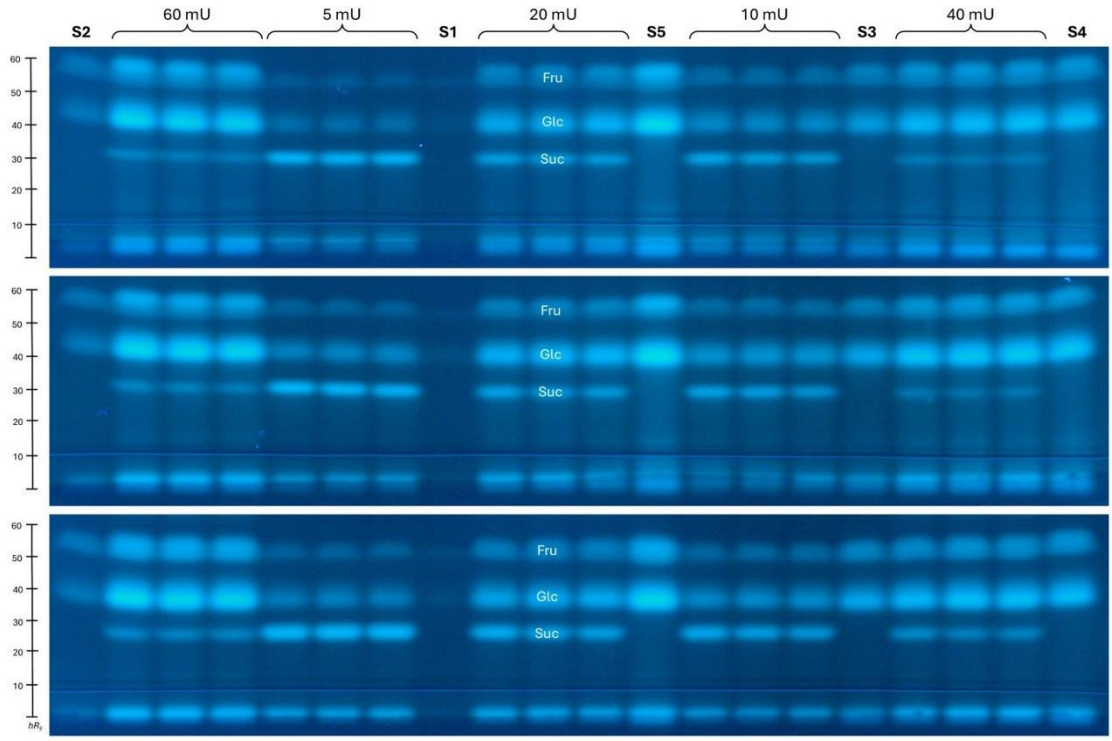

Figure 2 HPTLC-FLD chromatograms of the on-surface metabolization of sucrose (**Suc**, 2 µg/band) by invertase (5-60 mU/band) to fructose (**Fru**) and glucose (**Glc**) was used to determine the inter-day and intra-day precision of the enzyme reaction (n = 3). The plates were then incubated at 50 °C for 15 min. As a reference, the standards Glc and Fru (**S1–5**, 50-1200 ng/band) were applied onto the HPTLC plate silica gel 60, developed up to 60 mm with acetonitrile/water 4:1 (*V*/*V*) containing 2 mg/mL natural reagent A, and derivatised with *p*-aminobenzoic acid via immersion. Detected at FLD 366 nm and evaluated densitometrically in fluorescence mode at 366 nm.

precisions ≤14% were achieved which is acceptable for quantification of an on-surface enzymatic assay, but highlights the necessity of multiple determinations, preferably on different days. These challenges were expressed in terms of interday precision and have also been reported previously [5]. Although Glc showed good intraday precisions, the interday precisions (RSD% = 3–18) were high at the lowest (5 mU/band, RSD% = 18) and highest (60 mU/band, RSD% = 13) activity. The most robust results were obtained in the middle of the linear range of the enzymatic reaction (RSD% ≤ 7). Nevertheless, an outlier was detected in one (40 mU/band) or two (20 mU/band) sets, reflecting the hard-to-control immobilised enzyme reaction in the nanomolar range. The interday precisions for Fru (RSD% = 7–19) showed the same trend as for Glc, except for the activity of 40 mU/band (RSD% = 12), confirming the complexity of the immobilised enzyme assay. It was shown that the precise determination of robust ranges was essential for the .

Table 1 Intraday (n = 2–3) and interday (n = 8–9) precision of the HPTLC invertase nano assay at different enzyme activities (5–60 mU/band) determined on three different days with the resulting mean amount (ng/band) of the product release of fructose and glucose. Additionally, the conversion factor (Fru:Glc) was evaluated. The HPTLC invertase nano assay was performed using sucrose of standard purity.

Activity [mU/band]	Intraday precision [RSD%]	Interday precision [RSD%]	Mean amount ± SD [ng/band]	Intraday precision [RSD%]	Interday precision [RSD%]	Mean amount ± SD [ng/band]
	Fructose			Glucose		
5	3	19	138 ± 26.2	1	18	214 ± 39.4
	14			2		
	6			5		
	Conversion factor Fru:Glc = 65%					
10	13	10	246 ± 24.7	7	7	349 ± 24.7
	4			3		
	2			3		
	Conversion factor Fru:Glc = 70%					
20	0.4	7*	*498 ± 36.1	2	4*	*604 ± 23.4
	11			6*		
	3*			1*		
	Conversion factor Fru:Glc = 83%					
40	5	12	662 ± 78.8	1	3*	*827 ± 22.3
	12			3		
	7			2*		
	Conversion factor Fru:Glc = 80%					
60	6	8	888 ± 72.1	3	13	930 ± 119
	5			2		
	3			1		
	Conversion factor Fru:Glc = 95%					

*Outlier-corrected values using the interquartile range method with a cut-off of ±1.5

quantification of on-surface assays to obtain reliable results with a good precision. Based on the product release, the conversion factor of Fru:Glc was determined, revealing a non-equimolar conversion (65–95%) of both saccharides. With higher enzyme activities (≥ 60 mU/band), the conversion factor approached equimolar ratios, although these activities were outside the linear range of the enzyme reaction. This issue is discussed separately in a later troubleshooting section (3.7). Additionally, enzyme activity was calculated from the evaluated amount of products and compared to the assumed theoretical enzyme activity (Table 2). Surprisingly, the calculated activity differed significantly from the actual activity. The factor of difference was slightly lower for Glc (63–200) than for Fru (100–200). The sum of both saccharides (for comparability to the spectrophotometric assay) led to a factor of difference from 71–200, where with increasing activity the factor of difference grew. Excluding the lower (5 mU/band) and upper.

Table 2 Comparison of the calculated mean activity (mU/band) resulted from the HPTLC invertase nano assay with the true enzyme activity obtained from the supplier (mU/band) and the factor of difference. Enzyme activity was determined for each product separately (fructose and glucose) and summed (fructose + glucose).

True activity [mU/band]	5	10	20	40	60
Fructose					
Calculated mean activity [mU/band]	0.05	0.09	0.2	0.2	0.3
Factor of difference	100	111	100	200	200
Glucose					
Calculated mean activity [mU/band]	0.08	0.1	0.2	0.3	0.3
Factor of difference	63	100	100	133	200
Fructose + glucose					
Calculated mean activity [mU/band]	0.07	0.1	0.2	0.3	0.3
Factor of difference	71	100	100	133	200

(40–60 mU/band) borders of the linear range, a rather constant factor of difference of approximately 100 was obtained. It is not yet known whether this factor of difference can be applied for the quantification of all on-surface enzyme reactions or whether it must be evaluated individually for each enzyme; further studies are needed on this topic. For the quantification of on-surface enzyme reactions, it is recommended to compare the released quantities with other known validated assays to reliably interpret the results. In conclusion, a comparison of quantities, and thus enzyme activity, determined by spectrophotometric and HPTLC on-surface assays, cannot be made without knowing the factor of difference among the methods Nevertheless, statements about the products released by the enzymes and a detailed investigation of enzyme-substrate interactions can be made. Additionally, the determination of trends in the metabolism of different substrates is independent of the exact amount of product released, with particular attention paid to effects such as substrate or product inhibition. Therefore, enzyme reactions in the nanomolar range are preferred when only low amounts of enzyme/substrate are available; however, investigation via the HPTLC nano assay had shown clear limitations for miniaturised enzyme reactions.

3.6. Saccharide release and determination of invertase enzyme activity from sucrose-containing biscuits

To prove the concept of the invertase nano assay in addition to the matrix-free standards, sucrose was extracted from food, particularly from biscuits. Because of the ubiquitous use of fructose-glucose syrup and inverted sugar in bakery products, it was difficult to find foods

that did not interfere with the analytical method. Nevertheless, as previously proven [5,7,8], the analysis of matrix-rich samples is possible; however, this was not the focus of this study. The enzymatic conversion of sucrose extracted from biscuits by invertase (Figure 3) resulted in different amounts of Fru and Glu than those previously evaluated with the standards, even though the same amount of Suc and enzyme was used (Table 3, Table S3). Over the whole investigated range (5–60 mU/band) the mean amount of Fru (269–1063 ng/band, n = 5–6) and Glu (310–927 ng/band, n = 5–6) released was higher for the biscuit-extracted Suc than the release of Fru (138–888 ng/band, n = 5–6) and Glu (214–930 ng/band, n = 4–6) from Suc with standard purity. Additionally, in contrast to previously obtained results, the amount of Fru released was higher than the amount of Glc, leading to conversion factors >100%. Contrary to the standard substance, Suc was extracted from the biscuits via the dissolution of a representative amount of grounded biscuits (1.5 biscuits, 2.4 g). The amount of biscuit-extracted Suc used was not only based on calculations but was also previously compared with the corresponding amount of standard. A comparison of the extracted Suc with the previously used standard (Figure S3) showed comparable intensities and no other saccharides were present, assuming full comparability.

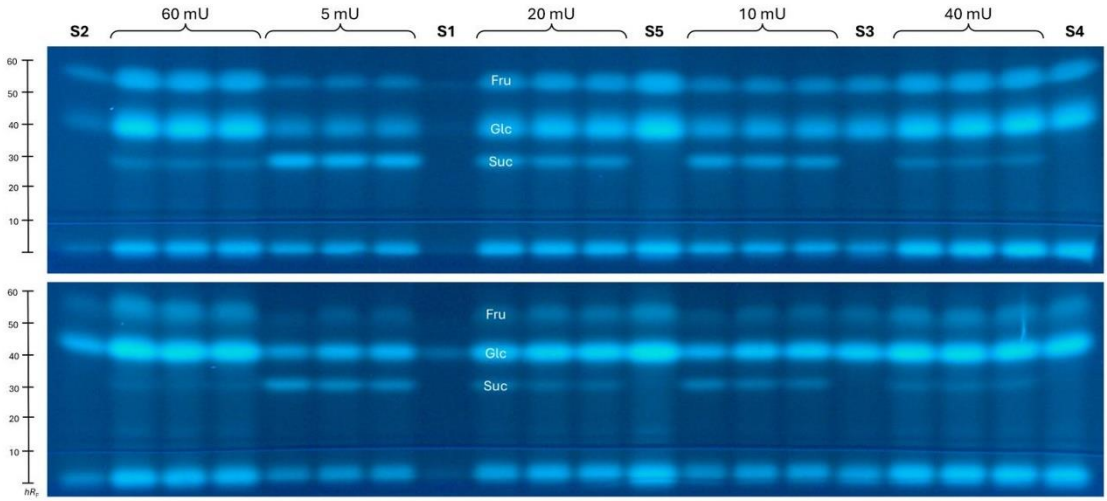

Figure 3 HPTLC-FLD chromatograms of the on-surface metabolization of sucrose (**Suc**, 2 µL/band) extracted from biscuits 2.5 mg biscuit/mL, i.e. 2 µg Suc/band) by invertase (5-60 mU/band) to fructose (**Fru**) and glucose (**Glc**) used for the determination of the inter-day and intra-day precision of the enzyme reaction (n = 2). The plates were then incubated at 50 °C for 15 min. As a reference, the standards Glc and Fru (**S1–5**, 50-1200 ng/band) were applied onto the HPTLC plate silica gel 60, developed up to 60 mm with acetonitrile/water 4:1 (*V*/*V*) containing 2 mg/mL natural reagent A, and derivatised with *p*-aminobenzoic acid via immersion. Detected at FLD 366 nm and evaluated densitometrically in fluorescence mode at 366 nm.

Table 3 Intraday (n = 2–3) and interday (n = 3–6) precision of the HPTLC invertase nano assay at different enzyme activities (5–60 mU/band) determined on three different days with the resulting mean amount (ng/band) of the product release of fructose and glucose. Additionally, the conversion factor (Fru:Glc) was evaluated. The HPTLC invertase nano assay was performed using biscuit-extracted sucrose.

Activity [mU/band]	Intraday precision [RSD%]	Interday precision [RSD%]	Mean amount ± SD [ng/band]	Intraday precision [RSD%]	Interday precision [RSD%]	Mean amount ± SD [ng/band]
	Fructose			Glucose		
5	9 1	7	269 ± 19	7 0.2*	7*	310 ± 22
	Conversion factor Fru:Glc = 87%					
10	9 11*	12	*392 ± 45	7 8*	6*	*446 ± 28
	Conversion factor Fru:Glc = 88%					
20	11 1	10	656 ± 66	11 19	16	604 ± 98
	Conversion factor Fru:Glc = 109%					
40	2 9	7	934 ± 70	8 4	10	869 ± 86
	Conversion factor Fru:Glc = 108%					
60	4 -	5	1063 ± 49	4 2*	3*	*927 ± 31
	Conversion factor Fru:Glc = 115%					

*Outlier-corrected values using the interquartile range method with a cut-off of ±1.5

However, the results of the enzymatic conversion using biscuit-extracted Suc were all in agreement with the previously determined interday precisions, and the proof of the concept was successful.

3.7. Troubleshooting and advice for dealing with immobilized enzyme reactions on solid surfaces (on-surface assays)

Several factors of influence were identified when dealing with the on-surface enzyme reaction despite the validation of the invertase nano assay, and were classified as important to be discussed in more detail.

Apart from the higher precision of the on-surface assays compared to the expected precision values of other common methods (except spectrophotometric assays), the immobilised enzyme reaction brings further challenges that need to be considered. Surprisingly, the release of Fru and Glc was not equimolar, as expected. The conversion factor (Fru:Glc) increased with increasing activity and reached equimolarity at higher activities (62% for 5 mU/band to 98% for 100 mU/band, Table S1), assuming a more complex relationship than simply the linearity. The reliability and calculation of the used well-established spectrophotometric assay is based on the equimolar conversion of Suc to

Fru and Glc in the validated linear enzyme range. Mentioned in advance, this observation of non-equimolarity would not be possible with spectrophotometric assays and thus would be overseen since a separation of single saccharides is not possible. Fortunately, this unexpected result draws attention to the complexity of enzyme reactions and the rash assumption that they are as simple as expected at the time of the establishment of those assays. In the last decades, the investigation of enzyme characterisation revealed a far more complex interaction of all assay components with the need to scrutinise the potentially outdated methods [24]. Intensive literature research has shown that invertase is not only known to convert Suc into Glc and Fru [26–28]. The non-equimolar conversion factor could be attributed to two reasons: I) the influence of the enzyme-to-substrate ratio (E/S) causing side reactions and/or II) different affinities of Fru and Glc for the derivatisation reagents.

The E/S ratio is a strongly underestimated parameter, and previous studies [7,8] have revealed the complexity of transferring aqueous (mobilised) to on-surface (immobilised) enzyme assays. Performing the enzyme reaction on the surface of an HPTLC plate led to a limited radius of action, where the enzyme and substrate could interact with each other. Substances that migrated into deeper layers during application owing to the capillary forces of the silica gel were not accessible for the enzyme-substrate reaction. This indicates that both may interact only in the first few layers of the HPTLC plate. This causes a different E/S ratio, even though the same amounts of enzyme and substrate were used for both assays. This was confirmed in this study by the determined factor of difference between the true and calculated activity (Table 2). To overcome this issue, it is recommended to use the same E/S ratio by applying small volumes of highly concentrated solutions to avoid migration to deeper layers. Nevertheless, this advice is limited by the application ability of the used components (solutions vs. suspensions, [5,7,8]) and the method of detection and its sensitivity (effects of dilution in aqueous solutions vs. concentration on HPTLC plates), as described previously. Different E/S ratios could lead to different enzyme interactions (side reactions, product or substrate inhibition) and thus complicating the comparison of both methods. Invertase not only converts Suc to Fru and Glc but also has transferring properties (fructosyltransferase) at high Suc concentrations [27], resulting in short-chain fructooligosaccharides [26,28]. These transferring interactions would result in higher amounts of Glc than Fru, and thus to a non-equimolar conversion since Fru is further converted, which can also be observed in this study. One advantage of the HPTLC approach is the possibility of simultaneously detecting a broad range of components. If fructooligosaccharides were produced, they would be detected in the application zone because they did not migrate in the polar mobile phase. Comparing the tracks

containing Suc treated with invertase and the tracks with standards (Fru and Glc) used for calibration (Figure 2–3), a higher fluorescence signal was detected in the application zones of the enzyme reaction. May, indicating fructooligosaccharide production. At higher standard concentrations, the tracks used for calibration also showed fluorescence signals in the application zone, which were identified as impurities in the saccharide standards. However, it is unclear whether the used derivatisation reagent (*p*-aminobenzoic acid) is sensitive enough to visualise long-chain saccharides because it is more sensitive to mono- and disaccharides than oligosaccharides [5,7] and to aldoses than to ketoses. A derivatisation reagent sequence on the same plate with a reagent that is more sensitive to long-chain saccharides [7,8] could provide further information regarding the suggested formation of side products. Another example of the easy handling and advantage of the HPTLC approach. The spectrophotometric assay only provides a mixture of all released products and requires further analytical investigation for the same information.

The investigation of the Michaelis-Menten constant (K_M) could also provide further information about the different enzyme interactions during both assay approaches and make them more comparable. Unfortunately, the determination of K_M was not successful for the HPTLC approach (data not shown) because data evaluation at small incubation intervals was impaired by the precision of the measurements. Adjustment of the incubation temperature is needed when using a spacious incubation oven to reach 50 °C on the plate surface within two or even 5 min. A change to an alternative heating method must be made to ensure rapid heating and constant incubation temperatures for the determination of K_M values for HPTLC enzyme assays. Nevertheless, the authors are confident that with further research on on-surface assays and an understanding of the behaviour of enzyme reactions on HPTLC plates, these minor uncertainties will be overcome in the future, making the HPTLC approach even more superior than spectrophotometric assays.

4. Conclusion

Overall, HPTLC nano assays are effective tools to open new doors for the research of already known or new unknown metabolisation reactions of all types, in contrast to spectrophotometric assays. Additionally, the increased sensitivity of the HPTLC approach concerning the amount of substrate used (12,500-fold less) at nearly equal amounts of enzyme (40-50 mU/band vs. 30-50 mU/band) was outstanding. Performing an assay in the nanomolar range makes it susceptible to minor changes in enzyme activity; thus, highly standardised conditions are needed for validation. However, the option of quantifying and separating even minor amounts of products of enzyme reactions would be a major benefit for the characterisation of enzymes.

Acknowledgement

Thank is owned to Lisa-Marie Niemeier and Ilka Scheibelhut for performing initial experiments.

Funding sources

Instrumentation was partially funded by Deutsche Forschungsgemeinschaft (DFG, German Research Foundation) - INST 162/536-1 FUGG and INST 162/471-1 FUGG.

Orcid

Gertrud Morlock https://orcid.org/0000-0001-9406-0351

Isabel Müller https://orcid.org/0000-0002-7392-7048

CrediT authorship contribution statement

Isabel Müller: Conceptualization, Methodology, Experimental Analysis, Data Analysis, Writing – Original Draft. **Viktoria H. Englert**: Experimental Analysis, Data Analysis. **Gertrud E. Morlock**: Conceptualization, Methodology, Supervision, Writing – Review and Editing.

Declaration of interests

The authors declare that they have no known competing financial interests or personal relationships that could have influenced the work reported in this study.

Supporting information

Supplementary information (PDF) can be found online.

References

[1] H. Troy AA, A Simplified Method for Measuring Secreted Invertase Activity in Saccharomyces cerevisiae, Biochem Pharmacol (Los Angel) 03 (2014) 1–5. https://doi.org/10.4172/2167-0501.1000151.

[2] U. Siegenthaler, Eine einfache und rasche Methode zur Bestimmung der a-Glucosidase (Saccharase) im Honig, MITT. GEB. LEBENSMITTELUNSTERS. HYG. 68 (1977) 251–258.

[3] G.L. Miller, Use of Dinitrosalicylic Acid Reagent for Determination of Reducing Sugar, Analytical Chemistry 31 (1959) 426–428. https://doi.org/10.1021/ac60147a030.

[4] B.V. McCleary, A.B. Blakeney, Measurement of inulin and oligofructan, Cereal Foods World 44 (1999) 398–406.

[5] I. Müller, G.E. Morlock, Quantitative saccharide release of hydrothermally treated flours by validated salivary/pancreatic on-surface amylolysis (nanoGIT) and high-performance thin-layer chromatography, Food Chem. 432 (2023) 137145. https://doi.org/10.1016/j.foodchem.2023.137145.

[6] I. Müller, A. Gulde, G.E. Morlock, Bioactive profiles of edible vegetable oils determined using 10D hyphenated comprehensive high-performance thin-layer chromatography (HPTLC×HPTLC) with on-surface metabolism (nanoGIT) and planar bioassays, Front. Nutr. 10 (2023) 1227546. https://doi.org/10.3389/fnut.2023.1227546.

[7] I. Müller, I. Scheibelhut, G.E. Morlock, Study of the quantitative α-amylase or trypsin inhibition by refined and whole wheat and einkorn using high-performance thin-layer chromatography–nanoGIT versus conventional spectrophotometry in submission.

[8] I. Müller, B. Schmid, L. Bosa, G.E. Morlock, Screening of α-amylase/trypsin inhibitor activity in wheat, spelt and einkorn by high-performance thin-layer chromatography, Anal. Methods. https://doi.org/10.1039/D4AY00402G.

[9] G.E. Morlock, L. Drotleff, S. Brinkmann, Miniaturized all-in-one nanoGIT+active system for on-surface metabolization, separation and effect imaging, Anal. Chim. Acta 1154 (2021) 338307. https://doi.org/10.1016/j.aca.2021.338307.

[10] S. Kulshrestha, P. Tyagi, V. Sindhi, K.S. Yadavilli, Invertase and its applications – A brief review, J. Pharm. Res. 7 (2013) 792–797. https://doi.org/10.1016/j.jopr.2013.07.014.

[11] F. Veana, A.C. Flores-Gallegos, A.M. Gonzalez-Montemayor, M. Michel-Michel, L. Lopez-Lopez, P. Aguilar-Zarate, J.A. Ascacio-Valdés, R. Rodríguez-Herrera, Invertase: An Enzyme with Importance in Confectionery Food Industry, in: M. Kuddus (Ed.), Enzymes in Food Technology: Improvements and Innovations, Springer Singapore, Singapore, 2018, pp. 187–212.

[12] K. Parker, M. Salas, V.C. Nwosu, High fructose corn syrup: Production, uses and public health concerns, Biotechnol. Mol. Biol. Rev. 5 (2010) 71–78.

[13] L.S.B. Upadhyay, N. Verma, Highly efficient production of inverted syrup in an analytical column with immobilized invertase, Journal of food science and technology 51 (2014) 4120–4125. https://doi.org/10.1007/s13197-013-0957-3.

[14] L.E. Trujillo Toledo, D. Martinez García, E. Pérez Cruz, L.M. Rivera Intriago, J.N. Pérez, J.M. Pais Chanfrau, Chapter 26 - Fructosyltransferases and Invertases: Useful Enzymes in the Food and Feed Industries, in: M. Kuddus (Ed.), Enzymes in Food Biotechnology: Production, Applications, and Future Prospects, Elsevier Science & Technology, San Diego, 2019, pp. 451–469.

[15] S.M. Kotwal, V. Shankar, Immobilized invertase, Biotechnol. Adv. 27 (2009) 311–322. https://doi.org/10.1016/j.biotechadv.2009.01.009.

[16] H. Manoochehri, N.F. Hosseini, M. Saidijam, M. Taheri, H. Rezaee, F. Nouri, A review on invertase: Its potentials and applications,

Biocatal. Agric. Biotechnol. 25 (2020) 101599. https://doi.org/10.1016/j.bcab.2020.101599.

[17] B.V. McCleary, L.M.J. Charmier, V.A. McKie, C. McLoughlin, A. Rogowski, Determination of Fructan (Inulin, FOS, Levan, and Branched Fructan) in Animal Food (Animal Feed, Pet Food, and Ingredients): Single-Laboratory Validation, First Action 2018.07, J. AOAC Int. 102 (2019) 883–892. https://doi.org/10.5740/jaoacint.18-0330.

[18] S. Bogdanov, P. Martin, C. Lüllmann, Harmonised methods of the European Honey Commission, Apidologie extra issue (1997).

[19] S. Kirchert, G.E. Morlock, Simultaneous determination of mono-, di-, oligo- and polysaccharides via planar chromatography in 4 different prebiotic foods and 60 naturally degraded inulin samples, Journal of chromatography. A 1569 (2018) 212–221. https://doi.org/10.1016/j.chroma.2018.07.042.

[20] Ich, Q2(R2): Validation of Analytical Procedures, International Council for Harmonisation, 1995/2023.

[21] A.A.N. Saqib, P.J. Whitney, Differential behaviour of the dinitrosalicylic acid (DNS) reagent towards mono- and di-saccharide sugars, Biomass Bioenergy 35 (2011) 4748–4750. https://doi.org/10.1016/j.biombioe.2011.09.013.

[22] K. Sato, A. Okuba, S. Yamazaki, Optimization of derivatization with 2-aminobenzoic acid for determination of monosaccharide composition by capillary electrophoresis, Analytical Biochemistry 262 (1998) 195–197. https://doi.org/10.1006/abio.1998.2798.

[23] G.E. Morlock, L.P. Morlock, C. Lemo, Streamlined analysis of lactose-free dairy products, J. Chromatogr. A 1324 (2014) 215–223. https://doi.org/10.1016/j.chroma.2013.11.038.

[24] J. Boeckx, M. Hertog, A. Geeraerd, B. Nicolai, Kinetic modelling: an integrated approach to analyze enzyme activity assays, Plant Methods 13 (2017) 69. https://doi.org/10.1186/s13007-017-0218-y.

[25] A.G. Tsuk, G. Oster, Determination of enzyme activity by a linear measurement, Nature 190 (1961) 721–722. https://doi.org/10.1038/190721a0.

[26] Y. Xie, H. Zhou, C. Liu, J. Zhang, N. Li, Z. Zhao, G. Sun, Y. Zhong, A molasses habitat-derived fungus Aspergillus tubingensis XG21 with high β-fructofuranosidase activity and its potential use for fructooligosaccharides production, AMB Expr 7 (2017) 128. https://doi.org/10.1186/s13568-017-0428-8.

[27] T. Shankar, P. Thangamathi, R. Rama, T. Sivakumar, Characterization of invertase from Saccharomyces cerevisiae MTCC 170, Afr. J. Microbiol. Res. 8 (2014) 1385–1393. https://doi.org/10.5897/AJMR2014.6612.

[28] D.C. Khandekar, T. Palai, A. Agarwal, P.K. Bhattacharya, Kinetics of sucrose conversion to fructo-oligosaccharides using enzyme (invertase) under free condition, Bioprocess Biosyst Eng 37 (2014) 2529–2537. https://doi.org/10.1007/s00449-014-1230-5.

Supplementary Information

Feasibility of HPTLC on-surface enzyme assays for the determination of enzyme activity in comparison to spectrophotometric approaches using invertase from *S. cerevisiae*.

Isabel Müller, Viktoria H. Englert, Gertrud E. Morlock*

Chair of Food Science, Institute of Nutritional Science, and Interdisciplinary Research Centre for Biosystems, Land Use and Nutrition, Justus Liebig University Giessen, Heinrich-Buff-Ring 26-32, 35392 Giessen, Germany

*Corresponding authors: Prof. Dr. Gertrud Morlock, phone: +49-641-9939141; fax +49-641-99-39149, email: gertrud.morlock@uni-giessen.de

Table of contents

Table S1 Calculated saccharide amounts (n = 2), relative percentage standard deviation (RSD%), and percentage conversion factor of fructose (Fru) to glucose (Glc) for determination of the linear range of the enzyme reaction.

Activity [mU/band]	Saccharide	Amount [ng/band]	Amount [ng/band]	Mean amount ± SD [ng/band]	RSD [%]	Conversion factor Fru:Glc [%]
2	Glucose	60.1	72.3	66.2 ± 8.6	13	-
	Fructose	<LOD	<LOD	-	-	
5	Glucose	111	156	134 ± 32	24	62
	Fructose	70.1	95.5	82.8 ± 18	22	
10	Glucose	214	328	271 ± 81	30	71
	Fructose	141	242	191 ± 71	37	
15	Glucose	332	488	410 ± 110	27	78
	Fructose	269	368	319 ± 70	22	
20	Glucose	458	621	540 ± 115	21	84
	Fructose	387	523	455 ± 96	21	
25	Glucose	527	651	589 ± 88	15	90
	Fructose	476	581	529 ± 74	14	
30	Glucose	647	741	694 ± 67	10	89
	Fructose	589	641	615 ± 37	6	
40	Glucose	792	867	829 ± 52	6	93
	Fructose	742	803	772 ± 43	6	
50	Glucose	811	906	859 ± 67	8	94
	Fructose	798	812	805 ± 10	1	
60	Glucose	822	1010	916 ± 133	14	95
	Fructose	849	895	872 ± 33	4	
70	Glucose	897	1043	970 ± 103	11	93
	Fructose	860	937	899 ± 55	6	
80	Glucose	941	951	946 ± 6.9	1	98
	Fructose	942	910	926 ± 23	2	
100	Glucose	1015	1070	1042 ± 39	4	98
	Fructose	1069	973	1021 ± 68	7	
150	Glucose	1117	1167	1142 ± 35	3	94
	Fructose	1108	1046	1077 ± 44	4	

Table S2 Intraday (*n* = 3) and interday (*n* = 9) precision of the HPTLC invertase nano assay at different enzyme activities determined on three different days with the resulting mean amount of product release of fructose and glucose. In addition, the calculated mean activity and conversion factors were evaluated. The HPTLC invertase nano assay was performed using sucrose in standard purity.

Activity [mU/band]	Saccharide	Amount [ng/band]	Intraday precision [RSD%]	Interday precision [RSD%]	Mean amount ± SD [ng/band]	Calculated mean activity [mU/band]	Conversion factor Fru:Glc [%]
5	Fructose	137	3	19	138 ± 26.2	0.05	65
		129					
		136					
		105	14				
		129					
		101					
		163	6				
		180					
		160					
	Glucose	192	1	18	214 ± 39.4	0.08	
		192					
		196					
		185	2				
		184					
		178					
		251	5				
		278					
		266					
10	Fructose	0.287	13	10	246 ± 24.7	0.09	70
		0.231					
		0.228					
		0.262	4				
		0.254					
		0.277					
		0.221	2				
		0.228					
		0.227					
	Glucose	0.360	7	7	349 ± 24.7	0.1	
		0.314					
		0.321					
		0.372	3				
		0.364					
		0.389					
		0.329	3				
		0.344					
		0.351					
20	Fructose	0.505	0.4	7**	**498 ± 36.1	0.2	83
		0.508					
		0.504					
		0.453	11				
		0.504					
		0.570					

Activity [mU/band]	Saccharide	Amount [ng/band]	Intraday precision [RSD%]	Interday precision [RSD%]	Mean amount ± SD [ng/band]	Calculated mean activity [mU/band]	Conversion factor Fru:Glc [%]
40		0.389*	3**				80
		0.481					
		0.460					
	Glucose	0.575	2	4**	**604 ± 23.4	0.2	
		0.594					
		0.591					
		0.589	6**				
		0.645					
		0.704*					
		0.525*	1**				
		0.618					
		0.613					
	Fructose	0.759	5	12	662 ± 78.8	0.2	
		0.728					
		0.689					
		0.709	12				
		0.739					
		0.583					
		0.545	7				
		0.623					
		0.586					
	Glucose	0.838	1	3**	**827 ± 22.3	0.3	
		0.832					
		0.842					
		0.814	3				
		0.834					
		0.859					
		0.728*	2**				
		0.812					
		0.787					
60	Fructose	0.849	6	8	888 ± 72.1	0.3	95
		0.826					
		0.756					
		0.937	5				
		0.910					
		0.853					
		0.971	3				
		0.969					
		0.924					
	Glucose	0.801	3	13	930 ± 119	0.3	
		0.791					
		0.754					
		0.980	2				
		0.966					
		0.939					
		1.061	1				
		1.047					
		1.033					

*Outlier and **outlier-corrected values using the interquartile range method with a cut-off of ±1.5

Table S3 Intraday (n = 3) and interday (n = 6) precision of the HPTLC invertase nano assay at different enzyme activities determined on three different days with the resulting mean amount of product release of fructose and glucose. In addition, the calculated mean activity and conversion factors were evaluated. The HPTLC invertase nano assay was performed using biscuit-extracted sucrose.

Activity [mU/band]	Saccharide	Amount [ng/band]	Intraday precision [RSD%]	Interday precision [RSD%]	Mean amount ± SD [ng/band]	Calculated mean activity [mU/band]	Conversion factor Fru:Glc [%]
5	Fructose	246	9	7	269 ± 19	0.1	87
		291					
		286					
		258	1				
		264					
	Glucose	294	7	7**	**310 ± 22	0.1	
		338					
		332					
		184*	0.2**				
		294					
		293					
10	Fructose	374	9	12**	**392± 45	0.1	88
		432					
		440					
		216*	11**				
		329					
		386					
	Glucose	411	7	6**	**446 ± 28	0.2	
		452					
		468					
		285*	8**				
		423					
		477					
20	Fructose	595	11	10**	**656 ± 66	0.2	109
		734					
		721					
		430*	1**				
		609					
		622					
	Glucose	573	11	16	604 ± 98	0.2	
		689					
		706					
		434	19				
		593					
		629					
40	Fructose	0.955	2	7	934 ± 70	0.3	108
		0.995					
		0.986					
		0.834	9				
		0.858					
		0.976					
	Glucose	0.871	8	10	869 ± 86	0.3	

Activity [mU/band]	Saccharide	Amount [ng/band]	Intraday precision [RSD%]	Interday precision [RSD%]	Mean amount ± SD [ng/band]	Calculated mean activity [mU/band]	Conversion factor Fru:Glc [%]
		0.920					
		1.010					
		0.833	4				
		0.777					
		0.802					
60	Fructose	1.085	4	5	1063 ± 49	0.4	115
		1.025					
		1.018					
		1.122	-				
	Glucose	0.977	4	3**	**927 ± 31	0.3	
		0.909					
		0.929					
		1.069*	2**				
		0.925					
		0.896					

*Outlier and **outlier-corrected values using the interquartile range method with a cut-off of ±1.5

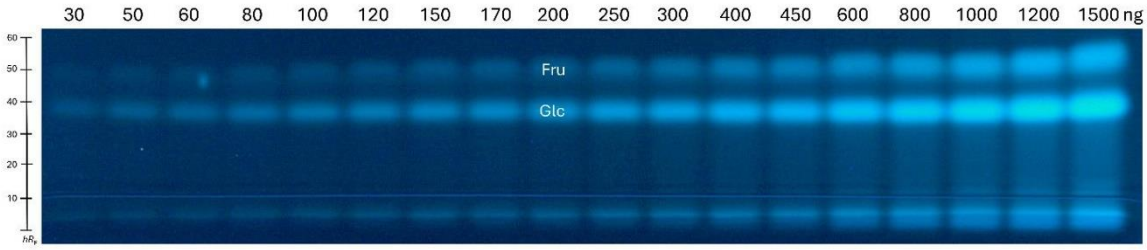

Figure S1 HPTLC-FLD chromatograms of the reference standards fructose (**Fru**) and glucose (**Glc**) to determine the limit of detection (LOD), limit of quantification (LOQ), and working range. Standards were applied in a range from 30-1500 ng/band onto the HPTLC plate silica gel 60, developed up to 60 mm with acetonitrile/water 4:1 (*V*/*V*) containing 2 mg/mL natural reagent A, and derivatized with *p*-aminobenzoic acid via immersion. Detected at FLD 366 nm and evaluated densitometrically in fluorescence mode at 366 nm.

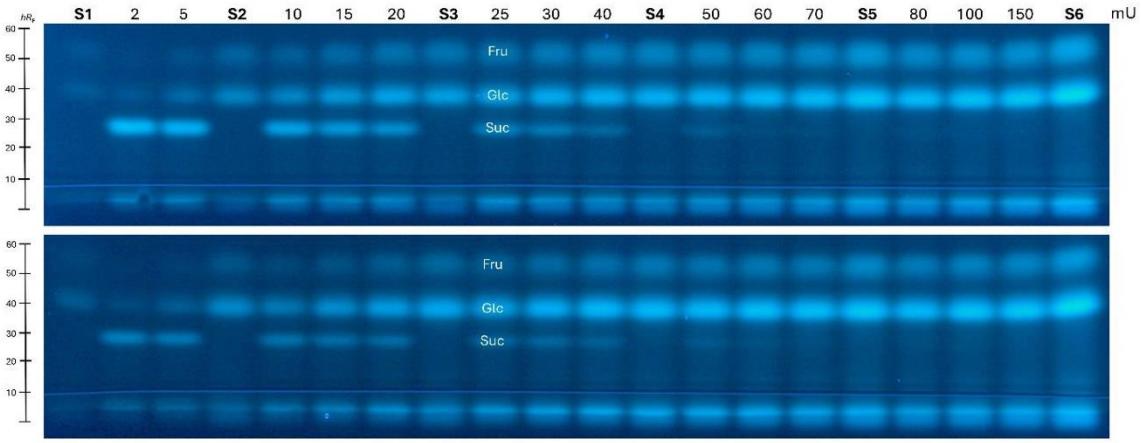

Figure S2 HPTLC-FLD chromatograms of the on-surface metabolization of sucrose (**Suc**, 2 µg/band) by invertase (2-150 mU/band) to fructose (**Fru**) and glucose (**Glc**) was used to determine the linear range of the enzyme reaction (n = 2). The plate was incubated at 50 °C for 15 min. As a reference, the standards Glc and Fru (**S1–6**, 100-1500 ng/band) were applied onto the HPTLC plate silica gel 60, developed up to 60 mm with acetonitrile/water 4:1 (*V*/*V*) containing 2 mg/mL natural reagent A, and derivatized with *p*-aminobenzoic acid via immersion. Detected at FLD 366 nm and evaluated densitometrically in fluorescence mode at 366 nm.

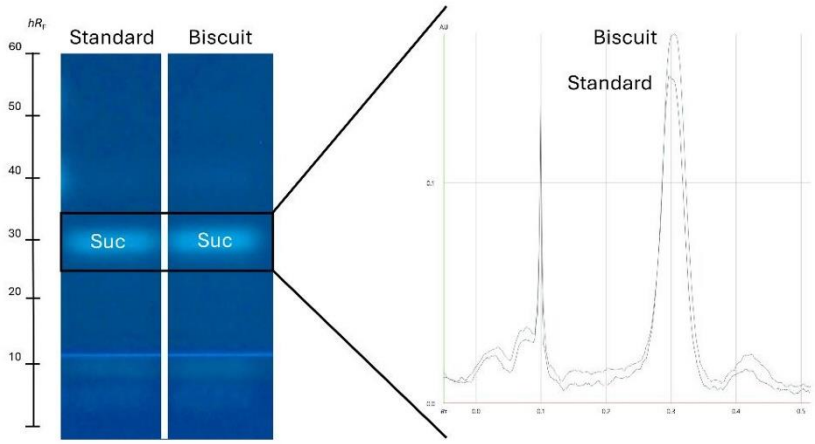

Figure S3 HPTLC-FLD chromatograms of sucrose (**Suc**, 2 µL/band) extracted from biscuits (2.5 mg biscuit/mL, i.e. 2 µg Suc/band) and Suc applied as standard substance (2 µg/band). For comparison of intensity, the corresponding densitogram was shown. Both applied onto the HPTLC plate silica gel 60, developed up to 60 mm with acetonitrile/water 4:1 (*V*/*V*) containing 2 mg/mL natural reagent A, and derivatized with *p*-aminobenzoic acid via immersion. Detected at FLD 366 nm and evaluated densitometrically in fluorescence mode at 366 nm.

Summary

This thesis discusses the progress achieved concerning the potential of on-surface metabolism hyphenated with HPTLC, established as HPTLC-nanoGIT. The developed methods and their wide range of applications offer several advancements in food science and nutrition research.

First, the previously published HPTLC-nanoGIT methodology was successfully validated for the quantification of starch digestibility by investigating various grain flours via saccharide release. It provides a novel approach to understand the digestibility of different flour types, as well as the differences between refined and whole grains. The possibility of quantifying each single saccharide provides a new detailed overview of amylolysis, which can help define dietary recommendations for obesity and diabetes management. Furthermore, the HPTLC-nanoGIT method was expanded to a 10D hyphenated technique to investigate the bioactive profiles of vegetable oils via on-surface lipolysis. The developed orthogonal HPTLC×HPTLC method allowed for a detailed metabolic profile. Additionally, the identification of genotoxic and antimicrobial effects of digested oils is helpful in the interpretation of food safety assessments. To further broaden the spectrum, the HPTLC-nanoGIT method was used to evaluate ATI-containing flour extracts and examine the potential as a novel inhibitory assay. This represents a major advancement over traditional spectrophotometric methods, particularly for matrix-rich samples. Finally, the feasibility of the HPTLC-nanoGIT method was investigated in detail and demonstrated enhanced sensitivity in contrast to spectrophotometric assays. However, some limitations were revealed when defining standardised protocols and determining kinetic parameters. Overall, the published results highlight the strong potential of the hyphenation of HPTLC and on-surface metabolisation for the detailed metabolic profiling of food components and their interpretation.

Zusammenfassung

Diese Arbeit diskutiert die erzielten Fortschritte bezüglich des Potenzials des on-surface Metabolismus kombiniert mit HPTLC, etabliert unter dem Namen HPTLC-nanoGIT. Die entwickelten Methoden und ihre breite Palette an Anwendungen bieten mehrere Fortschritte in der Lebensmittelwissenschaft und Ernährungsforschung.

Zunächst wurde die zuvor veröffentlichte HPTLC-nanoGIT Methodik erfolgreich validiert für die Quantifizierung des Stärkeverdaus durch die Untersuchung der Saccharidfreisetzung verschiedener Getreidemehle. Sie bietet einen neuartigen Ansatz, um die Verdaulichkeit verschiedener Mehlsorten sowie die Unterschiede zwischen Weißmehl und Vollkornmehl zu verstehen. Die Möglichkeit, jedes Saccharid einzeln zu quantifizieren, bietet einen neuen detaillierten Überblick über die Amylolyse. Dies könnte helfen, Ernährungsempfehlungen bezüglich Fettleibigkeit und Diabetes zu definieren. Darüber hinaus wurde die HPTLC-nanoGIT-Methode zu einer 10D-gekoppelten Technik erweitert, um die bioaktiven Profile von Pflanzenölen mittels on-surface Lipolyse zu untersuchen. Die entwickelte orthogonale HPTLC×HPTLC Methode ermöglichte ein detailliertes metabolisches Profil zu erstellen. Zusätzlich ist die Identifizierung genotoxischer und antimikrobieller Wirkung von verdauten Ölen hilfreich bei der Interpretation von Lebensmittelsicherheitsbewertungen. Um das Spektrum weiter zu erweitern, wurde die HPTLC-nanoGIT Methode verwendet, um ATI-haltige Mehlextrakte zu bewerten und das Potenzial als neuartigen Inhibitionsassay zu untersuchen. Die Methodik stellt einen bedeutenden Fortschritt gegenüber traditionellen spektrophotometrischen Methoden dar, insbesondere für matrixreiche Proben. Schließlich wurde die Durchführbarkeit der HPTLC-nanoGIT-Methode untersucht und zeigte eine erhöhte Empfindlichkeit im Gegensatz zu spektrophotometrischen Assays. Es wurden jedoch einige Einschränkungen bei der Definition standardisierter Protokolle und der Bestimmung kinetischer Parameter aufgedeckt. Insgesamt unterstreichen die veröffentlichten Ergebnisse jedoch das starke Potenzial der Kombination von HPTLC und on-surface Metabolisierung, um ein detailliertes Metabolitenprofil von Lebensmittelkomponenten zu erstellen und zu interpretieren.